Synthesis, complexation and reactivity studies of novel bis(1,2,3-triazol-5-ylidene)carbazolide ligands

by

George Kleinhans

Submitted in partial fulfilment of the requirements for the degree

Magister Scientiae

In the Faculty of Natural and Agricultural Sciences

University of Pretoria

Pretoria

October 2014

Declaration

I, George Kleinhans declare that the dissertation, which I hereby submit for the degree Magister Scientiae at the University of Pretoria, is my own work and has not previously been submitted by me for a degree at this or any other tertiary institution.

The X-ray structure determination was completed by Mr. David C. Liles at the University of Pretoria, and by Dr. Gaël Ung, at the University of California, San Diego.

Mass spectrometric analysis was performed by Dr. Dwayne Koot at the University of Pretoria, and by Dr. Gaël Ung, at the University of California, San Diego.

Part of the results in this dissertation has been published in D. I. Bezuidenhout, G. Kleinhans, G. Guisado-Barrios, D. C. Liles, G. Ung, G. Bertrand, *Chem. Commun.*, 2014, **50**, 2431 – 2433.

SIGNATURE:

DATE: 29/10/2014

Table of Contents

Summary

Synthesis, complexation and reactivity studies of novel bis(1,2,3-triazol-5-ylidene)carbazolide ligands

by

George Kleinhans

Supervisor: Dr DI Bezuidenhout

Submitted in partial fulfilment of the requirements for the degree Magister Scientiae, Department of Chemistry, University of Pretoria

During this study, novel tridentate ligands were synthesised, based on a rigid carbazole backbone whilst featuring triazolium flanking groups with bulky aryl wingtips. These ligands were coordinated to various late transition metals, including Ni, Cu, Rh, Ag and Au.

Deprotonation of the triazolium ligand salts with base yielded the potassium free carbene adducts, stable indefinitely under inert conditions. One of the free carbene adducts could also be characterised *via* X-ray diffraction analysis. The steric bulk 'enclosed' the tridentate pocket, where the two free triazolylidenes and the amido of the carbazolide backbone coordinated to two potassium metal ions. The free carbene adducts emitted a strong green fluorescence upon irradiating with ultra violet (UV) light at a wavelength of 354 nm.

The stabilisation imparted by the ligand adducts was evaluated when it was coordinated to reactive late transition metals. The first example of a neutral nickel(II)-hydride carbene complex was obtained after metallation of the ligand adduct with a nickel(II) precursor. Reacting the deprotonated ligand adduct with $CuCl_2$ lead to the isolation of a rare example of a copper(II) carbene complex. Reduction of copper(II) to copper(I) occurred readily. These complexes were characterised with various techniques, including X-ray diffraction analysis.

The stabilising ability of the ligand scaffolds was again probed, this time with regards to the heavier late transition metals. Metallation with Ag(I) or Au(I) yielded the corresponding metal complexes, where chelation around the metal centres, and not dinuclear complex formation, occurred. Pincer complex formation was accompanied by coordination of all three coordinating sites of the tridentate ligand scaffold to the metal. This is unusual because, in general, silver(I) and especially gold(I) metals, tend to form two-coordinated complexes with a linear geometry around the metal centre or trigonal planar complexes if the coordination number of the complex is three. Therefore, formation of the ''naked'' T-shaped Ag(I) and Au(I) complexes is unusual and remarkable indeed. The complexes are stable towards atmospheric conditions. Oxidation of Au(I) yielded a cationic gold(III)-hydroxo complex.

The bis(1,2,3-triazol-5-ylidene)carbazolide ligands not only proved to be excellent scaffolds for stabilising reactive metal complexes, but also proved to yield a catalytically active complex upon metallation of the ligand adduct with rhodium. Surprisingly, metallation yielded a rhodium(I)-dioxygen adduct. This complex coordinated reversibly to ammonia, and did not form an inert Werner complex, as heuristically expected. In order to probe the electronic properties of the ligand scaffolds, CO was reacted with the rhodium complexes. IR analysis of the Rh(I)-CO complexes revealed low energy values, giving evidence to the strong σ-donor and weak π-acceptor ability of the ligands. The rhodium-dioxygen adduct complex, which could be manipulated in air, was subjected to catalysis. The Rh(I)-O_2 species catalyses the dimerisation of 1-pentyne to 6-methylene-4-nonyne, with selectivity only towards the *gem*-enyne product. Such selectivity is scarcely reported. Full conversion of the alkyne to the enyne was observed when catalysis was executed in the presence of diethyl amine.

List of Precursors, Ligands and Complexes
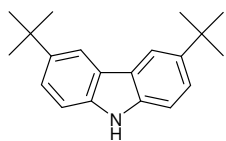
3,6-di-*tert*-butyl-9H-carbazole (**1**)
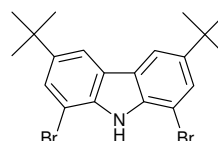
1,8-dibromo-3,6-di-*tert*-butyl-9H-carbazole (**2**)
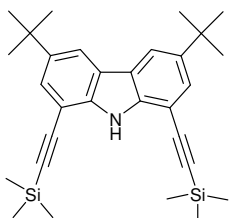
3,6-di-*tert*-butyl-1,8-bis(2-(trimethylsilyl)ethynyl)-9H-carbazole (**3**)
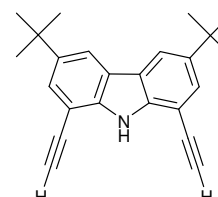
3,6-di-*tert*-butyl-1,8-diethynyl-9H-carbazole (**4**)
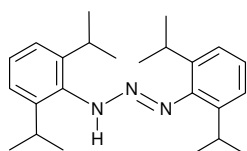
1,3-bis-(2,6-diisopropylphenyl)triaz-1-ene (**5**)
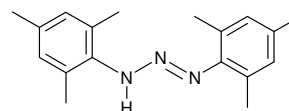
1,3-Bis-(2,4,6-trimethylphenyl)triaz-1-ene (**6**)
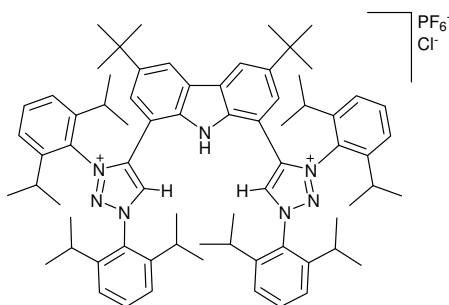
4,4'-(3,6-Di-*tert*-butyl-9H-carbazole-1,8-diyl)bis(1,3-bis(2,6-diisopropylphenyl)-1H-1,2,3-triazolium) hexafluorophosphate(V) chloride (**7**)

[(CNC$_{Dipp}$)PF$_6$] (**8**)

[(CNC_Dipp)K] (**9**)

4,4'-(3,6-Di-*tert*-butyl-9H-carbazole-1,8-diyl)bis(1,3-bis(2,4,6-trimethylphenyl)-1H-1,2,3-triazolium) hexafluorophosphate(V) chloride (**10**)

[(CNC_Mes)K] (**11**)

(CNC_Dipp)NiH (**12**)

(CNC_Mes)NiH (**13**)

(CNC_Dipp)CuCl (**14**)

IV
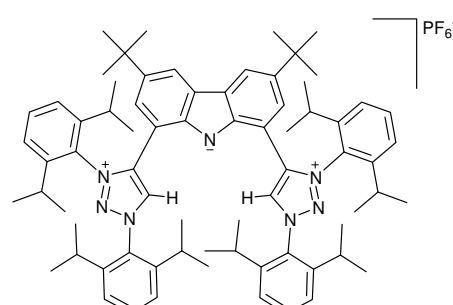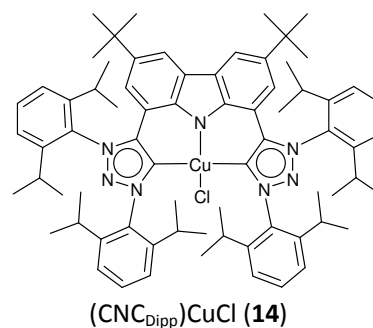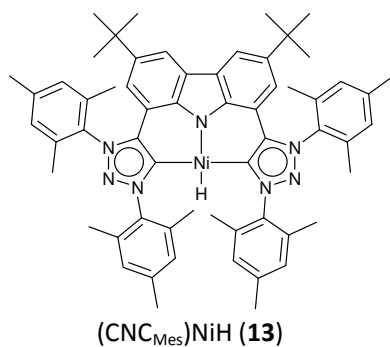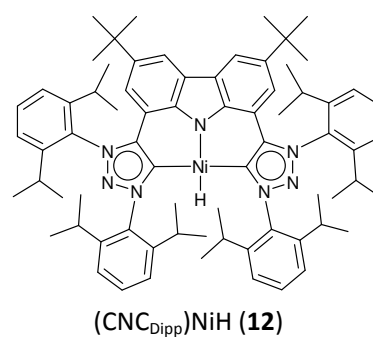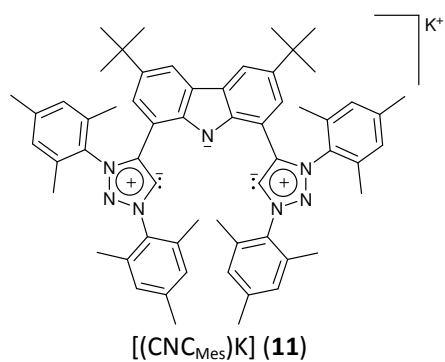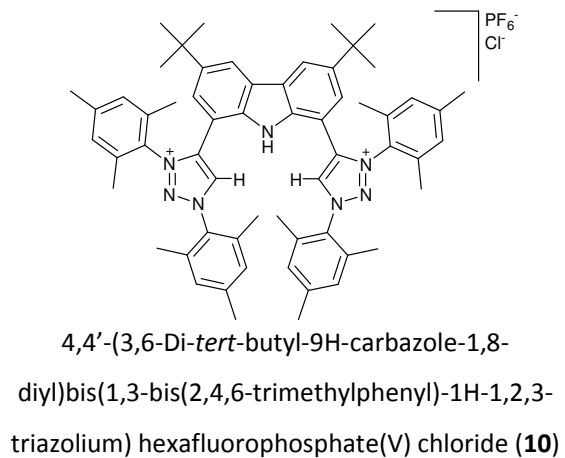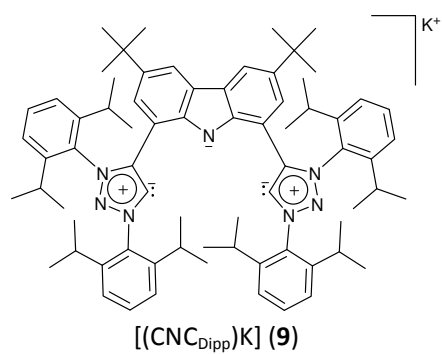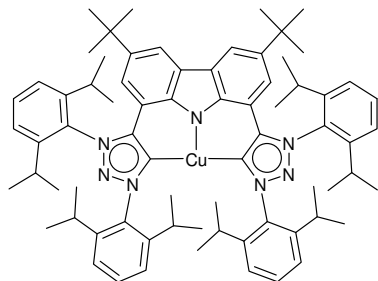
(CNC_Dipp)Cu (**15**)
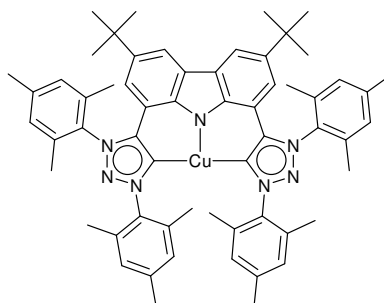
(CNC_Mes)Cu (**16**)
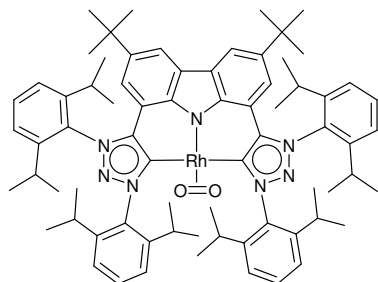
(CNC_Dipp)RhO₂ (**17**)
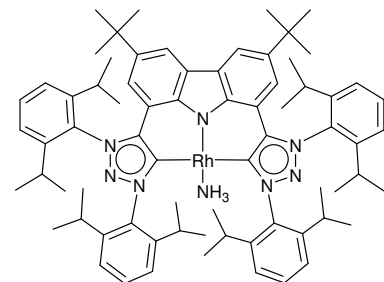
(CNC_Dipp)RhNH₃ (**18**)
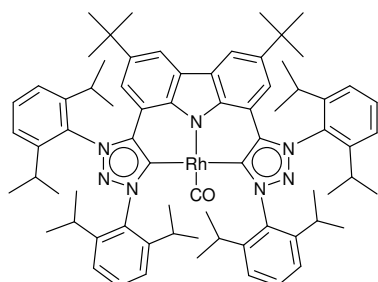
(CNC_Dipp)RhCO (**19**)
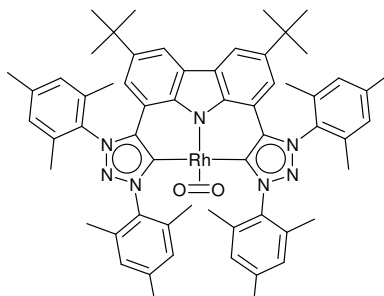
(CNC_Mes)RhO₂ (**20**)
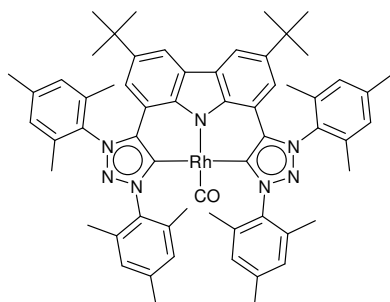
(CNC_Mes)RhCO (**21**)

(CNC_Dipp)Ag (**22**)

v

(CNC$_{Dipp}$)Au (**23**)

[(CNC$_{Dipp}$)Au(OH)]PF$_6$ (**24**)

(CNC$_{Mes}$)Au (**25**)

VI
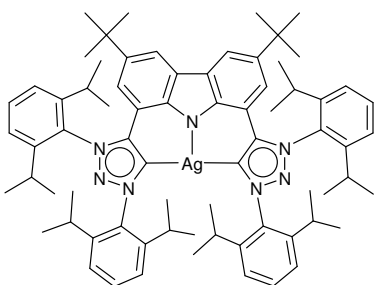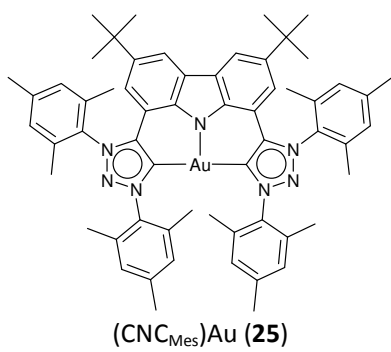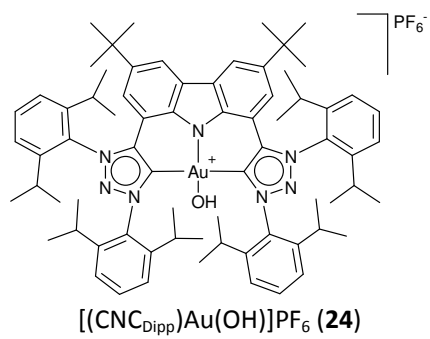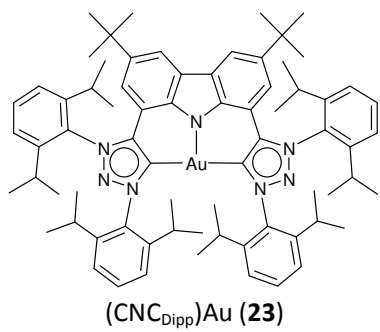
List of Abbreviations

aNHC	abnormal N-heterocyclic carbene
OAc	acetate
MeCN	acetonitrile
R	alkyl/aryl
Ar	aryl
atm	atmosphere
v_{av}	average stretching frequency
$i$bitz	4,4'-bis(1,2,3-triazol-5-ylidene)
Bu	butyl
^{t}Bu	$tert$-butyl
Boc	$tert$-butyloxycarbonyl
CuAAC	copper catalysed cycloaddition of alkynes with azides
J	coupling constant
CAAC	cyclic (alkyl)(amino)carbene
COD	1,5-cyclooctadiene
DFT	density functional theory
DCM	dichloromethane
Dipp	2,6-diisopropylphenyl
dme	dimethoxyethane
EPR	electro-paramagnetic resonance
ESI-TOFMS	electrospray ionization-time of flight-mass spectrometry
eq.	equivalents
Et	ethyl
FIA-ESI-MS	flow Injection analysis-electrospray ionization-mass spectrometry
NHC	N-heterocyclic carbene
HRMS	high resolution mass spectroscopy
HOMO	highest occupied molecular orbital
HCl	hydrochloric acid
H-bonding	hydrogen-bonding
Tp	hydrotris(3,5-di-2-propylpyrazolyl)borate
IR	infrared
^{i}Pr	iso-propyl

LUMO		lowest unoccupied molecular orbital
MS		mass-spectroscopy
MP		melting point
MIC		mesoionic carbene
MeOH		methanol
Me		methyl
nm		nanometer
nbd		norbornene
nNHC		normal/classical *N*-heterocyclic carbene
NMR		nuclear magnetic resonance
ppm		part per million
Ph		phenyl
KHMDS		potassium hexamethyldisilazide
rNHC		remote *N*-heterocyclic carbene
RT		room temperature
v		stretching freqeuncy
THF		tetrahydrofuran
tht		tetrahydrothiophene
TEP		Tolman Electronic Parameter
*trz*H		triazolium salt
trz		triazolylidene
OAc^F		trifluoroacetate
Mes		2,4,6-trimethylphenyl
TMS		trimethylsilyl
Tpz		trispyrazolylborate
UV		ultra-violet
UV-vis		ultra-violet-visible
XRD		X-ray diffraction
XPS		X-ray photoelectron spectroscopy

Chapter 1: Introduction

1.1) Overview

The carbene carbon has become a powerful tool in organometallic chemistry. Since the first correctly characterised organometallic carbene complex in the 1960's,[1] it has become the main focus of research of various research groups around the globe. Due to its characteristics, the carbene has found numerous applications, from fundamental template reactions in laboratories to industrial applications in catalysis and synthesis. There is no doubt that research in the field of carbene chemistry will continue for years to come, and that its potential has not yet been fully exploited.

1.1.1) Theoretical Bonding Aspects of Heteroatom-substituted Carbene

Carbenes are neutral divalent carbon atoms containing 6 valence electrons, and can either be linear or bent (Figure 1.1).[2] In the linear case the carbon atom consists of two sp-hybridised orbitals in addition to two p-orbitals, a p_x- and a p_y-orbital. The geometry around the carbon is linear, with both p-orbitals at 90° angles from each other orientated out of the plane. If the carbene is bent, the degeneracy of the carbene is lost, in which case it adopts sp^2-hybridisation. The p_x-orbital gains s-character, while the p_y-orbital remains unchanged and orthogonal to the sp^2 plane. The geometry around the sp^2-hybridised carbon atom is trigonal planar. The frontier orbitals are called the σ-orbital (sp^2-hybridised orbital) and the p_π-orbital (p_y-orbital).[2]

sp^2-hybridized orbital

p_x- and p_y-orbitals

120

p_y-orbital

sp-hybridized orbital

(**1$_a$**)

(**1$_b$**)
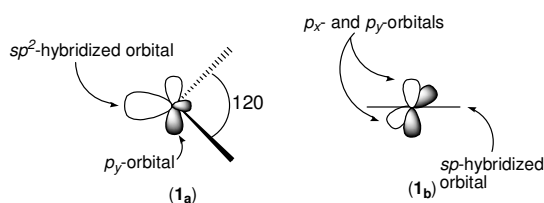
Figure 1.1: Carbon atom bent (**1$_a$**) or linear (**1$_b$**)[2]

The carbene carbon atom can either be in the singlet or in the triplet state, with each state consisting of two possible electron configurations (Figure 1.2). The singlet state occurs when the non-bonding pair of electrons are in either the σ-orbital or the p_π-orbital.[2] The σ^2 configuration (**2$_a$**), where both electrons are localised in the σ-orbital, is generally more stable than the $p_\pi{}^2$-

---

[1] E. O. Fischer, A. Maasböl, *Angew. Chem. Int. Ed. Engl.*, 1964, **3**, 580.
[2] D. Bourissou, O. Guerret, F. P. Gabbaï, G. Bertrand, *Chem. Rev.*, 2000, **100**, 39 – 91.

configuration (2_b) with both electrons localised in the p_π-orbital. Singlet carbenes are also classified as being ambiphilic in nature, due to the one orbital being fully occupied and the other orbital being vacant.[3] In the case of the triplet state, the two non-bonding electrons are located separately in different orbitals with either parallel (2_c) or anti-parallel (2_d) spins.[2] The one electron is localised in the σ-orbital, while the other electron is located in the p_π-orbital. As such, triplet carbenes are classified as diradicals.[3] The relative energy associated with the σ-orbital and p_π-orbital determines the ground state multiplicity of the carbene.[4] A large σ-p_π separation favours the singlet ground state configuration. Hoffmann determined that for the singlet ground state configuration, the σ-p_π separation must be at least 2 eV or higher, while for the triplet ground state configuration, the σ-p_π separation must be 1.5 eV or lower.[4]
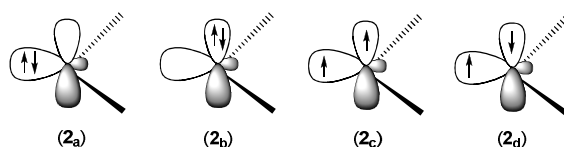
Figure 1.2: Singlet and triplet electron configuration of bent carbon with 6 valence electrons[2]

The carbene carbon atom is covalently bonded, in most cases to either one or two heteroatoms, except in the case of the Schrock carbene where no heteroatom is directly bonded to the carbene carbon atom (Figure 1.3). The heteroatom bonded to the carbene stabilises the highly reactive divalent carbon atom, through either inductive or resonance effects, or a contribution to the stability of the carbene from both effects. A σ-electron withdrawing heteroatom inductively stabilises the non-bonding σ-orbital of the carbene, increasing the s-character of the sp^2-hybridised orbital while leaving the p_π-orbital unchanged.[2] This results in an increase of the σ-p_π gap, favouring the singlet state. By contrast, the Schrock carbene is always in the triplet ground state configuration with alkyl- or aryl-substituents flanking the carbene, with an inductive electron donation towards the carbene atom. The σ-electron donation towards the carbene induces a small change in the energy of the σ-p_π gap, which is why the triplet ground state configuration is favoured.

R = alkyl or aryl
X = electronegative atom
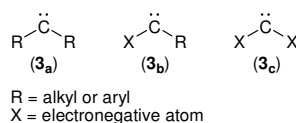
Figure 1.3: Schrock carbene (3_a) and carbene with either one (3_b) or two (3_c) heteroatoms

[3] G. B. Schuster, *Adv. Phys. Org. Chem.*, 1986, **22**, 311.
[4] R. Hoffmann, G. D. Zeiss, G. W. van Dine, *J. Am. Chem. Soc.*, 1968, **90**, 1458 – 1499.

For the heteroatom stabilised carbenes 3_b and 3_c (Figure 1.3), the divalent carbon is further stabilised by resonance. The heteroatom bonded to the carbene can either be a π-electron donating group (which will be referred to as X_{ED}) or a π-electron withdrawing group (X_{EW}).

A carbene can either be bonded to one or two X_{ED} substituents, and in both cases it is predicted that the carbene will have a bent geometry with a singlet ground state configuration.[5] X_{ED} substituents (such as -OR, -NR₂, -PR₂, -F, -Cl, -Br, -I, SR, etc.) are able to donate their electron lone pair into the vacant $p_π$-orbital (Figure 1.4), which results in the carbene obtaining a stable octet electron configuration. Upon donation of the X_{ED} lone pair, the heteroatom loses electron density and gains a partial positive charge. The σ-orbital remains unaffected, while the energy of the $p_π$-orbital increases, due to the interaction with the substituent lone pair.[2,5] The result is a further increase in the σ-$p_π$ gap, again favouring the singlet ground state configuration. The C-X_{ED} bond gains partial double bond character, as indicated in the resonance hybrids (4_c and 4_f, Figure 1.4). Examples of mono-heteroatom stabilised carbenes include Fischer carbenes (see later, Section 1.1.2, 7_b, Figure 1.7)[1] as well as Bertrand's cyclic alkyl amino carbenes.[6] When the carbene carbon is flanked by two X_{ED} substituents, electron delocalisation between the two X_{ED} p-orbitals and the $p_π$-orbital (4_a) results in a four-electron three-centred π-system and increased stabilisation of the divalent carbon.[2] The very reactive carbene is hereby stabilised to such an extent that it can be isolated and stored for a period of time. A representative example includes the well known Arduengo free N-Heterocyclic carbene (nNHC, see later, Section 1.1.2, 8_b, Figure 1.8).[7] Carbenes containing X_{ED} substituents will be classified, in this paper, as a σ-pull π-push system.
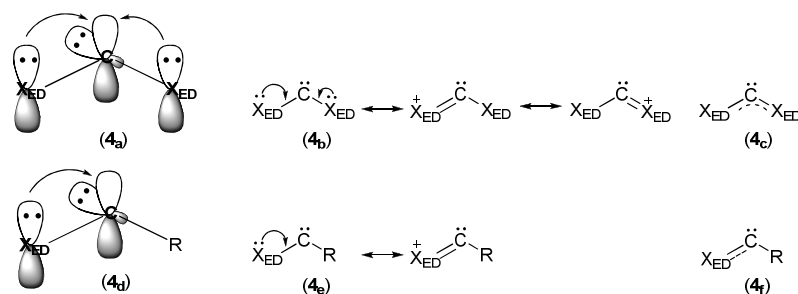
Figure 1.4: Carbenes with one (4_{d-f}) or two (4_{a-c}) X_{ED} substituents

[5] (a) W. W. Schoeler, J. Chem. Soc., Chem. Commun., 1980, **124**, 124 – 125; (b) L. Pauling, J. Chem. Soc., Chem. Commun., 1980, **688**, 688 – 689; (c) K. K. Irikura, W. A. Goddard, J. L. Beauchamp, J. Am. Chem. Soc., 1992, **144**, 48 – 51.

[6] (a) V Lavallo, Y. Canac, C. Präsang, B. Donnadieu, G. Bertrand, Angew. Chem. Int. Ed., 2005, **44**, 5705, (b) V. Lavallo, G. D Frey, B. Donnadieu, M. Soleilhavoup, G. Bertrand, Angew. Chem. Int. Ed., 2008, **47**, 5224 – 5228, (c) G. D. Frey, R. D. Dewhurst, S. Kousar, B. Donnadieu, G. Bertrand, J. Organomet. Chem., 2008, **693**, 1674 – 1682.

[7] A.J. Arduengo, R. L. Harlow, M. Kline, J. Am. Chem. Soc., 1991, **113**, 361 – 363.

3

Heteroatoms with no lone pair of electrons can accept electron density into their vacant p-orbital from the carbene (Figure 1.5). These heteroatoms are classified as π-electron withdrawing substituents (such as $-PR_3^+$, $-SiR_3$, $-BR_2$, $-CN$, $-CF_3$, etc.), while the carbenes are predicted to be mostly linear but still in the singlet ground state.[5] The vacant p-orbital of the substituent overlaps with the p_y-orbital of the carbene carbon atom, which has the lone pair of electrons localised in that orbital. The electron lone pair is donated into the vacant p-orbital of the substituent, which in most cases gains a stable electron configuration (eg. $-BR_2$ gains 2 electrons, resulting in a filled octet). Concurrently, the carbene carbon atom loses electron density around the carbon centre giving it a partial positive carbocation character.[2] The $C-X_{EW}$ single bond gains double bond character through electron delocalisation in the π-system. In the case of $\mathbf{5_b}$, electron delocalisation results in a two-electron three-centre π-system. These carbenes are even more reactive than X_{ED}-containing substituted carbenes. Borylmethyleneboranes are representative examples of such carbene systems.[8] Carbenes containing X_{EW} substituents will be classified, in this paper, as a σ-push π-pull system.
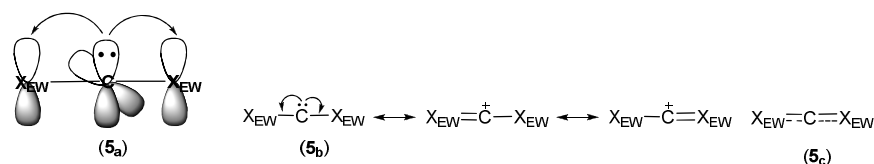
Figure 1.5: Carbene with two ($\mathbf{5_{a-c}}$) X_{EW} substituents

The carbene gains interesting properties when it is bonded to both X_{ED} and X_{EW} substituents, due to the electronic effects imparted by two different heteroatoms (Figure 1.6).[2] Both heteroatoms favour a singlet carbene ground state, with a quasi-linear geometry. The occupied X_{ED} p-orbital overlaps with the vacant p_y-orbital of the carbene, while the p_x-orbital of the carbene overlaps with the vacant X_{EW} p-orbital.[2] The lone pair of the X_{ED} substituent is donated into the vacant p_y-orbital, resulting in the X_{ED} substituent losing electron density to gain a partial positive charge. The carbene gains a partial carbanionic character, but in turn donates its lone pair of electrons localised in the p_x-orbital into the vacant X_{EW} p-orbital. The carbene loses some electron density, resulting in the formation of a neutral carbene. The X_{EW} substituent gains a stable electronic configuration, as well as a partial negative charge which intramolecularly compensates for the partial positive charge on the X_{ED} substituent. The zwitterionic allene system has an overall neutral charge, with each bond displaying double bond character. The carbenes are stable to a certain degree upon isolation and

[8] (a) A. Berndt, *Angew. Chem. Int. Ed. Engl.*, 1993, **32**, 985, (b) A. Berndt, D. Steiner, D. Schweikart, C. Balzereit, M. Menzel, H. J. Winkler, S. Mehle, M. Unverzagt, T. Happel, P. v. R. Schleyer, G. Subramanian, M. Hofmann, In *Advances in Boron Chemistry*, W. Siebert, Ed., The Royal Society of Chemistry: Cambridge, 1997, 61 – 72.

some of the most well known representative examples are reported by Bertrand and co-workers, including the well known (phosphino)(silyl)carbene which was the first correctly characterised free carbene (see later, Section 1.1.2, **8ₐ**, Figure 1.8).[9]
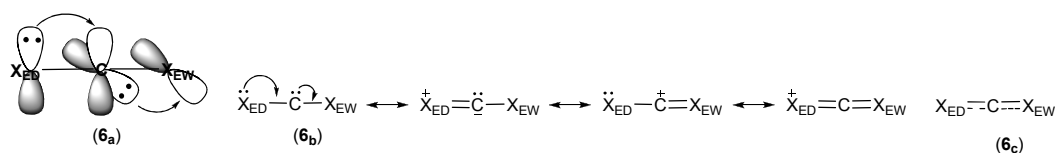
Figure 1.6: Carbene with one X_{ED} and one X_{EW} substituent

1.1.2) Brief History

The highly reactive free divalent carbon could only be synthesised, isolated and structurally characterised through Nuclear Magnetic Resonance (NMR) spectroscopy and X-ray Diffraction (XRD) analysis in the late 20th century, even though the idea received attention more than 150 years ago. In the year 1835 Dumas reported the attempted synthesis of methylene (**7ₐ**, Figure 1.7), a divalent carbon,[10] opening the door to the concept of a carbene carbon. However, it was only more than a 100 years later that the first metal-carbene complex was synthesised and correctly characterised. In 1964 E. O. Fischer and his graduate student A. Maasböl synthesised and characterised a tungsten-carbene complex, which marked the beginning of the metal-carbene chemistry era.[1] The Fischer carbene complex (**7ᵦ**, Figure 1.7) consists of a singlet carbene stabilised by a methoxy as heteroatom substituent, an alkyl or aryl substituent and a tungsten pentacarbonyl moiety. The carbene carbon is stabilised by both the oxygen heteroatom and even more so by metal π-back donation into the vacant $p_π$-orbital. The reports by Wanzlick and Öfele on the syntheses of diaminocarbenes followed a few years later, in 1968. Wanzlick and Öfele independently reported a dicationic mercury(II) bis(carbene)[11] complex (**7c**, Figure 1.7) and a diaminocarbene chromium(0)pentacarbonyl complex,[12] respectively (**7d**, Figure 1.7). Lappert, another pioneer in the field of carbene chemistry, also reported synthesis of a platinum carbene complex, three years after the publications by Wanzlick and Öfele.[13] Lappert synthesised a *trans*-platinum(II) carbene complex (**7e**, Figure 1.7) from an electron-rich olefin.[13] Another breakthrough in metal-carbene chemistry came in 1974, with the publication of Schrock on the synthesis and isolation of a tris(alkyl) tantalum(V) carbene complex (**7f**,

[9] A. Igau, H. Grutzmacher, A. Baceiredo, G. Bertrand, *J . Am. Chem. Soc.,* 1988, **110***,* 6463-6466.

[10] J. P. A. Dumas, E. M. Peligot, *Ann. Chim. Phys.*, 1835, **58**, 5 – 74.

[11] H. W. Wanzlick, H. J. Schönherr, *Angew. Chem. Int. Ed. Engl.*, 1968, **7**, 141 – 142.

[12] K. Öfele, *J. Organomet. Chem.*, 1968, **12**, 42 – 43.

[13] D. J. Cardin, B. Cetinkaya, M. F. Lappert, Lj. Manojlović-Muir, K. W. Muir, *Chem. Commun.*, 1971, 400 – 401.

5

Figure 1.7).[14] Unlike the Fischer carbene **7ᵦ** and diaminocarbenes **7c** to **7ₑ**, the Schrock carbene has a triplet ground state.
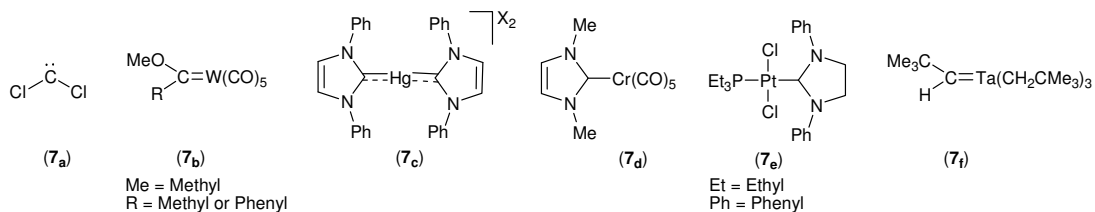
Figure 1.7: Early metal-carbene complexes

Finally, the synthesis and isolation of the first free carbene was reported by Bertrand in 1988.[9] The (phosphino)(silyl)carbene was characterised by NMR analysis in 1988, and in the year 2000 the structure was unambiguously assigned by single crystal X-ray diffraction (**8ₐ**, Figure 1.8).[15] Three years later, in 1991, Arduengo *et al*. reported the synthesis and crystal structure of 1,3-di-1-adamantylimidazol-2-ylidene, the first free crystalline *N*-Heterocyclic carbene (**8ᵦ**, Figure 1.8).[7] After the report by Arduengo in 1991, an exponential growth has been seen in the range of *N*-Heterocyclic carbene compounds.[16] Compound **8ᵦ** represents the classical *N*-Heterocyclic carbene (will be referred to as nNHC in this text), which has two nitrogen heteroatoms bonded to the carbene carbon. The carbene carbon occupies position 2 of the five-membered ring.
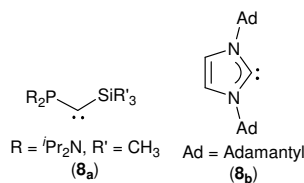
Figure 1.8: (phosphino)(silyl)carbene (**8ₐ**),[9] 1,3-di-1-adamantylimidazol-2-ylidene (**8ᵦ**)[7]

The first report of a 'mesoion-derived carbene' was published in 1993 by Araki and co-workers.[17] They reported a diaryl-tetrazolium salt, used as a ligand precursor in the synthesis of Hg and Pd complexes (Figure 1.9). Mercuration of the precursor tetrazolium salt with $Hg(OAc)_2$ yielded complex **9ₐ**, while oxidative addition of the 5-chloroazolium salt with $Pd(PPh_3)_4$ yielded complex **9ᵦ**.

---

[14] R. R. Schrock, *J. Am. Chem. Soc.*, 1974, **96**, 6796.

[15] T. Kato, H. Gornitzka, A. Baceiredo, A. Savin, G. Bertrand, *J. Am. Chem. Soc.*, 2000, **122**, 998 – 999.

[16] R. Corberán, E. Mas-Marzá, E. Peris, *Eur. J. Inorg. Chem.* 2009, 1700–1716.

[17] S. Araki, Y. Wanibe, F. Uno, A. Morikawa, K. Yamamoto, K. Chiba, Y. Butsugan, *Chem. Ber.*, 1993, **12**, 1149 – 1155.
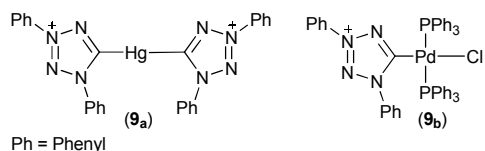
Figure 1.9: Hg (**9_a**) and Pd (**9_b**) aNHC complexes reported by Araki[17]

In 2001, Crabtree and co-workers reported the serendipitous discovery of an abnormal *N*-Heterocyclic carbene (aNHC) complex, where bond formation occurred at a remote position and not at the unsubstituted C-2 carbon.[18] They reacted 2-pyridylmethylimidazolium salt with $IrH_5(PPh_3)_2$ yielding the aNHC complex, as well as the NHC complex (Scheme 1.1). The reaction yielded mixtures of the nNHC and aNHC complexes when R = Me and $X^- = BF_4^-$. The formation of the imidazol-4-ylidene complex (aNHC) was favoured when bulky R-groups were used, when the proton transfer mechanism was avoided and when THF was used as the solvent of the reaction. By changing the R-groups to sterically less-hindered substituents and the solvent to CH_2Cl_2, the formation of the nNHC was favoured. Calculations showed that the free aNHC lies *ca*. 20 kcal/mol higher in energy than the free nNHC. This suggests that the aNHC would bind more strongly to the iridium metal than the corresponding nNHC.
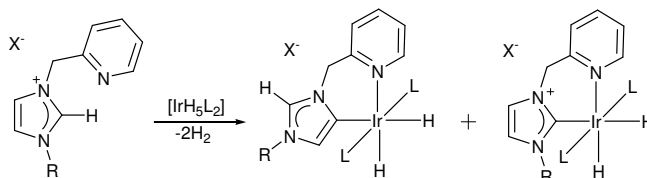
Scheme 1.1: [Ir(aNHC)L_2H_2] and [Ir(nNHC)L_2H_2] complexes reported by Crabtree[18]

In 2009 Bertrand and co-workers reported the first crystalline imidazole-based free aNHC.[19] Deprotonation at C-5 was achieved with potassium hexamethyldisilazide as base, after blocking the C-2 position with a phenyl substituent and with substituents present on N-1, N-3 and C-4 positions (Scheme 1.2). The successful synthesis of the crystalline imidazole-based free aNHC was unambiguously confirmed by XRD and NMR analysis. The very bulky 2,6-diisopropylphenyl substituents at N-1 and N-3 increased steric protection around the carbene carbon.

[18] S. Gründemann, A. Kovacevic, M. Albrecht, J. W. Faller, R. H. Crabtree, *Chem. Commun.*, 2001, 2274 – 2275.
[19] E. Aldeco-Perez, A. J. Rosenthal, B. Donnadieu, P. Parameswaran, G. Frenking, G. Bertrand, *Science*, 2009, **326**, 556 – 559.

7
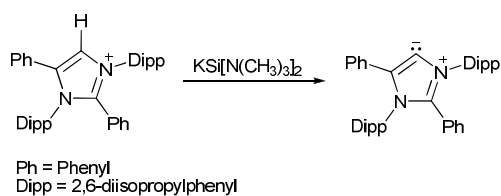
Scheme 1.2: Free crystalline aNHC reported by Bertrand and co-workers in 2009[19]

The synthesis of a second class of aNHC, namely 1,2,3-triazolylidenes and their use as ligands for metal complexes, was first reported in 2008 by Albrecht and co-workers (Figure 1.10).[20] The five-membered ring is substituted with three nitrogen heteroatoms, instead of the conventional two heteroatom-substituted five-membered ring. However, there is still only one heteroatom adjacent to the carbene carbon.
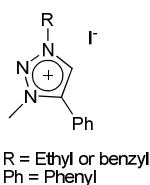
Figure 1.10: First triazolylidene synthesised by Albrecht and co-workers[20]

Bertrand and colleagues were again able to synthesise and isolate crystalline free aNHCs in 2010 and 2011 (Figure 1.11); this time triazole-based. In 2010 the 1H-1,2,3-triazol-5-ylidene precursor salt was reacted with potassium bis(trimethylsilyl)amide to deprotonate the triazolium C-H which yielded the free carbene (**11$_{a-b}$**, Figure 1.11).[21] The synthesis of the bis(1,2,3-triazol-5-ylidene) free aNHC or *i*bitz ligand (**11$_c$**, Figure 1.11),[22] as well as the 1,3-diaryl-1H-1,2,3,-triazol-5-ylidene (**11$_d$**, Figure 1.11)[23] was reported in 2011. In all three cases, crystal structures of the new aNHCs could be obtained.
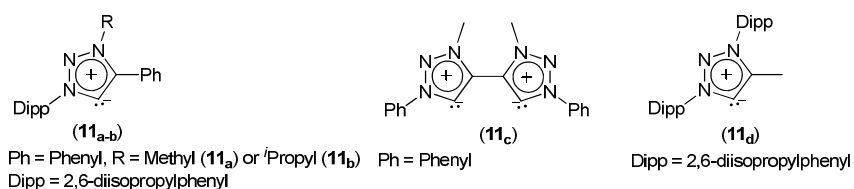
Figure 1.11: Free crystalline aNHC synthesised by Bertrand and colleagues in 2010 (**11$_a$**-**11$_b$**) and 2011 (**11$_c$** and **1$_d$**)

[20] P. Mathew, A. Neels, M. Albrecht, *J. Am. Chem. Soc.*, 2008, **130**, 13534 – 13535.

[21] G. Guisado-Barrios, J. Bouffard, B. Donnadieu, G. Bertrand, *Angew. Chem. Int. Ed.*, 2010, **49**, 4759 – 4762.

[22] G. Guisado-Barrios, J. Bouffard, B. Donnadieu, G. Bertrand, *Organometallics*, 2011, **30**, 6017 – 6021.

[23] J. Bouffard, B. K. Keitz, R. Tonner, G. Guisado-Barrios, G. Frenking, R. H. Grubbs, G. Bertrand, *Organometallics*, 2011, **30**, 2617 – 2627.

8

1.2) Classical *N*-Heterocyclic Carbenes

1.2.1) Overview

N-Heterocyclic carbenes have been studied and used extensively as ligands in catalyst design.[24] The exponential growth was spurred by the discovery and report by Arduengo's free crystalline NHC carbene (see **8_b**, Figure 1.8).[7] The most commonly known NHC structure, based on Arduengo's NHC, is indicated in Figure 1.12. NHCs are bent singlet carbenes with a σ^2 ground state electron configuration (see **2_a**, Figure 1.2) and consist of a five-membered ring, with C-2 flanked by two nitrogen atoms at positions N-1 and N-3 (Figure 1.12). Positions 4 and 5 are usually occupied by sp^2-hybridised carbons, but numerous reports feature sp^3-hybridised carbons.[2] In general, deprotonation and metallation occurs at the C-2 carbon, yielding the carbene. The formed diaminocarbene results in a σ-pull π-push system. As stated above, the σ-electron withdrawing effect of the two nitrogen substituents stabilises the *σ*-orbital, while π-donation from the nitrogen lone pairs stabilises the vacant p_π-orbital. This synergic effect increases the σ-p_π gap, which in turn increases the singlet-triplet energy gap resulting in a dramatic increase in the stability of the carbene. The outcome is a stable carbene, and subsequently even more stable upon metallation of the carbene with a metal precursor to yield the corresponding M-NHC complex.

The stable M-NHC bond formation is a result of the high covalent contribution from the NHC ligand to the metal.[25] A robust M-NHC complex is formed that is more stable, in contrast to the kinetically labile dative bond formation between a neutral N- or P-donor ligand, and the metal complex. In addition, NHCs have access to wide steric bulk and their electronic properties can be fine tuned more readily, compared to their phosphine analogues.[26] The strong σ-donor ability of the NHC ligands is one of the main reasons for their wide use in catalysis. The increased electron density on the metal centre could allow for oxidative addition of a substrate onto a metal centre more readily, facilitating (initiating) catalysis.
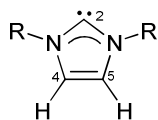
Figure 1.12: Classical *N*-Heterocyclic carbene

[24] O. Schuster, L. Yang, H. G. Raubenheimer, M. Albrecht, *Chem. Rev.,* 2009, **109**, 3445 – 3478.
[25] D. Canseco-Gonzalez, A. Petronilho, H. Mueller-Bunz, K. Ohmatsu, T. Ooi, M. Albrecht, *J. Am. Chem. Soc.*, 2013, **135**, 13193 – 13203.
[26] R. H. Crabtree, *Coord. Chem. Rev.*, 2013, **257**, 755 – 766.

M-NHC σ-bonding occurs through the NHC σ-orbital overlapping with the metal dz^2-orbital, with the carbene donating its lone pair of electrons into the metal dz^2-orbital (Figure 1.13).[27] In addition, π-orbital overlap occurs between the p_π-orbital and the d_{xz} and d_{yz} orbitals. Electron density in the π-system of the NHC is donated to the metal, and to a (much) lesser extent, backdonation from the metal to the NHC.

M to NHC pi''-backdonation

NHC to M pi-donation

NHC to M sigma-donation
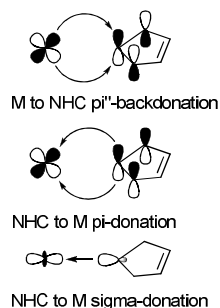
Figure 1.13: The three M-NHC bonding contributions[27]

1.2.2) Electronic Factors

Theoretical and experimental data suggest that electron delocalisation occurs throughout the five-membered ring.[28] The two lone pairs of electrons from the nitrogen p-orbitals overlapping with the p-orbitals of the C=C bond, as well as with the p_π-orbital result in six π-electrons being delocalised throughout the five-membered ring (Scheme 1.3).[29] Crystallographic analyses of nNHC carbenes indicate that the amino groups are always in a planar environment, and that the N-C bond lengths are quite short, indicating double bond character due to the lone pair(s) of electrons from the nitrogen(s) being donated into the p_π-orbital.[2] Double bond character is also supported by a large barrier to rotation around the N-C bond, which has been calculated for various cyclic diaminocarbenes.
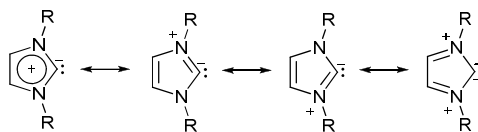
Scheme 1.3: Resonance structures of nNHC[29]

The electronic stability of the nNHC σ-orbital is further increased upon substitution of the hydrogens on positions C-4 and C-5 by a σ-electron withdrawing, π-donating group. Substitution of the

[27] H. Jacobsen, A. Correa, A. Poater, C. Costabile, L. Cavallo, *Coord. Chem. Rev.*, 2009, **253**, 687 – 703.
[28] S. Díez-González, S. P. Nolan, *Coord. Chem. Rev.*, 2007, **251**, 874 – 883.
[29] R. Sevinçek, H. Karabiyik, H. Karabiyik, *J. Mol. Model*, 2013, **19**, 5327 – 5341.

hydrogens on C-4 and C-5 with two Cl atoms allows for the isolation of an air stable crystalline free imidazol-2-ylidene, which was reported by Arduengo and co-workers (Scheme 1.4).[30] The high electronegativity of the Cl atom has a σ-electron withdrawing effect, resulting in stabilisation of the σ-lone pair. The basicity of the σ-lone pair is decreased to such an extent that the free Cl-substituted imidazole-2-ylidene is stable towards weakly acidic solvents such as $CHCl_3$, which is in stark contrast to the unsubstituted free imidazol-2-ylidene. The dichloroimidazol-2-ylidene is also stable towards air for a certain period of time.[30] The two Cl substituents can donate their lone pair of electrons into the π-system, increasing the aromaticity of the five-membered ring.

Mes = mesityl
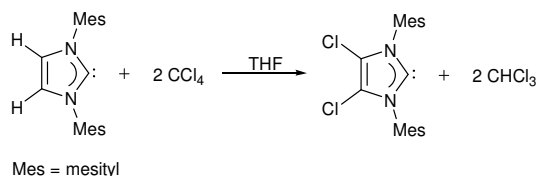
Scheme 1.4: Synthesis of 1,3-dimesityl-4,5-dichloroimidazole-2-ylidene[30]

1.2.3) Steric Factors

The steric stabilisation imparted by the bulky adamantyl substituents on N-1 and N-3, **together** with the electronic stabilisation, allowed for the isolation of Arduengo's crystalline free imidazol-2-ylidene.[7] Steric stabilisation by use of bulky wingtip groups substituted on the two nitrogen atoms impart extra stability to the nNHCs, however not as much as electronic effects do.[31] Indeed, it has been shown that unsaturated imidazol-2-ylidenes are more stable than their saturated imidazolin-2-ylidene analogues which readily dimerise into the corresponding dimer (**b-c**, Scheme 1.5).[32] This dimerisation occurs through the Wanzlick equilibrium due to the thermodynamic instability of the imidazolin-2-ylidenes. The lone pair of electrons located in the σ-orbital is donated into the vacant p_π-orbital of a second nNHC molecule, resulting in the formation of a stable double bond (**a**, Scheme 1.5).[2,31] The unsaturated imidazol-2-ylidenes are more stable due to the partial aromatic stabilisation and increased electron density in the five-membered ring. Bulky wingtip groups are not a necessity as in the case of the imidazolin-2-ylidene, however imidazol-2-ylidenes can still undergo dimerisation through the Wanzlick equilibrium pathway. Bulky alkyl substituents, either *tert*-butyl (*^{t}*Bu) or iso-

---

[30] A. J. Arduengo, F. Davidson, H. V. R. Dias, J. R. Goerlich, D. Khasnis, W. J. Marshall, T. K. Prakasha, *J. Am. Chem. Soc.*, 1997, **119**, 12742 – 12749.

[31] P. de Frémont, N. Marion, S. P. Nolan, *Coord. Chem. Rev.*, 2009, **253**, 862 – 892.

[32] *(a)* H. W. Wanzlick, E. Fjedo, K. H. Jerg, *Chem. Ber.*, 1963, **96**, 1208, *(b)* J. P. Malrieu, G. Trinquier, *J. Am. Chem. Soc.*, 1989, **111**, 5916, *(c)* H. Jacobsen, T. Ziegler, *J. Am. Chem. Soc.*, 1994, **116**, 3667, *(d)* A. J. Arduengo, *Acc. Chem. Res.*, 1999, **32**, 913.

propyl (^{i}Pr) groups; or aromatic substituents, either phenyl (Ph) or 2,4,6-trimethylphenyl (Mes), on the two nitrogen atoms hamper dimerisation through steric repulsion of the wingtip groups.
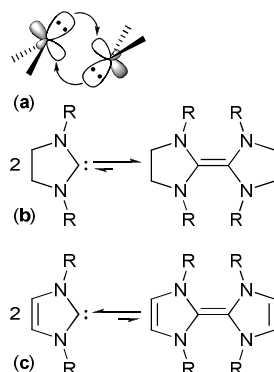
Scheme 1.5: Mechanism (**a**) of dimerisation for (**b**) imidazolin-2-ylidene and (**c**) imidazol-2-ylidenes

1.3) Abnormal *N*-Heterocyclic Carbenes

1.3.1) Overview

Abnormal *N*-Heterocyclic carbenes (aNHC) have only recently received interest since the serendipitous discovery in 2001 by Crabtree and co-workers,[18] although the first example of an aNHC was already reported by Araki in 1993.[17] All resonance forms of these carbenes cannot be drawn without introduction of a charge, hence this class of compounds are referred to as mesoionic carbenes (MIC) in addition to the classification of aNHC.[26] aNHCs consist of a five-membered ring with the carbene carbon flanked by one nitrogen atom, and not two as in the case of nNHCs (**14$_{b-e}$**, Figure 1.14). In addition, remote *N*-Heterocyclic carbenes (rNHC) refer to a carbene with nitrogen atoms in the *β* and/or *β'* positions, while carbon atoms occupy the *α* and *α'* positions flanking the carbene (**14$_f$**, Figure 1.14).[26] A direct result of the heteroatom position, and lack of a second heteroatom adjacent the carbene, is a decrease in stabilisation of the free carbene due to σ-pull/π-push effects, resulting in higher electron density located in the *σ*-orbital when compared to nNHC. Computational work, pK_a calculations, energy decomposition analysis and experimentally determined CO bond stretching frequencies all indicate the strong σ-donor ability of aNHCs.[24,26,33] The data obtained suggest that the donor gap between nNHC and aNHC is larger than the gap between nNHC and phosphines.[26] In some catalytic reactions, the aNHC has performed better than the nNHC analogue. This has been attributed, in several cases, to the increased donor ability of the aNHC which could allow for the metal centre to undergo oxidative addition much more readily.

---

[33] See review articles and reference therein: *a)* M. Albrecht, *Chem. Commun.*, 2008, 3601 – 3610, *b)* M. Melaimi, M. Soleilhavoup, G. Bertrand, *Angew. Chem. Int. Ed.*, 2010, **49**, 8810 – 8849.

Commonly known aNHCs include imidazol-4-ylidene (**14_b**, Figure 1.14), imidazol-5-ylidene (**14_c**, Figure 1.14), 1,2,3-triazolylidene (**14_d**, Figure 1.14), tetrazolylidene (**14_e**, Figure 1.14) and remote NHC (**14_e**, Figure 1.14).
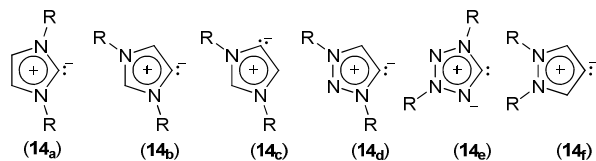
Figure 1.14: Representative examples of nNHC (**14_a**), aNHC (**14_{b-e}**) and rNHC (**14_f**) structures

In contrast to nNHCs, the free aNHC contains eight electrons in the valence shell of the carbene, but is still considered a free carbene.[26] The aNHC lacks a dimerisation pathway, in contrast to the Wanzlick equilibrium of classical carbenes. This should lead to relaxed steric requirements for their isolation (see Scheme 1.5 for Wanzlick dimerisation of nNHCs). Moreover, theoretical data suggest that derivatives of this type are even poorer π-acceptor ligands compared to nNHCs.[26] The poorer π-accepting ability of aNHCs can be attributed to their p_{π}-orbitals being almost fully occupied.[29] Instead of heteroatom electron lone pair donation into the p_{π}-orbital, a more accurate description would be heteroatom electron lone pair donation into the π-delocalised five-membered ring system. Indeed, the aromaticity of aNHCs is greater than that of nNHCs. The stronger donating ability of aNHCs is also due to the increased aromaticity of the five-membered ring. The higher the aromaticity of the imidazolylidene ligand, the higher the σ-donor ability of the ligand.[29] This opens interesting perspectives for their applications in organometallic catalysis.

For any NHC, the highest occupied molecular orbital (HOMO) describes the lone pair of electrons in the *σ*-orbital. A low-lying HOMO orbital has a decreased donating ability compared to energetically high-lying HOMO orbitals.[29] nNHCs have low-lying HOMO orbitals, while aNHCs have energetically high-lying HOMO orbitals. Therefore, increased donor ability of aNHCs is also due to the high energy associated with the HOMO orbitals.

In addition, aNHCs can be viewed as a vinyl or heteroarylium type complexes, which could also explain why they are stronger donors than nNHCs. Vinyls are intrinsically stronger donors than nNHCs, due to their anionic character.[34]

---

[34] A. Krüger, M. Albrecht, *Australian J. Chem.*, 2011, **64**, 1113 – 1117.

1.3.2) Imidazol-4-ylidene

Imidazol-4-ylidenes have two nitrogen heteroatoms at positions N-1 and N-3, two sp^2-hybridised C-2 and C-5 carbons that can either be substituted or unsubstituted, and the C-4 carbene carbon (**14$_b$**, Figure 1.14). The imidazol-4-ylidenes maintain an ensemble of interesting properties in addition to the properties of aNHCs already mentioned. Triazolylidenes have not yet received as wide-spread attention as paid to imidazol-4-ylidenes. For this reason, the imidazol-4-ylidenes will be discussed in more detail in order to compare the less explored triazolylidenes with the imidazol-4-ylidenes. The synthesis of imidazol-4-ylidenes will be discussed, followed by their electronic, steric and bonding properties.

1.3.2.1) Synthesis

Various methods have been employed in the synthesis of imidazolium salts as precursors to aNHCs.[26] By blocking the very acidic C-2 position in nNHC with a substituent, the aNHC can be synthesised. This method is commonly used in the synthesis of imidazolium aNHC where substituents are on N-1 and N-3, with the C-2 position blocked. The C-5 position is usually substituted, which leaves one proton in the five membered ring vulnerable towards deprotonation as well as metallation. Various metallation methods such as direct metallation,[18,35,36,37,38,39,40] oxidative addition,[41] transmetallation from the silver complex with an appropriate metal precursor,[38,42] or *in situ* deprotonation followed by metallation[43,44] have been employed in the synthesis of aNHC complexes of this type.

[35] A. R. Chianese, A. Kovacevic, B. M. Zeglis, J. W. Faller, R. H. Crabtree, *Organometallics*, 2004, **23**, 2461.

[36] *a)* M. Baya, B. Eguillor, M. A. Esteruelas, M. Loivan, E. Onate, *Organometallics*, 2007, **26**, 6556, *b)* B. Eguillor, M. A. Esteruelas, M. Olivan, M. Puerta, *Organometallics*, 2008, **27**, 445.

[37] M. Heckenroth, E. Kluser, A. Neels, M. Albrecht, *Angew. Chem. Int. Ed.*, 2007, **46**, 6293 – 6296.

[38] G. Song, Y. Zhang, X. Li, *Organometallics*, 2008, **27**, 1936.

[39] S. Gründemann, A. Kovacevic, M. Albrecht, J. W. Faller, R. H. Crabtree, *J. Am. Chem. Soc.*, 2002, **124**, 10473 – 10481.

[40] L. N. Appelhans, D. Zuccaccia, A. Kovacevic, A. R. Chianese, J. R. Miecznikowski, A. Macchioni, E. Clot, O. Eisenstein, R. H. Crabtree, *J. Am. Chem. Soc.*, 2005, **127**, 16299.

[41] *a)* D. Bacciu, K. J. Cavell, I. A. Fallis, L. L. Ooi, *Angew. Chem. Int. Ed.*, 2005, **44**, 5282, *b)* E. Kluser, A. Neels, M. Albrecht, *Chem. Commun.*, 2006, 4495, *c)* E. Stander-Grobler, O. Schuster, C. E. Strasser, M. Albrecht, S. Cronje, H. G. Raubenheimer, *Polyhedron*, 2011, **30**, 2776, *d)* A. Krüger, E. Kluser, H. Müller-Bunz, A. Neels, M. Albrecht, *Eur. J. Inorg. Chem.*, 2012, 1394.

[42] *a)* A. R. Chianese, A. Kovacevic, B. M. Zeglis, J. W. Faller, R. H. Crabtree, *Organometallics*, 2004, **23**, 2461, *b)* G. Song, Y. Zhang, X. Li, *Organometallics*, 2008, **27**, 1936.

[43] N. Stylianides, A. A. Danopoulos, N. Tsoureas, *J. Organomet. Chem.*, 2005, **690**, 5948.

[44] M. Alcarazo, S. J. Roseblade, A. R. Cowley, R. Fernandez, J. M. Brown, J. M. Lassaletta, *J. Am. Chem. Soc.*, 2005, **127**, 3290.

C-4 H-bond activation in imidazolium salts is worth noting. Theoretical and experimental calculations indicate that the acidity of the proton bonded to the C-2 position[45,46] ($pK_a = 24 \pm 1$) is nine pK_a units lower than the acidity of the proton attached to the C-4 position ($pK_a = 33$).[46] If the C-2 position is unprotected then it is expected that metallation will occur at the C-2 position due to the increased acidity of the C-2 bound proton.[46] However, it has been reported that both C-2 and C-4 bond formation occurs via two different pathways.[18] C-2 bonding occurs through C-H heterolytic bond cleavage, while C-4 bonding occurs via oxidative addition, as suggested by calculations (Scheme 1.6).[40] The calculation for two different reaction pathways was also supported by experimental data. The site of metallation is dependent on the counteranion and the size of the wingtip substituent used.[40] A large anion such as BF_4^- exhibits weak hydrogen bonding and small changes in charge distribution (Scheme 1.6). On the other hand, smaller anions such as Br^- exhibit stronger hydrogen bonding, which accelerates heterolytic C-H bond cleavage. The smaller anion interacts with the acidic C-2 proton, which supports proton migration from the imidazolium salt to the metal-bound hydride. The formation of the abnormally bound NHC-iridium complex through oxidative addition was supported by time dependant NMR analysis. The selectivity of metallation is also affected by the size of the wingtip groups. Small wingtip groups favour the formation of the C-2 bound metal complex, while bulky wingtip groups favour the C-4 bound metal complex.
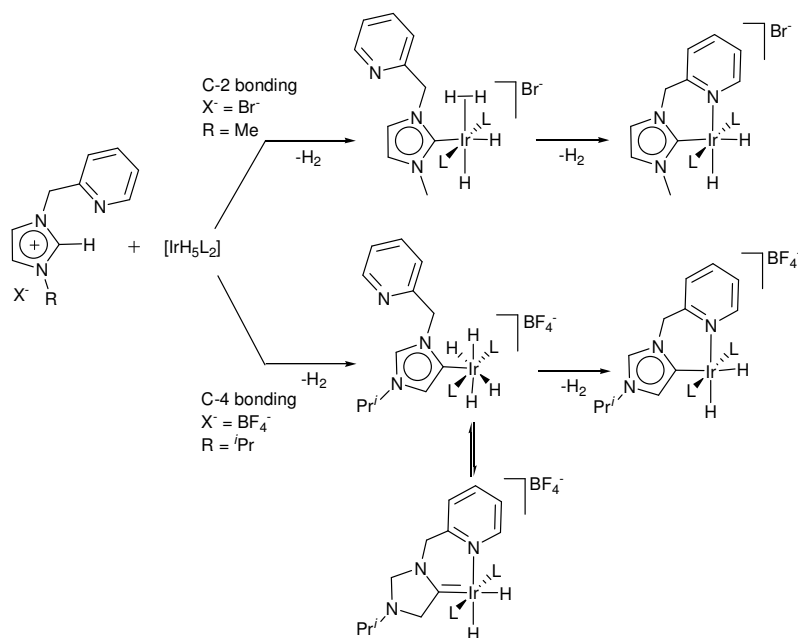
Scheme 1.6: C-2 and C-4 bond formation with Ir(III)[40]

[45] *a)* R. W. Alder, P. R Allen, S. J. Williams, *J. Chem. Soc., Chem. Commun.*, 1995, 1267, *b)* Y. J. Kim, A. J. Streitwieser, *J. Am. Chem. Soc.*, 2002, **124**, 5757, *c)* T. L. Amyes, S. T. Diver, J. P. Richard, F. M. Rivas, K. Toth, *J. Am. Chem. Soc.*, 2004, **126**, 4366.

[46] A. M. Magill, K. J. Cavell, B. F. Yates, *J. Am. Chem. Soc.*, 2004, **126**, 8717 – 8724.

1.3.2.2) Electronic Effects

Various methods used to assess the electronic properties all indicate that C-4 bound NHCs are stronger donors than C-2 bound NHCs.[24,26,33] XRD analysis indicates that the Pd-Cl bond length in complex **15a** is 2.404(4) Å, while the Pd-Cl bond length in complex **15b** is 2.357(2) Å (Figure 1.15). The longer bond length in **15a** is indicative of a larger *trans* influence due to the stronger donating effect of the aNHC ligand, compared to the nNHC ligand in **15b**.
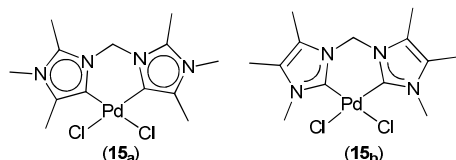
Figure 1.15: aNHC (**15a**) and nNHC (**15b**) PdCl$_2$ complexes

X-ray photoelectron spectroscopy (XPS) is another method used to evaluate the electronic effects of an abnormal versus normal bound imidazolylidene. XPS analysis demonstrates that the abnormally bound NHC Pd complex exhibits (**16a**, Figure 1.16) a positive 0.6 eV shift from the normally bound NHC Pd analogue complex (**16b**, Figure 1.16).[37] This considerably lower bonding energy of the 3*d* and 3*p* electrons is due to the stronger donor ability of the abnormally bound NHC.
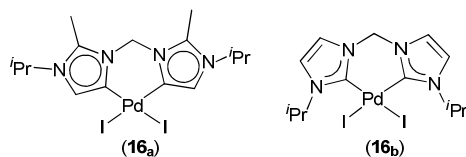
Figure 1.16: aNHC (**16a**) and nNHC (**16b**) PdI$_2$ complexes[37]

The Tolman Electronic Parameter (TEP) is another useful classification method for ligand donor strength, and is based on the CO stretching frequencies in a [M(L)(CO)] complex.[47] The average stretching frequencies for both C-4 and C-2 bound Ir and Rh complexes were measured. It was found that the CO stretching frequencies of C-4 bound carbenes are significantly lower than the ν(CO) of C-2 bound carbenes.[35,38,44,48] The lower stretching frequency is a result of the stronger donor ability of the C-4 bound ligand pushing electron density on to the metal centre, which in turn donates more electron density into the carbonyl carbon π*-orbital. The result is a decrease in the CO bond order, causing the decrease in the stretching frequency of the carbonyl ligand. In addition, from the data

[47] C. A. Tolman, *Chem Rev.*, 1977, **77**, 313 – 348.

[48] *a)* A. R. Chianese, X. Li, M. C. Janzen, J. W. Faller, R. H. Crabtree, *Organometallics*, 2003, **22**, 1663, *b)* R. A. Kelly, H. Clavier, S. Giudice, N. M. Scott, E. D. Stevens, J. Bordner, I. Samardjiev, C. D. Hoff, L. Cavallo, S. P. Nolan, *Organometallics*, 2008, **27**, 202 – 210.

16

obtained it was determined that the donor ability of C-4 bound carbenes is inductively tuneable over a broader range when compared to C-2 bound carbenes. Substitution of the hydrogen atom with more electron withdrawing functional groups results in a significant increase in the carbonyl stretching frequency (Figure 1.17). The inductive electron withdrawing substituents pull electron density out of the carbene carbon, which is positioned more than six atoms distant from the carbene carbon atom. Electron density is withdrawn from the electron rich carbene carbon, decreasing the donor ability of the C-4 bound imidazolylidene. This results in a decrease of electron density on the metal centre, in turn decreasing the extent of π-backbonding from the metal into the carbonyl carbon π*-orbital of the CO ligand. The CO ligand gains a higher bond order, which increases the stretching frequency of the CO ligand.

v_{av}(CO) = 1999cm^{-1}; R = H
v_{av}(CO) = 2008cm^{-1}; R = OCH$_3$
v_{av}(CO) = 2017cm^{-1}; R = CF$_3$
v_{av}(CO) = 2020cm^{-1}; R = F
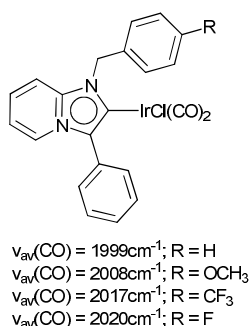
Figure 1.17: Inductive variation of the donor ability of C-4 bound NHC

Imidazol-4-ylidenes are more aromatic than imidazol-2-ylidenes (see Scheme 1.7). The enhanced *p*-electron character in the hybridisation of the carbene carbon increases π-delocalisation throughout the five-membered ring due to increased *p*-orbital overlap, which ultimately results in increased aromaticity.[29] Subsequently, the singlet-triplet energy gap decreases, in turn decreasing the stability of the aNHC. Indeed, the decreased stabilisation is supported by calculations which have indicated that imidazol-2-ylidenes are more stable than their imidazol-4-ylidene analogues.[29]

Scheme 1.7: Resonance structures of imidazol-4-ylidene[29]
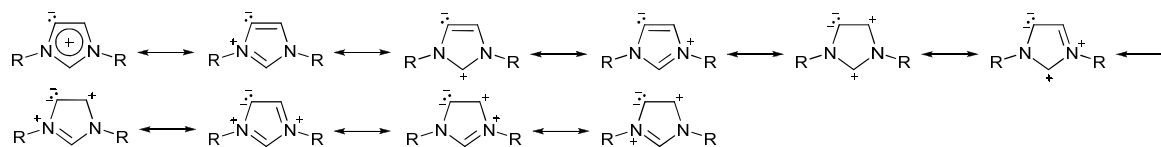
1.3.2.3) Steric Considerations

If the C-5 bound carbon is unsubstituted, the C-4 bound carbon is affected by the substituent bonded at the N-3 position. The substituent impinges into the coordination sphere of the metal

17

centre. Crystallographic analysis shows that the torsion angle between the abnormally bound N-heterocyclic biscarbene ligand (Figure 1.16) and the metal coordination plane is 20 – 30°,[37] while the torsion angle for the corresponding normally bound N-heterocyclic biscarbene complex is 35 – 45°.[49] The increased torsion angle in the nNHC complex is due to the second wingtip group in the α'-position, which twists the ligand out of the metal coordination plane by 35 – 45°. As a result, the smaller torsion angle in the C-4 bound NHC complex could allow for increased ligand to metal π-bonding, due to an increase in π-orbital overlap between the ligand and the metal. The absence of a second wingtip group in the α'-position of the C-4 bound carbene decreases the steric bulk around the metal centre, which increases the accessibility of the reagents and substrates towards the metal as well as increasing the sensitivity of the M-C bond, which in turn increases catalytic activity.

1.3.2.4) Bonding Considerations

The zwitterionic character of the C-4 bound carbene has a larger contribution to the overall binding mode in comparison with normally bound NHCs.[34] This can be deduced from the most relevant resonance forms of both aNHC and nNHC (Scheme 1.8).

Scheme 1.8: Resonance structures of metal bound nNHC and aNHC[34]
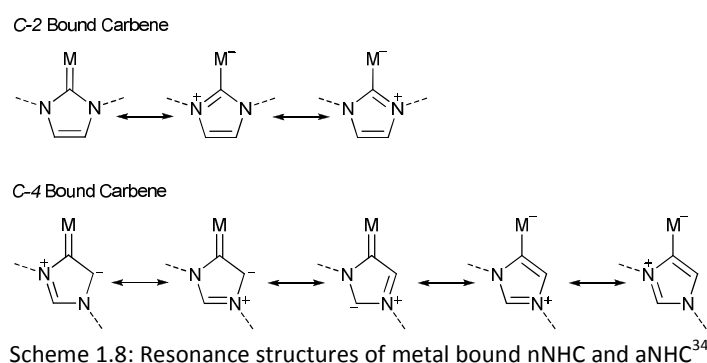
In some instances, unusual reactivity patterns have been noted which stem from the use of aNHCs. When a Rh complex bound to both an nNHC and aNHC was subjected to D_3PO_4, deuteration occurred at the C-5 position of the aNHC and not at the most acidic proton, which was at the C-2 position of the aNHC (Scheme 1.9). A possible mechanism, as indicated in Scheme 1.9, does not account for a simple electrophilic aromatic substitution, but rather a separation of the π-electron system in the aNHC ring which results in the formation of an olefinic C=C fragment and a cationic amidinium unit NCN^+.[34] The highly nucleophilic M-C=C unit reacts with D^+ through nucleophilic

---
[49] a) W. A. Herrmann, J. Schwarz, M. G. Gardiner, *Organometallics*, 1999, **18**, 4082, b) M. Heckenroth, A. Neels, H. Stoeckli-Evans, M. Albrecht, *Inorg. Chim. Acta*, 2006, **359**, 1929.

attack, either on the C-5 carbon or directly on the anionic metal centre. The cationic C-2 carbon is unreactive towards the electrophilic deuterium. The reactivity pattern could demonstrate that aNHCs can be used as more than just spectator ligands in catalysis, e.g. as co-catalyst or hydrogen donors and acceptors.
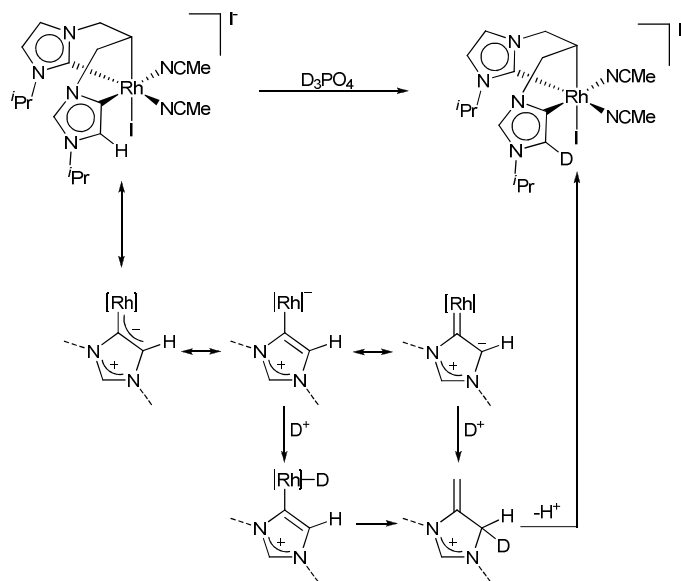
Scheme 1.9: Exclusive deuteration of the aNHC[34]

1.3.3) 1,2,3-Triazolylidenes

Triazolylidenes (abbreviated as *trz* in this paper), another subclass of nNHCs classified as aNHCs or MICs, have only recently received attention since their first report,[20] compared to the imidazol-4-ylidenes. Substitution of the C-2 carbon in imidazol-4-ylidenes with a nitrogen atom, yields the corresponding 1,2,3-triazol-4-ylidenes or 1,2,3-triazol-5-ylidenes. The substitution with a nitrogen atom changes the properties of the *trz*-ligand.[50] The nitrogen atom has an inductive σ-electron withdrawing effect, decreasing the electron density located in the carbene σ-orbital. This results in an increase in stability, as well as a slight decrease in donor ability when compared to the strongly donating imidazol-4-ylidenes. The *trz* is still however a stronger donor ligand than the classical imidazol-2-ylidenes and the basic diphosphine ligands. The electronic, steric and bonding properties of triazolylidenes will be discussed in this section, while the various synthetic procedures for preparation will be discussed in Chapter 2.

---

[50] K. F. Donnely, A. Petronilho, M. Albrecht, *Chem. Commun.*, 2013, **49**, 1145 – 1159.

1.3.3.1) Electronic Effects

The donor properties of *trz* were evaluated using similar methodologies as used for imidazol-4-ylidenes. The (*trz*)(allyl)palladium chloride[51] (**18$_a$**, Figure 1.18) and nNHC(allyl)palladium chloride[52] (**18$_b$**, Figure 1.18) complexes were prepared and their donor abilities compared. From the crystal structures, it was determined that the Pd-C(3) bond length for **18$_a$** is 2.212(3) Å, while the Pd-C(3) bond length for **18$_b$** is 2.183(5) Å. The considerably longer bond length in **18$_a$** is due to the stronger *trans* influence of the triazolylidene ligand compared to the nNHC ligand. The stronger *trans* influence is a result of the stronger donor ability of the *trz*-ligand, increasing the electron density on the metal centre, in turn resulting in a decrease in the Pd-C(3) bond strength, i.e. the bond length increases.

Ar = 2,4,6-trimethylphenyl
2,6-diisopropylphenyl

(**18$_a$**)   (**18$_b$**)
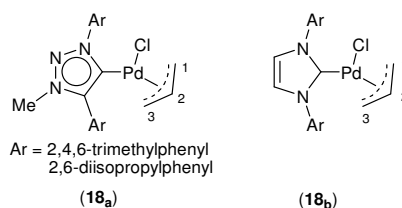
Figure 1.18: (η^3-allyl)(*trz*)PdCl (**18$_a$**)[51] and (η^3-allyl)(nNHC)PdCl complexes (**18$_b$**)[52]

XPS analysis was performed on the PdCl complexes **18$_a$** and **18$_b$** in Figure 1.18 to further investigate the donor strength of the *trz* versus the nNHC.[51] The Pd 3d electrons in complex **18$_b$** were found to have a binding energy of 336.2 eV, while the binding energy of the Pd 3d electrons in complex **18$_a$** is 335.7 eV. The 0.5 eV increase in binding energy of the *trz* complex **18$_a$** can be explained based on their stronger donor ability. XPS analysis revealed a large shift of 0.5 eV when the metal is bound to the triazolylidene ligand compared to the imidazol-2-ylidene ligand, but still not as large as the 0.6 eV shift brought about using the imidazol-4-ylidene ligand compared to the imidazol-2-ylidene ligand (**16$_a$**, Figure 1.16).

Measurement of the carbonyl stretching frequencies supports the stronger donor ability of triazolylidenes compared to nNHCs, as determined from XPS data analysis.[51] The (*trz*)(CO)$_2$IrCl complex exhibits a shorter carbonyl stretching frequency at v_{av}(CO) = 2019 cm^{-1}, compared to the (nNHC)(CO)$_2$IrCl complex (stated to be one of the most strongest donating imidazol-2-ylidene ligands)[50] with a carbonyl stretching frequency of v_{av}(CO) = 2024 cm^{-1} (Figure 1.19). The lower stretching frequency of **19$_a$** is a result of a decrease in the CO bond order. This is a direct result of the

[51] T. Terashima, S. Inomata, K. Ogata, S. Fukuzawa, *Eur. J. Inorg. Chem.*, 2012, 1387 – 1393.
[52] M. S. Viciu, O. Navarro, R. F. Germaneau, R. A. Kelly III, W. Sommer, N. Marion, E. D. Stevens, L. Cavallo, S. P. Nolan, *Organometallics*, 2004, **23**, 1629 – 1635.

stronger donor ability of the *trz* ligand, increasing the electron density on the metal centre; in turn the metal donates more electron density into the CO π^*-orbital.

v_{av}(CO) = 2019 cm^{-1}; Ar = 2,4,6-trimethylphenyl v_{av}(CO) = 2023 cm^{-1}; Ar = 2,4,6-trimethylphenyl
v_{av}(CO) = 2019 cm^{-1}; Ar = 2,6-diisopropylphenyl v_{av}(CO) = 2024 cm^{-1}; Ar = 2,6-diisopropylphenyl
(**19$_a$**)   (**19$_b$**)
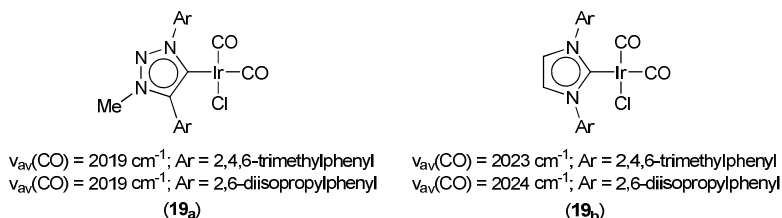
Figure 1.19: Stretching frequencies measured for the (*trz*)(CO)$_2$IrCl (**19$_a$**) and (nNHC)(CO)$_2$IrCl (**19$_b$**) complexes

From the crystal structures of the free *trz*-ligands (Figure 1.11), it could be deduced that the ligands are aromatic.[21-23] All the bond lengths have bond orders of between one and two, as observed in all three crystal structures. In addition, the heterocycles are also planar. Both characteristics are indicative of a π-delocalised system with a resonance hybrid throughout the five-membered ring, supporting the concept of aromaticity in the *trz* ligand. Calculations were performed on the free *trz* ligand (**11$_d$**, Figure 1.11).[23] The calculations indicated that the five-membered heterocycle has sizeable aromatic character, comparable to other five-membered heterocycles such as pyrrole, thiophene and 1,2-pyrazol-4-ylidenes.

In addition, the C4-C5-N1 bond angles in all three cases (Figure 1.11) are more acute compared to the triazolium salt. The decrease in the bond angle is consistent with an increase in s-character of the *σ*-orbital.[21-23] A higher s-character in the *σ*-orbital could allow for the increased stabilisation of the σ-lone pair of electrons. This in turn could explain the weaker donor ability compared to imidazol-4-ylidenes. The higher the energy of the *σ*-orbital, the stronger the σ-donation into the metal centre upon metallation.[29] The increased s-character increases the stability and decreases the energy of the *σ*-orbital.

The crystal structures of the complexes indicated in Figure 1.20 were obtained and analysed in order to gain more insight into the extent of aromaticity of the *trz* ligand.[25,53] The bond distance in the *trz* five-membered ring were measured and again averaged between that of a single and double bond for both complexes. In addition, the torsion angles of the *trz*-metal complexes were measured. The torsion angles of the complexes indicated in Figure 1.20 have values ranging from zero to one degree; therefore the *trz* ligands retain their planarity upon metallation. Both factors again support the possibility of an aromatic system with π-delocalisation throughout the five-membered ring.

---

[53] D. Canseco-Gonzalez, M. Albrecht, *Dalton Trans.*, 2013, **42**, 7424 – 7432.
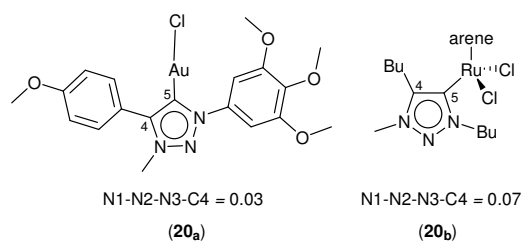
Figure 1.20: Torsion angle (N1-N2-N3-C4) of *trz*AuCl (**20$_a$**) and *trz*(arene)RuCl$_2$ (**20$_b$**) complexes

1.3.3.2) Steric Effects

As noted previously, dimerisation of aNHCs through the Wanzlick equilibrium pathway is unfavoured due to the filled p_π-orbital and aromatic character of the five-membered heterocycle, which leads to relaxed steric requirements for their isolation. Therefore, bulky substituents are not required as in the case of nNHC, however the choice of wingtip substituent is still very important due to the steric, and more importantly, electronic effects it has on the ligand and its donor ability. Albrecht and co-workers performed a detailed study of the effects of various substituents on the *trz*-metal complex.[54] Alkyl to aromatic groups were substituted on the Pd and Rh complexes (Figure 1.21). It was determined that aromatic wingtip groups deshield the carbene through a inductive σ-electron withdrawing effect, while alkyl wingtip substituents shield the carbene by increasing the electron density at the carbene carbon through an inductive σ-electron donating effect. The extent of shielding and deshielding effects of the wingtip groups was determined by NMR analysis and bond length determination. In both complexes, a general trend can be observed. The ^{13}C NMR spectra indicate that alkyl substituents induce an upfield shift of the carbene carbon, while aromatic substituents induce a downfield shift. The electronic trend observed through NMR analysis is supported by the XRD analysis. The Pd-I bond length is slightly shorter for phenyl substituted triazolylidene, compared to alkyl substituted triazolylidene. This indicates a larger *trans* influence resulting from the use alkyl versus aromatic substituents. Both observations point towards the trend of electron donating and electron withdrawing effects by choice of wingtip substituent.

Alkyl substituents decrease steric protection around the metal centre, which increases accessibility of incoming reagents or substrates towards the metal/catalyst, as well as electron density at the metal centre through its donating effect. Both factors could contribute towards a much more active catalyst. In contrast, aromatic substituents increase steric bulk and thus steric protection around the metal/catalyst, while decreasing electron density at the metal centre through σ-electron withdrawing effects. Both factors could contribute towards a more inactive catalyst. However, if the

---

[54] A. Poulain, D. Canseco-Gonzalez, R. Hynes-Roche, H. Müller-Bunz, O. Schuster, H. Stoeckli-Evans, A. Neels, M. Albrecht, *Organometallics*, 2011, **30**, 1021 – 1029.

22

aim is to stabilise very reactive compounds, the use of bulky aromatic substituents is desirable in order to increase steric protection around the metal centre.[21] The use of a bulky phenyl wingtip substituent resulted in the formation of a metallacycle, a special case which is discussed in Section 1.4.2.2.[54]
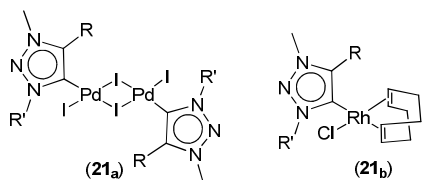
i) R = Ph and R' = Et
ii) R = Et and R' = Et
iii) R = Bu and R' = Bu
iv) R = Ph and R' = Bu
v) R = Bu and R' = Ph
vi) R = Ph and R' = Ph

Figure 1.21: Variation of wingtip groups in dinuclear PdI$_2$*trz*(NHC) complex (**21$_a$**) and *trz*(NHC)(COD)RhCl (**21$_b$**)

1.3.3.3) Bonding Considerations

Crystal structure analysis was performed and various conclusions made about the characteristics of triazolylidenes after metallation.[50] The N2-N3 bond length and the N3-C4 bond length of the triazolylidene remain constant after metallation of the triazolium salt. The C5-N1 and N1-N2 bonds length are slightly elongated after metallation. The most significant change upon metallation is the increase in the C4-C5 bond length, as well as the N1-C4-C5 bond angle which decreases (Scheme 1.10).[50] This could indicate a strong electrostatic contribution of the triazolylidene ligand, with a slight π-contribution.
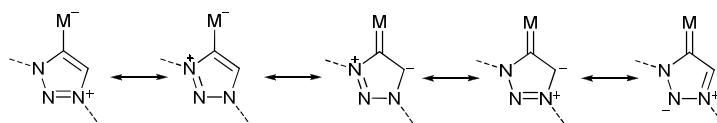
Scheme 1.10: Resonance structures of metallated *trz* ligand[50]

23

1.4) Mono-, Bi- and Tridentate Ligands

1.4.1) Monodentate Ligands

1.4.1.1) Monodentate nNHC Ligands

Some few examples of monodentate carbene ligands include nNHCs, widely used in catalysis for example, the Grubbs alkene metathesis catalyst (Figure 1.22).[55] The ligand consists of one coordination site which is used to coordinate to the metal precursor, a backbone responsible for the electronic properties of the ligand and in most instances, substituents imparting steric stabilisation in order to increase the stability of the formed ligand-metal complex. Variation of the electronic properties of the ligand is readily achieved by varying the nNHC backbone, in this case substitution of the hydrogens on the C-4 and C-5 carbon positions with electron donating or withdrawing substituents. The Ru metal contains a vacant site, which decreases the stability of the complex but increases the reactivity, in turn favouring a higher catalytic output.
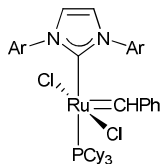
Figure 1.22: Grubbs alkene metathesis catalyst[55]

1.4.1.2) Monodentate *trz* Ligands

A monodentate *trz* ligand, like the nNHC monodentate ligand, coordinates to the metal through either the C-4 or C-5 carbene carbon. Some few examples of monodentate *trz* ligands and their corresponding metal complexes after metallation have been reported in literature.[50] These ligands can, just like the nNHC monodentate ligands, provide steric stabilisation towards the metal by appropriate choice of wingtip substituent, but the stability imparted is not nearly as much as the stabilising effect gained by using tridentate and even bidentate ligands. However, the decreased steric protection compared to bi- and tridentate ligands, allows for easier access of an incoming substrate or reagent towards the metal centre. Therefore, monodentate *trz* ligands could allow for increased catalytic activity of the synthesised catalyst, compared to bi- and tridentate ligands due to the metal coordination sites that are unprotected and easily accessible. In addition, their increased σ-donor ability increases electron density on the metal centre, which again should allow for increased catalytic activity compared to monodentate nNHC and phospine type ligands. Complexes

---

[55] R. H. Crabtree, *J. Organomet. Chem.*, 2005, **690**, 5451 – 5457 and references therein.

18$_a$, **19$_a$** and **20** (Figures 1.18, 1.19 and 1.20) are good representative examples of monodentate *trz* ligand-metal complexes.

1.4.2) Bidentate Ligands

1.4.2.1) Bidentate nNHC Ligands

Chelating bidentate ligands have found a prominent position in organometallic chemistry, especially in ligand design directed towards their use in catalysis. Formation of the metal chelated product improves the stability of the formed metal complex compared to monodenate ligand-metal complexes.[56] The improved stability is a direct result of one ligand coordinating to the metal at two different coordination positions. This decreases the tendency of the ligand to undergo dissociation or fragmentation. The ligand properties such as donor strength, steric hindrance, chirality and bite angle can be readily fine tuned to yield the desired ligand-metal complex/catalyst, with specific properties tailored for the specific catalytic reaction envisaged. A drawback during the synthesis of the chelated ligand-metal complex is the possible formation of a dinuclear bridged complex upon metallation where the ligand does not chelate around the metal, but coordinates to two metals forming the dinuclear bridged species (Scheme 1.11). The dinuclear bridged complex formation is an undesirable by-product in some cases, but the directed synthesis and use of the dinuclear bridged complex has been reported.[56] Various studies have been performed in order to determine the reaction conditions and ligand properties needed to favour either chelation or dinuclear bridged complex formation.
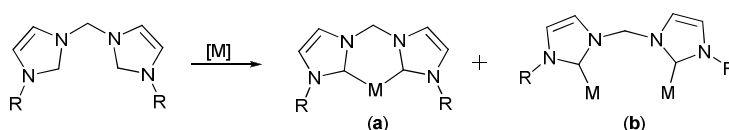
Scheme 1.11: Metallation of bidentate ligand yielding the (**a**) chelated ligand-metal complex and the (**b**) dinuclear bridged complex[56]

Chelating ligands have restricted rotation around the M-C bond. This results in the ligand axis being forced closer to the sterically crowded complex plane, but it is dependent on the length of the linker used (Figure 1.23).[56] Long linkers allow the five-membered ring to align in the sterically less crowded *z*-plane, while short linkers force the ring to occupy the sterically crowded *xy*-plane. Steric

---

[56] For relevant nNHC reviews and references therein see *a)* M. Poyatos, J. A Mata, E. Peris, *Chem. Rev.*, 2009, **109**, 3677 − 3707, *b)* R. Corberán, E. Mas-Marzá, E. Peris, *Eur. J. Inorg. Chem.*, 2009, 1700 − 1716, *c)* J. A. Mata, M. Poyatos, E. Peris, *Coord. Chem. Rev.*, 2007, **251**, 841 − 859.

considerations also play a pivotal role in the formation of the chelated or the dinuclear bridged complex. With a long linker between the two coordinating moieties and if bulky wingtip substituents are used, dinuclear bridged complex formation is favoured over chelation. This is a direct result of the bulky substituents experiencing steric clashes with each other (the ligand chelates around the metal, bringing the wingtip groups into close proximity of each other) and with the co-ligands substituted on the metal. However, the extent of steric repulsion can be decreased by using smaller wingtip substituents while still retaining the long linkers, which favours the formation of the chelated complex. As stated above, short linkers force the ligand to occupy the *xy*-plane. The bulky ligands and metal co-ligands are not forced close together, therefore experiencing less steric repulsion.[56] However, use of short linkers can still lead to the formation of bridged complexes where the ligand occupies the less sterically crowded *z*-plane.

In addition to the steric consideration, chelation or bridged dinuclear complex formation is also affected by the oxidation state of the metal, as well as the presence of halides in the reaction.[56] If the metal is in a higher oxidation state, formation of the mononuclear chelated biscarbene complex is favoured. The absence of halides in the reaction also favours the formation of the chelated complexes.

The electronic properties of the ligand can be fine tuned through substitution of the hydrogens on the C-4 and C-5 position of the azole rings, with either electron withdrawing or electron donating functional groups.[56] The wingtip groups can also affect the electronic properties of the ligand, but to a much smaller extent.

R1 = linker
R2 = wingtips
R3 = backbone
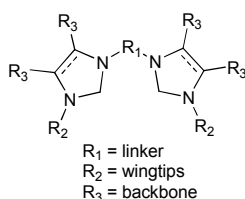
Figure 1.23: A representative bidentate nNHC ligand[56]

1.4.2.2) Bidentate *trz* Ligands

Bidentate *trz* ligands have been less explored than monodentate *trz* ligands.[26] However, due to the similarities between a bidentate nNHC and a bidentate *trz* ligand, predictions on whether or not a bidenate *trz* ligand will chelate or form a dinuclear bridged complex can be made. Similarly, the increased stability imparted towards a reactive metal centre when chelated by a bidentate nNHC ligand also holds for a bidentate *trz* chelating ligand. The only difference between a bidentate *trz*

26

ligand and a bidentate nNHC ligand is the substitution of the five-membered diamino-heterocyclic nNHC moiety with a five-membered 1,2,3,-triazolylidene moiety. The *trz* bidentate ligand is a stronger donor ligand compared to the nNHC bidentate ligand, as discussed above, but still retains the ability to chelate around the metal and yield a more stable complex when compared to a monodenate *trz* ligand-metal complex.

The free crystalline bidentate bis(1,2,3-triazol-5-ylidene), or *i*bitz ligand, was successfully synthesised by the group of Bertrand (**11c**, Figure 1.11).[22] The *i*bitz ligand was reacted with a weak base and a Rh metal precursor to yield the chelating bidentate bis-MIC Rh(I) COD (COD = 1,5-cyclooctadiene) complex, which was subsequently treated with carbon monoxide to yield the corresponding Rh(I) carbonyl complex (Scheme 1.12).
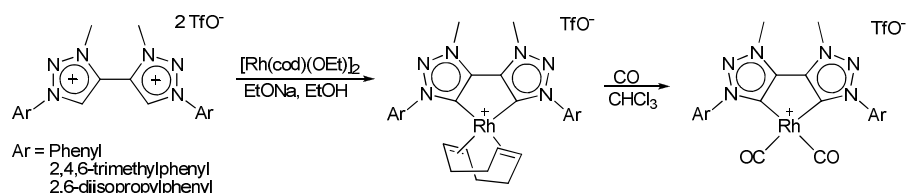
Scheme 1.12: Synthesis of mononuclear [Rh] bisMIC complex by Bertrand and co-workers[22]

The bis(*trz*)ligand salt (**a**, Scheme 1.13) was synthesised and metallated with Ag_2O, to yield the corresponding *trz*-Ag(I) complex (**b**, Scheme 1.13).[57] The silver complex was subsequently transmetallated with $[RuCl_2(p\text{-cymene})]_2$, which yielded the dinuclear chelated bis-*trz* ligand-metal complex (**c**, Scheme 1.13). The C-5 carbene carbon coordinates to the metal as an L-type ligand,[58] while the nitrogen of the pyrrole coordinates as an X-type ligand,[58] resulting in the formation of a five-membered metallacycle. The one bidentate Ru(II) moiety twists away from the other, in order to decrease the steric repulsion between the metal co-ligands.[57] It is predicted that the bidentate ligand occupies the metal *xy*-plane, due to the short linker length. As stated above, bidentate chelated metal complexes where the ligand occupies the *xy*-plane could have improved catalytic activity when compared to chelated metal complexes where the bidenate ligand occupies the *z*-plane. Indeed, complex **a** (Scheme 1.13) was reported to be active as a ring opening metathesis polymerisation catalyst.

[57] J. Cai, X. Yang, K. Arumugam, C. W. Bielawski, J. L. Sessler, *Organometallics*, 2011, **30**, 5033 – 5037.
[58] M.L.H Green, *J. Organomet. Chem.*, 1995, **500**, 127 – 148.
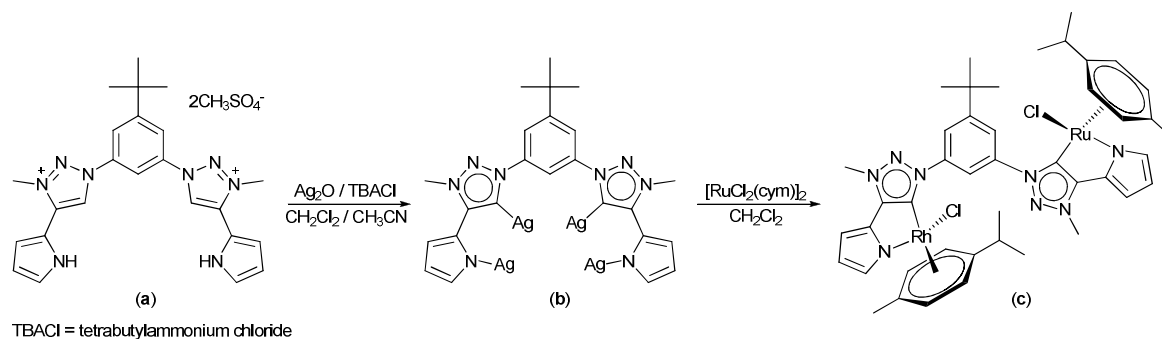
Scheme 1.13: Bidentate 1,2,3-triazol-5-ylidene Ru(II) complex[57]

In some instances, the use of phenyl wingtip substituents resulted in selective aromatic C-H bond activation, which yielded the chelated metallacycle complex containing a *trz* moiety. Figure 1.24 represents examples of *trz* containing bidentate ligands chelated around the metal centre.[54,59] Cyclisation is believed to occur by an electrophilic mechanism.[60] The π-electron releasing character of the nitrogen supports aryl functionalisation by stabilising the intermediate carbocation. Metallacycle formation in all three examples is reversible which could indicate a less stable chelated complex formed, but the number of possible applications for such complexes increases due to the ease with which bond making and bond breaking processes occur.[54,59]
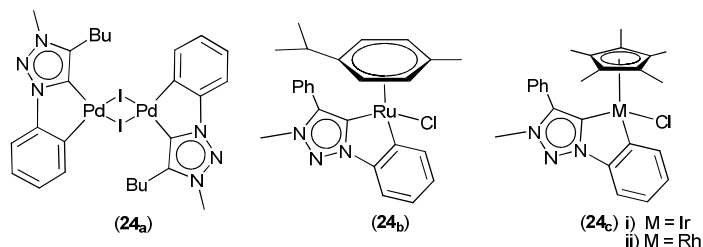
Figure 1.24: Representative examples of bidentate ligands chelated around a metal centre

1.4.3) Tridentate Ligands

As heuristically expected, the stability imparted by using tridentate ligands towards the synthesis of ligand-metal complexes and catalysts surpasses that of bidentate and monodentate ligands (in this thesis, tridentate ligands refers to ligands that form pincer complexes upon metallation, unless stated otherwise).[61] The increased stabilisation can be attributed to the sheltered environment of

---

[59] K. F. Donnelly, R. Lalrempuia, H. Müller-Bunz, M. Albrecht, *Organometallics*, 2012, **31**, 8414 – 8419.

[60] M. Albrecht, *Chem. Rev.*, 2010, **110**, 576 – 623.

[61] M. Albrecht, M. M. Lindner, *Dalton Trans.*, 2011, **40**, 8733 – 8744.

the metal in the 'pocket' of the pincer ligand. In most cases, the formed pincer ligand-metal complex is stable towards temperature degradation and ligand fragmentation.

The chemistry of pincer complexes have been extensively studied, especially the ligand system with a central carbon and two flanking phosphine groups coordinating to the metal. Various ligand systems have been synthesised, including incorporation of either an aromatic or aliphatic backbone, weak or strong central coordinating moieties and variation of the flanking groups through substitution with, for example, either P-, S-, N- or O-donor ligands. A general overview of the properties of pincer ligands will be discussed, followed by the discussion of a few examples of tridentate ligands containing nNHC moieties. Finally, the less explored *trz* pincer ligand system will be discussed.

1.4.3.1) Overview

Figure 1.25 represents the general structure of a metallated tridenate ligand coordinated to the metal in a meridonial configuration, with an aromatic backbone.[62] As depicted in Figure 1.25, different positions on the bulky tridentate ligand can be varied, in order to obtain a ligand system designed for a specific application. Electronic properties of the ligand can be remotely controlled through substitution of Z with other functionalities. Donor substituents will push or donate electron density into the ligand, which subsequently increases the electron density on the metal centre after metallation of the ligand. In contrast, substitution of Z with electron withdrawing substituents, decreases the electron density on the metal centre after metallation of the ligand. Steric consideration at Z is negligible, therefore substituents of various sizes are tolerated at that position.

The ligand electronic properties can be directly tailored by substitution of X with electron donating or withdrawing substituents.[62] This has a profound effect on the electron density at the metal centre, as well as directly influencing the *trans* effect of the ligand. Neutral two electron donor substituents coordinate as an L-type ligand[58] to the metal through dative covalent bond formation. These bonds are generally weak, and bond dissociation/association is commonly observed. In contrast, ionic substituents such as anionic nitrogen donors coordinate to the metal as X-type ligands.[58] X-M bond dissociation/association is not observed due to the stronger bond formed when compared to neutral donors. In addition, electron withdrawing and donating X substituents can either decrease or increase electron density at the metal centre. Substitution of X with a P- or S-

---

[62] J. Choi, A. H. Roy MacArthur, M. Brookhart, A. S. Goldman, *Chem. Rev.*, 2011, **111**, 1761 – 1779.

ligand allows for M→X π-backbonding whilst still donating electron density towards the metal through inductive effects. Donor ligands such as N or O are stronger π-donors.[62]
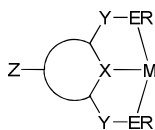
Z   = Control of electron density at
       remote position
X   = Direct electronic effects
Y   = Control of electron density and
       indirect control on steric properties
ER = Control of electron density and
       direct control of steric properties

Figure 1.25: Metallated tridentate ligand

Steric properties can be indirectly controlled by substitution of Y with other functionalities. In most cases, either one or two atom linkers are substituted at position Y.[63] Metallation of the ligand with a one atom linker at position Y is accompanied by the formation of two stable, five-membered metallacycles that are fused at the M-X bond. If the linker at Y has two atoms, formation of two six-membered metallacycles that are fused at the M-X bond results after metallation.[63] The formation of the six-membered metallacycle could decrease the distance between the R-groups substituted on E, which would result in a more sterically protected environment around the metal centre, but could also lead to steric clashes between the two R-groups. In contrast, five-membered metallacycle formation could increase the distance between the two R-groups. This could decrease the tendency of the two R-groups to sterically clash with each other, while decreasing the steric protection around the metal centre; a desired outcome for increased catalytic activity due to increased accessibility of the incoming substrate/reagent towards the metal centre. The electronic influence of the substituent at position Y is fairly subtle but complex and will not be further discussed.[62]

The two coordinating ER substituents flanking the metal centre significantly influence both steric and electronic properties of the ligand. More basic donor ligands can increase the electron density around the metal centre due to their increased donating ability, as discussed above. A more σ-donating R-substituent bonded to E can increase electron density on E, in turn donating more electron density towards the metal.[64] In addition, a bulky R-group imparts steric stabilisation towards the metal, enabling the isolation of reactive complexes. Substitution of the bulky groups with small functionalities decreases the steric hindrance around the metal centre, in turn increasing

---

[63] M. Albrecht, G. van Koten, *Angew. Chem. Int. Ed.*, 2001, **40**, 3750 – 3781.
[64] *Organometallic Pincer Chemistry*, *Top. Organomet. Chem.*, ed. G. van Koten, D. Milstein, Springer-Verlag, Berlin, 2013, vol. 40 and chapters therein.

30

the catalytic activity of the formed catalyst. The substituent at E can be varied in order to obtain a strong σ-donor and weak π-acceptor ligand, or a σ-donor and good π-acceptor ligand.

1.4.3.2) nNHC Pincer Ligands

The advantage of using an nNHC group as a coordinating moiety, in pincer ligands as stated above, results in increased σ-donor ability towards the metal centre due to the increased basicity of nNHC ligands. In this thesis, four different types of nNHC pincer ligands will be discussed.[65] The four groups are:

    I.   NCN pincer ligand – flanking groups coordinate through a N, while the centre coordinating functionality is a C.

    II.   CCC pincer ligand – all three coordinating groups coordinate through C.

    III.   Neutral CNC pincer ligand - flanking groups coordinate through a C, while the centre coordinating functionality is a neutral N donor.

    IV.   Anionic CNC - flanking groups coordinate through a C, while the centre coordinating functionality is a anionic N donor.

I) NCN pincer ligand

Ligands containing a central nNHC donor at position X (Figure 1.25) where the C-2 carbene coordinates to the metal, in addition to having two flanking N donors at both E positions, are generally known as NCN tridentate pincer ligands (Figure 1.26). The donor properties of the central nNHC moiety remain relatively unaffected compared to the properties discussed in Section 1.3, with the only difference being the substitution of the wingtip groups at N-1 and N-3 with flanking groups that can coordinate to the metal through a N functionality. The N functionality can either coordinate to the metal as an X-type ligand (**26$_a$**, Figure 1.26) or as an L-type ligand (**26$_b$**, Figure 1.26).[65] A stronger bond is formed if the N-donor ligand binds to the metal as an X-type ligand, yielding a more robust complex. The nitrogen does not bind to the metal through its lone pair, but through one of its *sp^2*-hybridised or *sp^3*-hybridised orbitals. This is generally achieved after deprotonation of one of the hydrogens bonded to the nitrogen, followed by metallation.

A dative covalent bond is formed when the N-donor ligand binds to the metal as an L-type ligand.[65] Dative covalent bond formation occurs through donation of the nitrogen lone pair to the metal

---

[65] D. Pugh, A. A. Danopoulos, *Coord. Chem. Rev.*, 2007, **251**, 610 – 641.

centre. The dative bond is relatively weak and can undergo dissociation, in which case the bond to the metal breaks or association, which results in bond formation again. This could be advantageous in situations where ligand dissociation/association is required in order to generate the active catalyst or assist in catalysis. Dissociation decreases the electron density on the metal, allowing for reductive elimination to occur more readily, while association would assist in increasing the electron density on the metal centre, allowing for oxidative addition across the metal to occur more readily. The R-groups substituted on the N-donor ligands can be varied in order to obtain the desired complex, either with bulky R-groups imparting increased steric stabilisation, or small R-groups resulting in increased catalytic activity.[56,64,65]
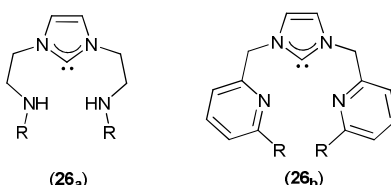
Figure 1.26: Representative examples of NCN pincer ligands

II) CCC pincer ligand

The CCC pincer ligand consists of two nNHC flanking groups and one central coordinating C moiety (Figure 1.27).[66] Both the nNHC groups coordinate to the metal through the C-2 carbene as L-type ligands. The central coordinating C moiety binds to the metal as an X-type ligand. In general, the central coordinating C moiety forms part of an aromatic backbone. If π-orbital overlap between the metal and the aromatic backbone is sufficient, it could allow for an increased π-delocalised system. Therefore, π-bonding and backbonding can occur more readily, but the aromatic ring can inductively withdraw electron density out of the metal.
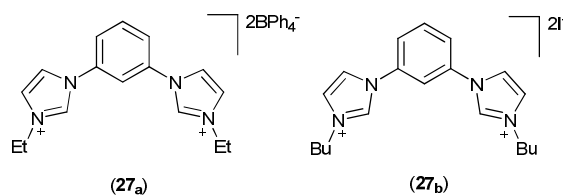
Figure 1.27: Representative examples of CCC pincer ligands[66]

[66] R. J. Rubio, G. T. S. Andavan, E. B. Bauer, T. K. Hollis, J. Cho, F. S. Tham, B. Donnadieu, *J. Organomet. Chem.*, 2005, **690**, 5353 – 5364.

III) Neutral CNC pincer ligand

The neutral CNC class of tridentate pincer ligands coordinates to the metal as L-type ligands at three positions. As indicated in Figure 1.28, the backbone can be either aliphatic or aromatic. Both nNHC moieties coordinate to the metal through the C-2 carbene. Weak dative covalent bond formation between the metal and the central N-donor ligand occurs upon metallation of the ligand, for readily occurring bond dissociation or association.
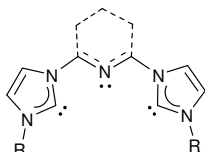
Figure 1.28: Neutral CNC tridentate pincer ligand

As with bidentate ligands, chelation with tridentate ligands does not always occur and the dinuclear bridged complex is formed (Scheme 1.14), as illustrated by the metallation of the CNC tridentate ligand with [RhCl(cod)]$_2$ in the presence of Et$_3$N, KBr and CH$_3$CN as solvent.[67] At lower temperatures, the dinuclear bridged complex is yielded, but at high temperatures the desired chelated ligand-metal complex is isolated. The desired pinced Rh complex was also obtained after heating the dinuclear bridged complex in the presence of one equivalent neutral CNC tridentate ligand, Et$_3$N, KBr and CH$_3$CN. The bulky COD co-ligand could sterically hinder the wingtip R-groups on the N-3 positions. The dinuclear bridged complex was obtained as a result of favourably decreasing the steric repulsion through occupation of the *z*-axis of the metal by the ligand. At elevated temperatures the lability of the COD co-ligand is increased, in turn allowing the ligand to dissociate more readily. In addition, at elevated temperatures oxidation of Rh(I) to Rh(III) occurs readily, and also the thermodynamic product, which is the chelated product, is favoured yielding the pseudo-octahedral complex.[67]
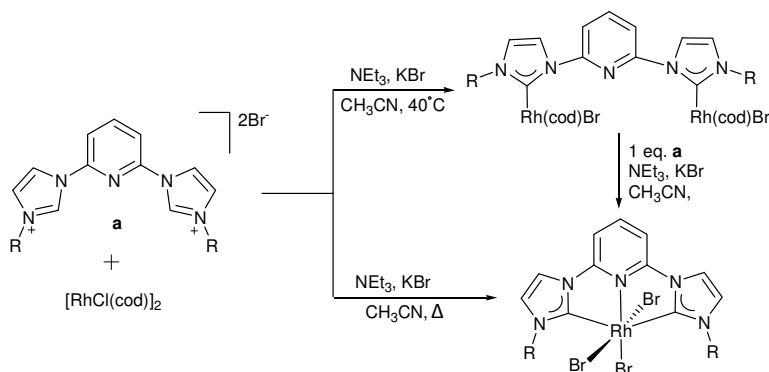
Scheme 1.14: Synthesis of CNC mono- and dinuclear Rh complexes[67]

[67] M. Poyatos, E. Mas-Marza, J. A. Mata, M. Sanau, E. Peris, *Eur. J. Inorg. Chem.*, 2003, 1215 – 1221.

33

IV) Anionic CNC pincer ligand

The anionic CNC pincer ligand comprises of two nNHC flanking groups that coordinate to the metal through the C-2 carbene as L-type ligands. The central coordinating moiety is an anionic N-donor that coordinates to the metal as an X-type ligand (Figure 1.29). The X-type ligand forms a strong bond to the metal, 'locking' the metal in position while the flanking L-type ligands can coordinate to the metal. This increases the robust nature of the ligand-metal complex, compared to the neutral CNC donor ligands.
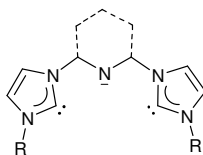
Figure 1.29: Anionic CNC tridentate pincer ligand

The anionic CNC pincer ligand system incorporating carbenes has not been studied as intensively as the other ligand systems have, and only four examples have been reported to date. All four examples are displayed in Figure 1.30. Complex **30a** in Figure 1.30 was the first reported complex comprising of a chelated anionic CNC ligand.[68] The ligand-metal complex was obtained after transmetallation from the dinuclear silver complex in CH_2Cl_2 and deprotonation with NaH in a CH_2Cl_2/THF (tetrahydrofuran) solvent mixture. The backbone of choice was aliphatic rather than an aromatic. An aliphatic backbone is not as rigid as an aromatic backbone, but it has stronger donor ability. The bulky ^{t}Bu wingtip groups impart steric stabilisation, while the nNHC moieties donate electron density towards the metal. Transmetallation from the silver complex with a Pd metal precursor yielded the chelated complex **30b** in Figure 1.30.[69] XRD analysis indicated that the two aromatic phenyl groups twist away from each other, presumably due to steric clashes. In addition, the nNHC moieties are not coplanar and are tilted out of the plane. The tridentate CNC ligand was complexed again to Pd as well as Pt via *in situ* deprotonation followed by metallation.[70]

[68] R. E. Douthwaite, J. Houghton, B. M. Kariuki, *Chem. Commun.*, 2004, 698 – 699.
[69] W. Wei, Y. Qin, M. Luo, P. Xia, M. S. Wong, *Organometallics*, 2008, **27**, 2268 – 2272.
[70] W. B. Cross, C. G. Daly, R. L. Ackerman, I. R. George, K. Singh, *Dalton Trans.*, 2011, **40**, 495 – 505.
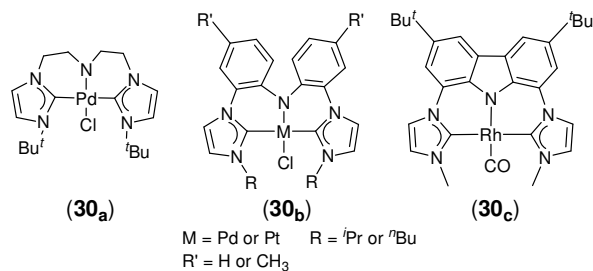
Figure 1.30: Chelated anionic CNC ligand-metal complexes

The synthesis and metallation of the rigid tridentate ligand, represented in Figure 1.30 as the metallated ligand complex **30_c**, was reported by Moser *et al.*[71] The free tridentate ligand was found to be stable in solution, in the absence of air or moisture. The anionic CNC tridentate ligand has a rigid carbazole backbone increasing the stability of the tridentate ligand even further. However, the crystal structure of complex **30_c** shows a slightly distorted carbazole backbone, and nNHC moieties that are not coplanar. The carbonyl stretching frequency of the Rh(I)CO complex was measured and found to be low at 1916 cm^{-1}, indicating that the ligand is a very strong donor. The strong nucleophilicity of the Rh(I) metal centre is supported by the almost instantaneous reaction with MeI, which oxidatively adds across the metal to yield the corresponding Rh(III) complex.[71]

1.4.3.3) *trz* Pincer Ligands

Substitution of the nNHC donor moiety/moieties in the tridentate ligand with a *trz* donor, yields the corresponding *trz* tridentate ligand. The stronger *trz* donor, in combination with the stability imparted by the chelate effect when using a tridentate ligand, could result in the synthesis of catalysts with high catalytic output and a high robust nature. However, reports on the use of *trz* donors in tridentate ligands are scarce. Some examples will be discussed below.

I) PCP *trz* pincer ligand

A PCP tridentate ligand was synthesised and successfully coordinated to both Pt and Pd (Figure 1.31).[72] The tridentate ligand coordinates to the metal through the C-5 carbene of the *trz* moiety and the two phosphine flanking groups. Chloride abstraction from complex **31_b** (Figure 1.31) with AgOTf and subsequent treatment with CO yielded the corresponding Pt carbonyl complex. The carbonyl stretching frequency of the compound was measured and reported to be 2124 cm^{-1}. This is relatively low, but not as low as other reported values (See section 1.3.3.1).[51] The higher value could be

---

[71] M. Moser, B. Wucher, D. Kunz, F. Rominger, *Organometallics*, 2007, **26**, 1024 – 1030.

[72] E. M. Schuster, M. Botoshansky, M. Gandelman, *Dalton Trans.*, 2011, **40**, 8764.

attributed to both the cationic Pt centre, and the inductive electron withdrawing effect of the CF_3 functional group substituted on the benzyl functionality.
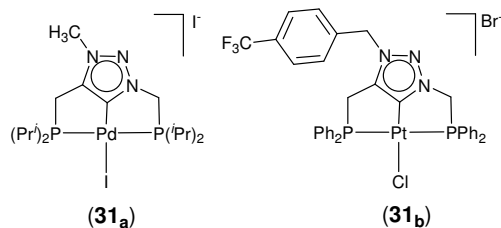
Figure 1.31: PCP *trz* tridentate ligand-metal complexes [72]

II) CCC *trz* pincer ligand

The CCC *trz* tridentate ligand consist, like the nNHC CCC tridentate ligand, of two *trz* flanking groups and a central coordinating C moiety. Chelation would be successful if both the *trz* C-5 carbenes coordinate to the metal as L-type ligands, while the central C moiety coordinates as an X-type ligand. However, chelation of the *trz* tridentate ligand proved to be non-trivial. A potential tridentate CCC pincer ligand was synthesised and treated with Ag_2O, yielding a dinuclear bridged silver metal complex where the central C-atom did not ligate (Scheme 1.15).[73] This is the first reported example of a silver MIC complex. Transmetallation of the silver MIC complex with [Rh] yielded the dinuclear [Rh] MIC complex, and not the chelated complex. The same ligand was coordinated to $PdCl_2$ in the presence of K_2CO_3 and pyridine, but again yielded the dinuclear complex.[74] In both cases, a possible reason for dinuclear bridged complex formation instead of chelation, would be that the bulky Dipp (2,6-diisopropylphenyl) wingtip groups could sterically clash with each other if chelation were to occur. Dinuclear complex formation twists the Dipp groups away from each other, resulting in the complex experiencing a dramatic decrease in steric strain.
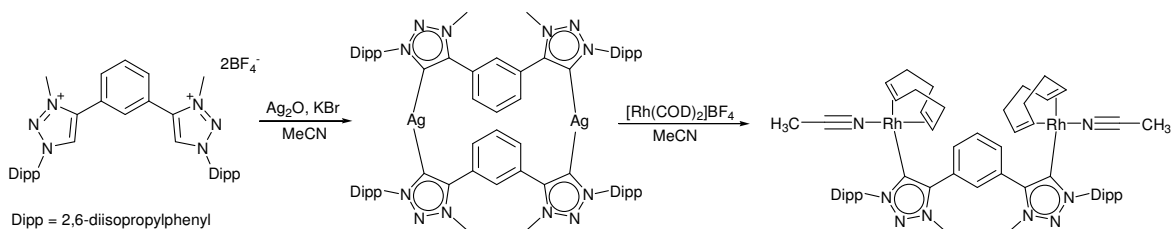
Scheme 1.15: Synthesis of a dinuclear [Rh] bisMIC complex[73]

[73] E. C. Keske, O. V. Zenkina, R. Wang, C. M. Crudden, *Organometallics*, 2012, **31**, 456 – 461.
[74] E. C. Keske, O. V. Zenkina, R. Wang, C. M. Crudden, *Organometallics*, 2012, **31**, 6215 – 6221.

36

Neutral CNC *trz* tridentate ligands consist of an N-donor moiety, coordinating to the metal through its lone pair of electrons as an L-type ligand. The two flanking groups can either consist of two *trz* donor ligands, or one *trz* donor ligand and another flanking group. Figure 1.32 represents a neutral CNC *trz* tridentate ligand and a neutral CNN tridentate ligand that was successfully chelated around a Ru(II) metal centre.[75] Complex **32$_a$** in Figure 1.32 has two flanking *trz* donor ligands, in addition to the N-donor ligand coordinating as an L-type ligand. Complex **32$_b$** in Figure 1.32 consists of one *trz* flanking group, the central coordinating N-donor L-type ligand and a second pyridyl flanking group.

$$a_i, R = CH_3, R' = 2,4,6\text{-trimethylphenyl}, R'' = H, X = BF_4$$
$$a_{ii}, R = C_8H_{17}, R' = CH_3, R'' = COOCH_3, X = PF_6$$
$$a_{iii}, R = C_8H_{17}, R' = CH_3, R'' = COOH, X = PF_6$$

$$b_i, R = H, X = PF_6$$
$$b_{ii}, R = COOCH_3, X = PF_6$$
$$b_{iii}, R = COOH, X = PF_6$$
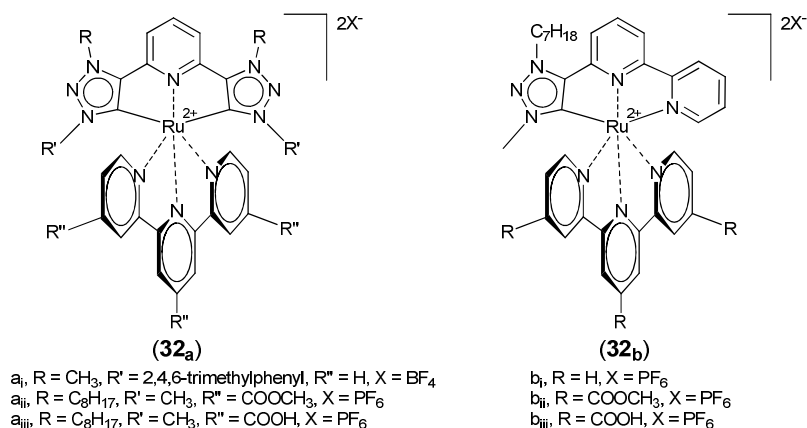
Figure 1.32: Chelated neutral CNC (**32$_a$**) and CNN (**32$_b$**) *trz* ligand-metal complexes[75]

1.5) Aim

Research into the activation and utilisation of small molecules (e.g. $CO_{2(g)}$, $CO_{(g)}$, $NH_{3(g)}$, H_2NNH_2, $O_{2(g)}$, etc.) has been an area of increasing interest over the past few years.[76] The Achilles heel of designing and synthesizing (pre)catalysts successful in the activation of small molecules, and/or active in homogenous catalysis utilizing small molecules as substrates, has been the significant challenges associated with these processes. These challenges include bond activation of so-called inert or unreactive substrates, bond cleavage and its utilisation as substrates in catalysis. The successful design and synthesis of a catalyst able to overcome these challenges could be associated with large-scale production of organic compounds from inexpensive substrates that are readily available.

---

[75] S. Sinn, B. Schulze, C. Friebe, D. G. Brown, M. Jäger, E. Altuntaş, J. Kübel, O. Guntner, C. P. Berlinguette, B. Dietzek, U. S. Schubert, *Inorg. Chem.*, 2014, **53**, 2083 – 2095.
[76] J. I. van der Vlugt, *Chem. Soc. Rev.*, 2010, **39**, 2302 – 2322.

The proposed project is aimed at the design and synthesis of novel ligands and its complexation to various metal precursors in order to synthesise (pre)catalysts that could be active in processes such as activation of small molecules and in catalytic processes.

The ligand scaffold will consist of a tridentate ligand with a rigid carbazole backbone and a central coordinating amido moiety. Triazolylidenes will be incorporated into the ligand scaffold as the two flanking groups. The wingtips substituted onto the triazolylidene will be bulky groups for steric stabilisation. The ligands will be complexed to various metals, including Ni(II), Cu(I), Cu(II), Rh(I), Ag(I), Au(I) and Au(III). The catalytic activity of selected complexes will subsequently be investigated.

38

Chapter 2: Ligand Design and Synthesis

2.1) Background

The strong σ-donating triazolylidenes (*trz*) are readily synthesised from their stable precursors, the triazolium salts (*trz*H). Two different methods are commonly employed in the synthesis of triazolium salts. The first method involves the copper catalysed cycloaddition of an alkyne and an azide (CuAAC), followed by alkylation as reported by Albrecht and co-workers.[1] The second synthetic method towards the synthesis of triazolium salts involves the cycloaddition of 1,3-diaryl-2-azoniaallene salts and alkynes, as reported by Bertrand and co-workers.[2] These two general methods will be discussed in this section.

2.1.1) Synthesis of Triazolium Salts *via* the CuAAC Method

The copper catalysed cycloaddition of a terminal alkyne and an azide (CuAAC), or the so-called 'click' chemistry reaction, is a well known method utilised in the synthesis of triazoles (Scheme 2.1).[1] The method is remarkably robust towards a large temperature (0 °C – 160 °C) and pH (*ca.* 4 – 12) range, tolerates aqueous environments and succeeds in the presence of various functional groups.[3] The CuAAC method provides access to a wide range of five-membered heterocycles and does not undergo side reactions readily.[4]
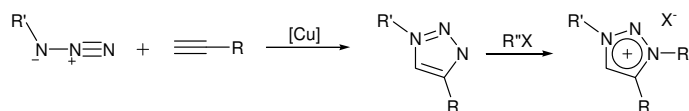
Scheme 2.1: Triazolium salt synthesis *via* [Cu] catalysed [3 + 2] cycloaddition[1]

The proposed mechanism for the cycloaddition between an azide and an alkyne in the presence of copper is outlined in Scheme 2.2.[3] The mechanism does not account for a concerted 3 + 2 cycloaddition reaction, but rather a stepwise formation of various intermediates. Step **A** involves the coordination of the alkyne to the copper species, forming the acetylide **2** by displacement of one of

[1] P. Mathew, A. Neels, M. Albrecht, *J. Am. Chem. Soc.*, 2008, **130**, 13534 – 13535.

[2] J. Bouffard, B. K. Keitz, R. Tonner, G. Guisado-Barrios, G. Frenking, R. H. Grubbs, G. Bertrand, *Organometallics*, 2011, **30**, 2617 – 2627.

[3] F. Himo, T. Lovell, R. Hilgraf, V. V. Rostovtsev, L. Noodleman, K. B. Sharpless, V. V. Fokin, *J. Am. Chem. Soc.*, 2005, **127**, 210 – 216.

[4] V. V. Rostovtsev, L. G. Green, V. V. Fokin, K. B. Sharpless, *Angew. Chem. Int. Ed.*, 2002, **41**, 2596 – 2599.

the ligands coordinated to the copper. The second step (**B**, Scheme 2.2) involves displacement of another ligand by the azide, yielding intermediate **3**. It is computationally predicted that the C-substituted nitrogen coordinates to the metal, due to its higher nucleophilic character.[3] The unusual six-membered ring **4** is formed by the interaction between the nitrogen distal to the carbon in the azide fragment, with the *sp*-hybridised carbon atom in the acetylide fragment (**C**, Scheme 2.2). Ring contraction by interaction of the allenic carbon with the azido nitrogen coordinated to the copper (**D**, Scheme 2.2) yields the triazole ring **5**. Proteolysis of **5** releases the triazole ring **6** and regenerates the copper starting material.[3]
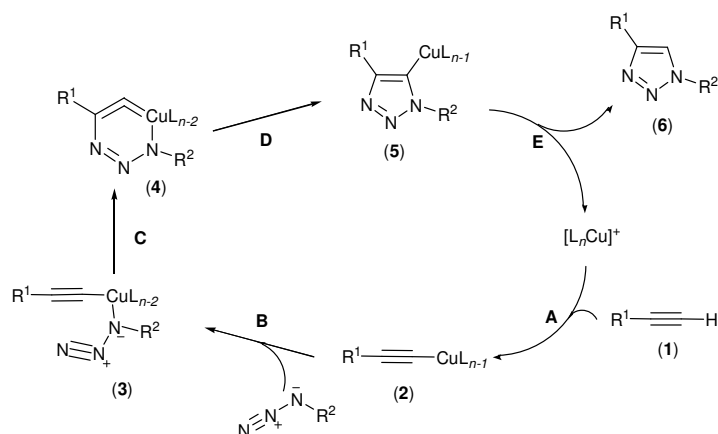
Scheme 2.2: Proposed mechanism for triazole synthesis *via* the CuAAC method[3]

Alkylation of triazole **6** (Scheme 2.2) with an appropriate alkylating agent yields the triazolium salt. The site of alkylation is at the N-3 position and is generally selective for that position.[5] The nucleophilic nitrogen attacks the electrophilic carbon of the alkylating agent, yielding a stable N-C bond. The leaving group of the alkylating agent serves as the counteranion of the triazolium salt after alkylation.

Metallation of the triazolium salt generally results in the formation of a stable metal complex.[5] However, deprotonation of the triazolium salt in order to isolate the free 1,2,3-triazolylidene leads to decomposition of the triazolylidene moiety through N-3 alkyl bond cleavage, as reported by Bertrand and co-workers.[2] Introduction of an aryl wingtip substituent at the N-3 position, together with a second aryl wingtip group at position N-1 would limit the decomposition pathway and yield a stable, free triazolylidene moiety upon deprotonation of the diaryl triazolium salt. The CuAAC method does not allow for the introduction of aryl wingtip functionalities at the N-3 position, a

---

[5] K. F. Donnelly, A. Petronilho, M. Albrecht, *Chem. Commun.*, 2013, **49**, 1145 – 1159.

40

disadvantage encountered when using the CuAAC method for triazolium salt synthesis.[2] In order to obtain the diarylated triazolium salt, an alternative method has to be employed.

2.1.2) Synthesis of Triazolium Salts *via* the Cycloaddition of 1,3-Diaryl-2-azoniaallene Salts and Alkynes

Synthesis of the diarylated triazolium salt is accomplished *via* cycloaddition of 1,3-diaryl-2-azoniaallene salts and alkynes in the presence of *tert*-butylhypochlorite (^{t}BuOCl) and KPF$_6$ or SbCl$_5$ (Scheme 2.3).[2] This method allows for the introduction of aryl wingtip substituents on N-1 and N-3, increasing the stability of the triazolium salt as well as the free or metallated triazolylidene.
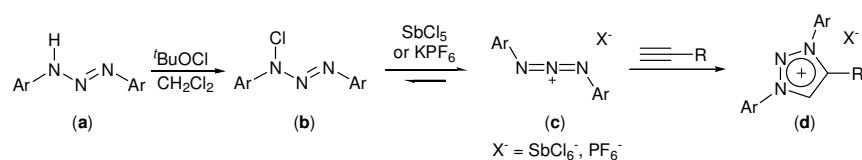
Scheme 2.3: Arylated triazolium salt synthesis *via* [3 + 2] cycloaddition reaction

As depicted in Scheme 2.3, oxidation of the diarylated triazene **a** with ^{t}BuOCl in CH$_2$Cl$_2$ affords the unstable, open chain *N*-chlorotriazene.[6] Compounds of type **b** exploded upon attempted isolation, attributable to their unstable nature as reported by Wirschum.[6] Treatment of **b** (Scheme 2.3) with antimony pentachloride (SbCl$_5$) or potassium hexafluorophosphate (KPF$_6$) yields the 1,3-diaryl-2-azoniaallene salt (**c**, Scheme 2.3), which is only stable below -30 °C. Addition of alkyne to the 1,3-diaryl-2-azoniaallene salt yields the triazolium salt **d** (Scheme 2.3) *via* a cycloaddition reaction between the alkyne and the salt. Both electron rich and poor alkynes react with the salt to yield the desired triazolium salt.[6] Calculations indicated that formation of the triazolium salt (**d**, Scheme 2.3) occurs through a concerted [4π + 2π]-cycloaddition reaction mechanism (Scheme 2.4).[6] In the transition state, the C-N bond lengths were calculated to be equal, supporting a concerted (synchronous) reaction mechanism.
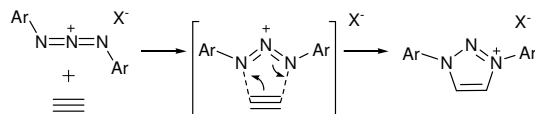
Scheme 2.4: Proposed mechanism for the cycloaddition of 1,3-diaryl-2-azoniaallene salts and alkynes[6]

---

[6] W. Wirschum, *J. prakt. Chem.*, 1998, **30**, 300 – 308.

2.2) Aim

Incorporation of the strongly donating triazolylidene moiety into an anionic tridentate ligand could potentially lead to a very strong donor ligand system. As such, synthesis towards an anionic CNC tridentate pincer ligand featuring two triazolylidene donor moieties and a rigid backbone will be attempted (Figure 2.1). A carbazole moiety will be used as the rigid backbone, similar to the ligand system incorporated by Moser *et al.* (see Section 1.4.3.2, Chapter 1).[7] In addition to the anionic rigid carbazole backbone, two *trz*H moieties will feature as the two flanking groups. The *trz*H moieties will have aryl functional groups substituted at the N-1 and N-3 positions of the *trz*H groups. Deprotonation of the synthesised tridentate ligand in order to isolate a crystalline free bis(triazolylidene)carbazolide ligand will be attempted.

Ar = 2,4,6-trimethylphenyl
= 2,6-diisopropylphenyl
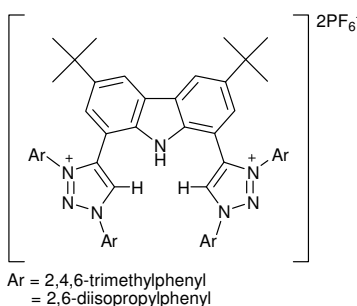
Figure 2.1: Proposed anionic tridentate pincer ligand to be synthesised

2.2.1) Synthetic Strategy

The proposed synthetic strategy towards the synthesis of the CNC tridentate ligand represented in Figure 2.1 is outlined in Scheme 2.5. Various synthetic steps are required in order to obtain the dialkyne precursor for the cycloaddition reaction, which will yield the triazolium salt. The first step is alkylation of the carbazole starting material with *tert*-butylchloride (*t*BuCl) in the presence of AlCl$_3$, which is generally known as a Friedel-Crafts alkylation reaction. Alkylation of the carbazole to yield the dialkylated carbazole **i**, serves two main purposes; first alkylation blocks the *para* position of the phenyl ring and the second purpose is the increased electron density in the benzene rings as a result of alkyl groups donating electron density towards the ring. Both factors contribute towards selective bromination at the *ortho* positions of compound **i**, which is the second step in the proposed synthetic strategy. The brominated compound **ii** is subjected to a Sonogashira coupling reaction with trimethylsilylacetylene, to yield compound **iii**. Deprotection of compound **iii** with K$_2$CO$_3$ and MeOH yields the dialkyne **iv**. The 1,3-diaryl-2-azoniaallene salt is generated *in situ* by treatment of the

---

[7] M. Moser, B. Wucher, D. Kunz, F. Rominger, *Organometallics*, 2007, **26**, 1024 – 1030.

42

triazene with ^{t}BuOCl in the presence of KPF$_6$, which subsequently reacts with the alkyne in order to yield the desired triazolium salt **v**. A more detailed explanation of each reaction will follow in the following subsections.
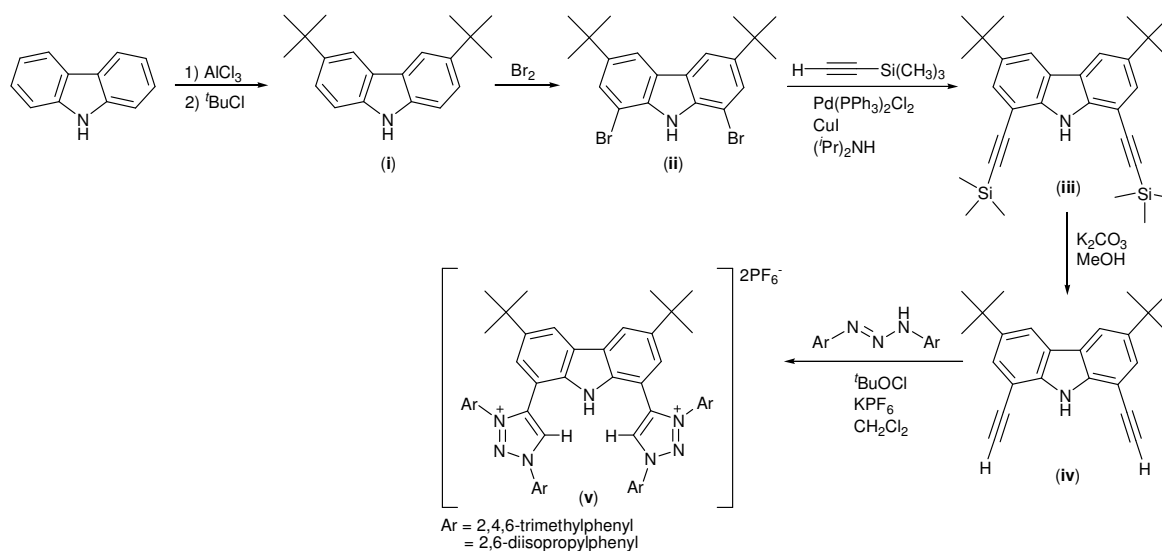
Scheme 2.5: Proposed synthetic strategy towards the synthesis of an anionic tridentate pincer ligand

2.2.1.1) 3,6-Di-*tert*-butyl-9H-carbazole

The Friedel-Crafts alkylation is a carbon-carbon coupling reaction, used to form new bonds between an alkyl substituent and an aromatic moiety. The reaction generally occurs in two steps, as depicted in Scheme 2.6.[8] The first step involves the formation of the electrophilic carbocation from the corresponding alkylchloride. The carbocation is formed when ^{t}BuCl reacts with aluminium trichloride (AlCl₃) in a Lewis acid-base reaction. This yields the Lewis acid-base complex and the tertiary carbocation through chloride abstraction. The tertiary carbocation will then, in step two of the reaction, react with the 9H-carbazole in an electrophilic aromatic substitution reaction.[8] The 9H-carbazole is subjected to two consecutive electrophilic aromatic substitution reactions, in order to yield the dialkylated 9H-carbazole. The Lewis acidic AlCl₃ is regenerated, and HCl is released as a by-product from the reaction.

---

[8] J. G. Smith, *Organic Chemistry*, 2nd Ed., Mc Graw Hill, New York, United States, 2008, 641 – 680.

Step 1: Formation of the Carbocation Electrophile

$(CH_3)_3C{-}Cl$ + $AlCl_3$ $\longrightarrow$ $(CH_3)_3C{-}\overset{+}{C}l{-}\overset{-}{A}lCl_3$ $\longrightarrow$ $(CH_3)_3\overset{+}{C}$ + $Al\overset{-}{C}l_4$
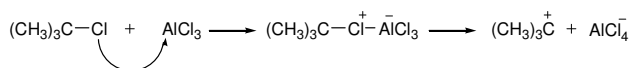
Step 2: Alkylation of Carbazole with Electrophile
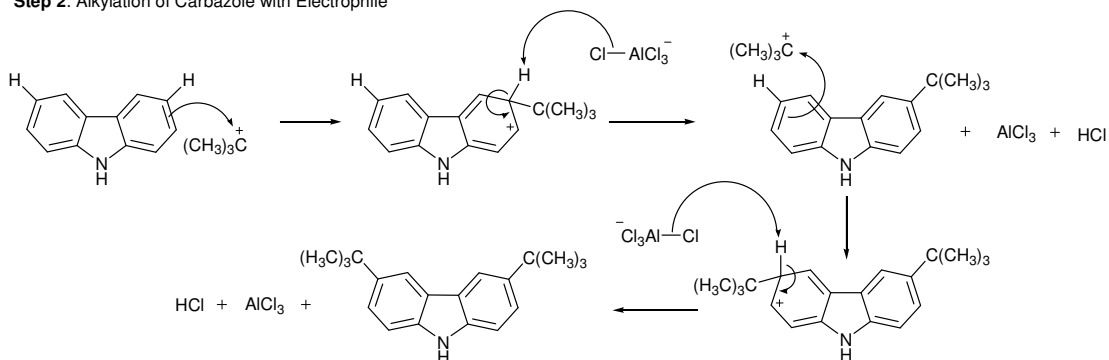
Scheme 2.6: Mechanism of Friedel-Crafts Alkylation of 9H-carbazole *via* Electrophilic Aromatic Substitution[8]

2.2.1.2) 1,8-Dibromo-3,6-di-*tert*-butyl-9H-carbazole

Bromination of a benzene ring does not readily occur. However, once a benzene ring is substituted with a nitrogen moiety, the situation changes significantly.[9] This is due to the nitrogen lone pair of electrons being donated into the aromatic benzene ring, which serves to 'activate' the benzene ring towards electrophilic aromatic substitution reactions. As such, the dialkylated carbazole can be readily brominated by the addition of bromine in acetic acid as solvent. The mechanism for the bromination of the dialkylated carabazole is depicted in Scheme 2.7. The nitrogen lone pair is donated into the π-electron delocalised conjugated system. The carbon at the *ortho* position of the carbazole gains nucleophilic character as a direct result of the electron donation from the nitrogen. The nucleophilic carbon induces a dipole moment on the incoming bromine reagent. The partially positive bromine atom in the bromine molecule is then attacked by the nucleophilic carbon, which forms a new carbon-bromine bond and breaks the bromine-bromine bond.[9] The acidic hydrogen can now react with the bromine anion, to yield hydrogen bromide and the brominated carbazole compound. The procedure is repeated again, to yield the 1,8-dibromo-3,6-di-*tert*-butyl-9H-carbazole product.

[9] J. Clayden, N. Greeves, S. Warren, P. Wothers, *Organic Chemistry*, Ed., Oxford University Press Inc., New York, United States, 2004, 546 – 579.
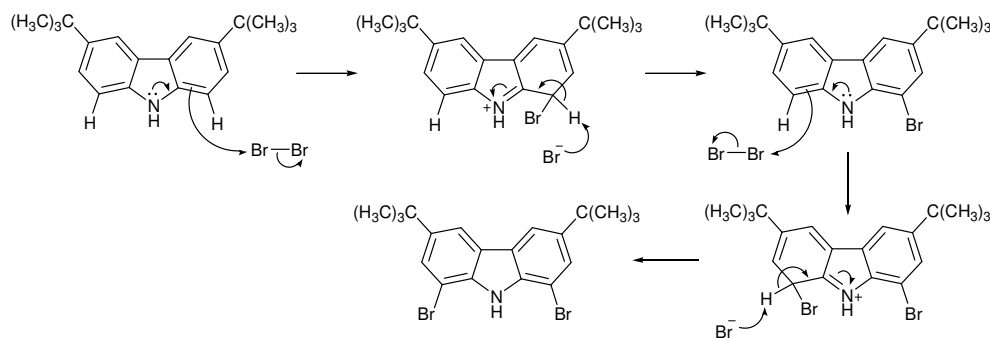
Scheme 2.7: Mechanism for bromination of 3,6-di-*tert*-butyl-9H-carbazole[9]

2.2.1.3) 3,6-Di-*tert*-butyl-1,8-diethynyl-9H-carbazole

The Sonogashira carbon-carbon coupling reaction can be utilised in order to replace the bromine functional groups on the 1,8-dibromo-3,6-di-*tert*-butyl-9H-carbazole compound with alkyne functionalities, forming new carbon-carbon bonds. The mechanism of the palladium catalysed Sonogashira coupling reaction, with the aid of a copper co-catalyst, is not fully understood.[10] However, various studies, including kinetic studies, have been sufficient in order to propose a plausible mechanism for the coupling reaction. As such, a proposed mechanism for the coupling reaction for the 1,8-dibromo-3,6-di-*tert*-butyl-9H-carbazole compound with an alkyne reagent will be presented in Scheme 2.8 (Note: Only one coupling reaction will be shown. The second coupling reaction should follow the same mechanism as proposed for the first coupling reaction, to yield the desired 3,6-di-*tert*-butyl-1,8-bis(2-(trimethylsilyl)ethynyl)-9H-carbazole). The active palladium(0) catalyst, generated from the palladium(II)chloride starting complex *via* an *in situ* reduction reaction, is oxidised to the palladium(II) intermediate through oxidative addition of the brominated reagent. At the same time, the copper co-catalyst serves to metallate the trimethylsilyl (TMS) protected acetylene.[10] This is accomplished by coordination of the copper(I) bromide salt through the π-bond of the alkyne, followed by formation of the copper-carbon bond after the acetylenic proton had been deprotonated by the basic amine added to the reaction mixture. This yields the copper-acetylide intermediate, which can now react with the palladium(II) intermediate. The bromine ligand is replaced by the TMS-protected copper-acetylide in a transmetallation reaction, to yield the palladium intermediate containing both the aryl functional group (the carbazole) and the TMS-acetylide ligand. Reductive elimination yields the palladium(0) starting catalyst with release of the desired TMS-acetylene carbazole compound.[10]

---

[10] See relevant review article and references therein: R. Chinchilla, C. Nájera, *Chem. Rev.*, 2007, **107**, 874 – 922.
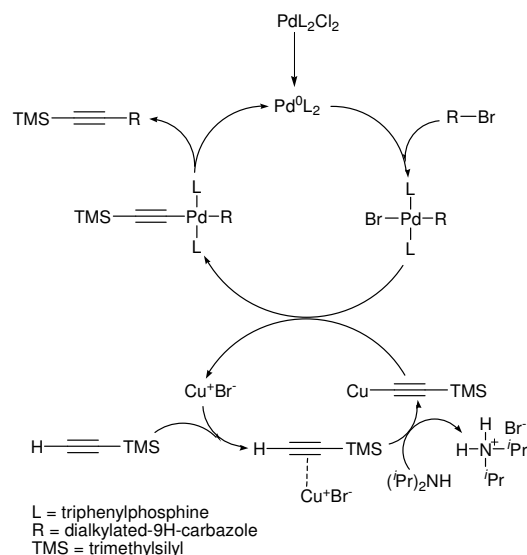
Scheme 2.8: Sonogashira coupling of the 1,8-dibromo-3,6-di-*tert*-butyl-9H-carbazole[10]

Upon completion of the Sonogashira coupling to yield the 3,6-di-*tert*-butyl-1,8-bis(2-(trimethylsilyl)ethynyl)-9H-carbazole, a simple deprotection reaction is utilised in order to remove the trimethylsilyl protecting groups bonded to the alkyne. The silicon protecting groups are replaced by hydrogen atoms, yielding the desired terminal alkyne carbazole product, which is the precursor compound for the cycloaddition reaction between the alkyne and a triazene reagent. Scheme 2.9 illustrates the deprotection reaction, where potassium carbonate in methanol is used to yield the desired product.
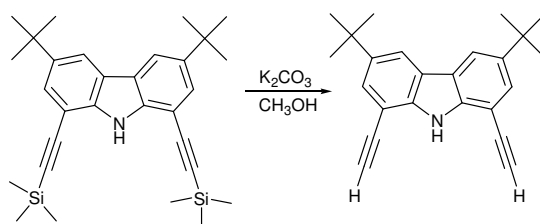
Scheme 2.9: Deprotection of the TMS-protected alkyne functional groups

2.2.1.3) 1,3-Diarylated triaz-1-ene

The second precursor for the cycloaddition reaction is the 1,3-diarylated triaz-1-ene reagent. The simple method[2] involves the addition of isoamyl nitrite to a cold ethereal solution of an aniline derivative. After the reaction, the product is obtained by recrystallisation techniques. However, the mechanism for the reaction is not as trivial. A mechanism for the reaction is postulated, and illustrated in Scheme 2.10. The first step involves a Schiff base reaction. Nucleophilic addition of the aniline to the nitrite followed by the elimination of water yields the arylated diazonium

46

intermediate. A second nucleophilic addition reaction, involving a second aniline molecule, displaces the *iso*-pentoxide leaving group in a substitution reaction. The *iso*-pentoxide, after being substituted, reacts as a base to deprotonate the acidic hydrogen from the ammonium moiety, to yield the desired 1,3-diarylated triazene product and *iso*-amyl alcohol as a by-product.

Ar = 2,6-diisopropylphenyl
2,4,6-trimethylphenyl
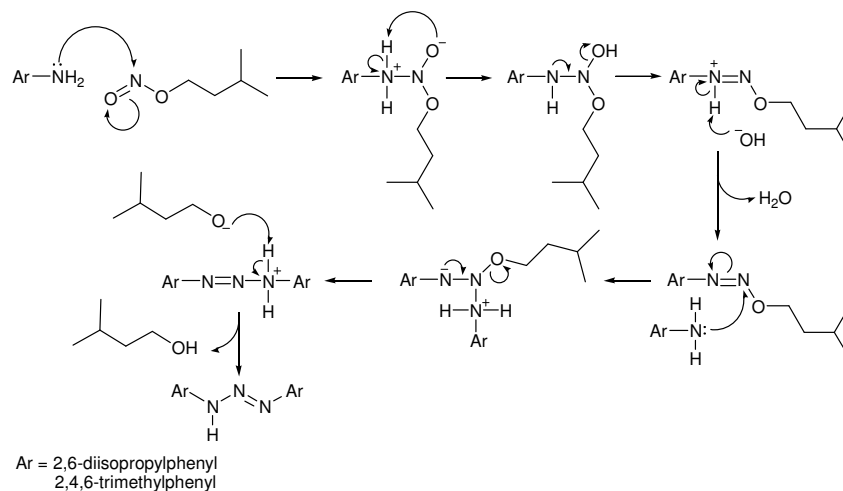
Scheme 2.10: A proposed mechanism for the formation of 1,3-diarylated triaz-1-ene

2.3) Results and Discussion

See Section 2.5 for the methods used during the synthesis of the compounds as well as the full characterisation thereof.

2.3.1) Synthesis of 1

In order to synthesise the bis(triazolium)carbazole ligand salt with aryl wingtip functionalities, the precursor compound, namely 9H-carbazole, had to undergo various organic transformation reactions. The first step involved the dialkylation of 9H-carbazole with ^{t}BuCl, in the presence of AlCl$_3$, as reported by Williams and co-workers.[11] After stirring a solution of 9H-carbazole, AlCl$_3$ and ^{t}BuCl in dichloromethane (DCM) for thirty hours at RT, a mixture of monoalkylated (Scheme 2.11) and dialkylated (**1**, Scheme 2.11) 9H-carbazole compounds as the main products of the reaction were obtained (Scheme 2.11). The formation of the monoalkylated product could have been a result of the coordination of the amino functional group of the carbazole, to the AlCl$_3$. The coordinated aluminium would subsequently be unreactive towards the ^{t}BuCl reagent and the formation of the

---

[11] V. C. Gibson, S. K. Spitzmesser, A. J. P. White, D. J. Williams, *Dalton Trans.*, 2003, 2718 – 2727.

47

carbocationic electrophile would decrease significantly. A decrease in the amount of electrophilic carbocation available would ultimately lead to the formation of mixtures of mono- and dialkylated carbazole products, as seen for this reaction. In addition, separation of the two compounds proved non-trivial, and was also accompanied by a large loss of product. To obtain the desired product as the only major product with acceptable yields, a different approach had to be employed.
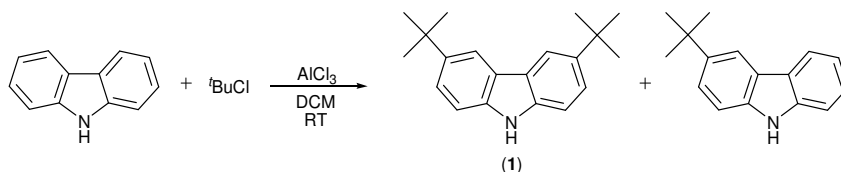
Scheme 2.11: Synthesis of dialkylated 9H-carbazole in the presence of AlCl₃

In order to synthesise **1** (Scheme 2.11) as the major product in high yields, the AlCl₃ reagent was substituted with a ZnCl₂ reagent, and an adapted procedure reported by Promarak *et al.* was employed for the synthesis of **1**.[12] The dialkylation reaction was done in the presence of ZnCl₂ and ^{t}BuCl, with nitromethane as the solvent of the reaction (Scheme 2.12). After stirring the reaction mixture for two days, followed by a basic work-up of the mixture, **1** could be obtained with a 99% purity as determined after NMR analysis, and with a yield of 97%.
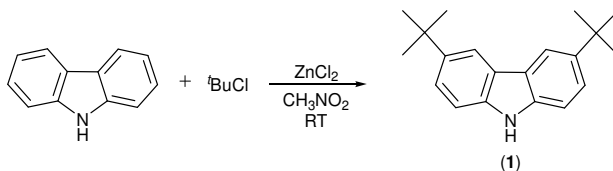
Scheme 2.12: Synthesis of **1** in the presence of ZnCl₂

2.3.2) Synthesis of 2

Compound **1** was halogenated by reaction with bromine, in order to obtain the dibromo-dialkylated-9H-carbazole compound. The method for halogenation of **1** was similar to that reported by Williams and co-workers.[11] Compound **1** was stirred in glacial acetic acid, with the slow addition of Br₂ (*l*) in the absence of light. Excess bromine reagent could be added to the reaction mixture without the possibility of bromination occurring at positions other than the *ortho* positions of the benzene rings. Polyhalogenation of the activated benzene ring is prevented by blocking the *para*-positions with alkyl-substituents. The solution was stirred for fourteen hours, and after a basic work-up of the reaction mixture, **2** was obtained as the only product with a yield of 96% (Scheme 2.13).

---

[12] P. Moonsin, N. Prachumrak, R. Rattanawan, T. Keawin, S. Jungsuttiwong, T. Sudyoadsuk, V. Promarak, *Chem. Commun.*, 2012, **48**, 3382 – 3384.

48
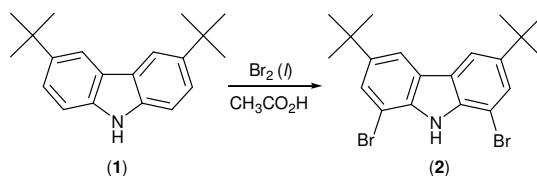
Scheme 2.13: Bromination of **1** with Br$_2$ (*l*)

2.3.3) Synthesis of 3

A Sonogashira carbon-carbon coupling reaction had to be employed, in order to obtain the dialkyne-9H-carbazole **3** derivative. As mentioned in Section 2.1.2, the alkyne is one of the precursors for the 3+2 cycloaddition reaction of 1,3-diaryl-2-azoniaallene salts and alkynes, yielding the corresponding triazolium salts. An adapted literature procedure, as reported by Bertrand and co-workers, was followed during the synthesis of **3**.[2] Reacting **2** with two equivalents of trimethylsilylacetylene (TMS-acetylene), using Pd(PPh$_3$)$_2$Cl$_2$ as catalyst and CuI as co-catalyst with the addition of diisopropylamine and toluene as solvent, a mixture of monocoupled (Scheme 2.14) and dicoupled (**3**, Scheme 2.14) alkyne carbazole compounds were obtained. After, subjecting the mixture of two compounds to a second Sonogashira coupling reaction, using the same equivalents of reagents and the same procedure as used before, the desired compound **3** could be obtained as the only product of the carbon-carbon coupling reaction (Scheme 2.14). The overall yield of the reaction was determined to be 89%.
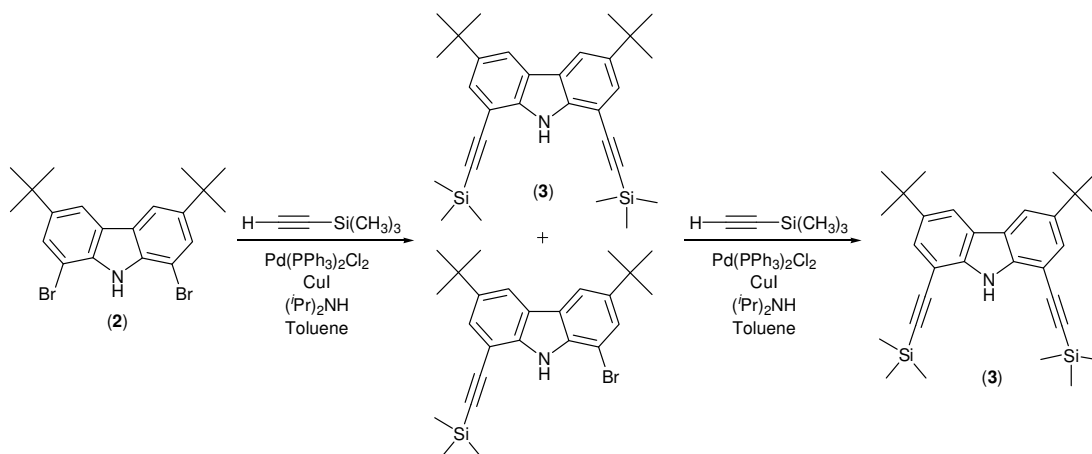
Scheme 2.14: Sonogashira coupling of **2** with TMS-acetylene to yield **3**

2.3.4) Synthesis of 4

Compound **3** was subjected to a deprotection reaction in order to remove the trimethylsilyl protecting groups, bonded to the alkynes. A mild deprotecting method was employed which makes

49

use of potassium carbonate as weak base and methanol as the solvent of the reaction. After deprotecting **3**, **4** was obtained as the only product with a yield of 96%. Scheme 2.15 outlines the deprotection reaction employed and the desired compound **4**, obtained as the only product after the reaction.
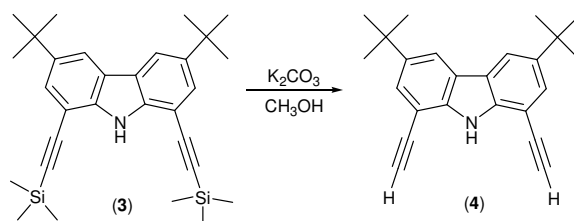
Scheme 2.15: Deprotection of **3** with K_2CO_3 to yield **4**

2.3.5) Synthesis of 5

The method of Bertrand[2] was slightly modified during the synthesis of **5** (Scheme 2.16). In the absence of light, isoamyl nitrite was added drop-wise to an ethereal solution of 2,6-diisopropylbenzenamine cooled down to -30 °C. The reaction was removed from the cold bath after one hour; left to settle overnight and after crystallisation, **5** was obtained as yellow crystals with a yield of 30%.
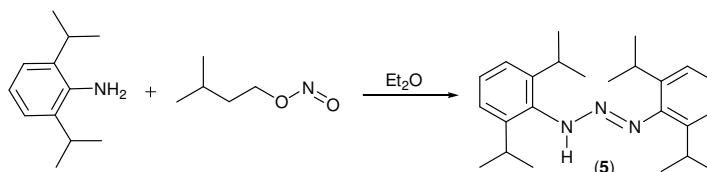
Scheme 2.16: 1,3-bis-(2,6-diisopropylphenyl)triaz-1-ene synthesis

2.3.6) Synthesis of 6

The method used for the synthesis of **5** was also employed for the synthesis of **6** (Scheme 2.17), using 2,4,6-trimethylbenzenamine as reagent. Compound **6** was obtained as yellow crystals with a yield of 22%.
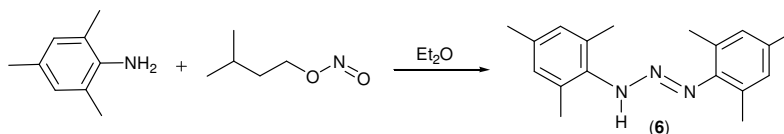
Scheme 2.17: 1,3-bis-(2,4,6-trimethylphenyl)triaz-1-ene synthesis

50

2.3.7) Synthesis of 7

Once the alkyne and triazene precursor compounds were obtained, the 3+2 cycloaddition reaction could be performed in order to synthesise the desired bis(triazolium) ligand salt. An adapted literature reported procedure[2] was followed during the synthesis of the ligand salt. To a DCM solution of **4**, **5** and potassium hexafluorophosphate (KPF$_6$) cooled down to -78 °C was added the oxidising reagent, ^{t}BuOCl, in a drop-wise manner (Scheme 2.18). The solution was stirred overnight and after filtration followed by trituration; compound **7** could be obtained as an off-white solid with a yield of 68%. Nuclear Magnetic Resonance Spectroscopy (NMR), High Resolution Mass Spectrometry (HRMS), X-Ray Diffraction analysis (XRD) and Melting Point (MP) determination all confirmed the formation of **7**.
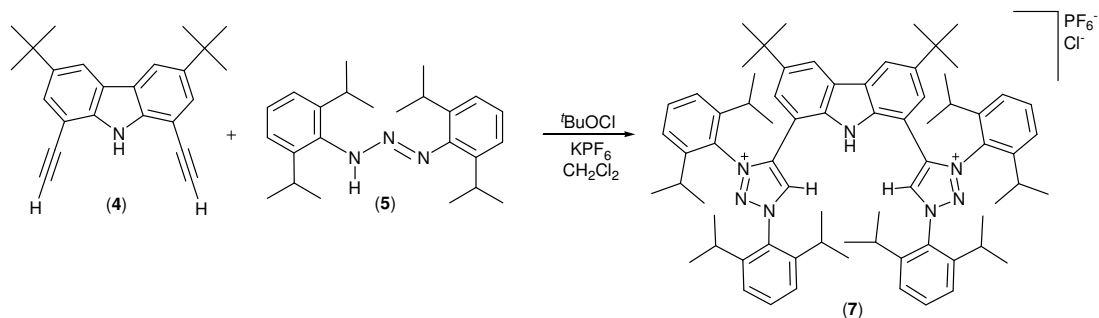
Scheme 2.18: Synthesis of **7** *via* a 3 + 2 cycloaddition reaction between **4** and **5**

The proton NMR of **7** (Figure 2.2) indicates that the three acidic protons, namely the two *trz*H protons at a resonance of 10.95 ppm and the carbazole amino proton at a resonance of 13.03 ppm, are significantly shifted downfield. The downfield shift can be attributed to the interaction of the protons with the chloride anion. The chloride anion with its high electronegativity will have an electron withdrawing effect on the protons.

51
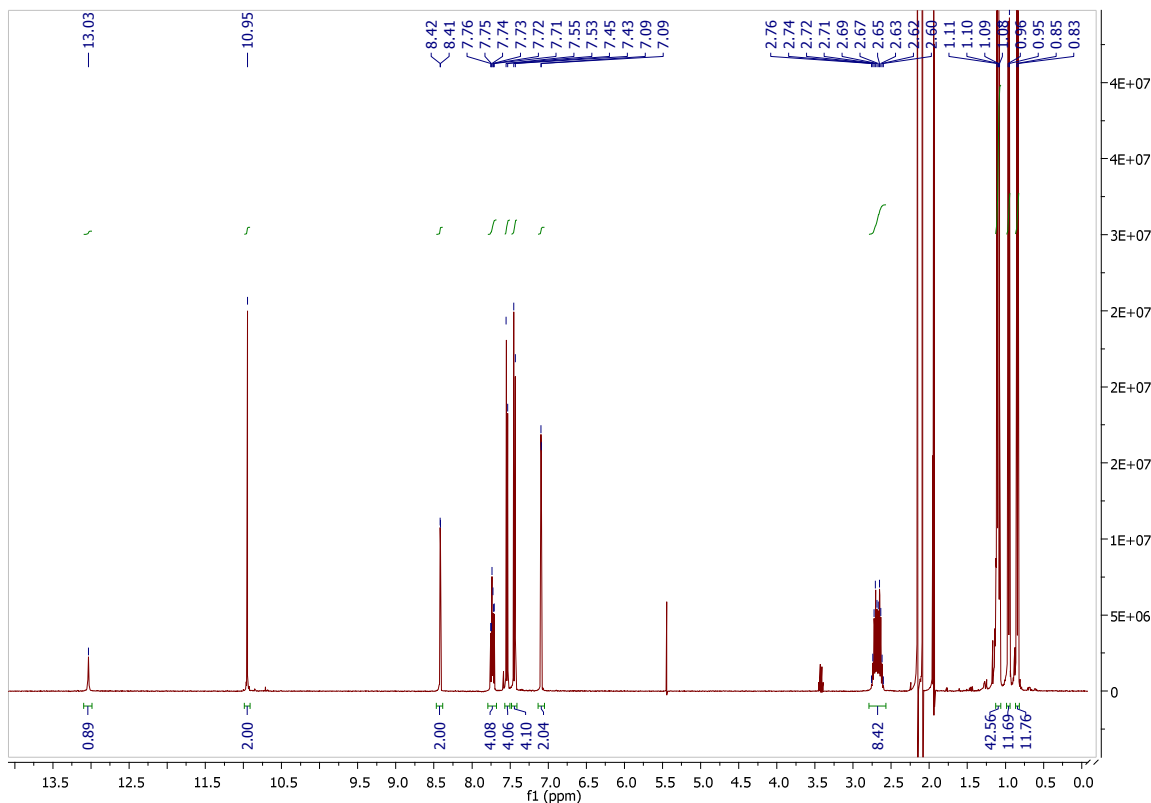
Figure 2.2: ^{1}H NMR of **7** in CD$_3$CN solvent

The crystal structure of **7** (Figure 2.3) indicates that the five-membered triazolium rings are not planar with the rigid carbazole backbone. The C1-C2-C3-C4 torsion angle is 31.7(3)° out of the carbazole plane. The second triazolium ring is also twisted out of the carbazole plane in the opposite direction as the first triazolium ring, with a C1M-C1L-C1K-C1F torsion angle of 18.6(4)°. The triazolium five-membered rings are however planar. This could be deduced from the torsion angles of the triazolium rings being almost 0°. The first triazolium ring has a C1-C2-N2-N3 torsion angle of 0.2(2)°, while the second triazolium ring has a C1M-C1L-N2'-N3' torsion angle of 0.5(2)°. The bond lengths on the triazolium rings are short, and are more characteristic of double bonds than of single bonds. The double bond character together with the torsion angle values being almost 0°, is indicative of a planar aromatic system. The C2-C1-N4 bond angle is 106.3(2)° while the C1L-C1M-N4' bond angle has a value of 106.6(2)°. These values are in the range of other diarylated triazolium ligand salts as reported by Bertrand and co-workers.[2]

From the solid state structure, it can be seen that the chloride counteranion does in fact occupy the centre of the tridentate pocket due to favourable bonding interactions between itself and the acidic protons. This supports the explanation of the large downfield shift of the three acidic protons observed in the ^{1}H NMR spectrum, due to the interaction of the protons with the chloride

52

counteranion. The H-bonding interaction is illustrated in Figure 2.3. The H1M-Cl1 bond distance is 2.4539(5) Å while the H1-Cl1 bonding distance is 2.15(6)Å. The H1a-Cl1 bond distance is longer (3.7502(6) Å), due to the triazolium ring being twisted in the opposite direction, increasing the distance between the chloride counteranion and the acidic proton.

The bulkiness of the ligand can be visualised when looking at the solid state structure. The 2,6-diisopropylphenyl wingtip substituents increases the steric bulk around the centre/pocket of the tridentate ligand. The wingtip substituents are twisted out of the triazolium plane, approximately perpendicular in order to decrease the steric repulsion experienced.
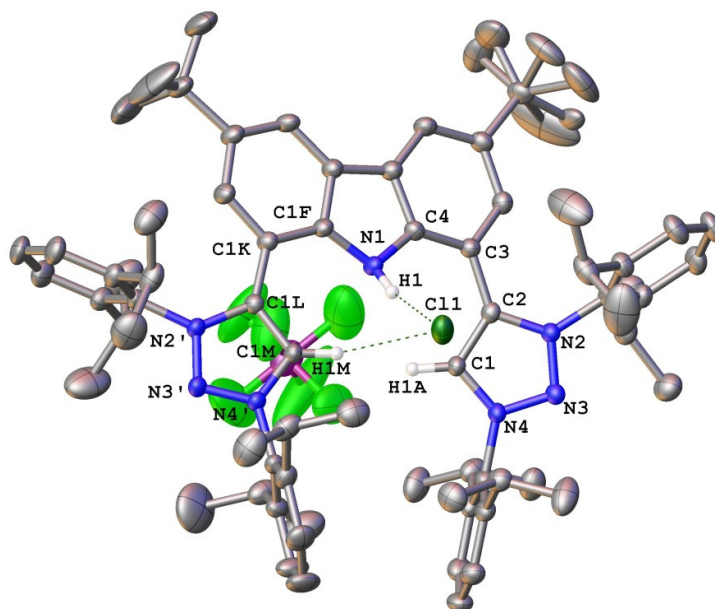
Figure 2.3: Crystal structure of **7**

2.3.8) Synthesis of 8

In order to deprotonate **7**, a strong non-nucleophilic base was used. Treatment of **7** with three equivalents of potassium hexamethyldisilazide (KHMDS) did not lead to the fully deprotonated ligand, where all three the acidic protons (eg. both *trz*H and carbazole-amino protons) were cleaved. Instead, only the amino moiety of the carbazole backbone was deprotonated to yield the mono-deprotonated amido-form **8**, with tetrahydrofuran (THF) as the solvent of the reaction mixture, illustrated in Scheme 2.19. Compound **8** is stable under aerobic conditions for a period of time. Product **8** bears a formal charge of +1.
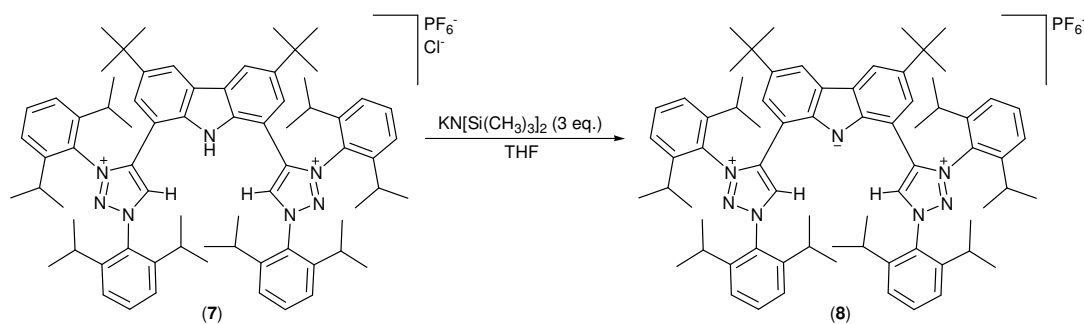
Scheme 2.19: Mono-deprotonation of **7** yielding **8**

The ¹H NMR spectrum (Figure 2.4) displays only one singlet with a large downfield shift, and not two as was the case with the ¹H NMR spectrum of **7**. The singlet peak with a downfield resonance of 10.04 ppm corresponds to the *trz***H** protons, integrating to 2H. The counteranion still present after the reaction was the hexafluorophosphate counteranion. This was supported by phosphorous NMR (³¹P NMR) and fluorine NMR (¹⁹F NMR) analysis, as well as mass spectrometry.
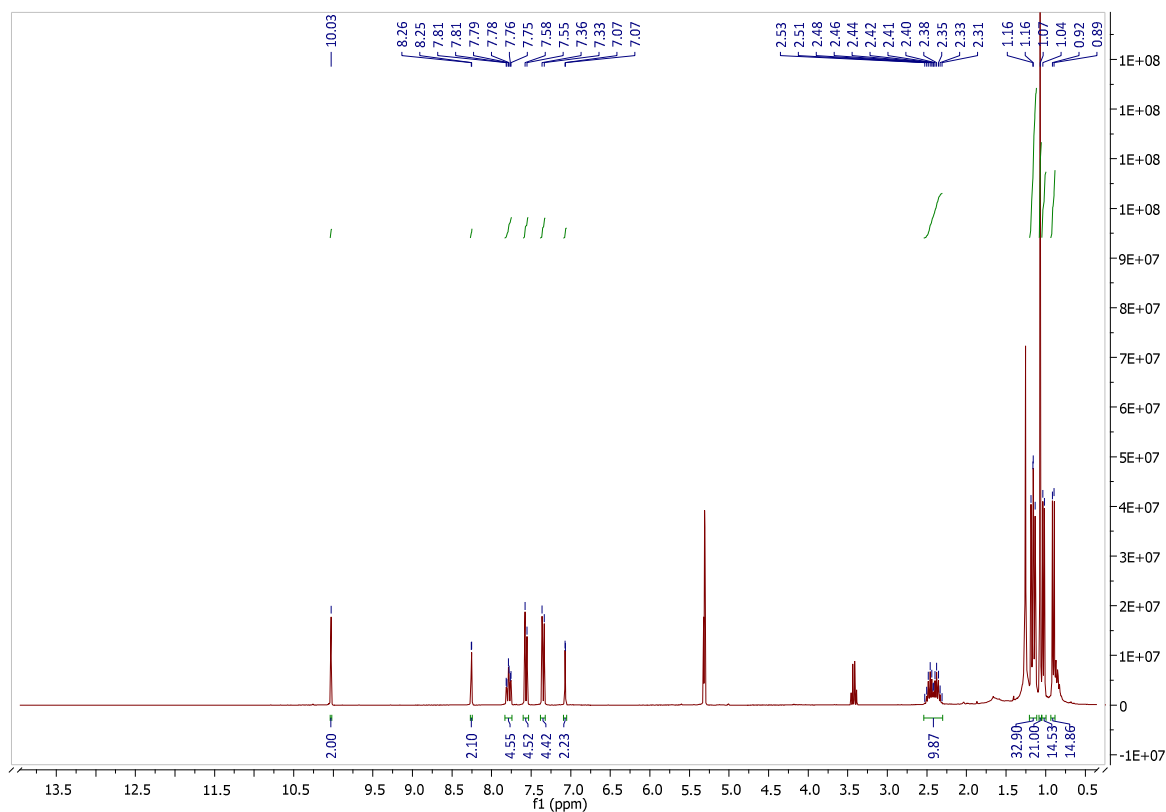
Figure 2.4: ¹H NMR of compound **8** in CD₂Cl₂ solvent

54

2.3.9) Synthesis of 9

The use of five equivalents of KHMDS, instead of three equivalents, allowed for the synthesis of **9** from **7**. Treatment of the dicationic ligand salt with excess base deprotonated all three acidic positions, leading to the formation of the tris-deprotonated free carbene adduct (Scheme 2.20). The reaction was completed using Et₂O as solvent. The two triazolium rings were deprotonated at the *trz***H** carbons, to yield the desired triazolylidenes. Both the triazolylidene five-membered rings have an overall neutral charge, due to the positive charge delocalised throughout the rings while the carbene carbons bear a negative charge. This results in a zwitterionic five-membered ring, or a mesoionic carbene. The amido moiety still retains its formal negative charge, which leaves the overall charge of the ligand as -1. As such, a potassium countercation stabilised the overall negative charge of the ligand, to yield the potassium free carbene adduct or the potassium free carbene salt. The potassium countercation was obtained from the KHMDS base after deprotonation of the acidic protons. Compound **9** could only be obtained working under strict anaerobic conditions, i.e. Schlenk techniques as well as utilisation of a glove box. The free carbene adduct decomposes immediately when exposed to aerobic conditions, but under anaerobic conditions, **9** is indefinitely stable, either in solution or in the solid state. The free carbene adduct **9** is also stable towards high temperatures, as was determined after refluxing a solution of **9** in THF. Once all three sites have been deprotonated, the ethereal free carbene adduct solution emits a green fluorescence when irradiated with ultra violet (UV) light at a wavelength of 354 nm. The emission of the fluorescence promises interesting application.
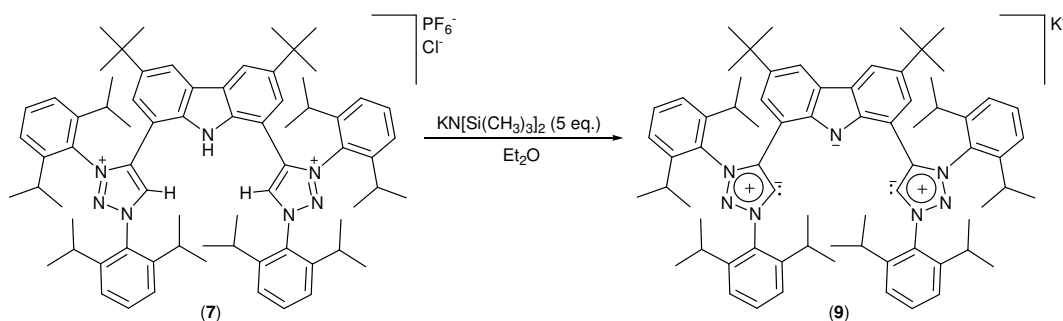
Scheme 2.20: tris-deprotonation of **7** yielding **9**

The tris-deprotonation of **7** to yield **9** was supported by NMR analysis. The disappearance of all three downfield acidic protons confirmed the loss of the two *trz***H** protons, and the carbazole amino proton. The ¹H NMR of **9** is displayed in Figure 2.5. The most downfield shifted resonance (8.57 ppm), is that of the aromatic protons of the carbazolide backbone.

55

In the ^{13}C NMR of **9**, a singlet peak at a downfield resonance of 195.0 ppm corresponds to the carbene carbon (Figure 2.6). A direct result of the carbene carbon being deprotonated is an increase in the amount of electron density situated around the carbene carbon. This increases the shielding around the carbene carbon, and as result, the downfield shift in the ^{13}C NMR spectra is not as far downfield as observed for other free carbene carbons that are generally more deshielded. In fact, the carbene carbon shift of **9** is upfield compared to some of the classical NHC free carbene carbons.[13] Compound **9** is also slightly shifted upfield when compared to the free triazolylidenes as reported by Bertrand and co-workers.[2,14] The carbene shift of **9** is not only characteristic of free triazolylidenes, but is also characteristic of K-**C**$_{carbene}$ adducts.[15] This supports the formation of a potassium adduct of the anionic ligand.
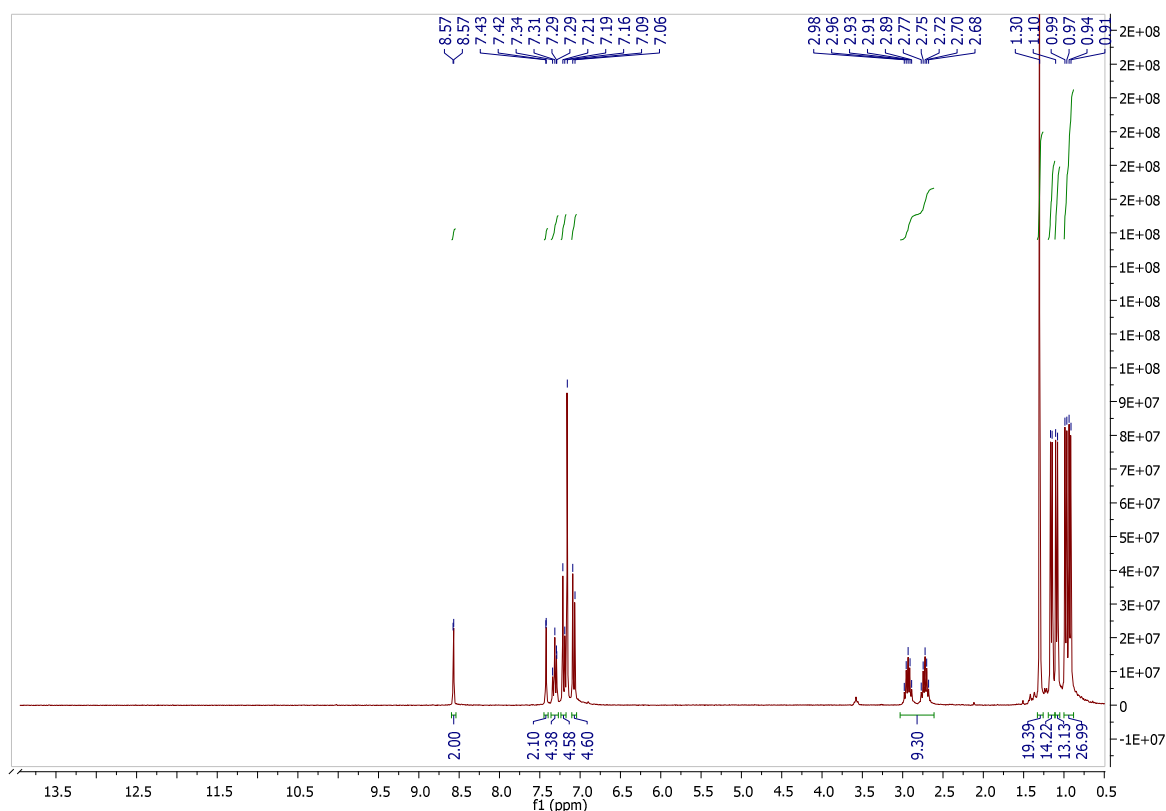
Figure 2.5: ^{1}H NMR of **9** in C$_6$D$_6$ solvent

[13] See review article and references therein: D. Bourissou, O. Guerret, F. P. Gabbaï, G. Bertrand, *Chem. Rev.*, 2000, **100**, 39 − 91.

[14] *(a)* G. Guisado-Barrios, J. Bouffard, B. Donnadieu, G. Bertrand, *Angew. Chem. Int. Ed.*, 2010, **49**, 4759 − 4762, *(b)* G. Guisado-Barrios, J. Bouffard, B. Donnadieu, G. Bertrand, *Organometallics*, 2011, **30**, 6017 − 6021.

[15] *(a)* M. S. Hill, G. Kociok-Köhn, D. J. MacDougall, *Inorg. Chem.,* 2011, **50**, 5234, (*b*) P. L. Arnold, M. Rodden, C. Wilson, *Chem. Commun.*, 2005, 1743, *(c)* M. Otto, S. Conejero, Y. Canac, V. D. Romanenko, V. Rudzevitch, G. Bertrand, *J. Am. Chem. Soc.,* 2004, **126**, 1016**,** (*d*) R. W. Alder, M. E. Blake, C. Borlotti, S. Bufali, C. P. Butts, E. Linehan, J. M. Oliva, A. G. Orpen, M. J. Quale, *Chem. Commun.*, 1999, 241.
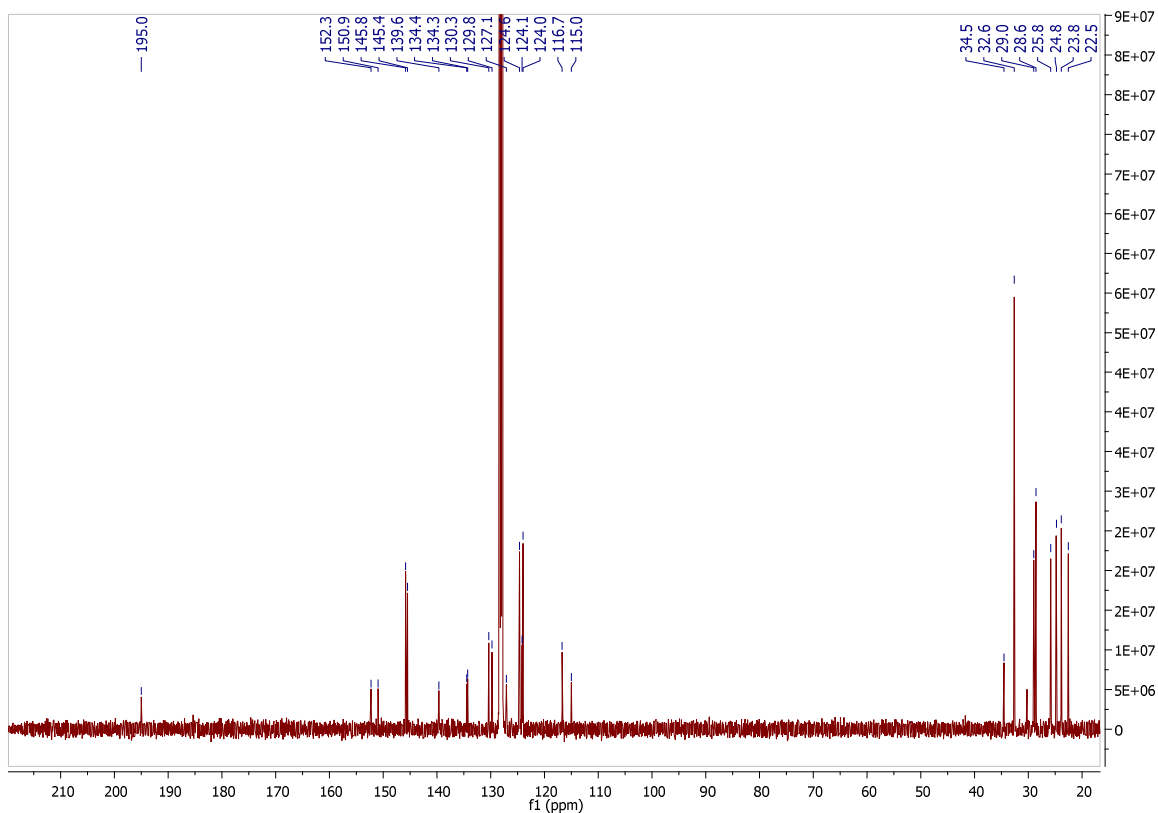
Figure 2.6: ^{13}C NMR of **9** in C$_6$D$_6$ solvent

Crystals suitable for single crystal X-ray diffraction could be obtained from a toluene and deuterated benzene mixture. The crystal structure confirms the formation of a potassium free carbene adduct. However, the resolved crystal structure (with atom numbering, Figure 2.7) features a dimer with two three-coordinated potassium atoms, bridging the two CNC ligands. The triazolylidene rings are not co-planar with the carbazolide backbone, as was the case with the triazolium rings of **7**. The one triazolylidene ring is twisted out of the carbazolide plane, with a C1-C2-C3-C4 torsion angle of 32.5(3)°. The second triazolylidene ring is also twisted out of the carbazolide plane in the same direction as the first triazolylidene, and not in the opposite direction as was the case for **7**. The C37-C38-C39-C40 torsion angle, for the second triazolylidene ring, is 69.3(3)°. This triazolylidene ring, the second triazolylidene ring, deviates significantly from the carbazolide plane, and is almost at a right angle to the plane of the carbazolide. This could be due to the favourable interaction between the C37 carbene carbon and both of the potassium atoms, facilitating the twist of the triazolylidene ring out of the carbazolide plane in order to maximize the C-K interactions. The free carbene adduct features K-**C**$_{carbene}$ bond distances that are well in accordance with other reported K-**C**$_{carbene}$ bond distances.[15] The shorter N1-K1 (bond distance of 2.6247(13) Å) could be due to the stronger interaction between the more basic amido moiety and the potassium cation. The C1-K1 bond

57

distance is 2.8693(17) Å, while the same potassium cation interacts with the C37 carbene, with a K1-C37 bonding interaction of 3.1576(18) Å. The same C37 carbene also interacts with the second potassium cation K1', and the bond distance for that interaction is 2.9684(17) Å. It is postulated that the longer K1-C37 bond distance is due to the C37-C38-N7-N6-N5 triazolylidene ring being twisted out of the carbazolide plane as mentioned above. This would certainly increase the C37-K1 bond distance, while the C37-K1' bond distance decreases because the C37 carbene carbon is now twisted closer to the second K1' atom. The triazolylidene ring orientates itself in such a position as to maximise interactions with both of the potassium countercations.

The five-membered triazolylidene heterocycles retain their planarity and aromatic character. This could be deduced from the torsion angles and bond distances. The C1-C2-N4-N3 torsion angle has a value of 0.0(2)°, while the C37-C38-N7-N6 torsion angle is 0.16(19)°. These torsion angle values are even smaller than the torsion angle values for **7**. The smaller torsion angle could be due to the increased aromatic character of the triazolylidene ring, which was gained from the increased electron density in the ring after deprotonation of **7**. The increased aromatic character would be accompanied by a more planar ring to increase the extent of π-orbital overlap. The electron delocalisation throughout the ring would therefore increase, and ultimately result in a torsion angle value being very close, or equal to, zero. The bond distances between the atoms in the ring have double bond character, supporting the concept of aromaticity throughout the triazolylidene ring.

The C2-C1-N2 bond angle is 100.49(14)° and the C38-C37-N5 has a bond angle of 100.65(17)°. These bond angles are more acute than the corresponding bond angles of **7**. Upon deprotonation of the *trz*H carbon to obtain the carbene carbon, the σ-orbital gains s-character. This is not an uncommon feature, and has been mentioned in numerous review articles.[5,16]

---

[16] See review articles and references therein: *(a)* K. F. Donnelly, A. Petronilho, M. Albrecht, *Chem. Commun.*, 2013, **47**, 1145 – 1159, *(b)* R. H. Crabtree, *Coord. Chem. Rev.*, 2013, **257**, 755 – 766, *(c)* M. Melaimi, M. Soleilhavoup, G. Bertrand, *Angew. Chem. Int. Ed.,* 2010, **49**, 8810 – 8849, *(d)* D. Martin, M. Melaimi, M. Soleilhavoup, G. Bertrand, *Organometallics,* 2011, **30**, 5304 – 5313, *(e)* A. Poulain, M. Iglesias, M. Albrecht, *Curr. Org. Chem.,* 2011, **15**, 3325, (*f*) A. Kruger, M. Albrecht, *Aust. J. Chem.,* 2011, **64**, 1113 – 1117, *(g)* M. Albrecht, *Chimia,* 2009, **63**, 105, *(h)* O. Schuster, L. Yang, H. G. Raubenheimer, M. Albrecht, *Chem. Rev.,* 2009, **109**, 3445 – 3478, *(i)* P. L. Arnold, S. Pearson, *Coord. Chem. Rev.*, 2007*,* **251**, 596 – 609.
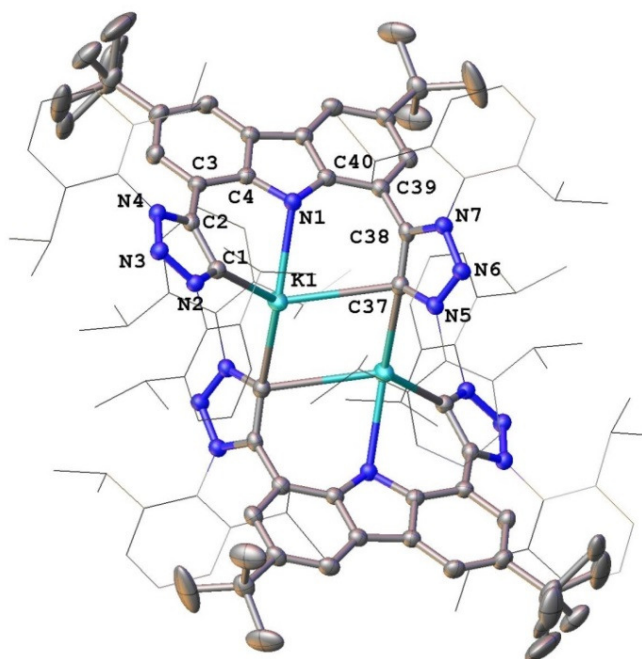
Figure 2.7: Dimeric crystal structure of **9**

The formation of a dimeric compound in the solid state could be a result of the formation of a cage-like compound that would increase the steric protection around the pocket formed in the CNC dimer, allowing the isolation of this extremely reactive compound. As is evident from the dimeric crystal structure and the space-filling model represented in Figure 2.8, the 2,6-diisopropylphenyl substituents are positioned around the centre of the dimeric ligand, which increase the steric protection around the four carbene carbons and the two amido moieties.
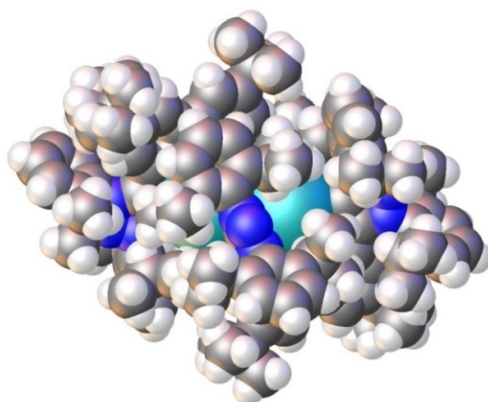
Figure 2.8: Space filling model for the dimeric crystal structure of **9**

59

2.3.10) Synthesis of 10

The same procedure that was used in order to synthesise **7**, was employed during the synthesis of **10**. The oxidising agent ^{t}BuOCl was added, in a drop-wise manner, to a DCM solution of **4**, **6** and KPF$_6$ which had been cooled down to -78 °C. After stirring of the reaction mixture for 20 hours, filtration followed by trituration yielded **10** as an off-white solid with a yield of 95% (Scheme 2.21). The formation of **10** was supported by NMR, MS, and XRD analysis.
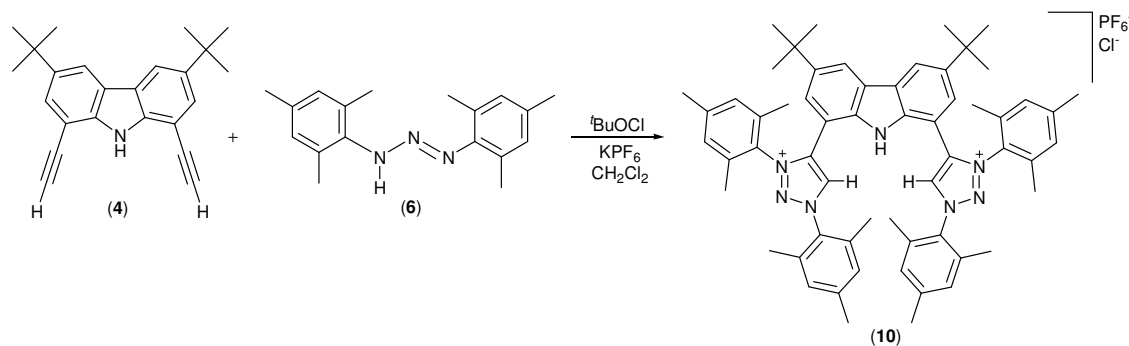
Scheme 2.21: Synthesis of **10** *via* a 3 + 2 cycloaddition reaction between **4** and **6**

The ^{1}H NMR spectrum displayed a broad signal with a resonance of 11.50 ppm and an integration of 1H, which corresponds to the carbazole amino proton (Figure 2.9). The two *trz*H protons appear as a singlet with a downfield shift of 10.06 ppm. As was the case for **7**, the three acidic protons of **10** also resonate at low field. This again points to the formation of the bis(triazolium)carbazole ligand salt with a chloride counteranion 'trapped' in the pocket of the tridentate ligand, where it will enjoy favourable interactions with the acidic protons. The second counteranion is a PF$_6^-$ anion, as determined with ^{19}F and ^{31}P NMR analysis.

60
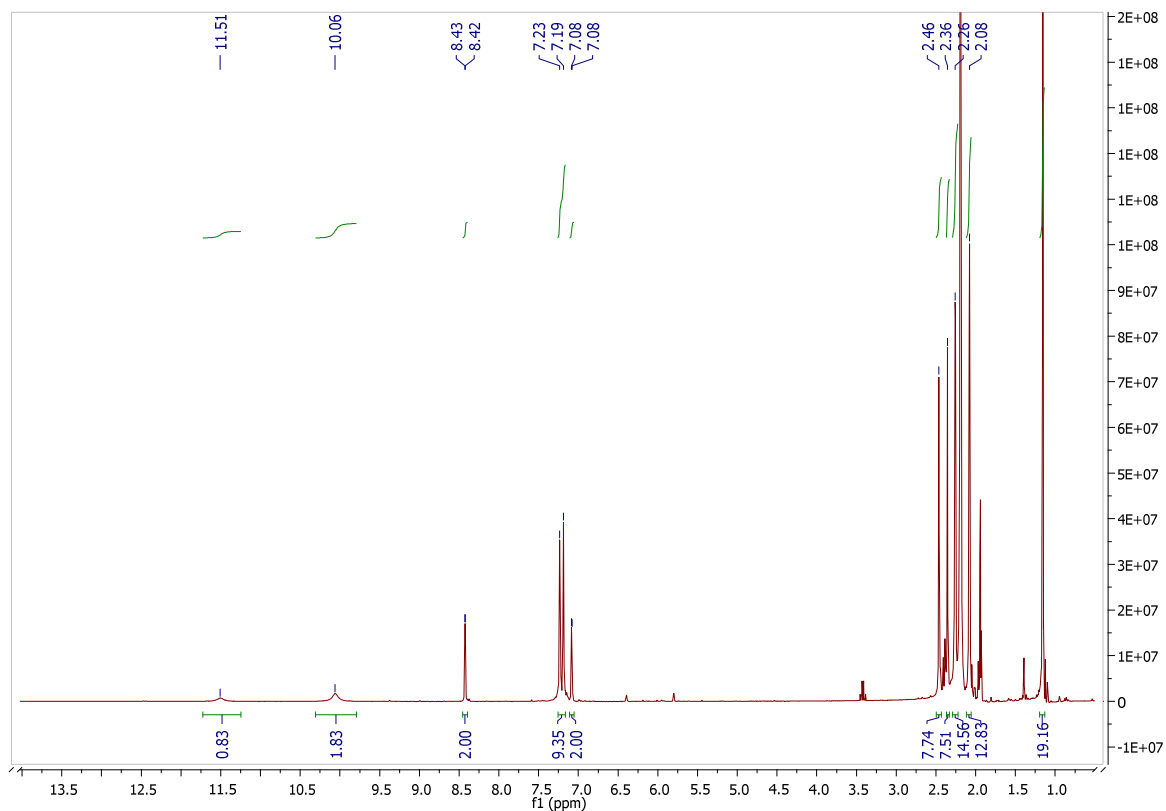
Figure 2.9: ¹H NMR of **10** in CD₃CN solvent

Crystals suitable for single crystal X-ray diffraction were obtained from an acetonitrile solution layered with hexanes. The crystal structure, displayed in Figure 2.10 with atom numbering, confirms that the tridentate ligand pocket does in fact contain a chloride counteranion interacting with the acidic protons. The triazolium rings are also not co-planar with the carbazole backbone. The first triazolium ring has a C24-C23-C12-C7 torsion angle of 16.7(3)°. The second triazolium ring is significantly twisted out of the carbazole plane with a C22-C21-C6-C1 torsion angle of 44.2(3)°. The second triazolium ring of **10** is twisted out of the carbazole plane with a value of more than 10° when compared to the triazolium ring of **7** (see Figure 2.3). This increased deviation from co-planarity can be a result of less steric hindrance due to the use of 2,4,6-trimethylphenyl wingtip groups and not the bulky 2,6-diisopropylphenyl wingtip substituents of **7**. The decreased steric hindrance can allow the wingtip substituents to twist with the triazolium ring even further out of the carbazole plane and not experience as great a steric repulsion from the wingtip groups on the other triazolium ring. The triazolium ring with a torsion angle of 16.7(3)° has orientated itself in order to maximise the interaction between the chloride counteranion and the *trz*H proton. The H22-Cl1 bond distance is 2.45(2) Å, which is slightly shorter than the H1M-Cl1 bonding distance of 2.4539(5) Å in compound **7** (see Figure 2.3). Compound **10** has an H1-Cl1 bond distance value of 2.202(19) Å, while

61

the H24-Cl1 bond distance is 3.15(2) Å long. The long H24-Cl1 bond distance is due to the triazolium ring being twisted away from the chloride anion, in the solid state structure.

The triazolium torsion angles of **10** are also close to zero. The C22-C21-N4-N3 torsion angle is 0.5(2)°, while the C24-C23-N7-N6 torsion angle has a value of 0.26(17)°. The bond distances within the triazolium ring are also more characteristic of double bonds than of single bonds. Similarly to **7**, both factors support aromaticity of the triazolium rings. The N2-C22-C21 and the N5-C24-C23 bond angles are also comparable to that of **7**, as well as other diarylated triazolium rings reported by Bertrand and co-workers.[2] The N2-C22-C21 bond angle is 106.11(13)° while the N5-C24-C23 bond angle has a value of 106.96(14)°.
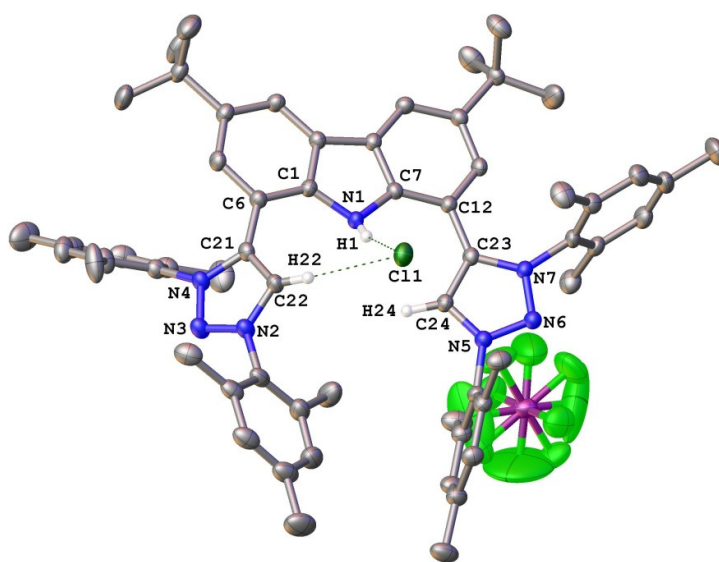
Figure 2.10: Crystal structure of **10**

2.3.11) Synthesis of 11

Reacting **10** with five equivalents of KHMDS yielded **11** after filtration and *in vacuo* evaporation of the solvent (Scheme 2.22). The reaction was completed using Et$_2$O as solvent. Deprotonation of the two *trz*H yields the mesoionic carbenes; the triazolylidenes. In addition, the amino moiety was also deprotonated to yield the amido moiety, as was the case for **9**. Disappearance of the acidic protons, and formation of the biscarbene **11**, was confirmed by NMR spectroscopy. Similar to the synthetic procedure employed for the synthesis of **9**, strict anaerobic conditions had to be enforced in order to obtain **11**. The free carbene adduct is stable under anaerobic conditions. However, **11** starts to slowly decompose after a few days at room temperature under a nitrogen gas atmosphere. Again,

an ethereal solution of the free carbene adduct **11** emits a green fluorescence when irradiated with ultra violet (UV) light at a wavelength of 354 nm.
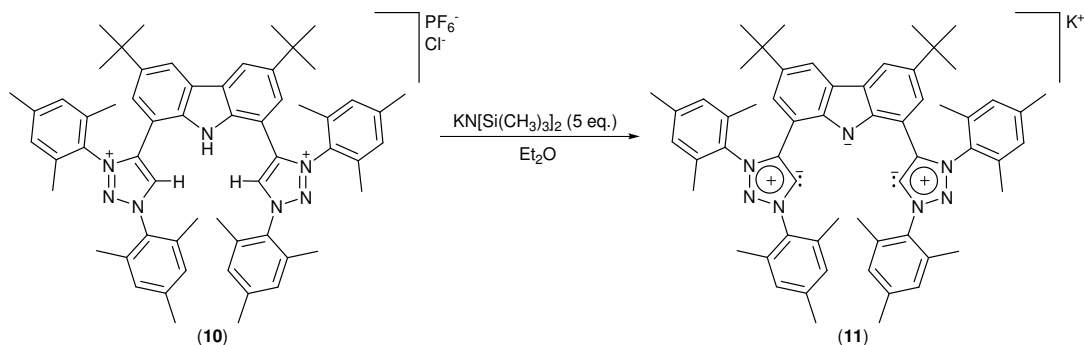
Scheme 2.22: Synthesis of the potassium free carbene adduct **11** from **10**

As is evident from the ^{1}H NMR spectrum (Figure 2.11), the peaks resonating at 8.44 ppm are the most downfield shifted protons, which correspond to the aromatic protons of the carbazole backbone. The disappearance of all three the acidic protons (see Figure 2.9 for ligand salt) confirms the clean deprotonation of the ligand salt. A downfield shifted singlet peak in the ^{13}C NMR spectra (Figure 2.12) resonating at 195.0 ppm, corresponds to the carbene carbon. The resonance of the carbene carbon for **11** is exactly the same as for the carbene carbon resonance of **9**. This is expected because the only difference between the two free carbene ligand adducts **9** and **11**, is the substitution of the 2,6-diisopropylphenyl wingtip groups of **9** for the 2,4,6-trimethylphenyl wingtip groups in **11**. Substitution of the bulky phenyl wingtip groups with alkyl functionalities will have a significant difference in the resonance of the carbene carbon, as discussed during Chapter 1. The carbene carbon resonance for **11** (195.0 ppm) is also characteristic of K-$C_{carbene}$ adducts, as mentioned earlier. NMR analysis of **11** and its expected similarities with the NMR spectra of **9**, clearly confirms the formation of **11** even though crystals for X-ray diffraction analysis could not be obtained.
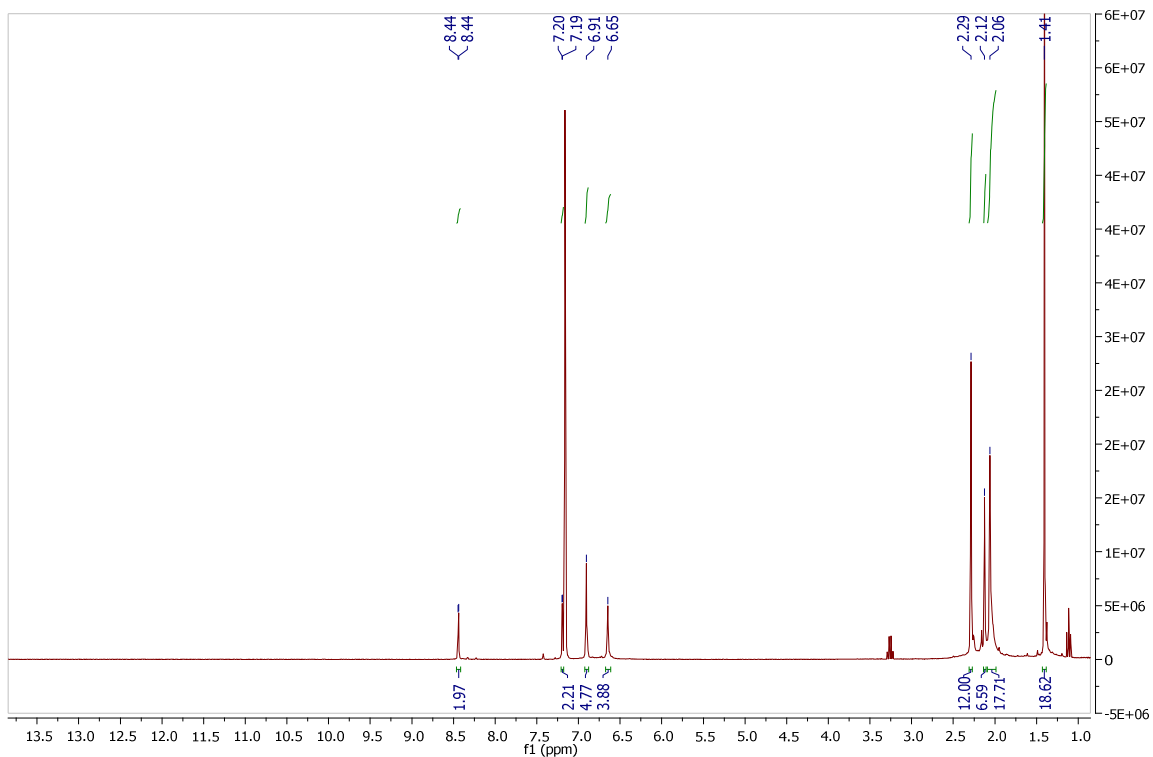
Figure 2.11: ^{1}H NMR of **11** in C$_6$D$_6$ solvent
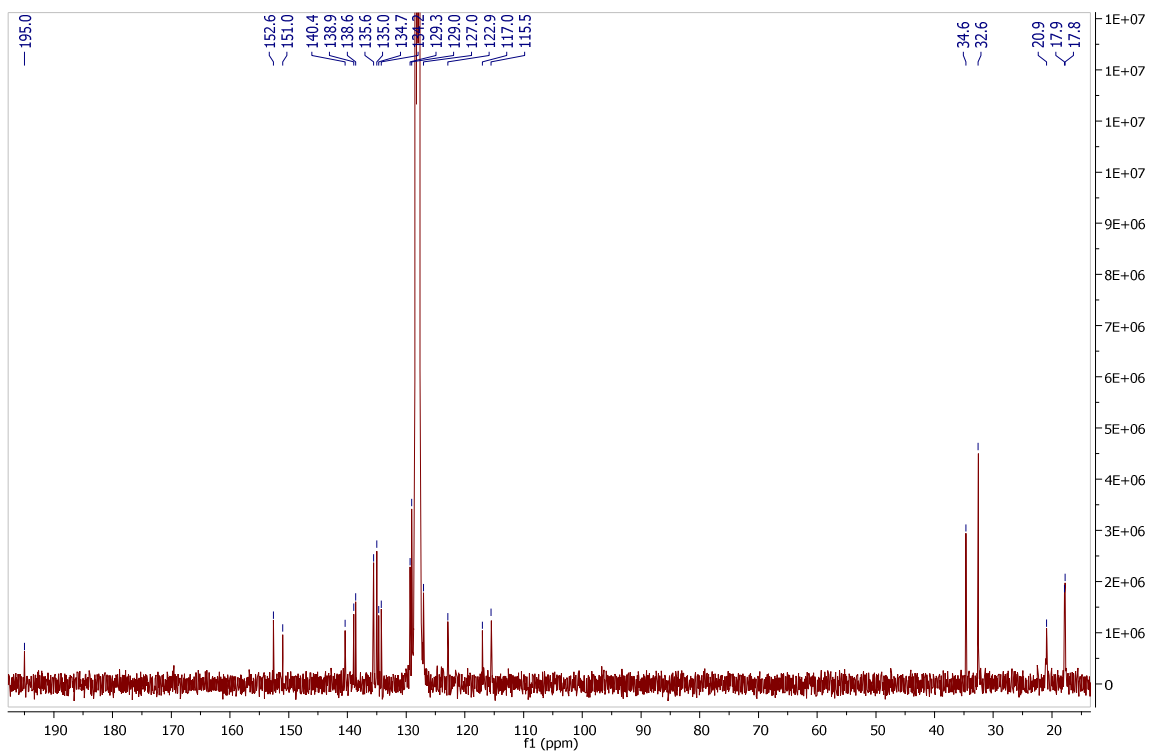
Figure 2.12: ^{13}C NMR of **11** in C$_6$D$_6$ solvent

64

2.4) Conclusion

The two tridentate bis(triazolium)carbazole ligand salts **7** and **10**, were obtained in good to excellent yields after subjecting the corresponding dialkynecarbazole and diarylated triazene reagents to a 3 + 2 cycloaddition reaction, using ^{t}BuOCl as the oxidising agent in the presence of KPF$_6$. The dialkynecarbazole and triazene reagents were individually obtained through various organic transformation reactions from the relevant starting compounds. The ligand salts had increased steric bulk, accessible only through employing the 3 + 2 cycloaddition approach, and not the CuAAC method (see Section 2.1). The novel compounds **7** and **10** constitute the first known examples of a ligand featuring an amino moiety together with two triazolium flanking groups.

The extremely reactive, tris-deprotonated, potassium free carbene adduct could be obtained by reacting compound **7** with five equivalents of KHMDS, using Et$_2$O as solvent. A green fluorescence is emitted once all three acidic positions had been cleaved, to yield the free carbene adduct. The disappearance of the acidic *trz*H and amino protons where unambiguously confirmed, not only with spectroscopic techniques, but also with X-ray diffraction analysis. The free carbene salt displayed a dimeric structure in the solid state, encapsulating the tridentate pocket and forming a 'cage-like' structure around the reactive amido and carbene moieties in the centre of the pocket (see, Figure 2.7 and 2.8). The steric bulk surrounding the triazolylidenes in compound **9** allowed for the isolation of compound **9**, which is indefinitely stable under anaerobic conditions.

In addition, compound **10** could also be deprotonated with five equivalents of KHMDS to yield the tris-deprotonated free carbene adduct **11**. The disappearance of the three acidic protons was confirmed with NMR analysis, supporting the formation of the free carbene salt. However, crystallisation was unsuccessful, due to the decomposition of this potassium carbene adduct after a few days. This could be attributed to the lesser steric bulk obtained when employing the 2,4,6-timethylphenyl substituents, rather than the 2,6-diisopropylphenyl wingtip groups, decreasing the steric bulk around the tridentate pocket.

The clean deprotonation of the ligand salts were accomplished, and as such, the ligands can now be metallated using various metal precursors. The metallation techniques, such as deprotonation of the ligand followed by metallation, will be discussed in the following chapters.

2.5) Experimental

2.5.1) 3,6-Di-*tert*-butyl-9H-carbazole (1)
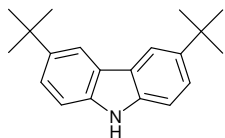
The synthesis of 3,6-di-*tert*-butyl-9H-carbazole (**1**) was done through an adaptation of the procedure reported by Promarak *et al*.[12] A 500 mL, 3-necked round bottom flask was charged with 9H-carbazole (10.00 g, 59.8 mmol) and dry $ZnCl_2$ (24.46 g, 179.4 mmol). The flask was purged with N_2 (g) and the solids were dissolved by the addition of nitromethane (90.0 mL). At room temperature (RT) whilst stirring, 2-chloro-2-methylpropane (20.1 mL, 179.4 mmol) was added drop-wise to the solution. The thick brown solution was stirred for 72 hours. The solution was added to water (200 mL), followed by the addition of DCM (100 mL). The aqueous phase was washed with DCM (3 x 100 mL) and the organic fractions were combined, washed with water (100 mL) and finally with sodium carbonate brine solution (100 mL). The organic phase was dried using anhydrous Na_2SO_4 and concentrated to yield **1** (16.18 g, 57.9 mmol, 97%) as an orange solid. ^1H NMR δ_H ($CDCl_3$, 300 MHz) 8.12 (2H, d, J = 1.8 Hz, Ar**H**), 7.78 (1H, s, N**H**), 7.49 (2H, dd, J = 8.4 Hz, 1.9 Hz, Ar**H**), 7.32 (2H, d, J = 8.4 Hz, Ar**H**), 1.49 (18H, s, C(C**H₃**)₃). ^{13}C NMR δ_C ($CDCl_3$, 75 MHz) 142.4 (Ar**C**q), 138.2 (Ar**C**q), 123.7 (Ar**C**H), 123.4 (Ar**C**q), 116.3 (Ar**C**H), 110.2 (Ar**C**H), 34.8 (**C**(CH₃)₃), 32.2 (C(**C**H₃)₃).

2.5.2) 1,8-Dibromo-3,6-di-*tert*-butyl-9H-carbazole (2)
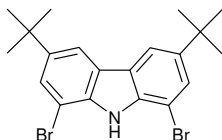
1,8-dibromo-3,6-di-*tert*-butyl-9H-carbazole (**2**) was synthesised through an adapted procedure as reported by Williams and co-workers.[11] A 500 mL, 3-necked round bottom flask was loaded with **1** (30.00 g, 107.4 mmol) and dissolved by the addition of glacial acetic acid (300 mL). The vessel was subsequently purged with N_2 (g). In the absence of light, Br_2 (*l*) (12.2 mL, 236.2 mmol) was added drop-wise to the reaction mixture while stirring vigorously at RT. The reaction was stirred in the dark for two days, after which water (400 mL) was added to the reaction mixture. A creamy brown solid was filtered and re-dissolved in Et_2O. The organic phase was washed with a 1M aqueous NaOH solution (4 x 200 mL) and subsequently with a 1M aqueous $NaHCO_3$ solution (4 x 200 mL). The organic phase was separated and dried over $MgSO_4$. The solvent was evaporated to obtain **2** (44.92 g, 102.7 mmol, 96%) as a brown solid. ^1H NMR δ_H ($CDCl_3$, 400 MHz) 8.15 (1H, br s, N**H**) 7.99 (2H, d, J = 1.6 Hz, Ar**H**), 7.65 (2H, d, J = 1.6 Hz, Ar**H**), 1.45 (18H, s, C(C**H₃**)₃). ^{13}C NMR δ_C ($CDCl_3$, 100 MHz) 144.9 (Ar**C**q), 136.5 (Ar**C**q), 126.8 (Ar**C**H), 125.0 (Ar**C**q), 116.1 (Ar**C**H), 104.1 (Ar**C**q), 35.1 (**C**(CH₃)₃), 32.1 (C(**C**H₃)₃).

2.5.3) 3,6-Di-*tert*-butyl-1,8-bis(2-(trimethylsilyl)ethynyl)-9H-carbazole (3)
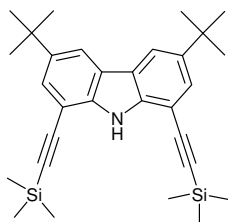
3,6-di-*tert*-butyl-1,8-bis(2-(trimethylsilyl)ethynyl)-9H-carbazole was synthesised by loading a 500 mL 3-necked round bottom flask with **2** (30.00 g, 68.6 mmol), Pd(PPh$_3$)$_2$Cl$_2$ (3.85 g, 5.5 mmol) and CuI (1.31 g, 6.9 mmol). The vessel was subsequently purged with N$_2$ (g). Toluene (250 mL) was added to the solid mixture, as well as degassed diisopropylamine (60 mL). The resulting solution was stirred at RT for 30 min, which was followed by the slow drop-wise addition of trimethylsilylacetylene (29.3 mL, 205.9 mmol). The resulting solution was stirred at RT for two days. The solvent was evaporated, and the solid mixture was dry loaded onto a silica plug. The mixtures of the mono- and di-coupled products were eluted from the silica plug with hexane as solvent. The solvent was evaporated, and the yellow product was subjected to a second coupling reaction. To the mixture of mono- and di-coupled products were added to Pd(PPh$_3$)$_2$Cl$_2$ (3.85 g, 5.5 mmol) and CuI (1.31 g, 6.9 mmol). The vessel was again purged with N$_2$ (g), followed by the addition of toluene (250 mL) and degassed diisopropylamine (60 mL). The resulting solution was stirred at RT for 30 min. Trimethylsilylacetylene (29.3 mL, 205.9 mmol) was added drop-wise to the solution, and allowed to stir again for two days. After two days, the solvent was evaporated. The solid mixture was dry loaded onto a silica plug and the product eluted with hexanes. Evaporation of the solvent yielded **3** (28.86 g, 61.2 mmol, 89%) as a yellow solid and as the only product of the reaction. ^{1}H NMR δ_H (CDCl$_3$, 300 MHz) 8.37 (1H, br s, N**H**) 8.07 (2H, d, J = 1.5 Hz, Ar**H**), 7.62 (2H, d, J = 1.8 Hz, Ar**H**), 1.46 (18H, s, C(C**H**$_3$)$_3$), 0.37 (18H, s, Si(C**H**$_3$)$_3$). ^{13}C NMR δ_C (CDCl$_3$, 75 MHz) 142.7 (Ar**C**$_q$), 139.2 (Ar**C**$_q$), 127.0 (Ar**C**H), 123.3 (Ar**C**$_q$), 117.9 (Ar**C**H), 105.1 (Ar**C**$_q$), 101.6 (**C**≡CSi(CH$_3$)$_3$)), 98.8 (C≡**C**Si(CH$_3$)$_3$)), 34.9 (**C**(CH$_3$)$_3$), 32.1 (C(**C**H$_3$)$_3$), 0.4 (Si(**C**H$_3$)$_3$).

2.5.4) 3,6-Di-*tert*-butyl-1,8-diethynyl-9H-carbazole (4)
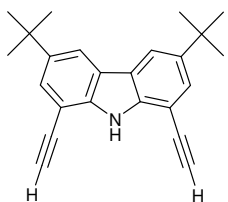
The synthesis of 3,6-di-*tert*-butyl-1,8-diethynyl-9H-carbazole was done through an adaptation of the previously reported literature procedure.[2] Compound **3** (15.00 g, 31.8 mmol) and anhydrous K$_2$CO$_3$ (35.15 g, 254.3 mmol) was loaded into a 500 mL, two 2-necked round bottom flask. To the solid mixture was added methanol (250 mL) at RT. The solution was stirred for 12

hours at RT. A white precipitate was filtered off and discarded from the creamy brown solution, with subsequent evaporation of the solvent. The brown residue was re-dissolved in DCM, with the addition of water. The two phases were separated, and the organic phase was washed three times with copious amounts of water. The organic phase was dried with $MgSO_4$ and the solvent evaporated *in vacuo* to yield **4** (9.99 g, 30.5 mmol, 96%) as a brown solid. No further purification was needed. ^{1}H NMR δ_H (CDCl₃, 300 MHz) 8.48 (1H, broad s, N**H**), 8.10 (2H, d, J = 1.5 Hz, Ar**H**), 7.66 (2H, d, J = 1.5 Hz, Ar**H**), 3.47 (2H, s, C≡C**H**), 1.46 (18H, s, C(C**H₃**)₃). ^{13}C NMR δ_C (CDCl₃, 75 MHz) 142.9 (Ar**C_q**), 139.3 (Ar**C_q**), 127.7 (Ar**C**H), 123.4 (Ar**C_q**), 118.1 (Ar**C**H), 104.0 (Ar**C_q**), 81.5 (**C**≡CH), 80.6 (C≡**C**H), 34.9 (**C**(CH₃)₃), 32.1 (C(**C**H₃)₃). HRMS (ESI-TOFMS): Calculated for $C_{24}H_{26}N^+$ (M+H)[+]: 328.2060, found: 328.2062.

2.5.5) 1,3-Bis-(2,6-diisopropylphenyl)triaz-1-ene (5)
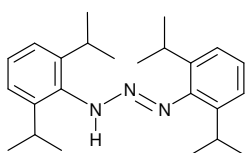
The 1,3-diarylated-triaz-1-enes were synthesised following an adaptation of the literature reported procedure.[2] A 500 mL, 2-necked round bottom flask was evacuated, purged with N_2 (g) and subsequently charged with 2,6-diisopropylbenzenamine (20.0 mL, 106.0 mmol). To the aniline was added Et₂O (200 ml) and the resulting solution cooled down to -30 °C. In the absence of light, isoamyl nitrite (7.1 mL, 53.0 mmol) was added drop-wise to the solution over a period of several minutes. The solution was stirred at -30 °C in the dark for one hour, before being removed from the cold bath and left to settle at RT overnight. The solvent was evaporated until 60% of the solvent had been removed. The concentrated dark orange solution was then left in the freezer at -15 °C until orange crystals crystallised out of the solution. The resulting crystals were washed with cold hexanes and dried under vacuum to yield **5** (5.81 g, 15.9 mmol, 30%) as yellow crystals. ^{1}H NMR δ_H (C₆D₆, 300 MHz) 9.61 (1H, broad s, N**H**), 7.22 – 7.08 (7H, broad m, Ar**H** overlaps with C₆D₆), 3.41 – 3.36 (4H, broad m, C**H**(CH₃)₂), 1.22 (24H, d, J = 6.9 Hz, CH(C**H₃**)₂).

2.5.6) 1,3-Bis-(2,4,6-trimethylphenyl)triaz-1-ene (6)
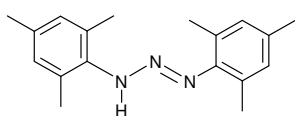
The preparation of **6** was done by using the same procedure as used for the synthesis of **5**. A 500 mL, 2-necked round bottom flask was evacuated and purged with N_2 (g) and subsequently charged with 2,4,6-trimethylbenzenamine (20.0 mL, 142.4 mmol). To the aniline was added Et₂O (200 mL) and the

68

resulting solution cooled down to -30 °C. The isoamyl nitrite (9.6 mL, 71.2 mmol) was added drop-wise to the solution over a period of several minutes, in the absence of light. The solution was stirred in the dark at -30 °C for one hour. After one hour, the vessel was removed from the cold bath and left to settle at RT overnight. The solvent was evaporated until 60% of the solvent had been removed. The concentrated dark yellow orange solution was then left in the freezer at -15 °C until yellow orange crystals crystallised out of the solution. The resulting crystals were washed with cold hexanes and dried under vacuum to yield **6** (4.41 g, 15.7 mmol, 22%) as yellow crystals. ^{1}H NMR δ_H (C_6D_6, 300 MHz) 8.76 (1H, broad s, N**H**), 6.75 (4H, broad s, Ar**H**), 2.24 (12H, broad s, ArC**H₃**), 2.13 (6H, broad s, ArC**H₃**).

2.5.7) 4,4'-(3,6-Di-*tert*-butyl-9H-carbazole-1,8-diyl)bis(1,3-bis(2,6-diisopropylphenyl)-1H-1,2,3-triazolium)hexafluorophosphate(V) chloride (**7**)
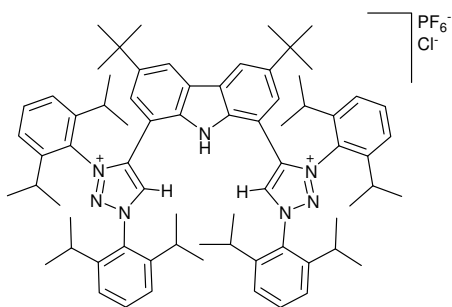
Compound **7** was prepared by modification of the literature reported procedure for 1,3-cycloaddition of triazenes and alkynes.[2] A 500 mL, 3-necked round bottom flask was charged with potassium hexafluorophosphate (3.81 g, 20.7 mmol), **3,6-di-*tert*-butyl-1,8-diethynyl-9H-carbazole** (2.00 g, 6.1 mmol) and **1,3-bis-(2,6-diisopropylphenyl)triaz-1-ene** (7.14 g, 19.5 mmol). The vessel was purged with N_2 (g) and the solids were dissolved in dry DCM (160 mL). The solution was cooled down to -78 °C and *tert*-BuOCl (2.2 mL, 18.3 mmol) was added drop-wise to the solution with subsequent stirring of the solution at -78 °C for two hours. After two hours, the solution was left to warm up to room temperature whilst stirring for 24 hours. The white precipitate was filtered from the red solution with subsequent evaporation of the solvent *in vacuo*. Trituration with hexanes followed by Et₂O yielded **7** as an off-white solid (5.14 g, 4.2 mmol, 68%); **m.p.** > 300 °C. Single crystals were grown from an acetone solution layered with hexane. ^{1}H NMR δ_H (CD₃CN, 400 MHz) 13.03 (1H, broad s, N**H**carb), 10.95 (2H, s, Ar**H**Triazolium), 8.42 (2H, d, *J* = 1.6 Hz, Ar**H**carb), 7.74 (2H, t, *J* = 7.8 Hz, Ar**H**Dipp), 7.73 (2H, t, *J* = 7.8 Hz, Ar**H**Dipp), 7.54 (4H, d, *J* = 8.0 Hz, Ar**H**Dipp), 7.44 (4H, d, *J* = 8.0 Hz, Ar**H**Dipp), 7.09 (2H, d, *J* = 2.0 Hz, Ar**H**Carb), 2.71 (4H, sept, *J* = 6.8 Hz, C**H**(CH₃)₂), 2.65 (4H, sept, *J* = 6.8Hz, C**H**(CH₃)₂), 1.10 (12H, d, *J* = 6.8 Hz, CH(C**H₃**)₂), 1.09 (18H, s, C(C**H₃**)₃), 1.09 (12H, d, *J* = 7.2 Hz, CH(C**H₃**)₂ overlaps with C(CH₃)₃), 0.96 (12H, d, *J* = 6.4 Hz, CH(C**H₃**)₂), 0.84 (12H, d, *J* = 6.8 Hz, CH(C**H₃**)₂). ^{13}C NMR

δ $_C$ (CD$_3$CN, 101 MHz) 146.7 (Ar**C**$_q$), 146.7 (Ar**C**$_q$), 145.2 (Ar**C**$_q$), 143.2 (Ar**C**$_q$), 140.0 (Ar**C**$_q$), 134.3 (Ar**C**H), 134.2 (Ar**C**H), 134.2 (Ar**C**H), 131.8 (Ar**C**$_q$), 131.1 (Ar**C**$_q$), 128.0 (Ar**C**$_q$), 127.0 (Ar**C**H), 126.1 (Ar**C**H), 125.9 (Ar**C**H), 122.4 (Ar**C**H), 107.9 (Ar**C**$_q$), 35.4 (**C**(CH$_3$)$_3$), 31.7 (C(**C**H$_3$)$_3$), 29.9 (**C**H(CH$_3$)$_2$), 29.6 (**C**H(CH$_3$)$_2$), 25.6 (CH(**C**H$_3$)$_2$), 24.8 (CH(**C**H$_3$)$_2$), 23.9 (CH(**C**H$_3$)$_2$), 22.5 (CH(**C**H$_3$)$_2$). ^{19}F NMR δ $_F$ (CD$_3$CN, 377 MHz) -72.9 (d, J = 708.0 Hz, P**F$_6$**). ^{31}P NMR δ $_P$ (CD$_3$CN, 162 MHz) -144.6 (sept, J = 706.4 Hz, **P**F$_6$). HRMS (ESI-TOFMS): Calculated for C$_{72}$H$_{93}$N$_7$$^{2+}$ [M]$^{2+}$: 527.8741, found: 527.8739.

2.5.8) Synthesis of (8)

A Schlenk tube was charged with **7** (200.0 mg, 1.6 x 10^{-4} mol) and KN[Si(CH$_3$)$_3$]$_2$ (96.8 mg, 4.9 x 10^{-4} mol) under a N$_2$ (g) atmosphere. The solids were dissolved by adding THF (12 mL) which was cooled down to -78 °C. The solution was stirred at -78 °C for 30 min, after which it was left to warm up to room temperature whilst stirring for an additional 3 hours. The solvent was evaporated and the residue washed with hexanes (4 x 10 mL) and Et$_2$O (3 x 10 mL), followed by extraction of the product with DCM (3 x 10 mL). Evaporation of the solvent yielded **8** (181.0 mg, 1.5 x 10^{-4} mol, 93%) as a red solid. ^{1}H NMR δ $_H$ (CD$_2$Cl$_2$, 300 MHz) 10.03 (2H, s, Ar**H**$_{Triazolium}$), 8.25 (2H, d, J = 1.8 Hz, Ar**H**$_{carb}$), 7.79 (2H, t, J = 7.8 Hz, Ar**H**$_{Dipp}$), 7.78 (2H, t, J = 7.8 Hz, Ar**H**$_{Dipp}$), 7.57 (4H, d, J = 7.8 Hz, Ar**H**$_{Dipp}$), 7.35 (4H, d, J = 8.1 Hz, Ar**H**$_{Dipp}$), 7.07 (2H, d, J = 1.8 Hz, Ar**H**$_{Carb}$), 2.46 (4H, sept, J = 6.9 Hz, C**H**(CH$_3$)$_2$), 2.38 (4H, sept, J = 6.9 Hz, C**H**(CH$_3$)$_2$), 1.17 (12H, d, J = 6.9 Hz, CH(C**H$_3$**)$_2$), 1.14 (12H, d, J = 6.9 Hz, CH(C**H$_3$**)$_2$), 1.07 (18H, s, C(C**H**$_3$)$_3$), 1.03 (12H, d, J = 6.9 Hz, CH(C**H$_3$**)$_2$), 0.90 (12H, d, J = 6.9 Hz, CH(C**H$_3$**)$_2$). ^{13}C NMR δ $_C$ (CD$_2$Cl$_2$, 101 MHz) 150.8 (Ar**C**$_q$), 145.8 (Ar**C**$_q$), 145.8 (Ar**C**$_q$), 145.5 (Ar**C**$_q$), 137.6 (Ar**C**$_q$), 133.8 (Ar**C**H), 132.5 (Ar**C**$_q$), 131.6 (Ar**C**$_q$), 130.5 (Ar**C**H), 128.0 (Ar**C**$_q$), 126.6 (Ar**C**H), 125.8 (Ar**C**H), 121.8 (Ar**C**H), 121.0 (Ar**C**H), 105.3 (Ar**C**$_q$), 34.6 (**C**(CH$_3$)$_3$), 32.0 (C(**C**H$_3$)$_3$), 30.0 (**C**H(CH$_3$)$_2$), 29.7 (**C**H(CH$_3$)$_2$), 25.1 (CH(**C**H$_3$)$_2$), 24.9 (CH(**C**H$_3$)$_2$), 24.1 (CH(**C**H$_3$)$_2$), 23.1 (CH(**C**H$_3$)$_2$). ^{19}F NMR δ $_F$ (CD$_3$CN, 377 MHz) -73.0 (d, J = 706.2 Hz, P**F$_6$**). ^{31}P NMR δ $_P$ (CD$_3$CN, 162 MHz) -144.63 (sept, J = 706.2 Hz, **P**F$_6$). HRMS (ESI-TOFMS): Calculated for C$_{72}$H$_{92}$N$_7$$^+$ [M]$^+$: 1054.7414, found: 1054.7418.

70

2.5.9) Synthesis of (9)
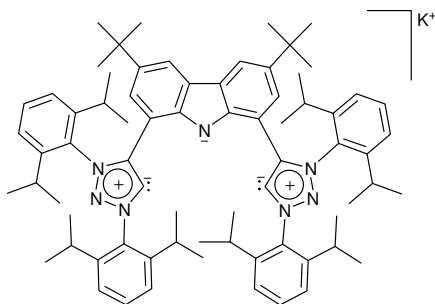
A flame dried Schlenk tube was charged with **7** (100.0 mg, 8.1×10^{-5} mol) and KN[Si(CH₃)₃]₂ (80.6 mg, 4.0×10^{-4} mol) inside the glove box. The solids were suspended in Et₂O (12 mL) at -78 °C, followed by stirring the mixture at -78 °C for 30 min before being removed from the cold bath and stirred an additional 3 hours at room temperature. The solvent was evaporated *in vacuo* and the product extracted with hexanes. Evaporation of the solvent yielded **9** (63.8 mg, 5.8×10^{-5} mol, 72%) as a yellow green solid; **m.p.** 262 - 264 °C (dec). ^{1}H NMR δ $_H$ (C₆D₆, 300 MHz) 8.57 (2H, d, *J* = 1.8 Hz, Ar**H**$_{carb}$), 7.42 (2H, d, *J* = 1.8 Hz, Ar**H**$_{carb}$), 7.32 (2H, t, *J* = 7.8 Hz, Ar**H**$_{Dipp}$), 7.32 (2H, t, *J* = 7.9 Hz, Ar**H**$_{Dipp}$), 7.20 (4H, d, *J* = 7.5 Hz, Ar**H**$_{Dipp}$), 7.08 (4H, d, *J* = 7.8 Hz, Ar**H**$_{Dipp}$), 2.93 (4H, sept, *J* = 6.9 Hz, C**H**(CH₃)₂), 2.72 (4H, sept, *J* = 6.9 Hz, C**H**(CH₃)₂), 1.30 (18H, s, C(C**H₃**)₃), 1.16 (12H, d, *J* = 6.9 Hz, CH(C**H₃**)₂), 1.09 (12H, d, *J* = 6.6 Hz, CH(C**H₃**)₂), 0.98 (12H, d, *J* = 6.9 Hz, CH(C**H₃**)₂), 0.93 (12H, d, *J* = 6.9 Hz, CH(C**H₃**)₂). ^{13}C NMR δ $_C$ (C₆D₆, 75 MHz) 195.0 (**C**$_{Carbene}$), 152.3 (Ar**C**$_q$), 151.0 (Ar**C**$_q$), 145.8 (Ar**C**$_q$), 145.4 (Ar**C**$_q$), 139.6 (Ar**C**$_q$), 134.5 (Ar**C**$_q$), 134.4 (Ar**C**$_q$), 130.4 (Ar**C**H), 129.8 (Ar**C**H), 127.1 (Ar**C**$_q$), 124.6 (Ar**C**H), 124.1 (Ar**C**H), 124.0 (Ar**C**H), 116.7 (Ar**C**H), 115.0 (Ar**C**$_q$), 34.5 (**C**(CH₃)₃), 32.6 (C(**C**H₃)₃), 29.0 (**C**H(CH₃)₂), 28.6 (**C**H(CH₃)₂), 25.9 (CH(**C**H₃)₂), 24.8 (CH(**C**H₃)₂), 23.8 (CH(**C**H₃)₂), 22.6 (CH(**C**H₃)₂).

2.5.10) 4,4'-(3,6-Di-*tert*-butyl-9H-carbazole-1,8-diyl)bis(1,3-bis(2,4,6-trimethylphenyl)-1H-1,2,3-triazolium) hexafluorophosphate(V) chloride (10)
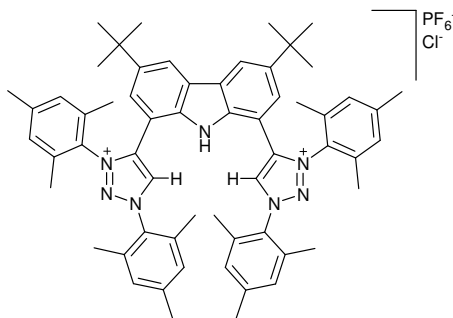
Compound **10** was prepared by a similar method as used for the synthesis of **7**. A 500 mL, 3-necked round bottom flask was charged with **3,6-di-*tert*-butyl-1,8-diethynyl-9H-carbazole** (8.00 g, 24.4 mmol), **1,3-bis-(2,4,6-trimethylphenyl)triaz-1-ene** (22.00 g, 78.2 mmol) and potassium hexafluorophosphate (15.24 g, 82.8 mmol). The vessel was purged with N₂ (g). The solids were dissolved in dry DCM (250 mL) and the solution was cooled down to -78 °C. To the solution was added *tert*-BuOCl (9.3 mL, 78.2 mmol) in a drop-wise manner with subsequent stirring of the

71

solution at -78 °C for two hours. After two hours, the solution was left to warm up to room temperature whilst stirring for 20 hours. The white precipitate was filtered from the brown red solution with subsequent evaporation of the solvent *in vacuo.* Trituration with hexanes followed by Et$_2$O yielded **10** as an off-white solid (24.70 g, 23.1 mmol, 95%); **m.p.** > 300 °C. Single crystals were grown from acetone layered with hexane. ^{1}H NMR δ$_H$ (CD$_3$CN, 300 MHz) 11.51 (1H, broads, N**H**$_{carb}$), 10.06 (2H, s, Ar**H**$_{Triazolium}$), 8.42 (2H, d, *J* = 1.8 Hz, Ar**H**$_{carb}$), 7.23 (4H, broad s, Ar**H**$_{Mes}$), 7.19 (4H, broad s, Ar**H**$_{Mes}$), 7.08 (2H, d, *J* = 1.5 Hz, Ar**H**$_{carb}$), 2.46 (6H, s, ArC**H₃**), 2.36 (6H, s, ArC**H₃**), 2.26 (12H, s, ArC**H₃**), 2.08 (12H, s, ArC**H₃**), 1.16 (18H, s, C(C**H**$_3$)$_3$). ^{13}C NMR δ$_C$ (CD$_3$CN, 75 MHz) 145.3 (Ar**C**$_q$), 144.5 (Ar**C**$_q$), 144.2 (Ar**C**$_q$), 142.3 (Ar**C**$_q$), 138.7 (Ar**C**$_q$), 136.1 (Ar**C**$_q$), 135.9 (Ar**C**$_q$), 133.6 (Ar**C**$_q$), 132.5 (Ar**C**$_q$), 131.3 (Ar**C**H), 130.9 (Ar**C**H), 127.2 (Ar**C**$_q$), 125.9 (Ar**C**H), 122.5 (Ar**C**H), 106.9 (Ar**C**$_q$), 35.4 (**C**(CH$_3$)$_3$), 31.5 (C(**C**H$_3$)$_3$), 21.4 (Ar**C**H$_3$), 21.2 (Ar**C**H$_3$), 18.1 (Ar**C**H$_3$), 18.1 (Ar**C**H$_3$). ^{19}F NMR δ$_F$ (CD$_3$CN, 282 MHz) -72.90 (d, *J* = 706.0 Hz, P**F₆**). ^{31}P NMR δ$_P$ (CD$_3$CN, 121 MHz) -144.6 (sept, *J* = 706.5 Hz, **P**F₆). HRMS (FIA-ESI): Calculated for C$_{60}$H$_{69}$N$_7$$^{2+}$ [M]$^{2+}$: 443.7802, found: 443.7835.

2.5.11) Synthesis of (11)
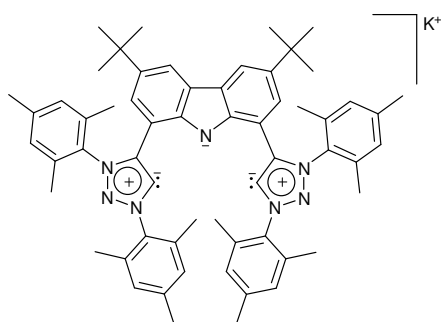
Into a flame dried Schlenk tube was loaded **10** (200.0 mg, 1.9 x 10^{-4} mol) and KN[Si(CH₃)₃]₂ (186.7 mg, 9.4 x 10^{-4} mol) inside the glove box. The solids were suspended in Et₂O (20 mL) at -78 °C. The reaction mixture was stirred at -78 °C for 25 min, after which the vessel was removed from the cold bath and stirred an additional 3 hours at room temperature. The solvent was evaporated *in vacuo* and the product extracted with benzene. Evaporation of the solvent yielded **11** (146.0 mg, 1.6 x 10^{-4} mol, 84%) as a brown solid. ^{1}H NMR δ$_H$ (C$_6$D$_6$, 300 MHz) 8.44 (2H, d, *J* = 2.1 Hz, Ar**H**$_{carb}$), 7.19 (2H, d, *J* = 2.1 Hz, Ar**H**$_{carb}$), 6.91 (4H, s, Ar**H**$_{Mes}$), 6.65 (4H, s, Ar**H**$_{Mes}$), 2.29 (12H, s, ArC**H₃**), 2.12 (6H, s, ArC**H₃**), 2.06 (18H, s, ArC**H₃**), 1.41 (18H, s, C(C**H**$_3$)$_3$). ^{13}C NMR δ$_C$ (C$_6$D$_6$, 75 MHz) 195.0 (**C**$_{Carbene}$), 152.6, 151.0, 140.4, 139.0, 138.6, 135.6, 135.0, 134.7, 134.2, 129.3, 129.0, 127.0, 122.9, 117.0, 115.5, 34.7 (**C**(CH$_3$)$_3$), 32.6 (C(**C**H$_3$)$_3$), 21.0 (ArC**H₃**), 20.9 (ArC**H₃**), 17.9 (ArC**H₃**), 17.8 (ArC**H₃**).

Chapter 3: Stabilisation of Reactive Late 3*d*-Transition Metal Complexes

3.1) Background

Nature utilises small molecules as building blocks for the synthesis of various larger organic products. These small molecules are transformed into their respective products through various enzymatic reactions, which make use of enzymes such as hydrogenases, oxidases and oxygenases, peroxidases, nitrogenases and various other enzymes and enzymatic systems.[1]

Catalyst design that mimics the catalytic reactions catalysed by these enzymes could allow for the large scale production of useful organic products, utilising these inexpensive small molecules that are readily available.[1] In addition, conversion of small unreactive molecules into useful organic products can be considered as "green processes". However, the design and synthesis of catalysts and catalytic systems able to activate these small molecules followed by the utilisation of these activated small molecules towards catalytic reactions are non-trivial. One of the main drawbacks is activating and cleaving these unreactive bonds.

Reactive transition metal complexes have shown promising results towards the activation of small molecules.[2] The small molecules of most relevance are CO_2 (g), CO (g), NH_3 (g), O_2 (g), CH_4 (g), and N_2 (g). However, various challenges are associated with the synthesis of these reactive transition metal catalysts. Their high reactivity result in their unstable nature and catalyst decomposition is not uncommon when using these reactive catalysts. Therefore, designing a ligand-metal catalyst that is resistant towards decomposition whilst retaining its high reactivity towards catalysis remains a major challenge in chemistry.

This chapter revolves around the synthesis and characterisation of reactive late 3*d*-transition metal complexes with the ligand scaffolds synthesised and presented in Chapter 2. In particular, the stabilisation of reactive nickel and copper complexes will be presented and discussed. A brief introduction regarding reactive transition metal complexes and stabilisation is presented below, which is followed by the Aim, Results and Discussion, Conclusion and Experimental sections.

---

[1] See review article and references therein: J. I. van der Vlugt, *Chem. Soc. Rev.*, 2010, **39**, 2302 – 2322.
[2] C. C. Lu, K. Meyer, *Eur. J. Inorg. Chem.*, 2013, 3731 – 3732.

3.1.1) Stabilisation of Reactive Ni and Cu Transition Metal Complexes

In stark contrast to the 4*d* and 5*d* transition metals, the nickel and copper 3*d* transition metals are considered as more earth abundant metals that are cheaper. Various reactive nickel and copper transition metal complexes, proposed to be key intermediates in catalytic reactions of importance, such as small molecule activation, have been synthesised and isolated in order to study their chemical and reactivity properties.[3] In most cases, these isolated metal complexes were also subjected to catalysis.

3.1.1.1) Nickel Hydride Complexes and Reactivity

Synthesis and isolation of nickel-hydride complexes have been reported in order to gain more insight into various nickel-catalysed reactions, and in particular where the formation of a nickel-hydride intermediate has been proposed.[4,5,6,7,8,9] Through investigations performed on these nickel-hydride complexes, a deeper understanding of the catalytic mechanism could be gained.

In 2004, Cavell *et al.* reported the first example of a (carbene)nickel-hydride complex.[4] Oxidative addition of an imidazolium salt across a low-valent bis(carbene)nickel(0) complex led to the formation of the corresponding cationic tris(carbene)nickel-hydride complexes (**a**, Figure 3.1). Formation of the nickel-hydride complexes were unambiguously confirmed with NMR and X-ray diffraction analyses. The complexes were surprisingly stable in the solid state and in solution, under anaerobic conditions. Manipulations could even be performed under aerobic conditions. The high stability of the nickel-hydride complex was attributed to the ligands coordinated to the nickel-hydride complex. Steric crowding around the square-planar nickel-hydride complex hindered orbital overlap between the hydride and the carbene carbon, which decreased the tendency for reductive elimination. In addition, steric crowding encapsulates the nickel-hydride centre, which further increases the stability towards unfavourable decomposition reactions. The catalytic activity of the nickel-hydride complexes were not investigated, however it could be postulated that the reactivity

---

[3] See review articles and references therein: *(a)* K. Ray, F. Heims, F. F. Ptaff, *Eur. J. Inorg. Chem.*, 2013, 3784 – 3807, *(b)* A. Arévalo, J. J. García, *Eur. J. Inorg. Chem.*, 2010, 4063 – 4074, *(c)* K. Hirano, H. Yorimitsu, K. Oshima, *Chem. Commun.*, 2008, 3234 – 3241, *(d)* M. Suzuki, *Acc. Chem. Res.*, 2007, **40**, 609 – 617, *(e)* J. R. Fulton, A. W. Holland, D. J. Fox, R. G. Bergman, *Acc. Chem. Res.*, 2002, **35**, 44 – 56.

[4] N. D. Clement, K. J. Cavell, C. Jones, C. J. Elsevier, *Angew. Chem. Int. Ed.*, 2004, **43**, 1277 – 1279.

[5] L-C. Liang, P-S. Chien, P-Y. Lee, *Organometallics*, 2008, **27**, 3082 – 3093.

[6] S. Chakraborty, J. A. Krause, H. Guan, *Organometallics*, 2009, **28**, 582 – 586.

[7] B. J. Boro, E. N. Duesler, K. I. Goldberg, R. A. Kemp, *Inorg. Chem.*, 2009, **48**, 5081 – 5087.

[8] T. Steinke, B. K. Shaw, H. Jong, B. O. Patrick, M. D. Fryzuk, J. C. Green, *J. Am. Chem. Soc.*, 2009, **131**, 10461 – 10466.

[9] J. Breitenfeld, R. Scopelliti, X. Hu, *Organometallics*, 2012, **31**, 2128 – 2136.

would be low, due to the high stability of the complexes resulting from steric protection. They also reported a tris(carbene)palladium-hydride analogue (**b**, Figure 3.1), and stated that low-valent group 10 metals tend to be susceptible towards oxidative addition reactions under mild reaction conditions.[4]

Figure 3.1: Tris(carbene) nickel (**a**) and palladium (**b**) hydride complexes reported by Cavell and co-workers[4]

A nickel-hydride complex, which displayed reactivity towards olefins to yield the corresponding metal alkyl complexes, was reported in 2008.[5] Oxidative addition of a Ni(COD)$_2$ (COD = 1,5-cyclooctadiene) precursor with various amido diphosphine ligand analogues at mild reaction conditions yielded the corresponding neutral nickel hydride complexes (Scheme 3.1). The formation of complexes **c$_{II}$**-**c$_{IV}$** (Scheme 3.1) was confirmed by NMR and X-Ray diffraction analyses. These complexes were also reported to be stable, except for complex **c$_I$** in Scheme 3.1. Complex **c$_I$** was only generated *in situ*, and decomposed upon attempted isolation due to its higher reactivity and steric properties when compared to **c$_{II}$**-**c$_{IV}$** (Scheme 3.1). The phenyl substituents decrease the electron density located at the metal centre through inductive electron withdrawing effects. This increases the electrophilicity of the metal centre. It could be concluded that the higher electrophilic character of the metal could increase the hydridic strength of the hydride, which subsequently increases its reactivity. The more reactive **c$_I$** complex reacted with the cyclooctadiene in the solution upon attempted isolation, to yield the corresponding nickel-alkyl complex. Complex **c$_I$**, prepared *in situ*, also reacted with other added olefin reagents such as ethylene, 1-hexene and norbornene to yield the corresponding [Ph-PNP]Ni-CH$_2$CH$_3$, [Ph-PNP]Ni-(*n*-hexyl) and [Ph-PNP]Ni-(2-norbornyl) complexes. Complex **c$_{IV}$** displayed similar reactivities, in contrast to complexes **c$_{II}$** and **c$_{III}$**, where no reaction towards olefins was observed. Therefore, the substituents on the phosphorous atoms determined reactivity, or lack thereof, of the nickel hydride complexes. No catalytic reactions of the nickel-hydride complexes were reported. After insertion of the olefin across the nickel-hydride bond, a stable nickel-alkyl complex is formed that is unreactive towards polymerisation or *β*-hydrogen elimination reactions.

75

(c)

I: $R^1 = R^2 = Ph$
II: $R^1 = R^2 = {}^iPr$
III: $R^1 = R^2 = Cy$
IV: $R^1 = Ph, R^2 = {}^iPr$

Scheme 3.1: Nickel hydride formation through oxidative addition of a Ni(0) precursor[5]

The nickel-catalysed hydrosilylation of carbonyl bonds was one of the few examples of an isolated nickel-hydride complex active in these type of catalytic reactions.[6] The nickel-hydride complex (**f**, Scheme 3.2) was synthesised through treatment of the nickel-chloride complex (**e**, Scheme 3.2) with LiAlH$_4$ (Scheme 3.2). Again, the R substituents substituted at the phosphine functionalities had a significant influence on the stability of the complexes synthesised. The nickel-hydride alkyl derivatives (**f$_I$** and **f$_{II}$**, Scheme 3.2) could be isolated and characterised, but the phenyl analogue of the nickel-hydride complex (**f$_{III}$**, Scheme 3.2) could not be obtained. This could have been due to the higher electrophilicity of the nickel-hydride complex with electron withdrawing phenyl substituents, which could increase the reactivity of the complex as mentioned above. After further studies, it was determined that the two synthesised and isolated nickel-hydride complexes were unreactive towards carbon-carbon double and triple bonds. However, upon addition of an organic compound containing a carbonyl functional group such as benzaldehyde, the insertion product was obtained almost instantaneously. This was the first reported example of a carbonyl insertion transformation across a nickel-hydride bond, which could be isolated.

(d)   (e)   (f)

I: R = ${}^iPr$
II: R = ${}^tBu$
III: R = Ph
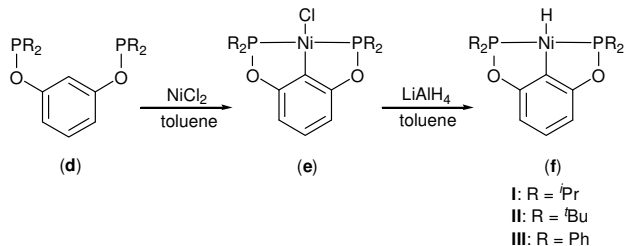
Scheme 3.2: Synthesis of NiCl (**e**) and NiH (**f**) complexes as reported by Chakraborty *et al.*[6]

The catalysis of the two isolated nickel-hydride derivatives (see **f$_I$** and **f$_{II}$**, Scheme 3.2) towards the hydrosilylation of aldehydes was tested (Scheme 3.3). As is evident from Scheme 3.3, the aldehyde inserts across the nickel-hydride bond, to yield the nickel-alkoxide intermediate. A phenyl-silyl reagent is added to regenerate the nickel-hydride catalyst, with subsequent release of the silyl ether.

76

Various aldehyde substrates were tested, and good to excellent yields for the silyl ethers were obtained, which were subsequently treated with 10% NaOH to yield the corresponding alcohol (Scheme 3.3).[6] Various substrates had other functional groups in addition to the aldehyde functional group. The nickel-hydride catalyst was selective only towards the aldehyde functional group. This indicated that the isolated nickel-hydride catalyst was both active in the hydrosilylation of aldehydes to the corresponding silyl ethers, and also selective only towards the aldehyde or carbonyl functional groups.
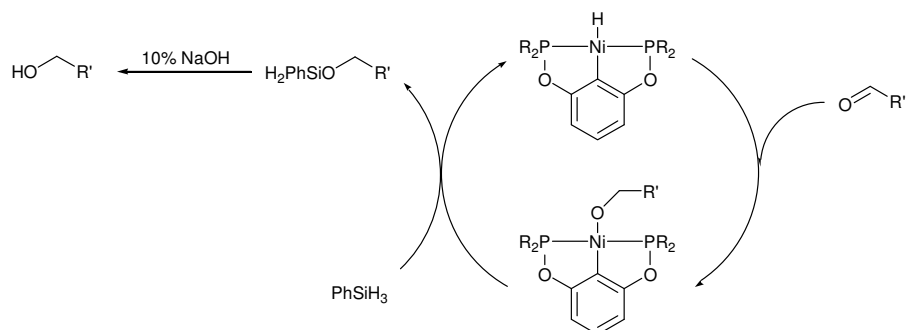
Scheme 3.3: Hydrosilylation of aldehydes catalysed by a nickel-hydride complex[6]

The reduction of carbon dioxide (CO_2 (g)) with a borane, using the nickel-hydride complex illustrated in Scheme 3.2 as catalyst, was reported in 2010 by the same group.[10] It was reported that the nickel-hydride complex f_{II} (see Scheme 3.2) catalytically converted CO_2 (g) at one atmosphere (1 atm) pressure, in the presence of catecholborane (HBcat), to the methoxide level (CH_3OBcat) (Scheme 3.4). Isolation and structural characterisation of the nickel formate complex was possible by treatment of the nickel-hydride complex with CO_2 (g) in toluene at room temperature, as depicted by reaction **I**, in Scheme 3.4. In order to complete a catalytic cycle by releasing the formate and regenerating the nickel-hydride starting complex, catecholborane (HBcat) was added to the mixture. This completed the catalytic reaction, forming the catechol-methoxide product and regenerating the nickel-hydride catalyst, as depicted by reaction **II**, in Scheme 3.4.[10]

---

[10] S. Chakraborty, J. Zhang, J. A. Krause, H. Guan, *J. Am. Chem. Soc.*, 2010, **132**, 8872 – 8873.
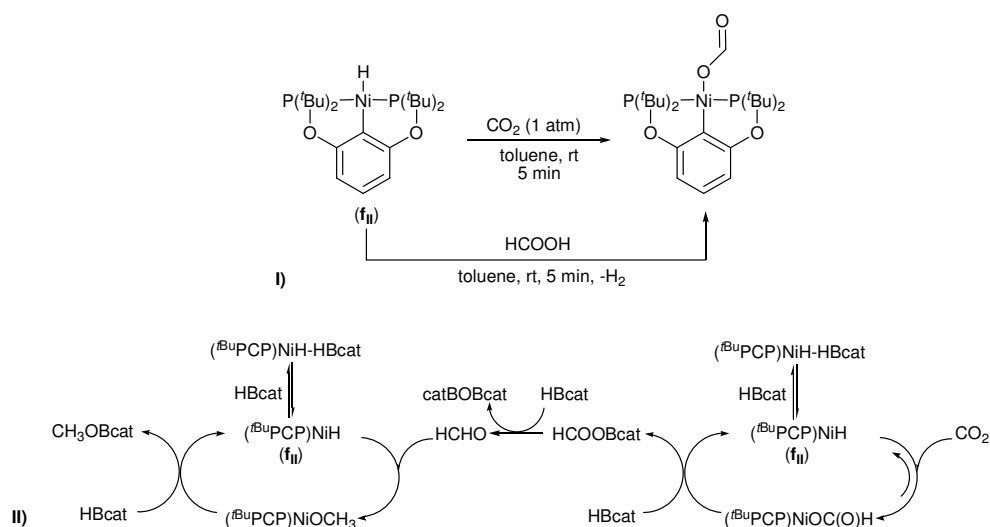
Scheme 3.4: **I)** CO_2 (g) insertion across Ni-H bond and **II)** CO_2 (g) reduction with Ni-H catalyst and HBcat[10]

A cationic nickel-hydride complex was also reported in 2009 by Steinke *et al.*[8] The cationic nickel-hydride complex was again synthesised through oxidative addition of a PCP ligand to a Ni(COD)$_2$ precursor. The reactivity of this nickel-hydride complex towards ethylene activation was investigated. The results obtained were somewhat surprising. After addition of excess ethylene to a THF solution of the nickel-hydride complex, a nickel(0) complex was isolated and characterised. Crystals of the unexpected nickel(0) complex were obtained. It was determined that the ethylene reagent had reacted with the hydride, yielding the ethyl moiety that formed a carbon-carbon bond to the former NHC carbene carbon and not to the nickel metal centre as expected. The nickel(II) had been reduced to nickel(0), and the NHC-ethyl ligand was now π-bonded to nickel(0) in a η² fashion. The formation of the cationic nickel-hydride complex and its subsequent reaction with ethylene is illustrated in Scheme 3.5. The expected complex **h** (Scheme 3.5) could not be isolated after reacting complex **g** with ethylene. Instead complex **i** was isolated and structurally characterised, probably resulting from a reductive elimination of complex **h** to complex **i**.[8] The vacant coordination site is then occupied by the π-C=N bond.

78
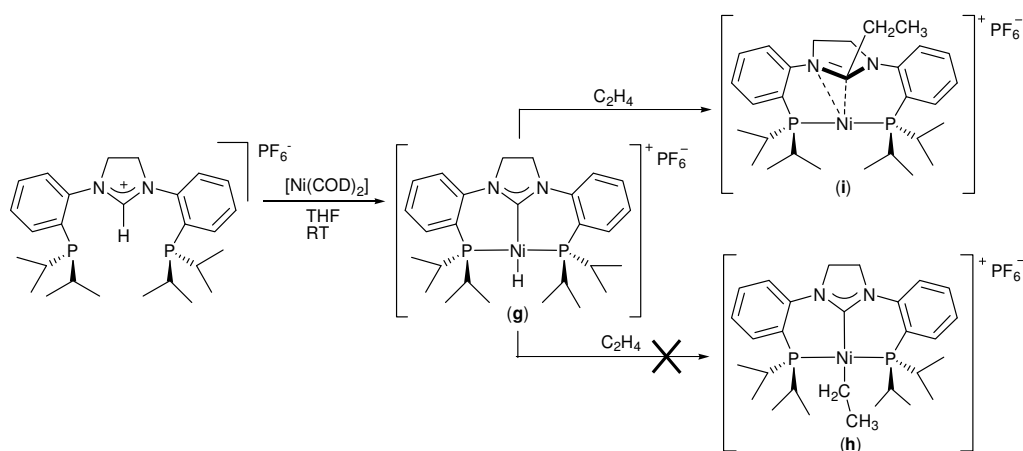
Scheme 3.5: Synthesis of a cationic (PCP)NiH complex and its reaction with ethylene[8]

A neutral [(Me$_2$N)$_2$NNiH] complex was isolated and structurally characterised in 2012 by Hu and co-workers.[9] The nickel-hydride complex was obtained by treatment of a [(Me$_2$N)$_2$NNi-OMe] with PhSiH$_2$, using toluene as solvent (Scheme 3.6). It should be noted that the complex gradually decomposed at room temperature, and could only be isolated and stored at temperatures of -28 °C or lower in the absence of light. Upon decomposition, nickel particles and the free ligand were obtained. This clearly indicated the higher reactivity of the nickel-hydride complex containing amine wingtip groups, instead of the phosphine wingtip groups as depicted in Schemes 3.2 to 3.4. The higher reactivity of the nickel-hydride complex was utilised. The nickel-hydride complex reacted with acetone, ethylene and alkyl halides to produce the corresponding [(Me$_2$N)$_2$NNi -O^{i}Pr], [(Me$_2$N)$_2$NNi -Et] and [(Me$_2$N)$_2$NNi-X] respectively. Treatment of complex **j** with an alkyl halide yielded the corresponding nickel-halide complex and alkane. Therefore, the complex did show promising reactivity towards a variety of substrates, and as such was further subjected to catalysis.
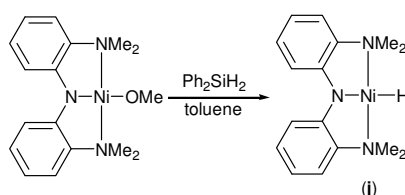
Scheme 3.6: Synthesis of a [(^{Me}N$_2$N)NiH] (**j**) from the [(^{Me}N$_2$N)Ni-OMe] precursor[9]

The catalytic activity of complex **j** (see Scheme 3.6) was tested towards the hydrodehalogenation of alkyl halides and displayed good to excellent catalytic activity for the reaction. Primary, secondary and tertiary alkyl halides were all converted to the corresponding alkanes. The catalyst was also active in the hydroalkylation of olefins yielding larger alkanes through carbon-carbon bond

formation. However, the catalyst showed poor reactivity in the hydroalkylation reaction and this was attributed to the instability of the nickel-hydride complex.

From these nickel-hydride examples discussed, it can be deduced that the stability of the nickel-hydride complexes depends greatly on the supporting ligand scaffold. In addition, some nickel-hydride complexes were active in various organic transformation and catalytic reactions. Activation of small molecules, such as CO_2 and C_2H_4, was accomplished by some of the nickel-hydride complexes reported. Therefore, the synthesis and stabilisation of reactive nickel-hydride complexes followed by subsequent studies to determine their catalytic activity and ability to activate small unreactive molecules, is an invaluable method from which valuable fundamental information regarding catalysis involving nickel complexes can be gained.

3.1.1.2) Copper(II) Complexes and Reactivity Towards Oxygen

The study of oxygen activation by use of reactive copper species has gained considerable attention over the past few years, due to their importance in biological and synthetic oxidation reactions.[11] Owing to the choice of ligand scaffold and reaction conditions, which were mostly carried out at low temperatures, isolation of Cu-O_2 adducts where the oxygen binds either side-on or end-on was possible, with subsequent studies performed on these isolated reactive complexes. A few selected examples of oxygen activation with either Cu(I) or Cu(II) species will be highlighted.

In general, a copper-oxygen adduct is formed through coordination of oxygen to the copper centre in a side-on fashion, or as a dimeric 2:1 Cu/O_2 adduct.[12] Various binding modes are illustrated in **I**, Scheme 3.7. However, in 2006 Schindler and co-workers reported an end-on superoxo-copper(II) complex, which was unambiguously characterised by X-ray diffraction analysis (**II**, Scheme 3.7).[12] This was the first reported example of an isolated and structurally characterised end-on superoxo-copper(II) complex. A Cu(I) salt (**II**, Scheme 3.7), with a basic and sterically demanding tripodal tetradentate NNNN ligand, was reacted with molecular oxygen to yield the oxidised Cu(II) salt with oxygen binding end-on to the copper (**II**, Scheme 3.7). Remarkably, the oxygen binds reversibly, as illustrated by **II** in Scheme 3.7. Through heating up a solution of **l** (**II**, Scheme 3.7), **k** (**II**, Scheme 3.7) could be regenerated. Cooling the same solution down in the presence of oxygen yielded **l** from **k** (**II**,

---

[11] See review articles and references therein: *a)* E. I. Solomon, D. E. Heppner, E. M. Johnston, J. W. Ginsbach, J. Cirera, M. Qayyum, M. T. Kieber-Emmons, C. H. Kjaergaard, R. G. Hadt, L. Tian, *Chem. Rev.*, 2014, **114**, 3659 – 3853, *b)* C. J. Cramer, W. B. Tolman, *Acc. Chem. Res.*, 2007, **40**, 601 – 608, *c)* E. I. Solomon, U. M. Sundaram, T. E. Machonkin, *Chem. Rev.*, 1996, **96**, 2563 – 2605.
[12] C. Würtele, E. Gaoutchenova, K. Harms, M. C. Holthausen, J. Sundermeyer, S. Schindler, *Angew. Chem. Int. Ed.*, 2006, **45**, 3867 – 3869.

Scheme 3.7). The crystal structure revealed that the geometry of complex **I** (**II**, Scheme 3.7) is trigonal-bipyramidal with the oxygen binding end-on as an axial ligand.[12]
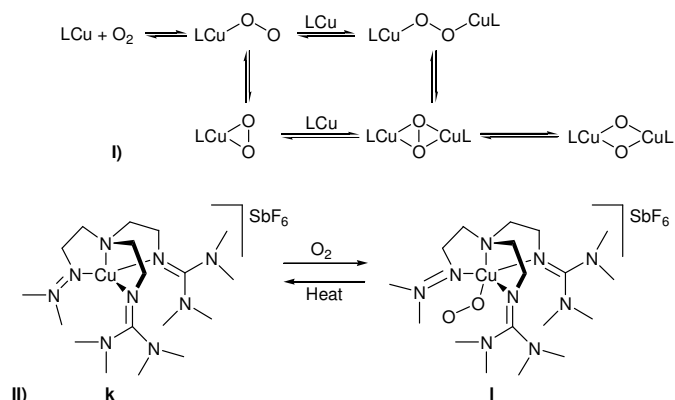
Scheme 3.7: **I)** Various copper-oxygen binding modes and **II)** oxygen activation by a tripodal tetradentate Cu(I) salt yielding the end-on superoxo-Cu(II) salt[12]

The end-on superoxo-copper(II) salt (**II**, Scheme 3.7) was subjected to reactivity tests towards various phenol organic substrates by Karlin *et al.* in 2008.[13] Complex **I** (**II**, Scheme 3.7) was reported to be active towards O-atom transfer, H-atom abstraction with subsequent oxidation or oxygenation, and C-H activation reactions with a phenolic substrate. Two of the various organic transformations facilitated by the end-on superoxo-copper(II) salt is displayed in Scheme 3.8. It can be concluded that the oxidising strength of complex **I** is high due to the fact that the *tert*-butyl alkyl group is oxidised to a ketone with cleavage of the alkyl substituent, in the absence of any co-oxidant or another oxidising agent.
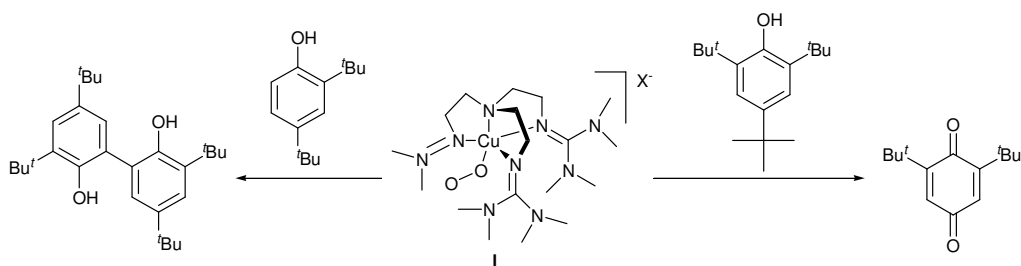
Scheme 3.8: Organic transformation reactions catalysed by an end-on superoxo-copper(II) salt[13]

Again it was illustrated that by choice of the correct ligand, a highly reactive copper species could be isolated and structurally characterised, and even used as a catalyst. A Cu(I) complex, also coordinated to a tripodal tetradentate NNNN ligand, was synthesised by the group of Schindler in

[13] D. Maiti, D-H. Lee, K. Gaoutchenova, C. Würtele, M. C. Holthausen, A. A. Narducci Sarjeant, J. Sundermeyer, S. Schindler, K. D. Karlin, *Angew. Chem. Int. Ed.*, 2008, **47**, 82 – 85.

2009.[14] The reported mononuclear complex reacted spontaneously in the solid state with air to yield the dinuclear complex bridged by molecular oxygen (**m**, Scheme 3.9). Complex **m** illustrated in Scheme 3.9 (and its analogues), can be stored in the presence of air at room temperature whilst in the solid state, for long periods of time. Surprisingly this complex is thermally stable at 70 °C also in the solid state.[14] However, it was reported that complex **m**, as well as its derivatives, decompose rapidly in solution at room temperature and is only stable at -80 °C in solution. The catalytic activity of complex **m** (and its derivatives) was tested towards the selective oxidation of technical grade toluene (Scheme 3.9). It was determined that the dinuclear copper peroxo complexes catalytically converted toluene to benzaldehyde with a yield of 20%. A small amount of benzyl alcohol was also obtained (Scheme 3.9).[14] It should be noted that these oxidation reactions discussed are, in general, carried out under harsh reaction conditions with reagents such as ozone, strong acids and also inorganic complexes comprising of chromium or manganese.
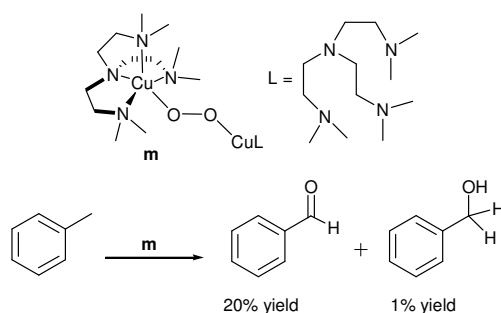
Scheme 3.9: Dinuclear copper peroxo complex and its catalytic activity towards the selective oxidation of toluene[14]

In addition to the various copper-oxygen binding modes displayed in Scheme 3.7, a new copper-oxygen binding mode was proposed in 2011 by Tolman *et al.*[15] They reported the synthesis of a Cu(II) hydroxide complex that was isolated, characterised and subsequently oxidised to the corresponding Cu(III) complex (Scheme 3.10). Due to its reactivity, this Cu(III)-OH complex was postulated to be an active intermediate in various catalytic oxidation reactions. The Cu(II)-OH (**o$_I$**, Scheme 3.10) or the Cu(II)-Cl (**o$_{II}$**, Scheme 3.10) salt complexes were obtained by reacting the neutral Cu(II) complex (**n**, Scheme 3.10) with Bu$_4$NX (X = OH or Cl), respectively. A one-electron oxidation reaction of the Cu(II)-OH salt (**o$_I$**, Scheme 3.10), using ferrocenium as the oxidant, yielded the corresponding neutral Cu(III)-OH complex (**p**, Scheme 3.10). This complex was thermally unstable, decomposing at temperatures above -60 °C. It was postulated that oxidation of the Cu(II) complex could have been either metal-based or ligand-based. A metal-based oxidation would have yielded a Cu(III) complex,

[14] C. Würtele, O. Sander, V. Lutz, T. Waitz, F. Tuczek, S. Schindler, *J. Am. Chem. Soc.*, 2009, **131**, 7544 – 7545.
[15] P. J. Donoghue, J. Tehranchi, C. J. Cramer, R. Sarangi, E. I. Solomon, W. B. Tolman, *J. Am. Chem. Soc.*, 2011, **133**, 17602 – 17605.

82

whereas a ligand-based oxidation could have yielded a Cu(II)-ligand radical.[15] After various characterisation techniques were applied, including EPR, IR and UV-vis spectroscopy that was supported by DFT calculations, it was concluded that a metal-based oxidation reaction occurred yielding the neutral Cu(III)-OH complex. The reactivity of the Cu(III)-OH complex (**p**, Scheme 3.10) towards dihydroanthracene was investigated. It was determined that H-atom abstraction occurred at high rates, yielding anthracene and the reduced Cu(II)-OH₂ complex (**q**, Scheme 3.10).[15]
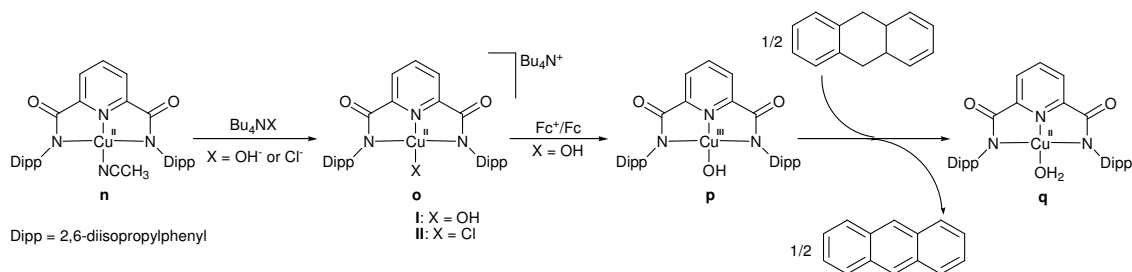
Scheme 3.10: Synthesis of Cu(III)-OH and reduction with dihydroanthracene[15]

The coordination of oxygen to the copper complex determines the ground state multiplicity of the complex and, subsequently, its stability.[16] Generally the coordination of oxygen to copper in an end-on fashion, as illustrated in Scheme 3.7 and Scheme 3.9, leads to the formation of a Cu-O bond with a triplet ground state configuration for the complex (Figure 3.2 right). The bonding/antibonding interaction between the superoxide π^*_σ-orbital and the Cu d-orbital does not possess enough energy to overcome the spin pairing energy. The two unpaired electrons occupy different orbitals, namely the π^*_v (superoxide character) and $d - \alpha\pi^*_\sigma$ (copper character) orbitals, leading to a triplet ground state electronic configuration. In contrast, side-on coordination of oxygen to the copper through two Cu-O bonds increases the HOMO (highest occupied molecular orbital)/LUMO (lowest unoccupied molecular orbital) gap significantly (Figure 3.2 left). The energy of the HOMO/LUMO gap is larger than the spin-pairing energy, resulting in the double occupation of the HOMO orbital, which is superoxide based (the π^*_v-orbital).[16] The antibonding copper $d_{x^2-y^2}$ forms the LUMO orbital. The singlet state is more stable compared to the triplet state. This could explain the fact that copper-superoxo complexes with triplet ground state configurations have only recently been isolated and characterised, while copper-superoxo complexes with singlet ground state configurations have been known and studied for some time.

[16] J. W. Ginsbach, R. L. Peterson, R. E. Cowley, K. D. Karlin, E. I. Solomon, *Inorg. Chem.*, 2013, **52**, 12872 – 12874.
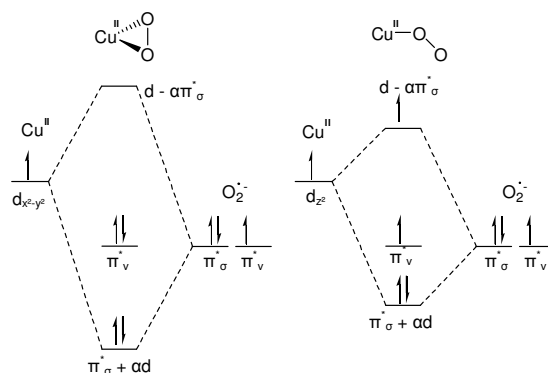
Figure 3.2: Frontier orbitals of superoxo-copper(II) complexes where oxygen coordinates side-on (left) or end-on (right)[16]

3.2) Aim

As exemplified in the preceding sections, numerous reports support the concept of utilising small molecules by activating the inert bonds of these difficult substrates through employing a reactive metal complex. It is postulated that, due to the rigid carbazole backbone and bulky aromatic wingtip substituents of the two ligands prepared and discussed in Chapter 2, reactive metal complexes could be stabilised and isolated through coordination of the required metal precursor (Ni, Cu) to the ligand scaffold. As such, synthesis and isolation of reactive nickel and copper metal complexes will be attempted. The general synthetic strategy involves *in situ* deprotonation of the bis(triazolium)carbazole ligand salt followed by metallation. The target metal complexes are illustrated in Figure 3.3.

Ar = 2,4,6-trimethylphenyl   M = Ni(II), Cu(II), Cu(I)
= 2,6-diisopropylphenyl
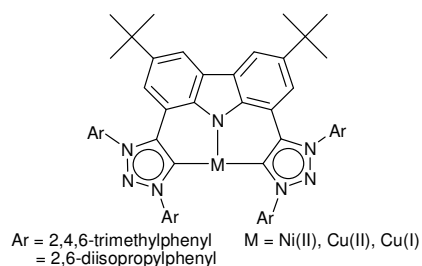
Figure 3.3: Proposed metal complexes containing CNC tridentate ligand

3.2.1) Synthetic Strategy

As was determined during the synthesis of compounds **9** and **11** (Chapter 2), deprotonation of all three acidic positions (the *trz*H and amino protons) is achieved by using five equivalents of the strong non-nucleophilic base, namely KHMDS. The potassium free carbene adduct can coordinate to

84

a metal precursor, either through substitution of the metal precursor co-ligands with the stronger donor L-type carbene ligands, or just simply coordinating to the vacant sites of the metal precursor, if such vacant sites are available. In addition to coordination of the carbene ligands, a metal X-type ligand will also have to be substituted, due to the amido moiety coordinating to the metal. The substitution of the weaker X-type ligand for the strong amido ligand will ensure that the metal retains its oxidation state. Both coordination of the carbene L-type and amido X-type ligands to the metal would yield the desired metal complex. The general method that will be employed during the synthesis of the metal complexes is outlined in Scheme 3.11.
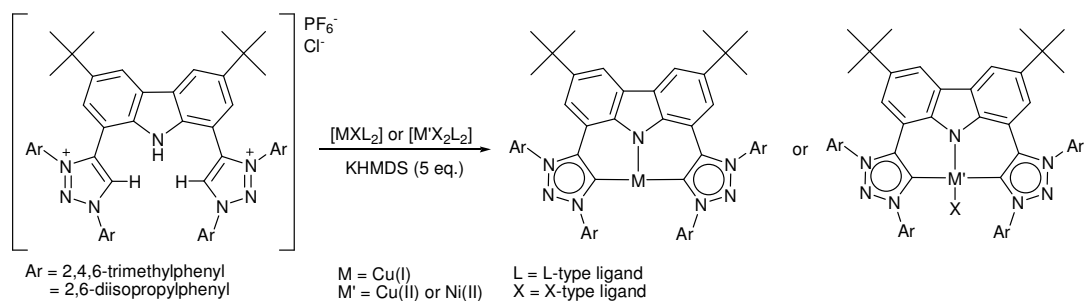
Scheme 3.11: Proposed synthetic strategy towards the synthesis of metal complexes containing the prepared tridentate pincer ligands

3.2.1.1) (CNC)NiCl and (CNC)NiH Complexes

The planned synthesis of the reactive nickel-hydride complex containing the tridentate ligand involves two steps (Scheme 3.12). The first step requires *in situ* deprotonation of the ligand with base and metallation with a dichloronickel(II) dimethoxyethane adduct. This could yield the (CNC)NiCl complex. The dimethoxyethane (dme) co-ligand can be readily substituted by the carbene ligands, due to the lability of the dimethoxyethane ligand.

The second step during the synthesis of the (CNC)NiCl complex will involve a nucleophilic substitution reaction (Scheme 3.12). The chloride ligand of the (CNC)NiCl complex will be reacted with a nucleophilic hydride source. A super hydride source such as LiEt₃BH could be used for the nucleophilic substitution reaction to yield the nickel-hydride complex. In both steps THF will be employed as the solvent of the reaction.

85

Step 1: Synthesis of the (CNC)NiCl complex
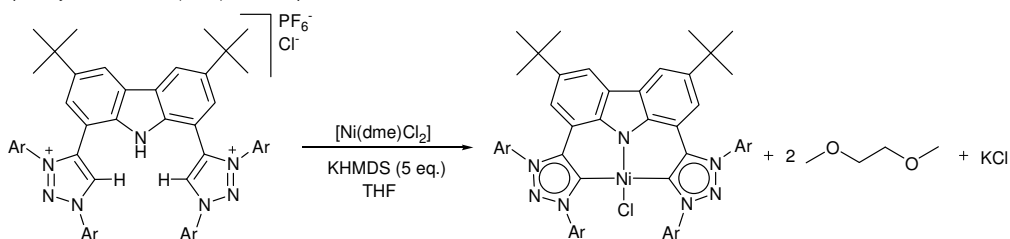
Ar = 2,4,6-trimethylphenyl
   = 2,6-diisopropylphenyl

Step 2: Nucleophilic substitution of (CNC)NiCl to yield the (CNC)NiH complex
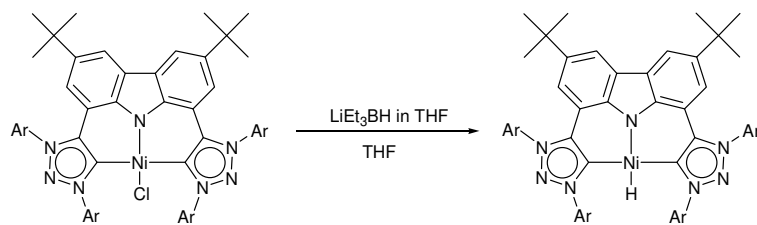
Scheme 3.12: Planned synthesis of the (CNC)NiH complex in two steps

3.2.1.2) (CNC)Cu, (CNC)CuCl and (CNC)CuH Complexes

The various copper complexes containing the tridenate ligand **7** or **10**, could also be synthesised using a similar method as proposed for the synthesis of the (CNC)NiCl and (CNC)NiH complexes.

The synthesis of the (CNC)Cu(I) complex could be accomplished by reacting the free carbene adduct generated *in situ*, with a CuX (X = Cl, Br, I) metal precursor. The halogen ligand will be substituted by the amido ligand, in addition to the coordination of the carbene ligands (Scheme 3.13). The (CNC)Cu(II)Cl complex can also be synthesised based on the same method, but employing a CuX₂ (X = Cl, Br) metal precursor. The planned isolation of a (CNC)Cu(II)H complex can be achieved, theoretically, by reacting the (CNC)Cu(II)Cl complex with a LiEt₃BH hydride source, as explained above (Scheme 3.13).

86
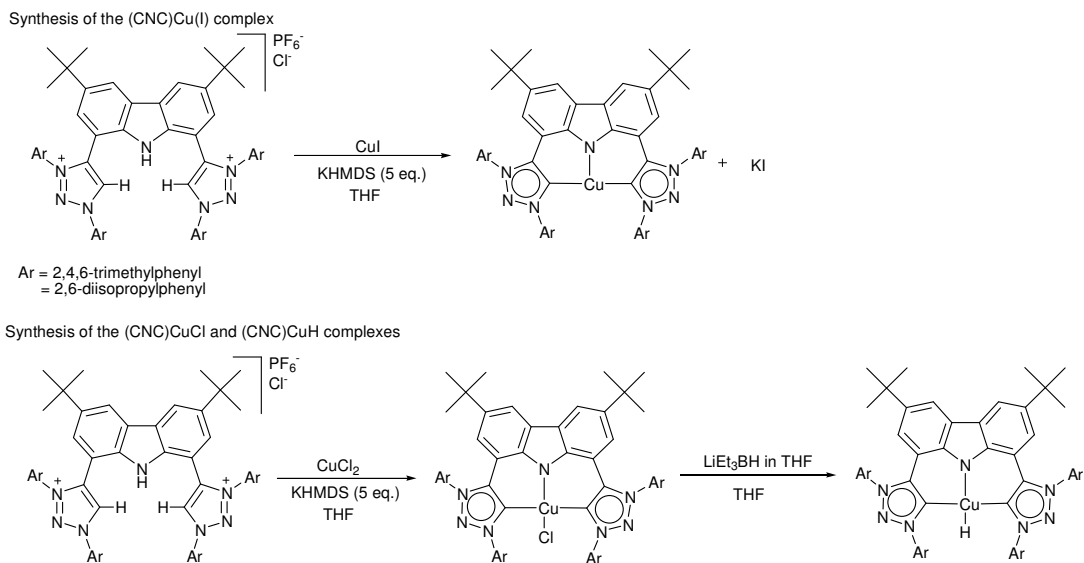
Scheme 3.13: Planned synthesis of copper(I) and copper(II) complexes

3.3) Results and Discussion

See Section 3.5 for the methods used during the synthesis of the compounds as well as the full characterisation thereof.

3.3.1) Synthesis of 12

The synthesis of **12** involved *in situ* deprotonation of **7** with KHMDS followed by metallation with [Ni(dme)Cl$_2$], at -78 °C, that unexpectedly yielded the nickel-hydride complex **12**, after extraction of the product with hexanes and evaporation of the solvent *in vacuo* (Scheme 3.14). Compound **12**, a red solid, was obtained with a yield of 39%. It was expected that metallation of the free carbene adduct with the nickel precursor should have first yielded the (CNC)NiCl complex, which if then treated with LiEt$_3$BH in THF as solvent, result in the formation of **12**. However, formation of the nickel-hydride complex as depicted in Scheme 3.14 was unambiguously confirmed with NMR, MS and X-ray diffraction analysis. It is postulated that the hydride resulted due to a triazolium C-H insertion reaction, similar to the C-H oxidative addition reaction yielding the nickel-hydride tris-carbene complex as reported by Cavell *et al.*[4] (see Section 3.1.1.1). The nickel-hydride **12** is the first example of a neutral nickel carbene hydride complex.

87
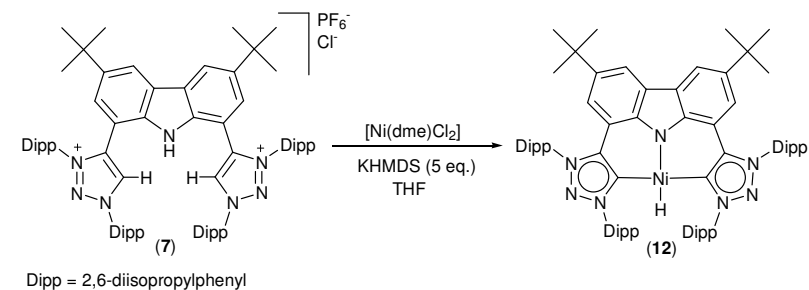
Scheme 3.14: Synthesis of **12** through *in situ* deprotonation and metallation of **7**

The ^{1}H NMR spectrum of **12** is given in Figure 3.4. The hydride is shifted upfield (-6.30 ppm) compared to the aromatic and aliphatic protons of compound **12**. The hydrogen atom is more electronegative compared to the nickel metal. As such, the hydride obtains a nucleophilic character and experiences more shielding as a result of the higher electron density situated on the hydrogen. However, the high field shift does not resonate as far upfield as do the hydride complexes discussed in Section 3.1.1.1. The hydrides of these complexes generally resonate between -10 and -15 ppm. Therefore, when compared to other nickel-hydride complexes, the hydride of complex **12** resonates downfield. It could be postulated that the Ni-H bond of **12** has more covalent character and less ionic character. In addition, the ^{13}C NMR spectrum (Figure 3.5) displays a singlet at 159.8 ppm which corresponds to the carbene carbon. The carbene carbon resonates upfield in the ^{13}C NMR spectrum when compared to the downfield shifted carbene carbons (185 to 190 ppm) of the nickel-hydride tris-carbene complex reported by Cavell.[4] This could support the postulation that the Ni-H bond has a high covalent character. The solid state decomposition temperature was determined to be between 282 and 285 °C, demonstrating the remarkable thermal stability of the complex.

88
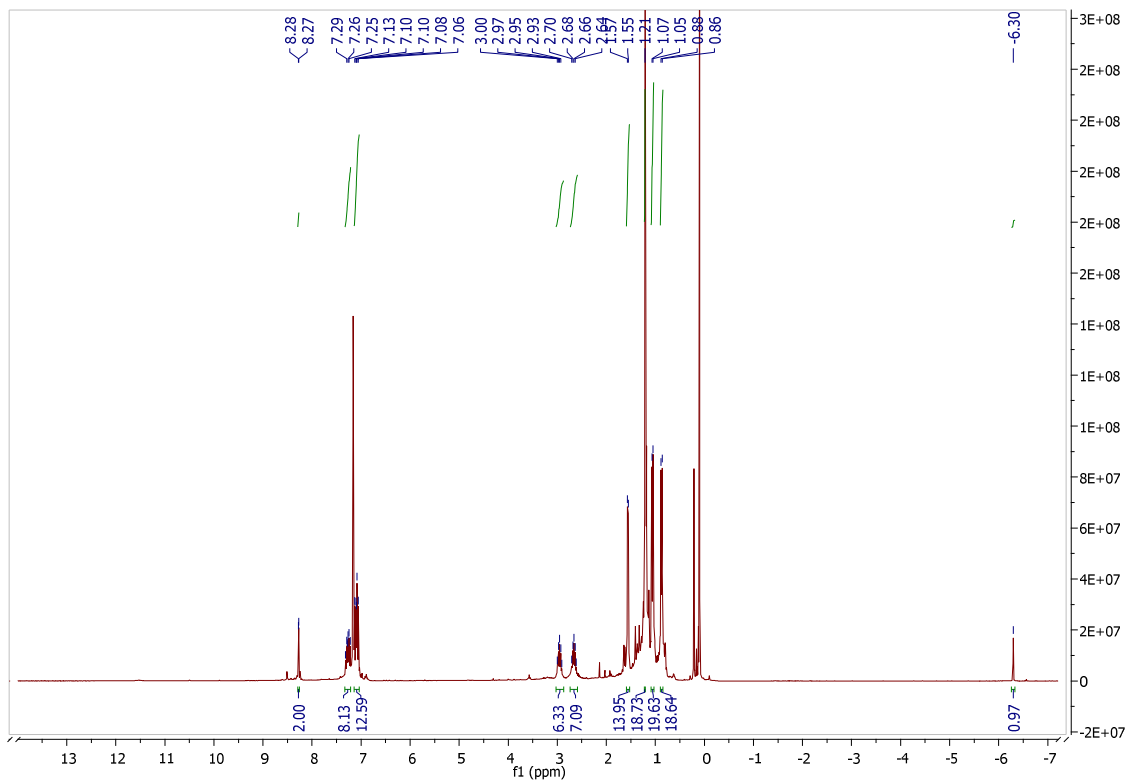
Figure 3.4: ^{1}H NMR of **12** in C_6D_6 solvent
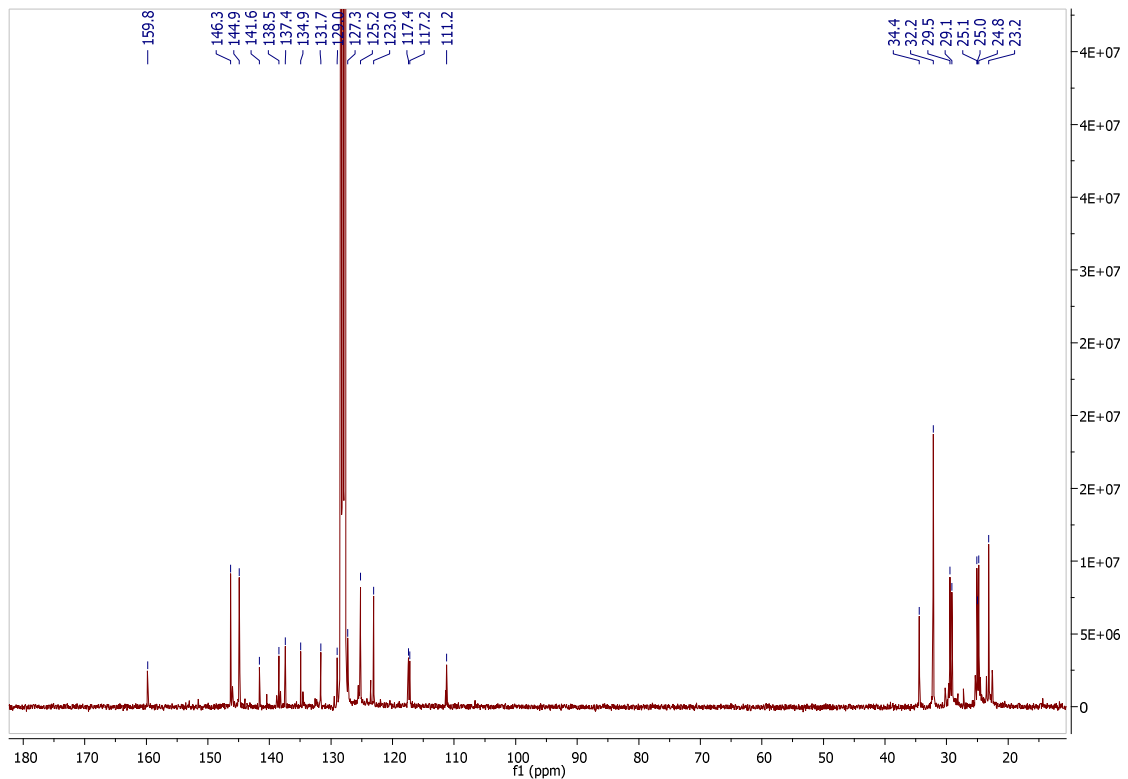
Figure 3.5: ^{13}C NMR of **12** in C_6D_6 solvent

89

Crystals suitable for crystal structure determination were obtained from a deuterated benzene solution. A two-fold symmetry axis for the molecule is situated parallel to the unit cell's b-axis with the nitrogen, nickel and hydride atoms lying on the symmetry axis. Upon coordination to the metal, the *trz* groups are forced to occupy a more planar environment with respect to the carbazole backbone, which is in stark contrast to the ligand salt **7** and free carbene adduct **9**. The triazolylidene moieties are twisted out of the carbazole plane, with a C1-C2-C3-C4 torsion angle of 7.7(2)°. The N1-Ni1-H1 bond angle is exactly 180° while the C2-C1-Ni1-C1 torsion angle is 170.84(14)°.

The geometry around the nickel centre is square planar, as is the case for other reported Ni-H complexes.[4,5,6,9] The bonds to the metal deviate slightly from a 90° angle with respect to each other. The C1-Ni-H1 bond angle is 88.78(5)° and the C1-Ni-N1 angle is 91.22(5)°, while the C1-Ni1-C1 angle is 177.56(10)° and not exactly linear. The Ni1-H1 bond length (1.45(2) Å), is shorter than the corresponding bond length of the nickel-hydride complex reported by Hu and co-workers (see **j**, Scheme 3.6).[9] This observation contrasts with the N1-Ni1 bond length of **12** being 1.9016(18) Å, while the N2-Ni1 bond length of complex **j** (Scheme 3.6) is shorter (1.881(2) Å). From the observations it could be concluded that the amido moiety for **12** has a weaker *trans* influence than the corresponding amido moiety for **j** (Scheme 3.6). As such, the N1-Ni1 bond is weaker while the Ni1-H1 bond is stronger for **12**. This would support a Ni-H bond with high covalent character. The stronger Ni-H bond could increase the stability of the complex, but decrease the reactivity or catalytic activity of the **12** to various organic substrates.

The C1-Ni1 bond length of **12** is 1.9183(17) Å. This C1-Ni1 bond length is longer than the carbene-nickel bond length of **a** (see Figure 3.1).[4] Again, in both cases the carbene ligand is *trans* to a second carbene ligand, which allows for direct comparison between the carbene-nickel bond lengths. Complex **a**, reported by Cavell and co-workers,[4] is cationic while **12** is neutral. The overall increased electrophilicity of the cationic complex **a** (Figure 3.1) should result in increased σ-donation from the nNHC ligands, explaining the shorter carbene-nickel bond of the complex.

The C1-C2-N2-N3 torsion angle has a value of 0.42(18)°, while the bond lengths in the *trz* moieties have double bond character. Both factors point to an aromatic five-membered heterocylce with delocalisation of the electron density throughout the ring. The C2-C1-N4 bond angle is 101.81(14)°, which is more acute than the corresponding bond angle of **7**, but not as acute as the C2-C1-N2 bond angle of compound **9**. The carbene σ-orbital overlaps with the metal orbital, which decreases the s-character and increases the p-character of the σ-orbital, resulting in an increase in the bonding angle, in comparison with **9**.

90
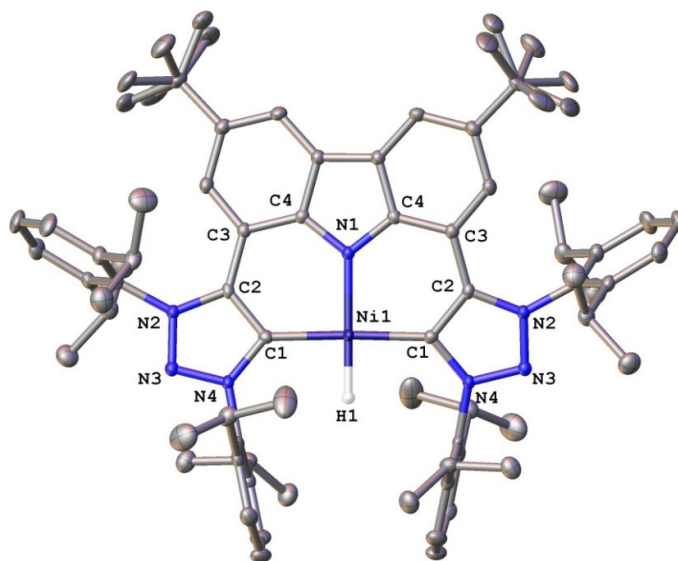
Figure 3.6: Crystal structure of **12**

3.3.2) Synthesis of 13

The 2,4,6-trimethylphenyl analogue of **12**, namely compound **13**, was synthesised using the same procedure as used for the synthesis of **12**. The ligand salt **10**, was metallated with [Ni(dme)Cl$_2$] through *in situ* deprotonation of the ligand with KHMDS followed by metallation. Again, the unexpected nickel-hydride complex was obtained after extraction of the product with hexanes from the crude residue, followed by evaporation of the hexane solvent *in vacuo*, yielding **13** as a red solid with a yield of 57% (Scheme 3.15). Characterisation of **13** with NMR and MS analysis confirmed the formation of the nickel-hydride complex.
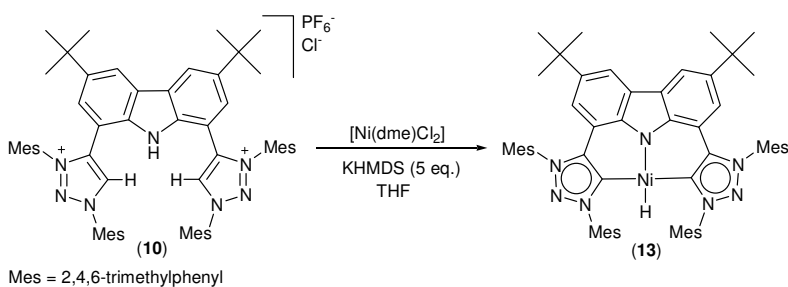
Scheme 3.15: Synthesis of **13** through *in situ* deprotonation and metallation of compound **10**

The clear disappearance of the acidic protons in the region of 10 and 13 ppm indicates the tris-deprotonation of the ligand (Figure 3.7). The singlet peak resonating at -6.31 ppm with an integration of 1H corresponds to the hydridic hydrogen. Both factors point to the successful metallation of the ligand and formation of the nickel-hydride complex and not the (CNC)Ni-Cl

91

complex. In addition, the carbene carbon, with a singlet peak in the carbon NMR spectrum resonating at 158.6 ppm, supports the formation of the carbene-metal complex (Figure 3.8). These values for **13**, the hydride and carbene carbon resonance, are almost identical to that of **12**, giving further clear evidence to the formation of **13**.

Due to the decreased steric protection from using the 2,4,6-trimethylphenyl wingtip groups, **13** is predicted to be less stable than **12**. This was indeed observed upon attempts at crystallisation of **13**. No crystals suitable for X-ray diffraction analysis were obtained. However, the increased reactivity of **13** will prove advantageous towards the reactivity of **13** with organic substrates and small molecules, as well as towards catalysis.
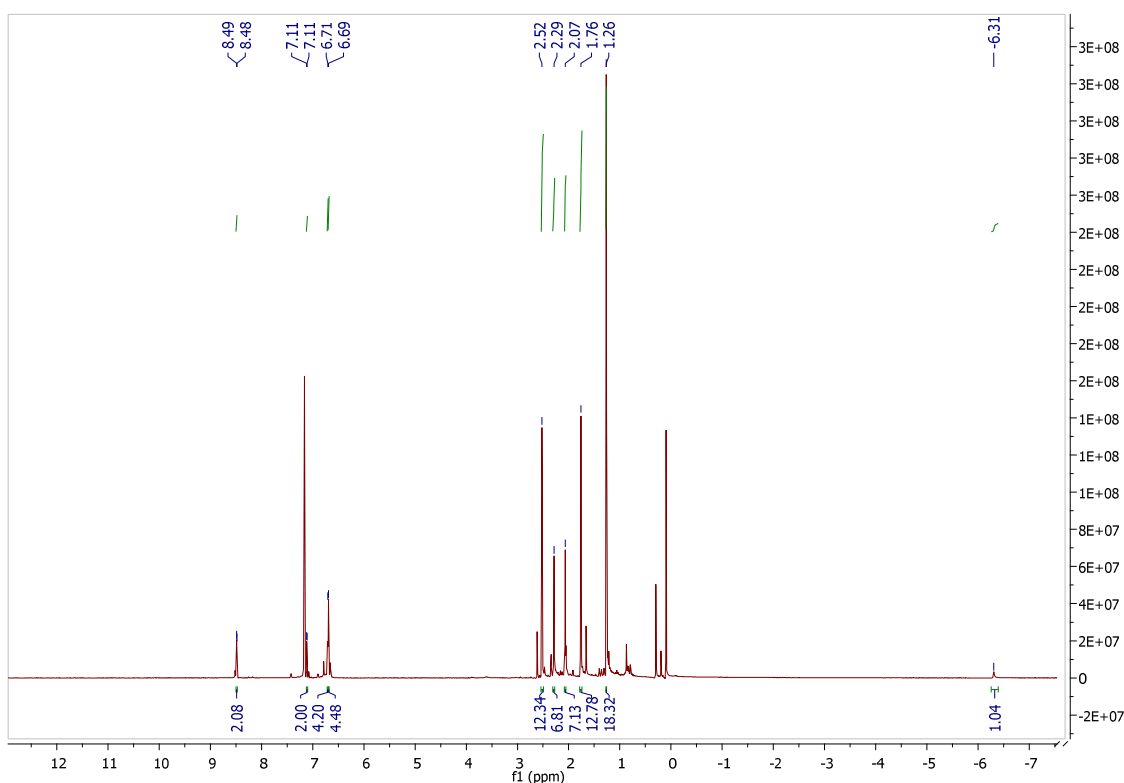
Figure 3.7: ^{1}H NMR of **13** in C$_6$D$_6$ solvent

92
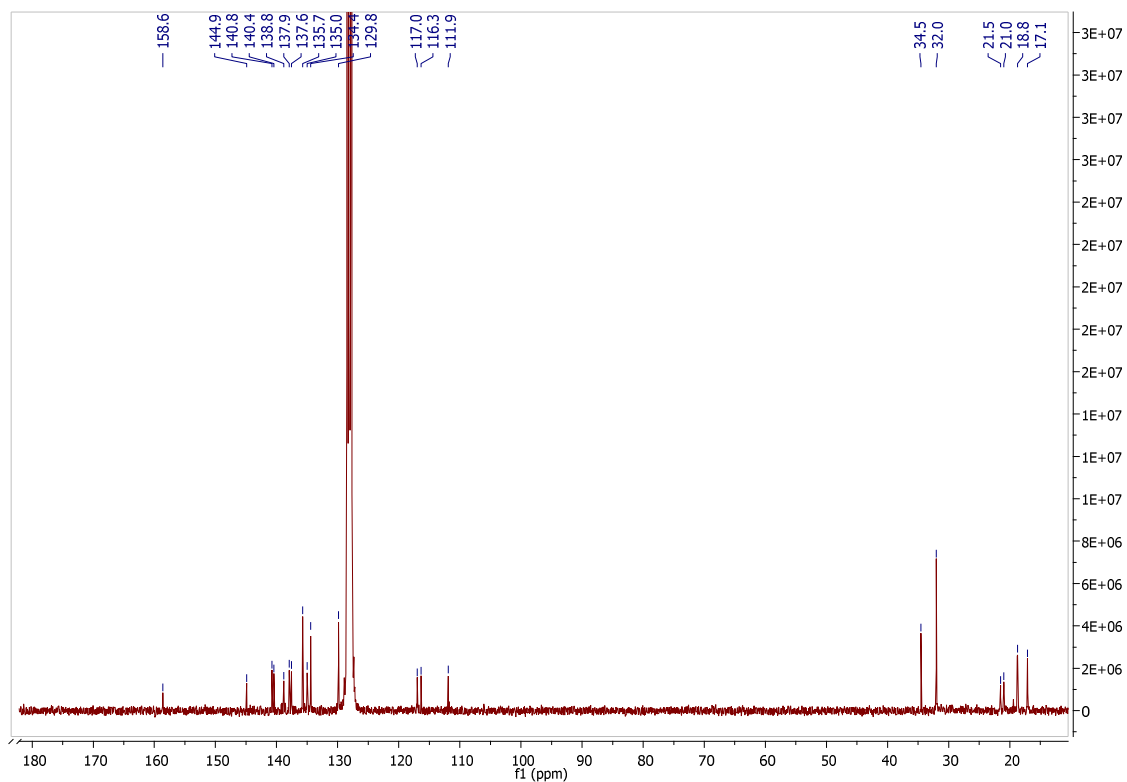
Figure 3.8: ^{13}C NMR of **13** in C_6D_6 solvent

3.3.3) Synthesis of 14

The synthesis of a Cu(II) carbene complex that could be active towards oxygen activation (see Section 3.1.1.2) was attempted. Deprotonation of the ligand salt **7** followed by metallation with CuCl$_2$, which was completed almost instantaneously at room temperature, yielded **14** as a brown solid with a yield of 86% after washing the residue with hexanes, extracting with Et$_2$O and *in vacuo* evaporation of the solvent (Scheme 3.16). The paramagnetic nature of **14** was confirmed by the NMR silent spectrum obtained. In addition, both MS and X-ray diffraction analysis confirmed the formation of **14**. The (CNC)CuCl **14** was stable only under anaerobic conditions. Decomposition of **14** was observed if the reaction depicted in Scheme 3.16 was allowed to react for twelve hours, instead of just two hours. To date, only two other examples of Cu(II)-carbene complexes have been reported, where only the report by Arnold and co-workers feature a crystal structure of the Cu(II) carbene complex.[17,18]

---

[17] P. L. Arnold, M. Rodden, K. M. Davis, A. C. Scarisbrick, A. J. Blake, C. Wilson, *Chem. Commun.*, 2004, 1612 – 1613.
[18] X. Hu, I. Castro-Rodriguez, K. Meyer, *J. Am. Chem. Soc.*, 2003, **125**, 12237 – 12245.

93
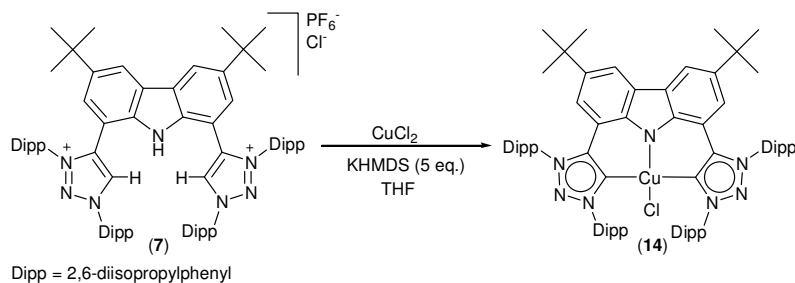
Scheme 3.16: Synthesis of the paramagnetic Cu(II) complex **14**

The Cu(II) centre has a distorted square-planar geometry, approaching a see-saw molecular geometry. This was deduced from the crystal structure (Figure 3.9). The *trz* moieties are almost exactly planar to the carbazole plane, with a C1-C2-C3-C4 torsion angle of 0.2(4)°. The C2-C1-Cu1-C1 torsion angle is 110.6(4)°, displaying the significant distortion of the metal atom out of the plane. The orientation of the metal is out of the *trz* and carbazole plane. The angles around the copper centre are more characteristic of a see-saw geometry, than of a sqaure planar geometry. The N1-Cu1-Cl2 angle is 123.61(9)° while the C1-Cu1-C1 angle (160.63(14)°) deviates substantially from 180°. The C1-Cu1-N1 angle is perpendicular at 91.14(7)°, but the C1-Cu1-Cl2 angle is 97.36(7)°. A possible explanation for the observed see-saw type geometry could be due to steric repulsion experienced by the chloro ligand from both the 2,6-diisopropylphenyl groups, forcing the chloro ligand out of the ligand scaffold plane.

The C1-Cu1 and N1-Cu1 bond distances are 1.983(3) Å and 1.956(3) Å, respectively. The Cu1-Cl2 bond distance has a value of 2.2997(11) Å. This bond length is longer than the Cu2-Cl2 bond distance of 1.971(15), the only other crystalline copper(II)-carbene complex reported to date.[17] The longer bond length in **14** is a result of the stronger *trans* influence of the amido ligand versus the oxygen *trans* ligand in the complex reported by Arnold.[17]

The triazolylidene moieties are planar (C1-C2-N2-N3 torsion angle is 0.3(3)°), with bond lengths being short, indicating electron delocalisation and thus aromaticity throughout the five-membered heterocycle. The C2-C1-N4 bond angle is 102.4(2)°, which is not as acute as for **9**. This difference can be explained by an increase in the p-character of the σ-orbital. It has been reported that aNHCs and *trz* ligands can behave as non-innocent ligands, stabilising metals of various oxidation states (see Section 1.3.2.4, Chapter 1). In the neutral *trz* ligand state, the ligand stabilises metals in low oxidation states.[19] If the metal increases its oxidation state, the *trz* moiety can stabilise the metal through intramolecular charge separation, forming a cationic iminium unit and an anionic vinyl unit.

---

[19] R. Lalrempuia, N. D. McDaniel, H. Müller-Bunz, S. Bernhard, M. Albrecht, *Angew. Chem. Int. Ed.*, 2010, **49**, 9765 – 9768.

94

This *trz* unit will still retain its aromaticity, but the percentage of s- and p-character of the σ-orbital could change. The vinylic unit will have sp^2-hybridised orbitals. The carbene carbon will also have sp^2-hybridised orbitals, but with a higher s- and lower p-character. The formation of the vinyl unit, resulting in charge separation, would decrease the s-character and increase the p-character of the σ-orbital. This then, leads to an increase in the C2-C1-N4 angle compared to the free carbene adduct.
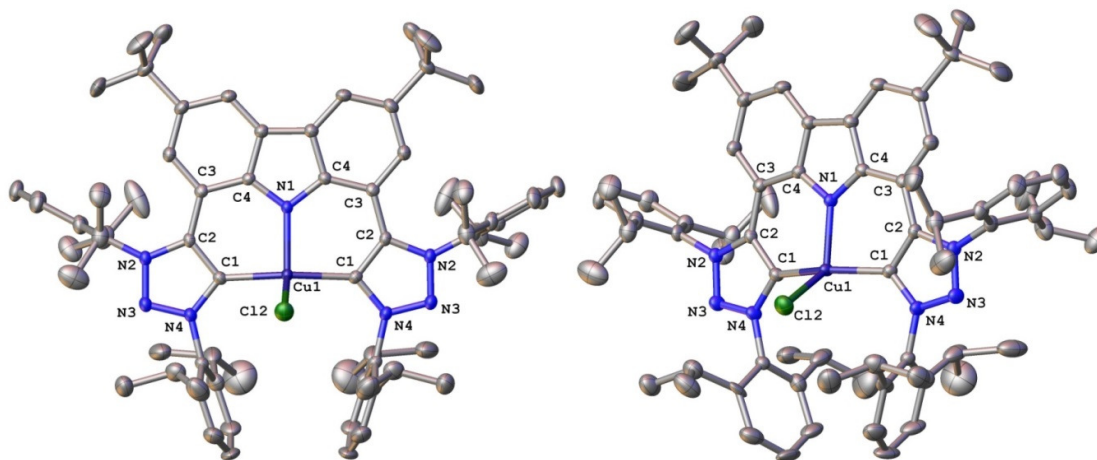
Figure 3.9: Frontal (left) and side on (right) images of crystal structure of **14**

3.3.4) Synthesis of 15

The unusual stability of **12** under anaerobic conditions inspired the attempted synthesis of the first example of a neutral carbene copper(II)-hydride complex, through the reaction of **14** with super hydride. However, the reaction of **14** with lithium triethylborohydride resulted in the reduction of the Cu(II) complex to the corresponding Cu(I) complex, **15** (Scheme 3.17). The brown solid **15** was obtained with a yield of 95%. The formation of **15** was determined by NMR, MS and XRD analysis.

Alternatively, the (CNC)Cu(I) complex could be synthesised directly from the ligand precursor **7**, employing CuI as metal precursor. Deprotonation followed by metallation of **7** with CuI yielded **15** after extraction from the crude residue with Et$_2$O, followed by evaporation of the solvent *in vacuo*. The yield of **15**, a brown solid, was determined to be 52% (Scheme 3.17). NMR analysis again confirmed a Cu(I) species, further supporting the formation of **15** through reduction of **14** with super hydride.

95
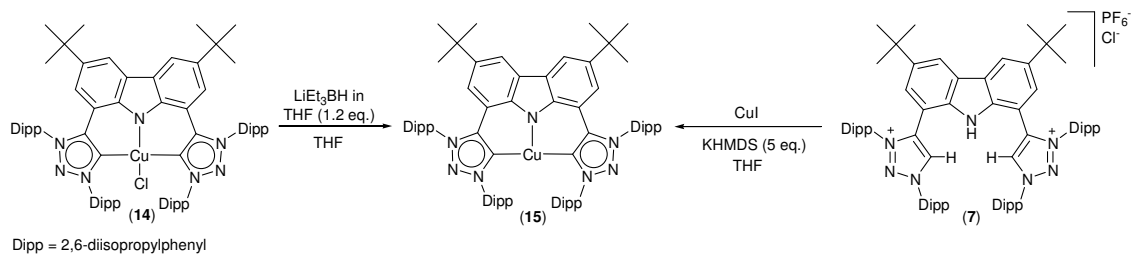
Scheme 3.17: Synthesis of **15** *via* two independent routes

There are no hydrogens resonating downfield from the aromatic hydrogens of the carbazole backbone, which resonates downfield at 8.58 ppm (Figure 3.10). This clearly indicates the disappearance of the acidic hydrogens. Also, no upfield hydridic resonance is observed in Figure 3.10, further supporting the formation of **15** and not the desired copper(II)-hydride complex. The formation of the metal-carbon bond is justified by the singlet peak resonating at 176.7 ppm in the ^{13}C NMR spectrum, which corresponds to the carbene carbon (Figure 3.11). In addition, as is evident from both the proton and carbon NMR spectra (Figure 3.10 and Figure 3.11 respectively), **15** is not paramagnetic.
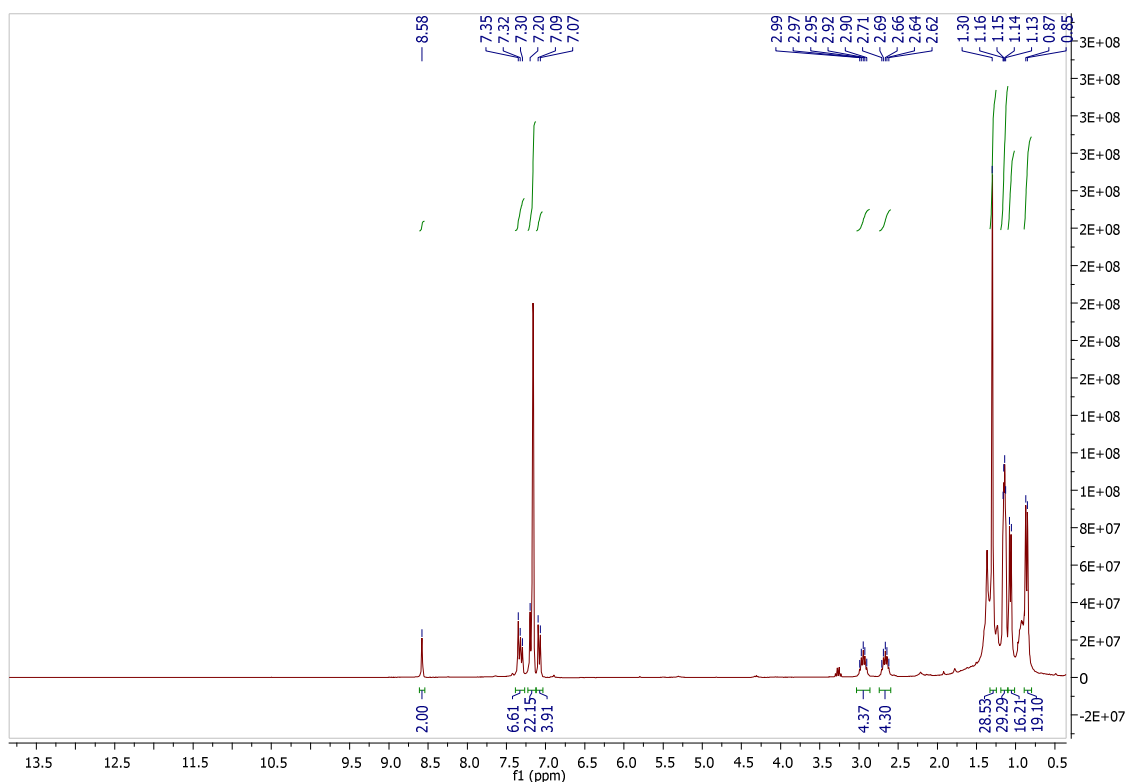
Figure 3.10: ^{1}H NMR of **15** in C_6D_6 solvent

96
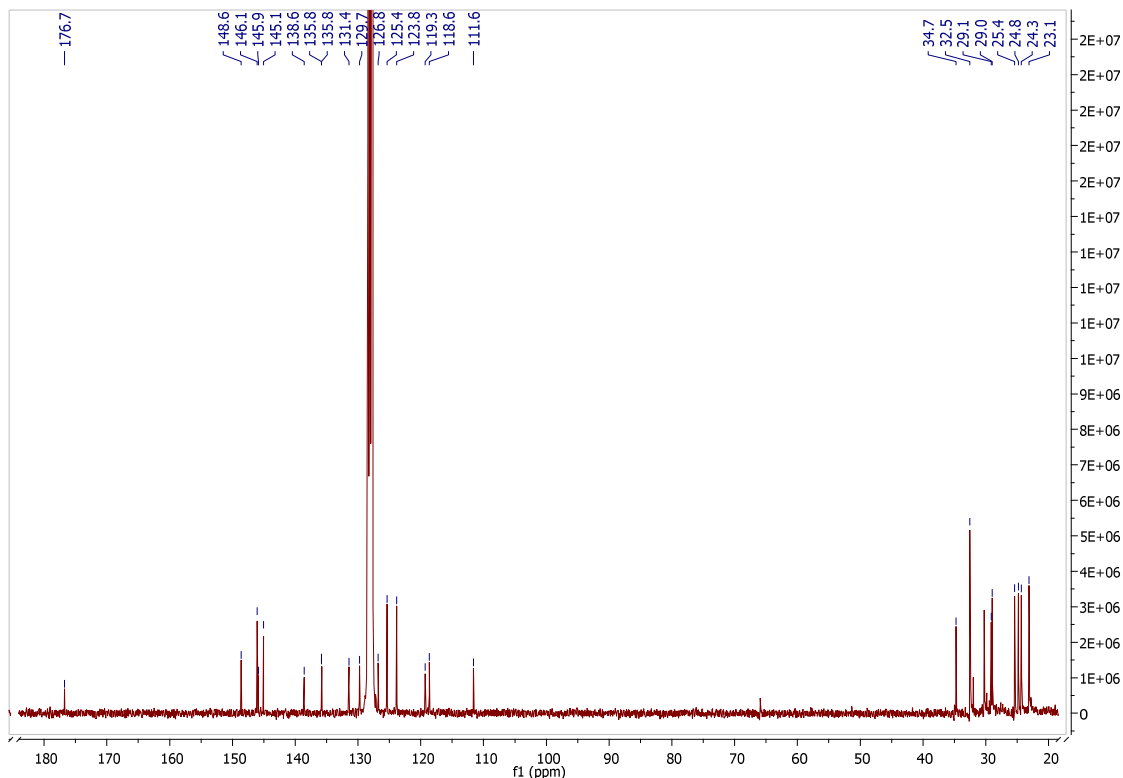
Figure 3.11: ^{13}C NMR of **15** in C$_6$D$_6$ solvent

The crystal structure of **15** was determined and is shown in Figure 3.12. The molecule has a two-fold symmetry axis with the nitrogen and copper atoms lying on the axis, and parallel to the unit cell's b-axis. The crystal structure displays a T-shaped geometry around a "naked" Cu(I) centre. The Cu(I) centre is orientated in the planar environment of the ligand scaffold, with a C2-C1-Cu1-C1 torsion angle of 175.81(15)°. The C2-C1-Cu1-C1 torsion angle of **15** is in striking contrast to that of **14**. The lack of a *trans* ligand in **15**, such as the chloride ligand in **14**, does not result in steric repulsion through occupation of the tridentate pocket by the metal and the co-ligand of the metal.

The C1-Cu1-N1 angle of 92.47(6)° deviates slightly from the expected 90° value for T-shaped complexes. The C1-Cu1-C1 angle is also not linear as expected and decreased from linearity to 175.06(12)°. The angles indicate that the tridentate ligand contracted around the Cu(I) centre, perhaps in order to increase orbital overlap between the ligand and metal. This contraction, however, decreased the distance between the two 2,6-diisopropylphenyl wingtip groups, increasing the steric repulsion experienced by these wingtip substituents on each other. The steric repulsion could be alleviated by the deviation of the *trz* moieties from carbazole planarity, which is observed for **15**. The C1-C2-C3-C8 torsion angle of **15** is 9.8(3)°.

97

The Cu(II) metal of **14** will have a larger charge density ratio, due to the higher charge and smaller metal radius when compared to the Cu(I) metal. In addition, Cu(II) is a harder Lewis acid. The amido moiety, being a hard Lewis base ligand, will form stronger bonds with hard acids. These two factors would explain why the N1-Cu1 bond for **15** is weaker, compared to the stronger N1-Cu1 bond of **14**. The difference in bond strength for both complexes can be inferred from the N1-Cu1 bond lengths. The N1-Cu1 bond length for **15** is 2.017(2) Å, which is significantly longer than the N1-Cu1 bond of **14**, which is 1.956(3) Å in length. The C1-Cu1 bond length of **15** is 1.913(2) Å, which is shorter than the C1-Cu1 bond length of **14**.

The C2-C1-N2 angle is 101.81(18) which is more acute than the corresponding angle of **14**. This could be due to the metal being in a lower oxidation state than **14**, resulting in a decrease in the extent of intramolecular charge separation (or the need for charge separation). This would not amount to as large an increase in the percentage of p-character of the σ-orbital. The angle will not increase, and will be smaller than the corresponding angle of the same metal in a higher oxidation state, as observed for the (CNC)Cu(I) and (CNC)Cu(II)Cl complexes. The *trz* ligand is also more planar than the *trz* heterocycle for **14**. The C1-C2-N4-N3 torsion angle is 0.1(2)°. This value, being very close to zero, supports aromaticity and electron delocalisation throughout the five-membered heterocycle. This also points to the intramolecular charge separation postulation. Due to the decrease in the extent of charge separation, the electron delocalisation will remain almost completely unaffected, maintaining the high aromatic character of the *trz* ligand and ultimately resulting in a planar ring system.
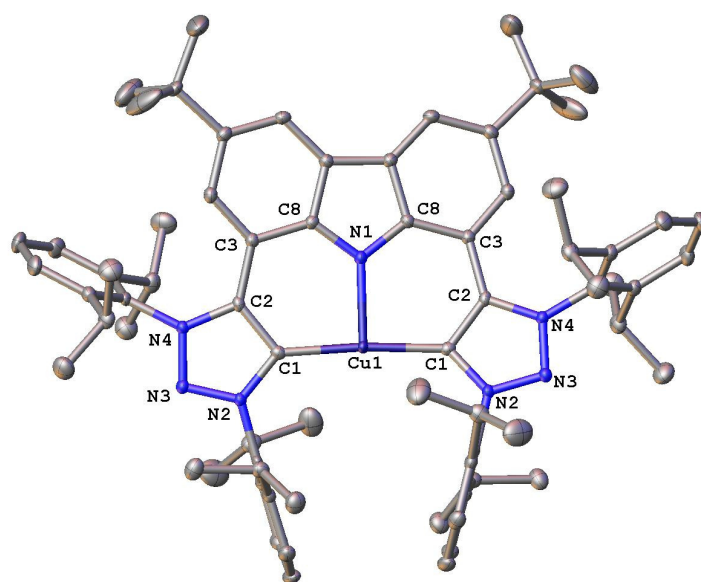
Figure 3.12: Crystal structure of **15**

98

3.3.5) Synthesis of 16

Preparation of **16**, the analogue of **15**, was done *via in situ* deprotonation of the ligand followed by metallation of the free carbene adduct with CuI. Extraction of the product from the solid residue with hexanes, and subsequent evaporation of the solvent *in vacuo*, yielded **16** as a brown solid with a yield of 69% (Scheme 3.18). NMR and MS analysis confirmed the formation of **16**, however crystals suitable for X-ray diffraction analysis were not obtained.
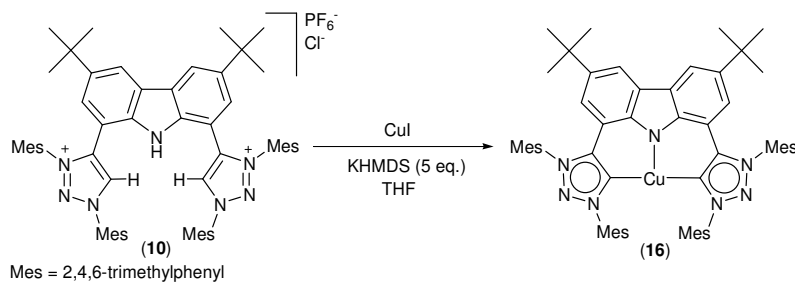
Scheme 3.18: Synthesis of **16**

As is the case for **15**, the clear disappearance of the acidic amino and *trz***H** protons is observed in the ¹H NMR spectrum of **16**. The downfield resonating protons at 8.72 ppm correspond to the aromatic hydrogens of the carbazole backbone. The carbon NMR spectrum displays a singlet at 175.7 ppm in deuterated benzene as solvent. The resonance of the carbene carbon for **15** was 176.7 ppm. The upfield shift of 1 ppm for **16** when compared to **15** is negligible.
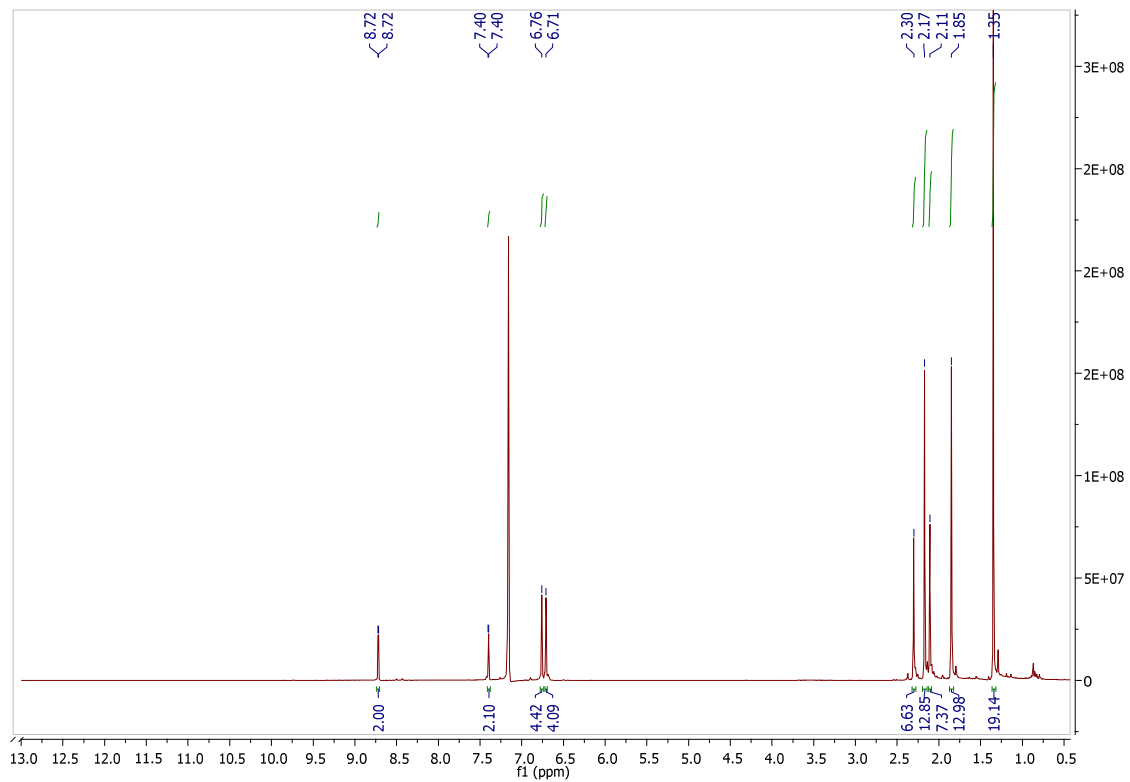
Figure 3.13: ^{1}H NMR of **16** in C_6D_6 solvent
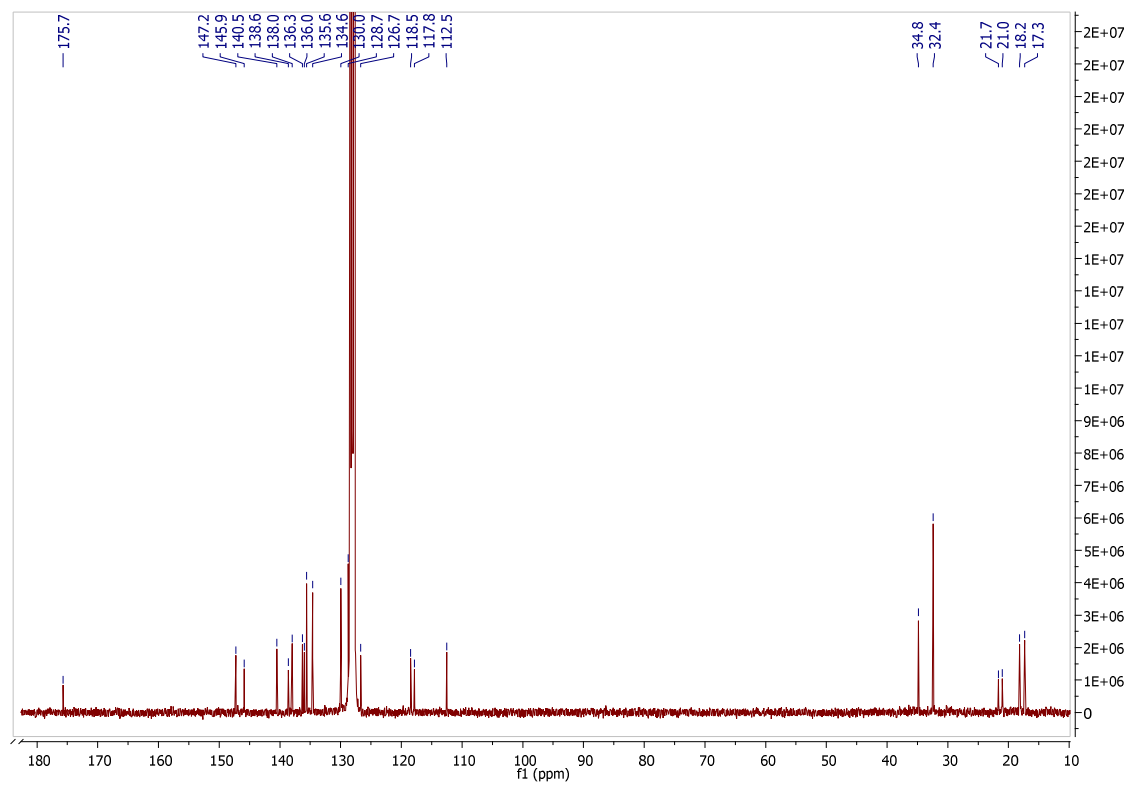
Figure 3.14: ^{13}C NMR of **16** in C_6D_6 solvent

100

3.4) Conclusion

The two triazolium ligand salts discussed in Chapter 2 were successfully coordinated to two different, late 3d-transition metals. The transition metals of interest are nickel and copper. The synthesised complexes were characterised with various techniques including NMR, XRD and MS analysis.

Coordination of either **7** or **10** to a [Ni(dme)Cl$_2$] metal precursor, *via in situ* deprotonation followed by metallation, unexpectedly yielded a nickel-hydride complex in both cases. The (CNC)NiH complexes **12** and **13** are the first examples of neutral nickel-hydride carbene complexes. The formation of both **12** and **13** were confirmed with NMR and MS spectrometric techniques, while **12** was additionally characterised with X-ray diffraction analysis. The crystal structure of **12** displayed a square-planar geometry. The (CNC)NiH complexes are surprisingly stable under anaerobic conditions at room temperature, but decompose in the presence of moisture.

The reaction between **7** and a CuCl$_2$ metal precursor yielded a rare example of a carbene-copper(II) complex, **14**, that was characterised by X-ray diffraction and mass spectrometric analysis. The paramagnetic nature of **14** was observed upon attempted characterisation with NMR techniques. The crystal structure revealed an unusual see-saw type geometry around the four coordinated Cu(II) metal. The (CNC)CuCl complex **14** was unstable under aerobic conditions and decomposed, but indefinitely stable under a N$_2$ (g) or Ar (g) atmosphere at room temperature. In addition, extended reaction time also resulted in decomposition of **14**.

The reaction of **14** with LiEt$_3$BH did not yield the desired (CNC)CuH complex. The super hydride acted as a reducing agent, resulting in the reduction of **14** to the Cu(I) complex, **15**. An independant method involving **7**, CuI and KHMDS also led to the synthesis of **15**. Spectroscopic characterisation, through NMR, MS and XRD analysis, unambiguously confirmed the formation of **15**. The crystal structure of **15** revealed that the geometry around the Cu(I) metal centre was T-shaped. The harder Lewis acid Cu(II) metal formed a stronger bond with the hard Lewis amido base ligand. This was confirmed with the short bond length for **14** and longer bond length for **15**. The unavailability of EPR instrumentation precluded the characterisation of the paramagnetic Cu(II) complex with EPR spectroscopy. Additionally, the analogue of **15**, namely **16** which is supported by **11**, could be synthesised by deprtotonation of **10**, yielding **11** that was metallated *in situ* with CuI. NMR and MS analysis confirmed the formation of **16**. Crystals suitable for X-ray diffraction analysis could not be obtained.

3.5) Experimental

3.5.1) (CNC$_{Dipp}$)NiH (**12**)
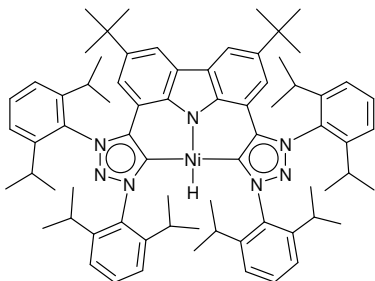
To a flame dried Schlenk was added **7** (200.0 mg, 1.6 x 10^{-4} mol), [Ni(dme)Cl$_2$] (39.1 mg, 1.8 x 10^{-4} mol) and KN[Si(CH$_3$)$_3$]$_2$ (161.3 mg, 8.1 x 10^{-4} mol). The reaction vessel was purged with Ar (g) and cooled down to -78 °C. The solids were dissolved by adding THF (12 mL) which was cooled down to -78 °C. The solution was stirred for 30 min at -78 °C before being removed from the cold bath and stirred an additional 24 hours at room temperature. The solvents were evaporated *in vacuo* and the product extracted with hexanes (5 x 10 mL). Evaporation of the solvent *in vacuo* yielded **12** as a red solid (70.0 mg, 6.3 x 10^{-5} mol, 39%); **m.p.** 282-285 °C (dec). Crystallisation from benzene yielded single crystals suitable for XRD analysis. ^{1}H NMR δ$_H$ (C$_6$D$_6$, 300 MHz) 8.28 (2H, d, *J* = 1.8 Hz, Ar**H**$_{carb}$), 7.29 (2H, t, *J* = 7.8 Hz, Ar**H**$_{Dipp}$), 7.25 (2H, t, *J* = 7.8 Hz, Ar**H**$_{Dipp}$), 7.15 (4H, d, Ar**H**$_{Dipp}$ overlaps with C$_6$D$_6$), 7.10 (2H, d, *J* = 1.8 Hz, Ar**H**$_{Carb}$), 7.07 (4H, d, *J* = 7.8 Hz, Ar**H**$_{Dipp}$), 2.95 (4H, sept, *J* = 6.9 Hz, C**H**(CH$_3$)$_2$), 2.66 (4H, sept, *J* = 6.9 Hz, C**H**(CH$_3$)$_2$), 1.56 (12H, d, *J* = 6.6 Hz, CH(C**H$_3$**)$_2$), 1.21 (18H, s, C(C**H**$_3$)$_3$), 1.19 (12H, d, CH(C**H$_3$**)$_2$ overlaps with C(C**H**$_3$)$_3$), 1.06 (12H, d, *J* = 6.9 Hz, CH(C**H$_3$**)$_2$), 0.87 (12H, d, *J* = 6.9 Hz, CH(C**H$_3$**)$_2$), -6.30 (1H, s, Ni**H**). ^{13}C NMR δ$_C$ (C$_6$D$_6$, 75 MHz) 159.8 (**C**$_{Carbene}$), 146.3 (Ar**C**$_q$), 144.9 (Ar**C**$_q$), 141.6 (Ar**C**$_q$), 138.5 (Ar**C**$_q$), 137.4 (Ar**C**$_q$), 134.9 (Ar**C**$_q$), 131.7 (Ar**C**H$_{Dipp}$), 129.0 (Ar**C**H$_{Dipp}$), 127.3 (Ar**C**$_q$), 125.2 (Ar**C**H$_{Dipp}$), 123.1 (Ar**C**H$_{Dipp}$), 117.4 (Ar**C**H$_{Carb}$), 117.2 (Ar**C**H$_{Carb}$), 111.2 (Ar**C**$_q$), 34.4 (**C**(CH$_3$)$_3$), 32.2 (C(**C**H$_3$)$_3$), 29.5 (**C**H(CH$_3$)$_2$), 29.1 (**C**H(CH$_3$)$_2$), 25.1 (CH(**C**H$_3$)$_2$), 25.0 (CH(**C**H$_3$)$_2$), 24.8 (CH(**C**H$_3$)$_2$), 23.2 (CH(**C**H$_3$)$_2$). HRMS (ESI-TOFMS): Calculated for C$_{72}$H$_{90}$N$_7$Ni$^+$ [M]$^+$: 1110.6611, found: 1110.6609.

3.5.2) (CNC$_{Mes}$)NiH (**13**)
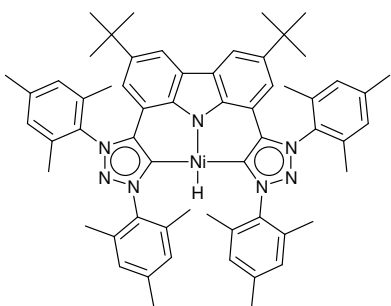
The same procedure used in order to synthesise **12** was employed during the synthesis of **13**. A flame dried Schlenk was charged with **10** (200.0 mg, 1.9 x 10^{-4} mol), [Ni(dme)Cl$_2$] (49.35 mg, 2.2 x 10^{-4} mol) and KN[Si(CH$_3$)$_3$]$_2$ (186.66 mg, 9.4 x 10^{-4} mol). The Schlenk was purged with Ar (g) and cooled down to -78 °C, with subsequent addition of THF (12 mL) which was also cooled down to -78 °C. The solution was stirred for one hour at -78 °C

before being removed from the cold bath and stirred an additional 18 hours at room temperature. The solvents were evaporated *in vacuo*. The product was extracted with hexanes (5 x 15 mL), followed by evaporation of the solvent *in vacuo* to yield **12** (95.0 mg, 1.0x 10^{-4} mol, 54%) as a red solid. ^{1}H NMR δ $_H$ (C$_6$D$_6$, 300 MHz) 8.49 (2H, d, *J* = 1.8 Hz, Ar**H**$_{carb}$), 7.11 (2H, d, *J* = 1.8 Hz, Ar**H**$_{carb}$), 6.71 (4H, s, Ar**H**$_{Mes}$), 6.69 (4H, s, Ar**H**$_{Mes}$), 2.52 (12H, s, Ar**CH$_3$**), 2.29 (6H, s, Ar**CH$_3$**), 2.07 (6H, s, Ar**CH$_3$**), 1.76 (12H, s, Ar**CH$_3$**), 1.26 (18H, s, C(**CH$_3$**)$_3$), -6.31 (1H, s, Ni**H**). ^{13}C NMR δ $_C$ (C$_6$D$_6$, 75 MHz,) 158.6 (**C**$_{Carbene}$), 144.2 (Ar**C**$_q$), 140.8 (Ar**C**$_q$), 140.4 (Ar**C**$_q$), 138.8 (Ar**C**$_q$), 137.9 (Ar**C**$_q$), 137.6 (Ar**C**$_q$), 135.7 (Ar**C**$_q$), 135.0 (Ar**C**$_q$), 134.4 (Ar**C**$_q$), 129.8 (Ar**C**H), 117.0 (Ar**C**H), 116.3 (Ar**C**H), 111.9 (Ar**C**$_q$), 34.5 (**C**(CH$_3$)$_3$), 32.0 (C(**CH$_3$**)$_3$), 21.5 (Ar**CH$_3$**), 21.0 (Ar**CH$_3$**), 18.8 (Ar**CH$_3$**), 17.1 (Ar**CH$_3$**). HRMS (FIA-ESI): Calculated for C$_{60}$H$_{66}$N$_7$Ni$^+$ [M]$^+$: 942.4733, found: 942.4767.

3.5.3) (CNC$_{Dipp}$)CuCl (14)
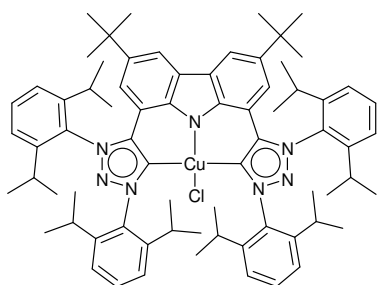
A flame dried Schlenk was charged with **7** (100.0 mg, 8.1 x 10^{-5} mol), CuCl$_2$ (12.0 mg, 8.9 x 10^{-5} mol) and KN[Si(CH$_3$)$_3$]$_2$ (80.6 mg, 4.0 x 10^{-4} mol). The vessel was purged with N$_2$ gas. THF (10 mL) cooled down to -78 °C was added to dissolve the solids. The solution was stirred for 30 min at -78 °C before being removed from the cold bath and left to warm up to room temperature whilst stirring for an additional 2 hours. The solvent was evaporated *in vacuo*. The product was extracted from the residue with Et$_2$O (4 x 15 mL) followed by evaporation of the solvent *in vacuo* to yield compound **14** as a brown solid (80.0 mg, 6.9 x 10^{-5} mol, 86%); **m.p.** > 300 °C (dec). Crystallizing from benzene yielded single crystals suitable for XRD analysis. No usable NMR spectra could be recorded due to the paramagnetic nature of the Cu(II) atom. HRMS (ESI-TOFMS): Calculated for C$_{72}$H$_{90}$N$_7$Cu$^+$ [M-Cl]$^+$: 1115.6548, found: 1115.6547.

3.5.4) (CNC$_{Dipp}$)Cu (15)
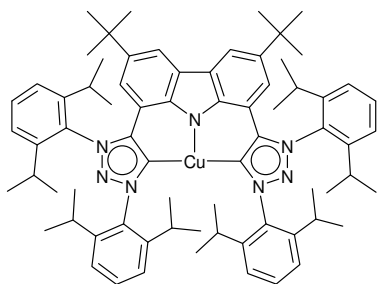
Method 1: A Schlenk was charged with compound **14** (54.5 mg, 4.7 x 10^{-5} mol) and purged with N$_2$ gas. The solid was first dissolved by adding THF (8 mL) cooled down to -78 °C, followed by the drop-wise addition of LiHBEt$_3$ (6.7 x 10^{-2} mL, 5.7 x 10^{-5} mol). The solution was stirred for 15 min at -78 °C before being removed from the cold bath and left to warm up to room temperature whilst stirring for 1 hour. The solvent was evaporated *in vacuo* and the product was extracted with hexanes (3 x 10 mL). Evaporation of the solvent *in vacuo* yielded compound **15** as a brown solid (50.0 mg, 4.5 x 10^{-5} mol, 95%).

Method 2: Compound **15** was prepared by addition of CuI (18.5 mg, 9.7 x 10^{-5} mol) to a Schlenk tube with compound **7** (100.0 mg, 8.1 x 10^{-5} mol), and KN[Si(CH$_3$)$_3$]$_2$ (80.6 mg, 4.0 x 10^{-4} mol). The Schlenk was purged with N$_2$ gas and cooled down to -78 °C. The solids were dissolved by adding THF (10 mL) cooled down to -78 °C. The solution was stirred for 30 min before being removed from the cold bath and left to warm up to room temperature whilst stirring overnight. The solvent was evaporated *in vacuo* and the residue was washed with hexanes (4 x 10 mL) followed by extraction of the product with Et$_2$O (4 x 15 mL). Evaporation of the solvent *in vacuo* yielded **15** as a brown solid (47.0 mg, 4.2 x 10^{-5} mol, 52%); **m.p.** > 300 °C (dec). Crystallizing from benzene yielded single crystals suitable for XRD analysis. ^{1}H NMR δ$_H$ (C$_6$D$_6$, 300 MHz) 8.58 (2H, br s, Ar**H**$_{carb}$), 7.35 (2H, br s, Ar**H**$_{carb}$), 7.32 (4H, t, *J* = 7.8 Hz, Ar**H**$_{Dipp}$), 7.18 (4H, d, Ar**H**$_{Dipp}$ overlaps with C$_6$D$_6$), 7.08 (4H, d, *J* = 7.8 Hz, Ar**H**$_{Dipp}$), 2.95 (4H, sept, *J* = 6.9, C**H**(CH$_3$)$_2$), 2.67 (4H, sept, *J* = 6.9, C**H**(CH$_3$)$_2$), 1.30 (18H, s, C(C**H$_3$**)$_3$), 1.15 (12H, d, *J* = 6.6 Hz, CH(C**H$_3$**)$_2$), 1.14 (12H, d, *J* = 6.6 Hz, CH(C**H$_3$**)$_2$), 1.07 (12H, d, *J* = 6.6 Hz, CH(C**H$_3$**)$_2$), 0.86 (12H, d, *J* = 6.6 Hz, CH(C**H$_3$**)$_2$). ^{13}C NMR δ$_C$ (C$_6$D$_6$, 75 MHz) 176.7 (**C**$_{Carbene}$), 148.6 (Ar**C**$_q$), 146.1 (Ar**C**$_q$), 145.9 (Ar**C**$_q$), 145.1 (Ar**C**$_q$), 138.6 (Ar**C**$_q$), 135.8 (Ar**C**$_q$), 135.8 (Ar**C**$_q$), 131.4 (Ar**C**H$_{Dipp}$), 129.8 (Ar**C**H$_{Dipp}$), 126.8 (Ar**C**$_q$), 125.4 (Ar**C**H$_{Dipp}$), 123.9 (Ar**C**H$_{Dipp}$), 119.3 (Ar**C**H$_{Carb}$), 118.6 (Ar**C**H$_{Carb}$), 111.6 (Ar**C**$_q$), 34.7 (**C**(CH$_3$)$_3$), 32.5 (C(**C**H$_3$)$_3$), 29.1 (**C**H(CH$_3$)$_2$), 29.0 (**C**H(CH$_3$)$_2$), 25.4 (CH(**C**H$_3$)$_2$), 24.8 (CH(**C**H$_3$)$_2$), 24.3 (CH(**C**H$_3$)$_2$), 23.1 (CH(**C**H$_3$)$_2$). HRMS (ESI-TOFMS): Calculated for C$_{72}$H$_{90}$N$_7$Cu$^+$ [M]$^+$: 1115.6554, found: 1115.6551.

3.5.5) (CNC$_{Mes}$)Cu (16)
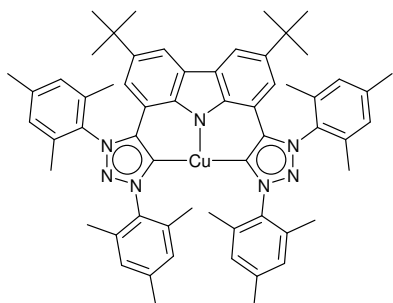
Compound **16** was prepared by loading a flame dried Schlenk with CuI (42.77 mg, 2.2 x 10^{-4} mol), **10** (200.0 mg, 1.9 x 10^{-4} mol), and KN[Si(CH$_3$)$_3$]$_2$ (186.7 mg, 9.4 x 10^{-4} mol). The Schlenk was purged with N$_2$ (g) and cooled down to -78 °C. The solids were dissolved by adding THF (20 mL) also cooled down to -78 °C. The solution was stirred for 30 min before being removed from the cold bath and left to warm up to room temperature whilst stirring overnight. The solvent was evaporated *in vacuo* and the product extracted with hexanes (5 x 15 mL). Evaporation of the solvent *in vacuo* yielded **16** as a brown solid (122.0 mg, 1.3 x 10^{-4} mol, 69%). ^{1}H NMR δ$_H$ (C$_6$D$_6$, 300 MHz) 8.72 (2H, d, *J* = 1.5 Hz, Ar**H**$_{carb}$), 7.40 (2H, d, *J* = 1.8 Hz, Ar**H**$_{carb}$), 6.76 (4H, s, Ar**H**$_{Mes}$), 6.71 (4H, s, Ar**H**$_{Mes}$), 2.30 (6H, s, Ar**C**H$_3$), 2.17 (12H, s, Ar**C**H$_3$), 2.11 (6H, s, Ar**C**H$_3$), 1.85 (12H, s, Ar**C**H$_3$), 1.35 (18H, s, C(**C**H$_3$)$_3$). ^{13}C NMR δ$_C$ (C$_6$D$_6$, 75 MHz,) 175.7 (**C**$_{Carbene}$), 147.2 (Ar**C**$_q$), 145.9 (Ar**C**$_q$), 140.5 (Ar**C**$_q$), 138.6 (Ar**C**$_q$), 138.0 (Ar**C**$_q$), 136.3 (Ar**C**$_q$), 136.0 (Ar**C**$_q$), 135.6 (Ar**C**$_q$), 134.6 (Ar**C**$_q$), 130.0 (Ar**C**H), 128.7 (Ar**C**H), 126.7 (Ar**C**$_q$), 118.5 (Ar**C**H), 117.8 (Ar**C**H), 112.5 (Ar**C**$_q$), 34.8 (**C**(CH$_3$)$_3$), 32.4 (C(**C**H$_3$)$_3$), 21.7 (Ar**C**H$_3$), 21.0 (Ar**C**H$_3$), 18.2 (Ar**C**H$_3$), 17.3 (Ar**C**H$_3$). HRMS (ESI-TOFMS): Calculated for C$_{60}$H$_{66}$N$_7$Cu^{2+} [M + K + H]$^{2+}$: 493.7189, found: 493.7182.

Chapter 4: Synthesis of (CNC)Rh(I) Complexes and Reactivity Studies

4.1) Background

The activation of small molecules and the importance thereof were discussed, with relevant examples, in Chapter 3. In particular, oxidation reactions of organic substrates with metal-peroxo and/or metal-superoxo species, obtained by the activation of molecular oxygen with a reactive metal complex. However, activation of other so-called 'inert' molecules, such as NH_3 (g) and O_2 (g), and their use as catalytic substrates are also of major importance due to their low cost and the fact that they are readily available.[1] Little progress has been made in this area of research, and not due to a lack of interest, but due to difficulty of utilising these small molecules in catalysis.

The coordination of rhodium to various ligand scaffolds to yield the corresponding rhodium complex, and their reactivity towards a broad range of catalytic reactions have been extensively studied and reported.[2] In fact, rhodium, palladium and nickel have been dubbed the heavyweights of the late transition metals in terms of catalytic reactivity. The catalytic reactions catalysed by rhodium carbene complexes include hydrosilylation to hydroformylation, transfer hydrogenation to hydrogenation, and coupling as well as cyclisation reactions.[2] In contrast, the activation of various amines including NH_3 (g) as well as O_2 (g), using a rhodium complex as catalyst, has received much less attention compared to the catalytic reactions already mentioned. A rhodium complex with a high nucleophilic metal centre could facilitate catalysis of these 'difficult' substrates, especially during the oxidative addition of the substrate across the metal centre.

4.1.1) Reactivity and Catalysis of Metal Complexes Towards Amines

The large scale production of various chemical feedstocks, pharmaceuticals and fertilizers involves the synthesis of organic products containing the ubiquitous carbon-nitrogen bond.[3] Classical

---

[1] J. I. van der Vlugt, *Chem. Soc. Rev.*, 2010, **39**, 2302 – 2322.

[2] See relevant review articles and references therein: *a)* M. Poyatos, J. A Mata, E. Peris, *Chem. Rev.*, 2009, **109**, 3677 – 3707, *b)* R. Corberán, E. Mas-Marzá, E. Peris, *Eur. J. Inorg. Chem.*, 2009, 1700 – 1716, *c)* J. A. Mata, M. Poyatos, E. Peris, *Coord. Chem. Rev.*, 2007, **251**, 841 – 859, *d)* D. Pugh, A. A. Danopoulus, *Coord. Chem. Rev.*, 2007, **251**, 610 – 641.

[3] V. Lavallo, G. D. Frey, B. Donnadieu, M. Soleilhavoup, G. Bertrand, *Angew. Chem. Int. Ed.*, 2008, **47**, 5224 – 5228.

methods for the utilisation of amines towards the synthesis of new C-N functionalised products involve salt elimination or dehydrogenation reactions. Both methods are accompanied by a large production of waste and require a high energy input. Metal complexes active in catalysis of amines towards the formation of carbon-nitrogen containing organic products, would certainly decrease the amount of waste production and energy requirement, as well as the cost of producing these valuable organic products.

Synthesis of metal complexes active in the catalysis of amines/ammonia is non-trivial. This is due to the tendency of amines to form stable Lewis acid-base complexes, also known as inert Werner complexes (**a**, Figure 4.1).[4] The nitrogen lone pair of the incoming amine coordinates to the metal with formation of a dative-covalent bond. In most cases, this renders the metal complex inactive towards subsequent reactions.

The oxidative addition of amines and/or NH_3 is more favoured with the use of a high nucleophilic metal centre.[1] This oxidative addition would circumvent the possible formation of a Werner complex, to yield the corresponding amido hydride complex (**b**, Figure 4.1). This complex could subsequently be reacted with a substrate such as an alkene or an alkyne, to yield the primary or secondary amine, depending on the substrate employed. The hydroamination, hydroaminomethylation, reductive amination, aryl halide amination and reduction of nitriles are some of the known examples for N-H bond functionalisation.[5]

$$L_nM \longleftarrow NH_3 \qquad L_nM \big\langle {}^{NH_2}_{\ \ H}$$

(**a**)   (**b**)
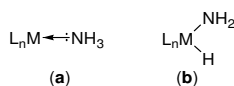
Figure 4.1: Coordination of NH_3 (g) to a metal centre yielding (**a**) the Werner complex or (**b**) the amido hydride complex

Formation of the amido hydride complex is not always a necessity during the catalytic amination reaction. In addition, the coordination of the amine substrate to the metal centre through its lone pair of electrons does not always yield an inert Lewis acid-base complex. A pioneering example includes the hydroamination of unactivated alkenes and alkynes with NH_3 (g) using a cationic (CAAC)-gold(I) complex (CAAC = cyclic (alkyl)(amino)carbene).[3] Addition of condensed NH_3 (*l*) to a solution of the cationic (CAAC)-gold(I) complex resulted in the formation of the Werner complex, which surprisingly, was not inert. The Werner complex was attributed to be the resting state of the catalyst. Addition of the unsaturated carbon substrate yielded the amine product through an insertion reaction, and the starting gold cationic complex coordinated to NH_3, was again obtained.

---

[4] Z. A. Werner, *Anorg. Chem.*, 1893, **3**, 267.
[5] M. Feller, Y. Diskin-Posner, L. J. W. Shimon, E. Ben-Ari, D. Milstein, *Organometallics*, 2012, **31**, 4083 – 4101.

107

4.1.1.1) Parent Amido and Amido Hydride Species

The synthesis and isolation of the amido and/or the amido hydride metal complexes, though not always a necessity in amination catalysis, are still important and valuable. These complexes can be studied, which would most certainly result in a deeper understanding of these important species as well as their role in catalysis. In addition, these species can also be reacted with various substrates in reactivity tests or catalytic reactions. Several synthetic methodologies towards the parent amido complex include the salt metathesis reaction (**II**, Scheme 4.1), dehydrohalogenation of the M-NH$_3$ adduct with a strong base (**III**, Scheme 4.1) and halide abstraction followed by coordination of the NH$_3$ molecule and subsequent deprotonation (**IV**, Scheme 4.1).[1] Synthesis of the parent amido and/or amido hydride complex through oxidative addition of the amine/ammonia is one of the more difficult reactions (**I**, Scheme 4.1).
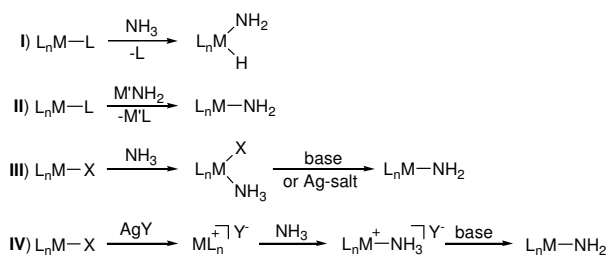
Scheme 4.1: Synthetic methodologies towards the parent amido or amido hydride metal complex[1]

The controlled N-H bond activation of ammonia to yield the metal-amido complex was first reported in the year 1987 by Calabrese and Milstein.[6] The reaction of ammonia with **c** (Scheme 4.2) in the presence of NaBPh$_4$ yielded the binuclear amido complex **d** (Scheme 4.2). Upon substitution of the ethyl phosphine substituents with *iso*-propyl phosphine functionalities, the Werner complex **e** (Scheme 4.2) was obtained after the reaction of **c** with NH$_3$. The dinuclear iridium complex **d** was structurally characterised, the first example of a crystalline metal-amido complex. It was postulated that a 14-electron iridium intermediate is present during the reaction. The loss of the ethylene ligand yields the reactive 14-eletron intermediate. No reaction with CO (g), excess ethene or phosphine with **c** was observed. It was later reported that the ligand *trans* to the incoming ammonia as well as the size of the functional groups substituted at the coordinating phosphine either resulted in oxidative addition or no reaction with ammonia.[7] If the phosphine ligand is *trans* to the incoming ammonia substrate, oxidative addition occurred due to the large *trans* effect. In contrast, the chloride ligand has a small *trans* effect, and did not mediate oxidative addition of the incoming

---

[6] A. L. Casalnuovo, J. C. Calabrese, D. Milstein, *Inorg. Chem.*, 1987, **26**, 973 – 976.
[7] M. Schulz, D. Milstein, *J. Chem. Soc., Chem. Commun.*, 1993, 318 – 319.

ammonia substrate. With *iso*-propyl functional groups on the phosphine instead of the ethyl moieties, intramolecular C-H activation of either the ethene or *iso*-propyl groups occurred, yielding the iridium-hydride ammonia adduct **e**.[7] These studies suggested that oxidative addition of ammonia might occur more readily using reactive late transition metals with strong *trans* donor ligands.
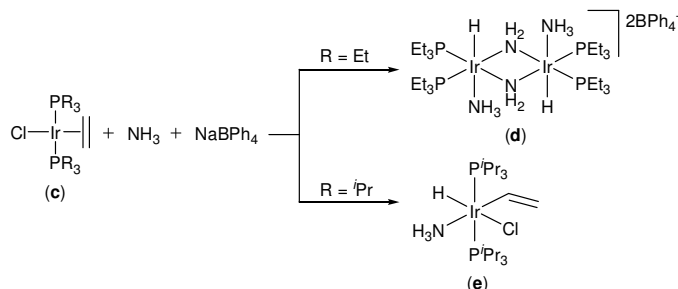
Scheme 4.2: Ammonia N-H activation by an Ir(I) metal centre[6]

The group of Hartwig *et al.* reported the oxidative addition of ammonia across an iridium metal centre (Scheme 4.3).[8] Hartwig postulated that synthesis of a metal complex with a high electron density might favour thermodynamics for oxidative addition of ammonia. In addition, formation of the metal-amido hydride complex would further favour thermodynamics, due to the increased electron density at the metal centre. As such, the group of Hartwig synthesised an iridium tetrahydride complex with a strongly donating, aliphatic PCP ligand backbone (**f**, Scheme 4.3) which was subsequently reacted with propene. Treatment of the iridium propene complex (**g**, Scheme 4.3) with four equivalents of ammonia yielded the iridium amido hydride complex in 5 minutes with a yield of 90% (**g**, Scheme 4.3). It was also proven that the oxidative addition of ammonia is thermodynamically more favourable compared to the oxidative addition of 3,5-dimethylaniline. This is unusual because it is expected that the more acidic aromatic amine with a weaker N-H bond strength, would oxidatively add across the iridium centre more readily compared to ammonia. This was not the case and the reason for this observation was based on the fact that the smaller ammonia substrate experience less steric repulsion compared to the bulky aniline substrate and also, the π-donating ability of the basic ammonia is greater than that of the aromatic amine. Catalysis of the iridium amido hydride complex was not reported.
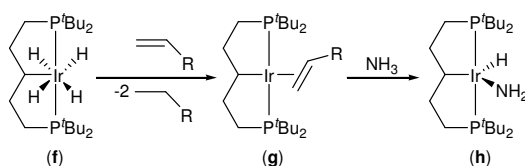
Scheme 4.3: Ammonia activation with a (PCP)Ir complex reported by Hartwig *et al.*[8]

---

[8] J. Zhao, A. S. Goldman, J. F. Hartwig, *Science*, 2005, **307**, 1080 – 1082.

Recently it was reported that a (PNP)Ir complex with a phosphaalkene moiety was active towards the N-H bond activation of ammonia as well as various other amines.[9] It was hypothesized that the low-lying π^*-orbital of the phosphaalkene unit would feature strong π-accepting properties and increase the Lewis acidity of the metal centre. This would subsequently allow for N-H bond cleavage to occur more readily. In addition, the basic phosphine ligands would increase electron density on the metal centre. The iridium complex **j** (Scheme 4.4), synthesised by treatment of **i** with three equivalents of potassium *tert*-butoxide, was reacted with ammonia to yield the parent iridium-amido complex quantitatively and instantaneously at room temperature (**k**, Scheme 4.4). The amido protons resonated, in the ^{1}H NMR spectrum, as a broad singlet at 3.82 ppm and crystal structure determination unambiguously confirmed the formation of the iridium-amido complex **k**. Density Functional Theory (DFT) calculations supported the formation of the iridium-amido complex in a concerted, three-step process. The ammonia coordinates to the apical site at the iridium centre, followed by the cooperative cleavage of the N-H bond by iridium and the vinylic carbon. Finally, the iridium-chloride bond elongates, inducing migration of the amido moiety from the apical to the equatorial position and subsequent chloride ligand dissociation.[9] The N-H bond activation was also shown to occur with aniline and hexylamine using the (PNP)Ir complex.
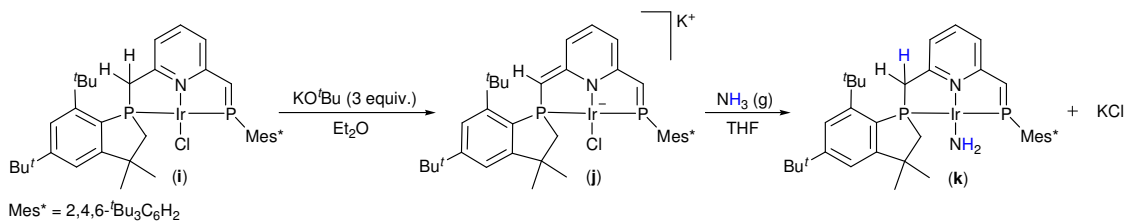
Scheme 4.4: N-H bond cleavage *via* a (PNP)Ir complex containing a phosphaalkene moiety[9]

Only a few discoveries have been made regarding the catalysis of various organic substrates with metal-amido or metal-amido hydride complexes as the intermediates or resting states during the catalytic reactions.[10] An example of a metal-amido complex which was formed from the reaction between ammonia and the catalyst, that is active in catalysis, was reported by Hartwig and co-workers.[11] The palladium-catalysed amination of aryl halides with ammonia to yield the aniline derivative was investigated (Scheme 4.5). Reacting ammonia with a palladium catalyst yielded the palladium-amido complex, which could be isolated, and reacted with an aryl halide to reductively eliminate an aryl amine. However, for catalytic purposes, stoichiometric amounts of NaO^{t}Bu had to

[9] Y-H. Chang, Y. Nakajima, H. Tanaka, K. Yoshizawa, F. Ozawa, *J. Am. Chem. Soc.*, 2013, **135**, 11791 – 11794.
[10] J. L. Klinkenberg, J. F. Hartwig, *Angew. Chem. Int. Ed.*, 2011, **50**, 86 – 95.
[11] Q. Shen, J. F. Hartwig, *J. Am. Chem. Soc.*, 2006, **128**, 10028 – 10029.

110

be added, and reactions were carried out with 1 mol% of catalyst. The aryl amines where obtained in good to excellent yields.

Scheme 4.5: Catalysis of ammonia occurring through a metal-amido complex[11]
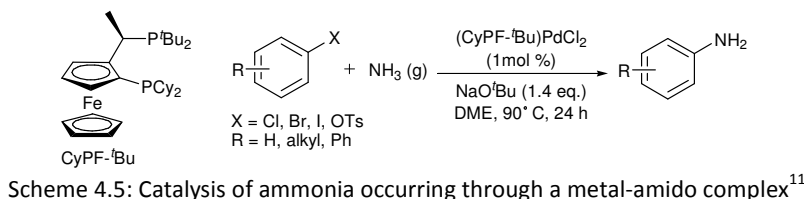
4.1.1.2) Catalytic Amination Reactions using a Rhodium Complex

Rhodium complexes, ranging from a simple $[Rh(cod)Cl]_2$ complex to a Milstein type PNP-pincer complex, has shown some promising results towards the reactivity of rhodium complexes with amines as well as the amination reaction of various organic substrates with amines. Rhodium can tolerate ammonia, binding to ammonia either reversibly or through formation of a Werner complex in general.[10] This has been attributed to the soft, late-transition metal character of rhodium. An insertion reaction similar to the insertion reaction reported by Bertrand,[3] would then be a better description for the catalytic reaction mechanism through which rhodium complexes could catalyse the conversion of amines, rather than the metal-amido intermediate formation.

An elegant example, regarding N-H bond cleavage and N-H bond reformation through a rhodium complex with the ligand displaying non-innocent behaviour, was reported in 2012 by the group of Milstein.[5] The aromatised pyridine starting complex **l** (Scheme 4.6) was treated with ^{t}BuOK in THF to yield the dearomatised complex **m**. Deprotonation of the benzylic phosphine 'arm' and precipitation of potassium tetrafluoroborate salt enforced the changing of the coordination mode of the pyridine-N from an L-type to an X-type ligand. The rhodium metal retained its oxidation number of one, but due to the nitrogen binding as an X-type ligand, a neutral complex was obtained from the starting salt complex. It is interesting to note that the rhodium vacant site was occupied by a nitrogen molecule. In solution, 30% of **m** formed the dimer **n**, by coordination of a second rhodium complex to the second nitrogen atom from the N_2 molecule. Reacting **m** with a primary amine resulted in N-H bond cleavage.[5] The nitrogen from the pyridine moiety changed its coordination mode from an X-type back to an L-type ligand, regaining aromaticity in the pyridine moiety. The benzylic phosphine 'arm' was protonated, while the amine coordinated to the rhodium metal as an X-type amide ligand (**o**, Scheme 4.6). As intuitively expected, electron poor amines reacted faster compared to more basic, alkyl amines. The primary amine was eliminated when reacted with carbon monoxide to yield **p** (Scheme 4.6). The elimination of the amine occurred through proton transfer from the benzylic

111

phosphine 'arm' to the amide and dearomatisation of the pyridine unit, with the nitrogen of the pyridine binding as an X-type ligand.[5]
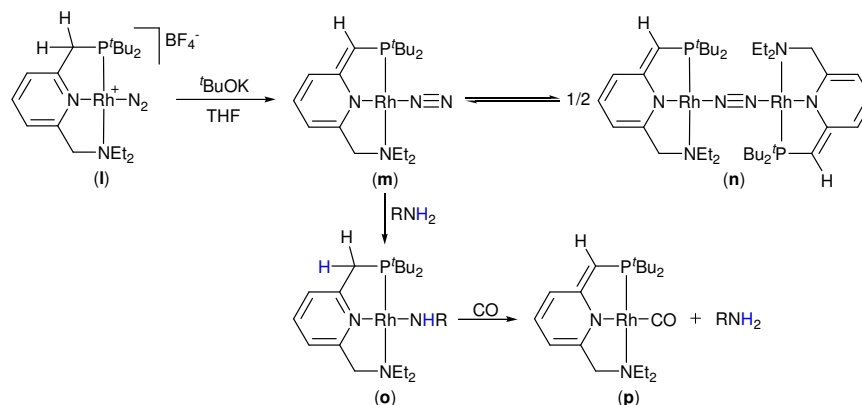
Scheme 4.6: Rhodium complex facilitating N-H bond scission and formation[5]

Tailor-made catalysts were employed by Beller and co-workers towards the high regioselective hydroaminomethylation of various olefins, a problem that had not been comprehensively addressed before their report in 2003.[12] Atom economic conversion of terminal olefins with carbon monoxide and primary or secondary amines to yield the corresponding amines with good regioselectivities was obtained using a rhodium catalyst with the addition of a chelating diphosphine ligand. The added diphosphine ligand coordinates *in situ* to the rhodium complex, yielding the chelated complex as catalyst. The high regioselectivities were attributable to the presence of the chelating ligand which prevented other potential ligands in solution, such as the added amine substrate, to substitute the phosphine ligand and form a mixture of unknown complexes in solution. Scheme 4.7 outlines the catalytic reaction. The reaction can be described as a domino or cascade reaction. The aldehyde is first synthesised from the catalyst that catalyses the hydroformylation of the olefin to the aldehyde, employing carbon monoxide.[12] This is followed by the reaction of the aldehyde with the amine to yield the enamine or imine with elimination of water. Finally, the catalyst hydrogenates the enamine or imine with hydrogen gas to yield product amine. The olefin was almost completely converted to the alkyl amine, with the desired *n*-alkylamine obtained as the major product of the reaction with the minor product being the branched alkylamine (ratio of 98>2).[12]

---

[12] M. Ahmed, A. M. Seayad, R. Jackstell, M. Beller, *J. Am. Chem. Soc.*, 2003, **125**, 10311 – 10318.
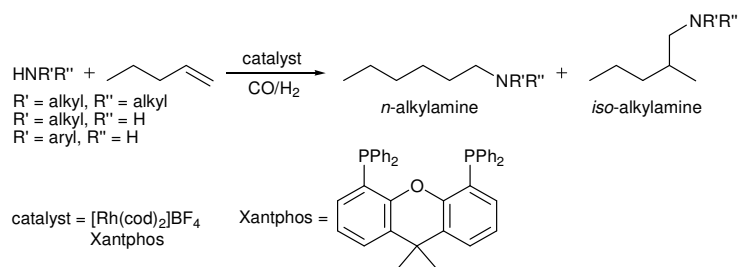
Scheme 4.7: Catalysis of olefins with synthesis gas, amines and a rhodium catalyst[12]

The hydroaminaion of terminal alkynes with primary or secondary amines to yield anti-Markovnikov products was reported in 2007 by Fukumoto *et al.*[13] The catalysis of 1-octyne with various primary or secondary amines using a $TpzRh(C_2H_4)_2$ (Tpz = trispyrazolylborate) catalyst with PPh_3 as additive, yielded the corresponding *E*-enamines or imines, respectively (**I**, Scheme 4.8). The rate and yield of enamine formation from a secondary amine was higher compared to using a primary amine as substrate. This is expected, due to the N-H bond of a secondary amine being more reactive. The presence of other functional groups on the alkyne substrate did not inhibit the reaction or resulted in any side-reactions or undesirable product formation. A plausible reaction mechanism is indicated as **II** in Scheme 4.8. It is postulated that a vinylidene-rhodium complex forms upon reaction of the rhodium catalyst with the terminal alkyne. Nucleophilic attack of the amine, either primary or secondary, at the α-carbon atom of the vinylidene-rhodium complex yields the α-aminovinylrhodium complex.[13] If a secondary amine was used as nucleophile, reductive elimination from the α-aminovinylrhodium complex releases the rhodium catalyst as well as the *E*-enamine. It is suggested that when employing a primary amine as the nucleophile, the imine forms from either tautomerisation of the *E*-enamine or from an iminorhodium complex.
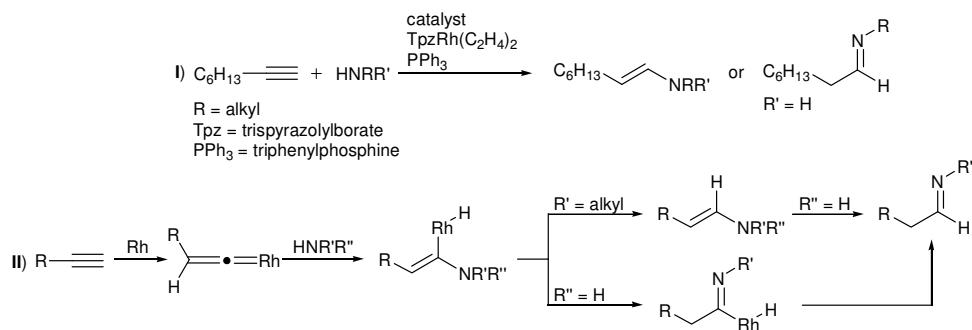
Scheme 4.8: The amination of **I**) terminal alkynes with primary or secondary amines and a **II**) postulated reaction mechanism for the catalytic reaction[13]

---

[13] Y. Fukumoto, H. Asai, M. Shimizu, N. Chatani, *J. Am. Chem. Soc.*, 2007, **129**, 13792 – 13793.

113

The less explored carbene complexes were also investigated towards amination reactions. The dinuclear biscarbene complex **q** (Scheme 4.9) was determined to be active towards the intramolecular hydroamination/cyclisation reaction of terminal alkenes with secondary amines.[14] When primary amines were employed as substrate, only alkene isomerisation products were obtained. The conversion of the secondary amine to the five-membered heterocycle proceeded in good to excellent yields, with formation of only a small amount of trace impurities. The catalytic reaction could be done in toluene, benzene or THF as the solvent of the reaction. Remarkably, the reaction could also be performed in water as the solvent of the reaction, with no decrease in the catalytic activity or without the occurrence of side-reactions. The catalyst was also stable towards open atmospheric conditions.[14] This inherent stability of carbene complexes makes them good candidates for catalysis.
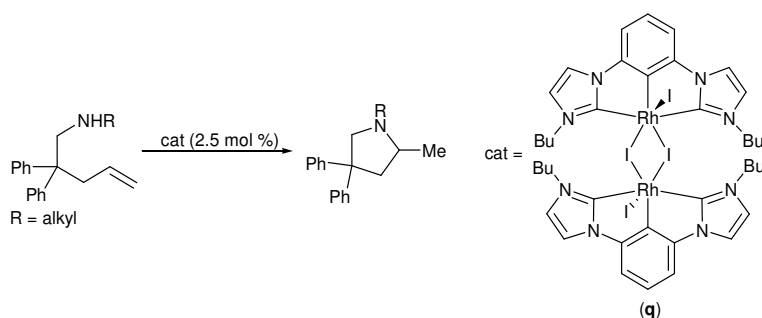
Scheme 4.9: Intramolecular hydroamination/cyclisation of unactivated alkenes with secondary amines[14]

Another rhodium-biscarbene complex was synthesised and its catalytic activity towards the intramolecular hydroamination/cyclisation reaction of terminal alkynes and primary amines tested.[15] The chelated rhodium complex **r** was synthesised from a rhodium dimer and the NHC salt precursor (**I**, Scheme 4.10). Substituting the COD (1,5-cyclooctadiene) ligand with carbonyl yielded the metal salt complex **s** (**I**, Scheme 4.10). The rhodium complex **s**, counteranion being either BPh_4^- or PF_6^-, displayed catalytic activity towards the intramolecular hydroamination/cyclisation reaction of a terminal alkyne with a primary amine, a reaction that was unsuccessful when the rhodium-carbene complex **q** was used (see Scheme 4.9). With a catalyst loading of 1.5 mol%, at 60 °C and employing deuterated THF as solvent, 85% of the starting aminoalkyne was converted to the pyrroline product (**II**, Scheme 4.10).[15] These examples support the concept of rhodium-carbene complexes active in hydroamination of alkenes or alkynes, with catalytic activity comparable to other reported catalytic systems.

[14] E. B. Bauer, G. T. Senthil Andavan, T. Keith Hollis, R. J. Rubio, J. Cho, G. R. Kuchenbeiser, T. R. Helgert, C. S. Letko, F. S. Tham, *Org. Lett.*, 2008, **10**, 1175 – 1178.
[15] S. Burling, L. D. Field, H. L. Li, B. A. Messerle, P. Turner, *Eur. J. Inorg. Chem.*, 2003, 3179 – 3184.

114
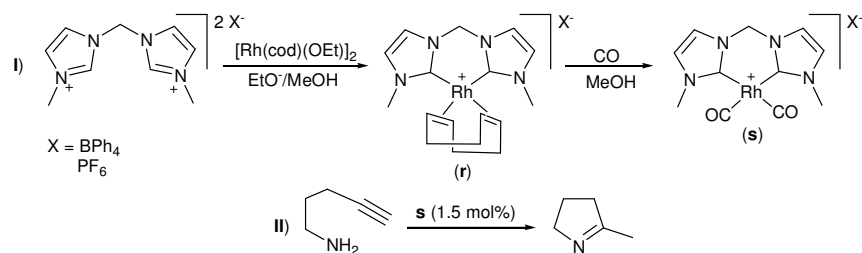
Scheme 4.10: Synthesis of **I)** bidentate rhodium-carbene complex and **II)** catalytic activity towards intramolecular hydroamination/cyclisation[15]

4.1.2) Reactivity of Rhodium Complexes with Oxygen

In Chapter 3, the importance of utilising molecular oxygen was mentioned with discussions of relevant examples. In particular, oxygen activation using copper complexes yielding oxo-, peroxo- or hydroperoxo-copper complexes. In some instances, these highly reactive species were active in various organic transformations such as oxidation or oxygenation reactions. Ligand-metal complexes of rhodium and their reactivity towards molecular oxygen have also been studied and documented. In some instances, these rhodium-oxygen species were active towards transformation reactions. In contrast to the reactivity tests showing positive results, the rhodium-oxygen species in selected examples are even more stable than the copper-oxygen complexes.

Minor ligand scaffold modifications, such as decreasing the steric hindrance imparted by the ligand, can alter the reactivity of a complex altogether. This point is illustrated by the formation of a rhodium(III)-hydroperoxo complex from the rhodium(III)-peroxo complex.[16] Stirring of a rhodium(I) species (**t**, Scheme 4.11) in the presence of a diisopropylpyrazole ligand and molecular oxygen yielded the oxidised rhodium(III)-peroxo complex (**u**, Scheme 4.11). The same reaction was repeated, however in the presence of a less bulky unsubstituted pyrazole ligand. This reaction yielded the oxidised rhodium(III)-hydroperoxo complex (**v**, Scheme 4.11). In addition, **u** could be converted to **v** by substitution of the bulky diisopropylpyrazole ligand with the pyrazole ligand in a deuterated benzene solution stirred at 60° C. In contrast to the unstable copper oxygen complexes, these two rhodium(III) complexes could be purified by silica gel chromatography. Both complexes were characterised with various techniques, including X-ray diffraction analysis. A mechanism was proposed involving first the coordination of molecular oxygen to the rhodium complex.[16] The adduct is readily converted through oxygenation of the phosphine moieties, which further reacts with a second oxygen molecule yielding the rhodium(III)-peroxo complex after dissociation of the bis(phosphine oxide) and association of the substituted or unsubstituted pyrazole ligand.[16] The

---

[16] Y. Takahashi, M. Hashimoto, S. Hikichi, M. Akita, Y. Moro-oka, *Angew. Chem. Int. Ed.*, 1999, **38**, 3074 – 3077.

substituted diisopropyl ligand does not allow for coordination of a second pyrazole moiety as a result of steric hindrance, terminating the reaction. The decreased steric hindrance experienced when employing the unsubstituted pyrazole ligand, allows for the incorporation and coordination of a second unsubstituted pyrazole moiety to the rhodium metal centre. The second pyrazole ligand inserts into one of the rhodium-oxygen bonds. The coordinated oxygen is very basic due to back-bonding from the rhodium metal. This basic oxygen abstracts the N-H proton from the second coordinated pyrazole moiety, yielding the rhodium(III)-peroxo complex with hydrogen bonding interaction between the nitrogen of the second pyrazole ligand and the –OOH moiety. The reactivity towards organic substrates was only suggested, and no reactivity or catalysis was reported.[16]
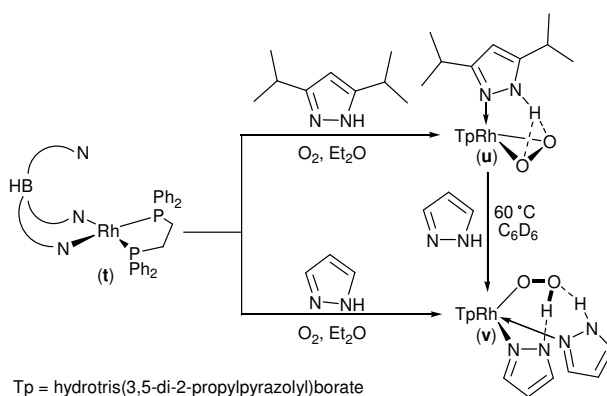
Scheme 4.11: Reactivity of a rhodium complex towards oxygen yielding either the peroxo- or hydroperoxo-rhodium complexes[16]

In 2011 Braun and co-workers reported an unprecedented reaction revolving around a rhodium-peroxo complex, which could directly transfer the peroxo unit to an organic substrate during an oxidation reaction.[17] An elegant method was employed during the synthesis of the rhodium(III)-peroxo complex from the rhodium(I) complex (Scheme 4.12). Reacting **w** with oxygen in the presence of methylene blue as sensitizer whilst irradiating with a tungsten halogen lamp to generate, *in situ*, singlet oxygen from triplet oxygen yielded the distorted octahedral rhodium(III)-peroxo complex **x**. Treatment of **x** with three equivalents of tetrakis(dimethylamino)ethylene whilst irradiating with a Xe UV lamp in deuterated benzene, resulted in the transfer of both oxygen atoms to the substrate, yielding two equivalents of the tetramethylurea product.[17] The rhodium(I) complex **w** was regenerated during the reaction. The dioxygen unit from **x** was directly transferred to a 9,10-dimethylanthracene substrate, yielding the 9,10-dimethylanthracene-9,10-endoperoxide product and **w**.[17]

---

[17] G. Meier, T. Braun, *Angew. Chem. Int. Ed.*, 2011, **50**, 3280 – 3284.
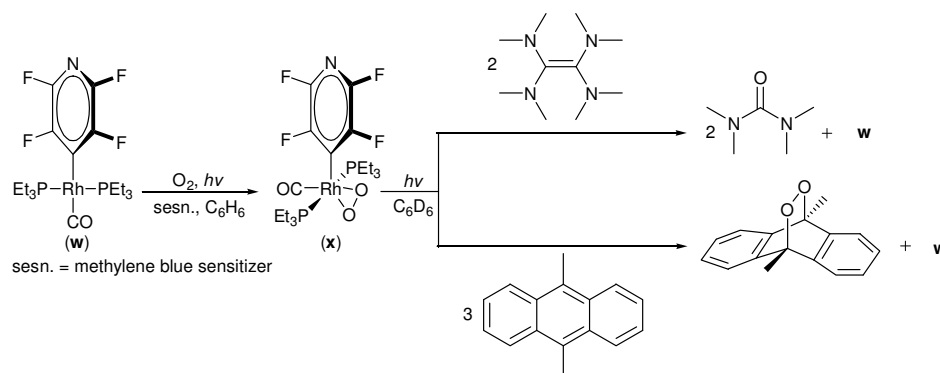
Scheme 4.12: Oxidation of organic substrates with a Rh(III)-peroxo complex[17]

Employing rhodium-carbene complexes towards reactivity with molecular oxygen furnished interesting results. A rhodium(I) complex substituted with a carbene and a phosphine ligand was exposed to oxygen/air, yielding the rhodium(I)-oxygen adduct.[18] However, the rhodium-oxygen adduct decomposed after a certain period of time due to further oxidation of the phosphine ligand to phosphine oxide. Substituting the phosphine ligand with a second carbene ligand yielded a more stable complex that was easy to manipulate. The biscarbene-rhodium complex, generated *in situ*, treated with oxygen and air yielded the corresponding rhodium-oxygen adduct **y** (Scheme 4.13). Crystallographic analysis of the adduct revealed a square-planar geometry around the rhodium(I) metal, with oxygen coordinating to the metal in a side-on fashion. Bonding results due to σ donation from the filled O_2 π-orbital and backbonding from the metal to the empty O_2 π^*-orbital. Bonding is considered to be similar to metal-olefin coordination.[18] The rhodium(I) complex was not oxidised in the presence of oxygen, in contrast to the examples discussed above.
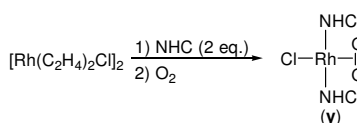
Scheme 4.13: Oxygen coordination to biscarbene-rhodium complex[18]

Crudden and co-workers further studied this rare and unusual binding mode of oxygen to the rhodium-carbene complex.[19] Reacting the rhodium(I)-oxygen adduct **y** (see Scheme 4.13 for synthesis of **y**) with one equivalent of a silver salt in acetonitrile (CH₃CN) as solvent, yielded the rhodium salt **z** after two hours (Scheme 4.14). The silver salt abstracted the chloride ligand with formation of insoluble silver(I) chloride. The crystal structure of **z** was compared with the crystal

[18] J. M. Praetorius, D. P. Allen, R. Wang, J. D. Web, F. Grein, P. Kennepohl, C. M. Crudden, *J. Am. Chem. Soc.*, 2008, **130**, 3724 – 3725.
[19] J. Cipot-Wechsler, D. Covelli, J. M. Praetorius, N. Hearns, O. V. Zenkina, E. C. Keske, R. Wang, P. Kennepohl, C. M. Crudden, *Organometallics*, 2012, **31**, 7306 – 7315.

117

structure of **y**. The oxygen moiety in complex **y** had an O-O bond length of 1.323(3) Å, which is short but falls well within the range of metal-oxygen adducts (range of metal-oxygen adduct O-O bond lengths is 1.24 – 1.39 Å).[19,20] This contrast with the cationic rhodium complex **z**, which had an O-O bond length of 1.428(3) Å. The longer O-O bond length of **z** is in the metal-oxygen O-O bond length range reminiscent of metal-peroxo complexes, which is 1.43 – 1.50 Å.[19,20] Upon removal of the chloride ligand from **y**, the coordinated oxygen could oxidise rhodium(I) to rhodium(III), yielding the rhodium-peroxo complex **z**, which would explain the longer O-O bond length. Further spectroscopic analysis of **z** and data comparison with that obtained for **y** confirmed the formation of the rhodium(III)-peroxo complex from the rhodium(I)-oxygen adduct. The IR-stretching frequencies for both **y** and **z** was well within the range with respect to other metal-oxygen adducts and metal-oxygen peroxidic complexes, respectively. The O-O bond stretching frequency for **z** shifted by more than 100 cm^{-1} compared to the stretching frequency observed for **y**. The lower O-O stretching frequency for **z** is a result of a decrease in the bond order, supporting the formation of the peroxo complex from the oxygen adduct. The reducing ability of the cationic complex was attributable to both the ligand *trans* to the oxygen and the change in the coordination number through the introduction of the acetonitrile ligand.

Ar = 2,6-diisopropylphenyl
X = BF$_4$, OTf, SbF$_6$
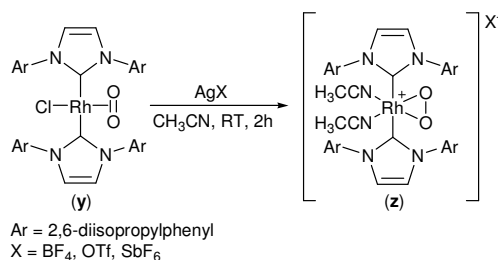
Scheme 4.14: Oxidation of Rh(I)-O$_2$ adduct to Rh(III)-peroxo complex[19]

4.2) Aim

Reactive late transition metal complexes with highly nucleophilic centres could be active in various catalytic reactions involving substrates such as amines and ammonia or molecular oxygen. As such, synthesis of a reactive 14-electron rhodium complex employing the bulky ligand scaffold, either **7** or **10** (Chapter 2), will be attempted. These ligand scaffolds have been demonstrated to stabilise reactive late transition metal complexes (Chapter 3). The triazolylidene and strongly donating amido moieties could yield a rhodium complex with adequate nucleophilic character.

---

[20] E. C. Keske, O. V. Zenkina, A. Asadi, H. Sun, J. M. Praetorius, D. P. Allen, D. Covelli, B. O. Patrick, R. Wang, P. Kennepohl, B. R. James, C. M. Crudden, *Dalton Trans.*, 2013, **42**, 7414 – 7423.

The proposed 14-electron rhodium complex, illustrated in Figure 4.2, will then be subjected to reactivity tests towards a variety of amines. It is postulated that, due to the potential properties of the rhodium complex being similar to what was reported by Hartwig and co-workers for their iridium complex (see Section 4.1.1.1), oxidative addition of amines to yield the metal-amido hydride complex, could occur. This metal-amido hydride complex would then be reacted with unsaturated carbon substrates. However, formation of the Werner complex is also a possibility. But this could indeed promise interesting reactivities, such as nucleophilic attack of an alkene or alkyne to the coordinated amine, which would be similar to the reported examples discussed for rhodium-carbene complexes above.

In addition, the reactivity of the proposed 14-electron rhodium complex towards molecular oxygen will also be investigated. The proposed rhodium-carbene complex (Figure 4.2) could display similar reactivities towards molecular oxygen as did the rhodium-carbene complexes reported by Crudden *et al.*

Ar = 2,6-diisopropylphenyl
2,4,6-trimethylphenyl
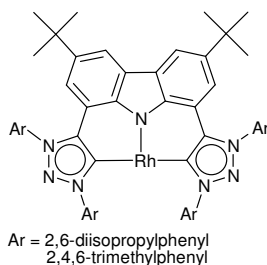
Figure 4.2: Proposed 14-electron rhodium complex

4.2.1) Synthetic Strategy

The synthesis of the 14-electron rhodium complex will be attempted by employing similar methodologies as used for the synthesis of the metal complexes discussed in Chapter 3. All manipulations, including the reaction itself and subsequent purifications will have to be performed under strict inert conditions if the reactive 14-electron complex is to be isolated. The ligand salt, either **7** or **10**, will be deprotonated with KHMDS, followed by *in situ* metallation of the carbene adduct (Scheme 4.15). The $[Rh(C_2H_4)_2Cl]_2$ dimer will be used as the metal precursor during the reaction, where the highly labile, small ethylene co-ligand should readily dissociate to allow for pincer-complex formation.

119
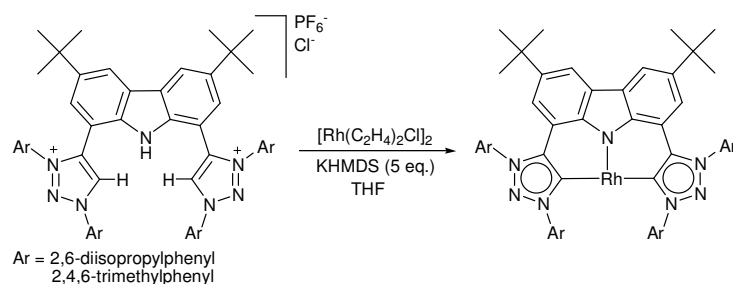
Scheme 4.15: Synthetic method that will be employed for the synthesis of the 14-electron rhodium complex

4.3) Results and Discussion

See Section 4.6 for synthetic procedures and catalytic reactions employed, as well as the full characterisation of the synthesised compounds.

4.3.1) Synthesis of 17

Attempted synthesis of a 14-electron rhodium complex through *in situ* deprotonation of **7** with KHMDS, followed by metallation with a dimeric rhodium [Rh(C$_2$H$_4$)$_2$Cl]$_2$ precursor, did not yield the desired complex even when working under strict inert conditions, i.e. Schlenk techniques as well as utilisation of a glove box. Instead, a 16-electron rhodium-oxygen adduct **17**, was obtained after extraction of the product from the crude reaction mixture with hexanes and subsequent *in vacuo* evaporation of the solvent (Scheme 4.16). The product was obtained with a yield of 55%, as a brown solid (Scheme 4.16). Characterisation by NMR, MS, as well as X-ray diffraction analysis confirmed the formation of **17**.
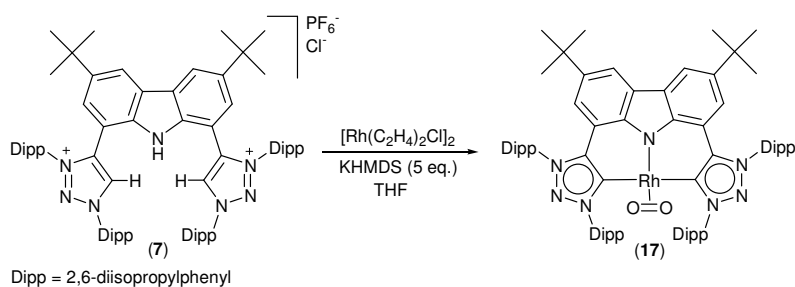
Scheme 4.16: Synthesis of Rh(I)-O$_2$ adduct **17**

Proton NMR spectroscopic analysis shows the clear disappearance of the three acidic protons (the amido and two *trz***H** protons). The upfield resonance at 8.41 ppm corresponds to the aromatic protons of the carbazole backbone (Figure 4.3). The rhodium complex **17** is symmetrical in solution,

120

as is evident from the proton NMR spectrum. A carbene signal, resonating as a doublet at 168.4 ppm, confirms the coordination of the two *trz* carbene carbons to the rhodium metal (Figure 4.4). The carbene carbons resonate upfield compared to rhodium complexes with nNHCs as ligands.[15,18,19,20,21] This observation is not surprising due to the stronger donating carbene carbons being more shielded compared to classical NHCs. In addition, the carbene resonance is characteristic of other rhodium complexes containing *trz* carbene ligands.[22,23] A carbene doublet is observed due to coupling of the ^{103}Rh(I) nuclei to the ^{13}C nuclei of the carbene carbons. The coupling constant has a value of 39.2 Hz which is consistent with other rhodium-carbene coupling constants that feature molecular oxygen coordinating in a side-on fashion to the rhodium metal.[19,20]
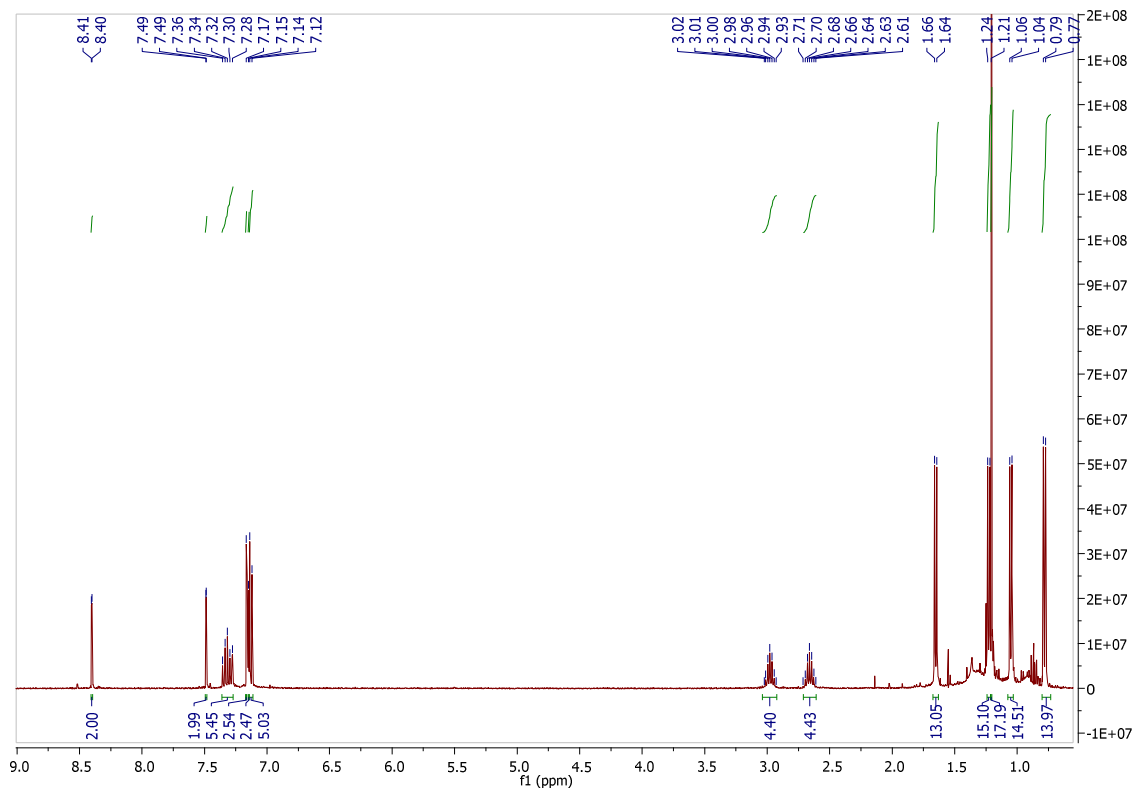
Figure 4.3: ^{1}H NMR of **17** in C$_6$D$_6$ solvent

[21] M. Moser, B. Wucher, D. Kunz, F. Rominger, *Organometallics*, 2007, **26**, 1024 – 1030.
[22] G. Guisado-Barrios, J. Bouffard, B. Donnadieu, G. Bertrand, *Organometallics*, 2011, **30**, 6017 – 6021.
[23] E. C. Keske, O. V. Zenkina, R. Wang, C. M. Crudden, *Organometallics*, 2012, **31**, 456 – 461.

121
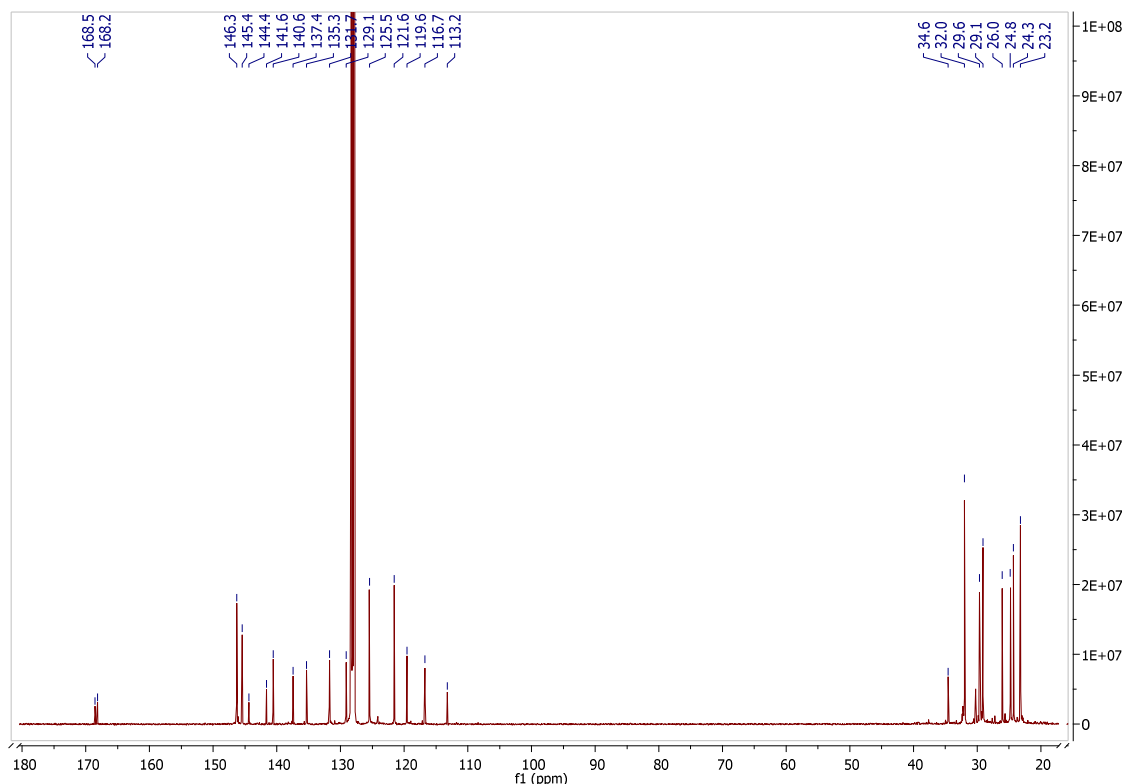
Figure 4.4: ^{13}C NMR of **17** in C$_6$D$_6$ solvent

The crystal structure (Figure 4.5) unambiguously confirmed the formation of a rhodium(I)-oxygen adduct, and not the rhodium(III)-peroxo or the desired rhodium 14-electron complex. The rhodium metal centre, carbene carbons and amido moieties are almost planar with respect to each other. There are only slight deviations in the bonding angles. The carbene-rhodium-nitrogen right angles are close to 90°, with values of 88.94(16)° and 89.75(16)° for the C24-Rh1-N1 and C22-Rh1-N1 angles, respectively. The metal is orientated in the plane of the carbene carbons. This can be deduced from the C22-Rh1-C24 angle (178.41(18)°) being very close to linearity. The **C**$_{\text{carbene}}$-Rh1-O$_{\text{oxygen}}$ bonding angles are also approximately perpendicular. These bonding angles are all consistent with square planar complexes, suggesting that the oxygen moiety binds as an L-type ligand in a side-on fashion, yielding the oxygen adduct and not the distorted trigonal bipyramidal rhodium(III)-peroxo complex. These observations are similar to that reported by Crudden and co-workers (see Section 4.1.2). Coordination of the molecular oxygen moiety through donation of π-electron density to the metal yields a σ-bond. Backbonding from the metal to the oxygen π*-orbital can also occur. This backbonding would certainly decrease the O-O bond order, increasing the O-O bond length from double bond character to single bond character. The O8-O9 bond length was determined to be 1.374(4) Å. This O-O bond length is slightly elongated from the O-O bond length values for rhodium-oxygen adducts, reported by Crudden, which might support metal-to-oxygen backbonding. However,

122

the O-O bond length of **17** is still short and falls well within the range of O-O bond lengths where rhodium-oxygen adduct formation occurred. This further supports the formation of a Rh(I)-O_2 adduct.

The square planar centre retains its planarity with the deviation of the ligand scaffold, in order to accommodate the large Rh(I) metal and the oxygen moiety in the pocket of the pincer ligand. The C23-C24-Rh1-C22 torsion angle is 32(6)° while the C21-C22-Rh1-C24 torsion angle value is 41(6)°. This indicates that the triazolylidene moieties are twisted significantly out of the carbene-rhodium plane. In addition, the *trz* functionalities are also twisted out of the plane of the carbazole backbone, as is evident from the C24-C23-C12-C7 and C22-C21-C6-C1 torsion angles being 3.1(7)° and 6.9(7)°, respectively. The deviation of the ligand backbone from planarity was also observed for the Rh(bimca)CO complex reported by Kunz and co-workers.[21]

The C24-C23-N7-N6 triazolylidene ring is planar, with a torsion angle value being 0.7(4)°. The C22-C21-N4-N3 torsion angle is 0.5(5)°. Both values, in addition to the triazolylidene bond lengths being short and indicative of double bonds, suggest adequate electron delocalisation and therefore supports aromaticity throughout the five-membered heterocycle. The C23-C24-N5 angle is 101.8(4)° and the C21-C22-N2 angle is 101.2(4)°. The bond angles are acute compared to that of **7**, but again, not as acute as that of **9**. This is expected because upon coordination of the potassium free carbene adduct to the metal, the carbene σ-orbital loses s-character and gains p-character. This increases the carbene bonding angle.

The Rh1-**C**$_{carbene}$ bond lengths (C24-Rh1 and C22-Rh1) are equal with a value of 2.037(5) Å. The N1-Rh1 bond length is 1.982(4) Å which is short, while the Rh1-O8 and Rh1-O9 bond lengths are 1.976(3) Å and 1.977(4) Å, respectively.
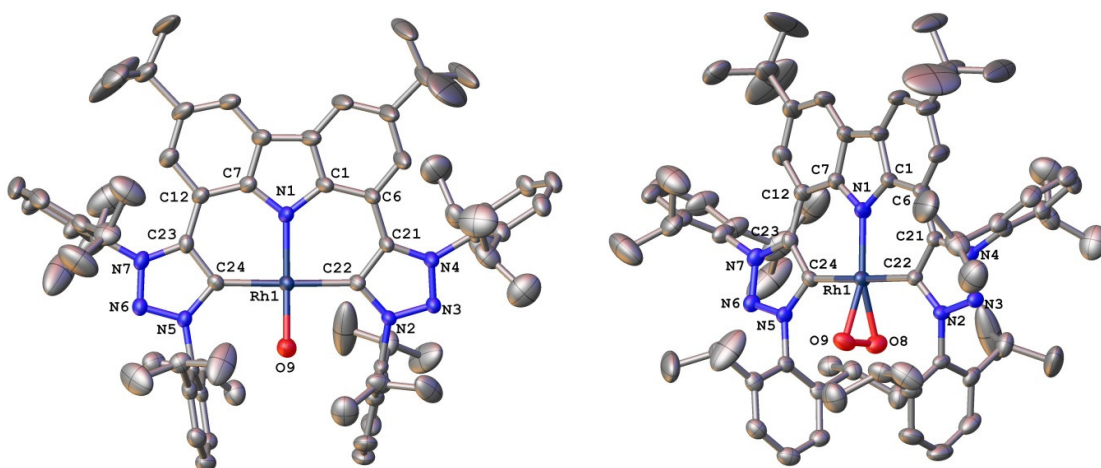
Figure 4.5: Crystal structure of **17** (Left: frontal and Right: side-on views)

4.3.2) Synthesis of 18

The reactivity of **17** was tested towards ammonia, in order to determine whether or not N-H activation and thus oxidative addition across the rhodium metal centre, or if Werner complex formation, would occur. Ammonia gas was bubbled through a brown coloured, deuterated benzene solution of **17**, which yielded a red coloured solution (Scheme 4.17). The solvent was not evaporated and the solution subjected to NMR experiments. NMR analysis (Figure 4.6 and 4.8) suggested the quantitative formation of **18**, a Rh(I)-NH$_3$ adduct, and not the rhodium(III)-amido hydride complex.

Dipp = 2,6-diisopropylphenyl
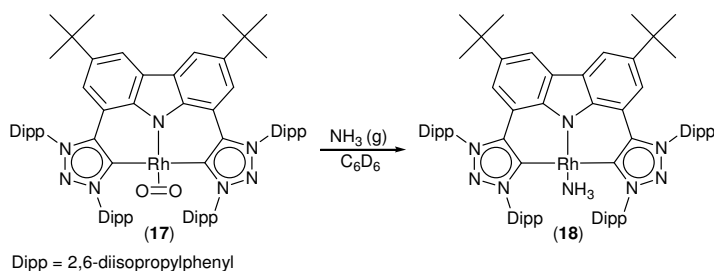
Scheme 4.17: Coordination of NH$_3$ yielding the Rh(I)-NH$_3$ adduct **18** form **17**

The ^{1}H NMR spectra of **18** is depicted in Figure 4.6. The most striking observation is the broad singlet resonating at -0.13 ppm corresponding to the excess ammonia. No hydridic M-H singlet or amido M-NH$_2$ protons were observed. The chemical shift for the protons of the coordinated NH$_3$ could not be unambiguously assigned. It resonates as a very broadened peak in the aliphatic region from 2.3 – 4.0 ppm, which could not be clearly distinguished in Figure 4.6 due to overlap with the ligand scaffold's aliphatic protons resonating in that region. This broad singlet of NH$_3$ for a Rh(I)-NH$_3$ adduct resonating upfield is not uncommon, and has been reported previously.[24] In addition, organometallic complexes where ammonia adduct formation with metals such as iridium and gold occurred, has also been reported.[3,25] In order to directly compare **18** with **17**, a deuterated benzene solution of **17** was again analysed by NMR spectroscopy. The exact same solution (the solution was not removed from the NMR tube) was treated with NH$_3$ (g). The ^{1}H NMR spectra of **17** is overlapped with the ^{1}H NMR spectra of **18** (Figure 4.7). The red curve in Figure 4.7 corresponds to **17** (**not treated** with NH$_3$ (g)) while the blue curve corresponds to **18** (**treated with** NH$_3$ (g)). Both the carbazole protons are orientated in the *meta*-position with respect to the amido moiety. However, the two protons resonating downfield in **17** shifted further downfield after bubbling NH$_3$ (g) through the solution, while the other two upfield carbazole protons resonating at 7.49 ppm, shifted further upfield. The

[24] Y. S. Varshavsky, M. R. Galding, T. G. Cherkasova, S. N. Smirnov, V. N. Khrustalev, *J. Organomet. Chem.*, 2007, **692**, 5788 – 5794.

[25] M. Kanzelberger, X. Zhang, T. J. Emge, A. S. Goldman, J. Zhao, C. Incarvito, J. F. Hartwig, *J. Am. Chem. Soc.*, 2003, **125**, 13644 – 13645.

^{13}C NMR spectrum strongly supports the formation of a Rh(I)-NH$_3$ adduct (Figure 4.8). The carbene carbon doublet (^{103}Rh-^{13}C) has slightly shifted downfield with 1 ppm. The coupling constant value has decreased significantly by 4.5 Hz, from 39.2 Hz (**17**) to 34.7 Hz (**18**). This result clearly indicates coordination of the amine and can be supported based on the following explanation. Stronger donor ligands induce smaller coupling constants between the nuclei coupling with each other.[26] The ligand which influences the ^{103}Rh-^{13}**C**$_{Carbene}$ coupling constant J for **17** and **18** is in the *cis*-position with respect to the carbene carbons. The basic amine, being a stronger donor ligand due to σ-overlap compared to the weaker donating, π-overlap from the dioxygen ligand, results in the coupling constant of **18** decreasing with respect to **17**.
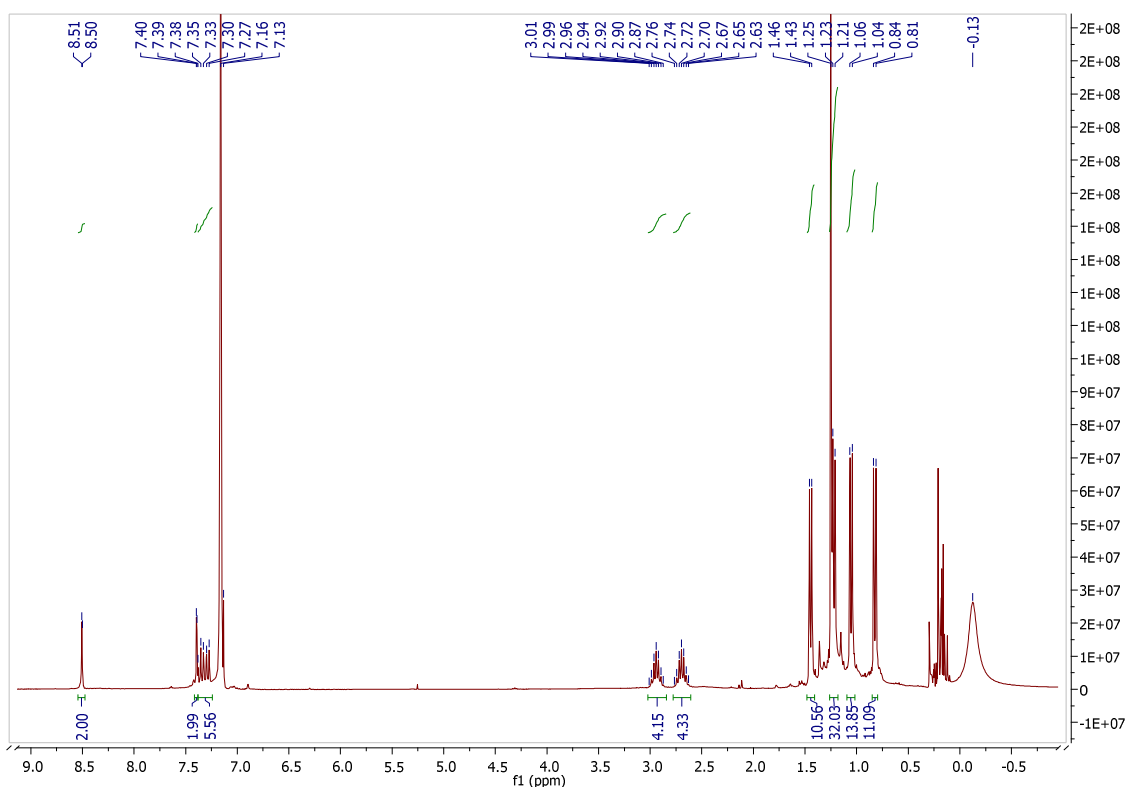
Figure 4.6: ^{1}H NMR of **18** in C$_6$D$_6$ solvent

---

[26] *NMR in Organometallic Chemistry*, P. S. Pregosin, WILEY-VCH Verlag GmbH & Co. KGaA, Weinheim, Germany, 2012, pp 207 – 277.
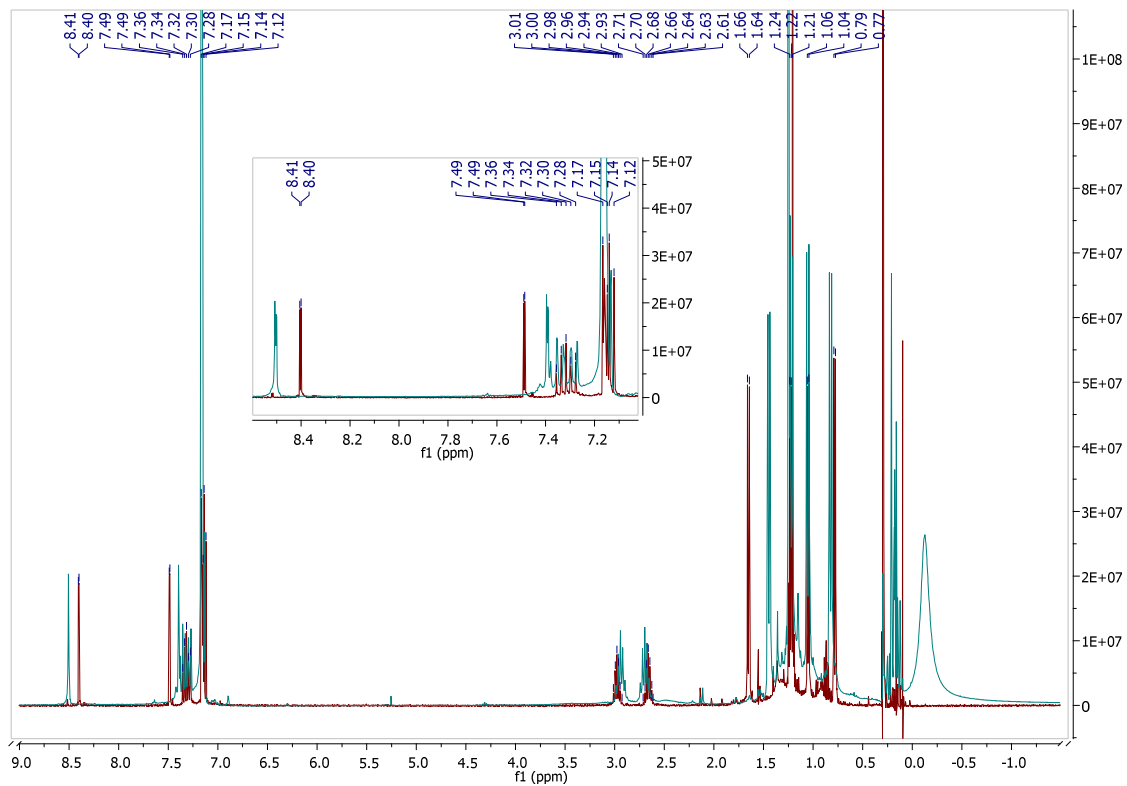
Figure 4.7: ¹H NMR overlap of **17** (red spectra) and **18** (blue)
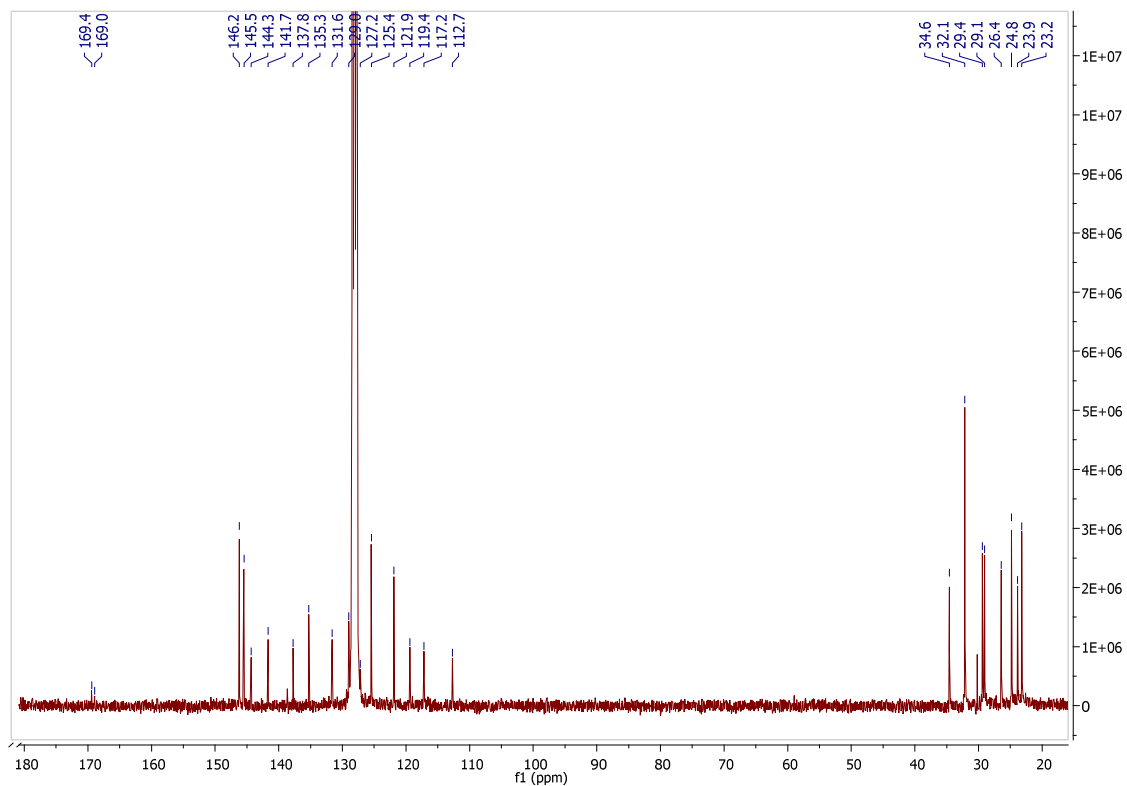
Figure 4.8: ¹³C NMR of **18** in C_6D_6 solvent

126

The reaction depicted in Scheme 4.17 was repeated as before, but instead of using deuterated benzene as the solvent, deuterated tetrahydrofuran was used (THF-d_8). A deuterated tetrahydrofuran solution of **17** was analysed by NMR spectroscopy. Again, the same solution that was not removed from the NMR tube, was treated with NH$_3$ (g). The three protons of the coordinated amine can again, not be unambiguously confirmed by proton NMR spectroscopy. The broad upfield resonance for the three protons of the coordinated ammonia is speculated to overlap with the aliphatic protons of the ligand scaffold. However, the singlet of the ammonia protons are not as broadened as in the case with deuterated benzene as solvent. Figure 4.9 displays the overlap of the ^{13}C NMR spectrum of **17**, which is the red curve (**not treated** NH$_3$ (g)), and **18**, which is the blue curve (**treated with** NH$_3$ (g)). The carbene doublet of **17** (in THF-d_8) has a resonance of 168.5 ppm with a coupling constant of 39.0 Hz, while the carbene doublet of **18** resonates at 170.7 ppm (in THF-d_8), with a coupling constant of 34.0 Hz. Using deuterated thf as solvent, the difference between the coupling constant of the doublet carbenes are 5 Hz, while the carbene carbon of the Rh(I)-NH$_3$ adduct resonates further downfield with a difference of 2 ppm.
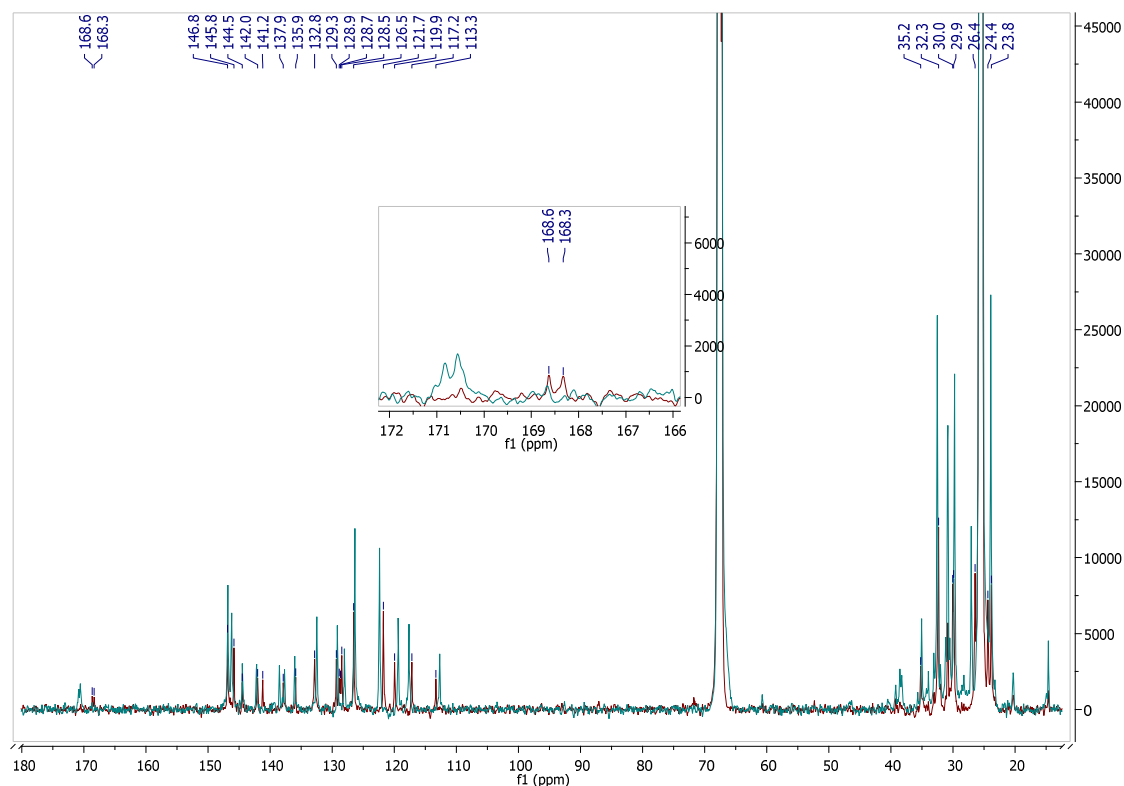
Figure 4.9: ^{13}C NMR overlap of **17** (red spectra) and **18** (blue)

Infrared spectroscopy unambiguously confirmed the formation of the Rh(I)-NH$_3$ adduct **18**. A broad band is observed at 3407 cm^{-1}, attributable to the stretching N-H absorption. The region between

127

2965 – 3686 cm^{-1} in the infrared spectrum of **17** did not display any absorption bands. In addition, the N-H stretching absorption of 3406 cm^{-1} is well within the range for metal-amine complexes.[27] The asymmetric δ N-H frequency of the NH$_3$ moiety has a strong absorption at 1627 cm^{-1}, whilst the infrared spectrum of **17** only indicated a weak absorption at 1604 cm^{-1}. The asymmetric δ N-H absorption fits well into the range for other metal-amine complexes with asymmetric δ N-H absorptions.[27] Further support of the stretching and asymmetric absorptions mentioned comes from a broad band displaying a strong absorption observed at 1033 cm^{-1} for **18**. This broad band overlapped with two weaker absorption bands observed at 1097 cm^{-1} and 1012 cm^{-1} for **17**. Even though there is overlap in the region displaying the symmetric δ N-H absorption band (at 1033 cm^{-1}) of **18**, it is still significant due to the strong vibration and the fact that there is no absorption band at 1033 cm^{-1} observed for **17**.

Remarkably, ammonia coordination is reversible. Ammonia gas was bubbled through a solution of **17** yielding **18**, followed by *in vacuo* evaporation of the solvent (Scheme 4.18). NMR analysis confirmed the formation of **17** from **18**. The Rh(I)-NH$_3$ adduct **18** is an example of a Werner complex, but not an inert Werner complex where ammonia binds non-reversibly as a Lewis base. This is evident by removing the ammonia moiety simply by applying a vacuum. To the best of our knowledge, reversible coordination of ammonia to a rhodium metal centre supported by a ligand scaffold, is unknown.
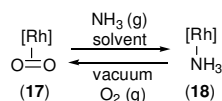
Scheme 4.18: Oxygen (**17**) and ammonia (**18**) adduct formation through reversible ammonia coordination

4.3.3) Synthesis of 19

The reaction of **17** towards carbon monoxide was investigated. A solution **17** (10.0 mg, 8.4 x 10^{-6} mol) in DCM (5 mL) was treated with carbon monoxide by bubbling CO (g) through the solution for two minutes. A colour change occurred from dark to light brown upon formation of **19**. NMR analysis confirmed quantitative formation of **19** after evaporation of the DCM solvent and redissolving the light brown residue in deuterated benzene.

---

[27] *A critical survey of the infrared and Raman spectra of metallic and organometallic compounds, Metal-ligand and Related Vibrations*, D. M. Adams, Edward Arnold, London, 1967, pp 274 – 277.

128
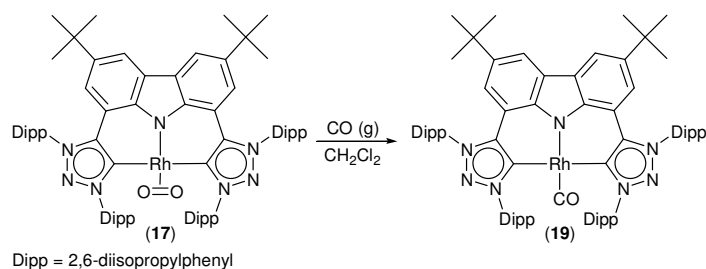
Scheme 4.19: Reacting **17** with carbon monoxide yielding **19**

The proton and carbon NMR spectra of **19** are displayed in Figures 4.10 and 4.11, respectively. It was immediately determined that four aromatic protons where unaccounted for, and it is predicted that these protons are overlapped by the benzene resonance at 7.16 ppm. All the other protons were accounted for and assigned (see Section 4.5.3). In addition, the resonance of all the protons had shifted, either upfield or downfield, supporting substitution of the oxygen for the carbonyl ligand. The carbon NMR spectra unambiguously confirmed a rhodium-carbonyl complex. Again, one carbon was unaccounted for, due to overlap with the benzene solvent. Two independent doublets resonate downfield, corresponding to the carbonyl carbon and the carbene carbon. The carbene carbon doublet resonates downfield (compared to **17** and **18**) at 173.4 ppm with a coupling constant of 41.6 Hz. The carbonyl ligand, being a weak L-donor and strong π-acceptor ligand, is directly responsible for the larger coupling constant. The coupling constant of **19** is 2.4 Hz more than **17** and 6.9 Hz more than **18**. This is a direct result of substituting stronger donor ligands with weaker donor ligands. The relatively small differences between the coupling constants of **17**, **18** and **19** are attributable to the position of the ligand which influences the coupling constant of the two nuclei coupling with each other. If the ligand was *trans* to the $C_{Carbene}$, the effect resulting from changing the ligands on the coupling constant would be much more dramatic. However, in the *cis*-position the effect from changing the ligands is still significant and undoubtedly conclusive.[26] The *sp*-hybridised carbon of the carbonyl ligand resonates downfield with respect to the carbene carbon, at 195.4 ppm. The ^{103}Rh-^{13}CO coupling constant is 70.2 Hz. The larger ^{103}Rh(I)-^{13}CO coupling, in comparison with the ^{103}Rh(I)-^{13}**C**carbene coupling constant, is a result of the high percentage s-character of the CO *sp*-hybridised orbital versus the *sp²*-hybridised carbene carbon orbital.[26] The ^{13}C NMR spectra of **19** displayed three additional, unassigned resonances at 167.6, 68.1 and 39.2 ppm, indicating formation of a side-product. These resonances correspond to possible acyl-type side-products, but as no acidic aldehyde resonance was observed in Figure 4.10, only possible ketone formation can be speculated. However, this unknown product does not coordinate to the metal as there are no other doublet or doublets, except for the two already discussed.

129
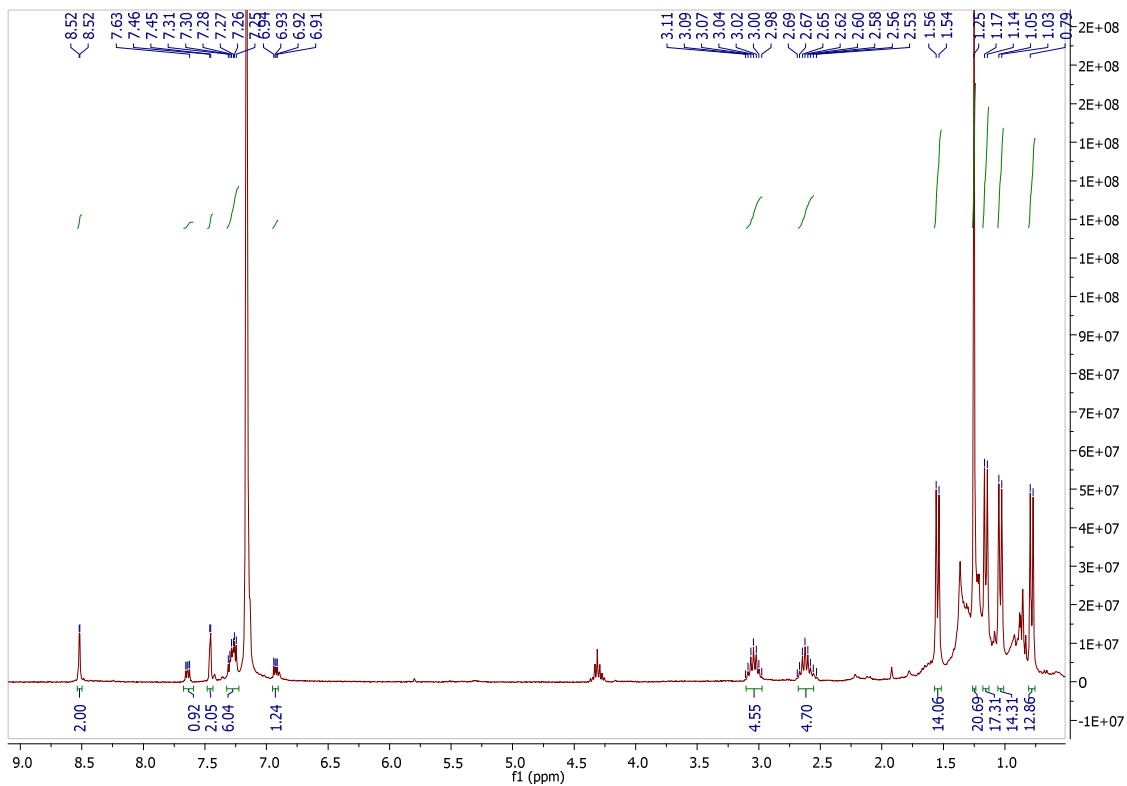
Figure 4.10: ^{1}H NMR of **19** in C_6D_6 solvent
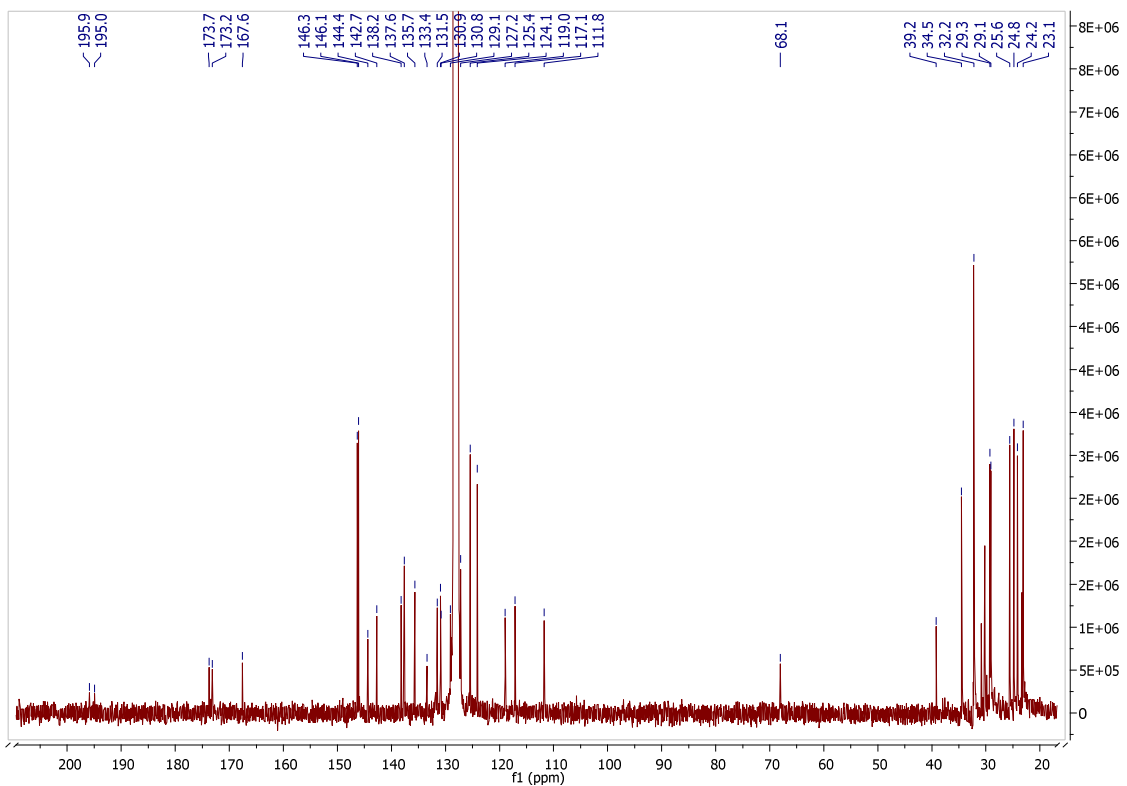
Figure 4.11: ^{13}C NMR of **19** in C_6D_6 solvent

130

Infrared spectroscopic analysis, in addition to NMR studies, unambiguously confirmed the formation of **19**. The carbonyl carbon has a strong absorption band at 1955 cm^{-1}. Detection of the absorption band is trivial, due to the absence of other absorptions in that region. No absorptions were observed in that region for **17** and **18**. This value, being of very low energy, gives clear evidence of the ligand scaffold's strong σ-donor and weak π-acceptor properties. The strong donating ability is a direct result of employing a very basic amido moiety, in addition to the two *trz* carbenes, which were already discussed in Chapter 1 to be strongly donating systems. The π-acceptor ability of the *trz* functionalities are lower compared to the already weak π-acceptor nNHC. It is generally known that amines are also weak π-acceptors due to their basic properties. The low wavenumber is even lower than the values reported for most nNHC, aNHC and *trz* ligand systems (see Chapter 1). The strong donating ligand scaffold results in a metal centre with a high nucleophilic character. However, the high nucleophilic centre did not allow for the oxidative addition of ammonia across the metal centre yielding the (CNC)Rh(H)(NH$_2$) complex.

4.3.4) Synthesis of 20

The analogue of **17**, namely **20**, was synthesised based on the same procedure as used for the synthesis of **17**. The ligand salt **10** was deprotonated with KHMDS followed by *in situ* metallation with [Rh(C$_2$H$_4$)$_2$Cl]$_2$. Evaporation of the THF solvent, followed by extraction of the product from the crude reaction mixture with hexanes and subsequent *in vacuo* evaporation of the solvent yielded a dark brown coloured residue (Scheme 4.20). NMR and MS analysis confirmed the formation of **20** with a yield of 68%. Again, the 16-electron rhodium-oxygen adduct was obtained and not the desired 14-electron rhodium complex, even when working under strict inert conditions. Crystal suitable for X-ray diffraction could not be obtained.

Scheme 4.20: Metallation of **10** with Rh(I) yielding the Rh(I)-O$_2$ adduct **20**
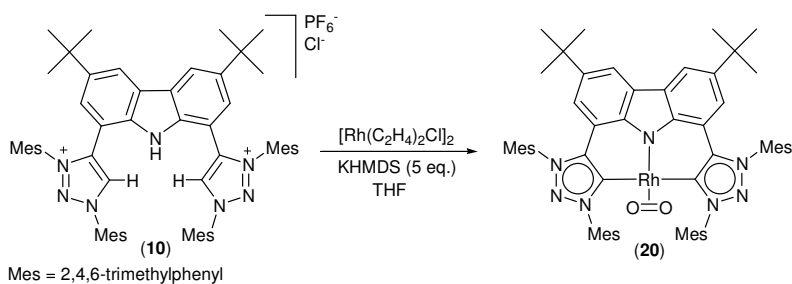
As is evident from the proton NMR spectra displayed in Figure 4.12, no acidic *trz***H** or amido protons are present, confirming that the ligand had been deprotonated. The carbon NMR spectrum (Figure

131

4.13) confirmed the metallation of the ligand, which could be deduced from the carbene carbon resonance at 167.4 ppm. The ^{103}Rh(I)-^{13}**C**carbene doublet has a coupling constant of 38.9 Hz. The carbene resonance, as well as the ^{103}Rh(I)-^{13}**C**carbene coupling constant is similar to that of **17**, re-affirming the formation of the Rh(I)-O_2 adduct **20**. One carbon could not be assigned, and it is postulated that the benzene solvent overlaps with the carbon resonance. In solution, the complex appears to be symmetric.
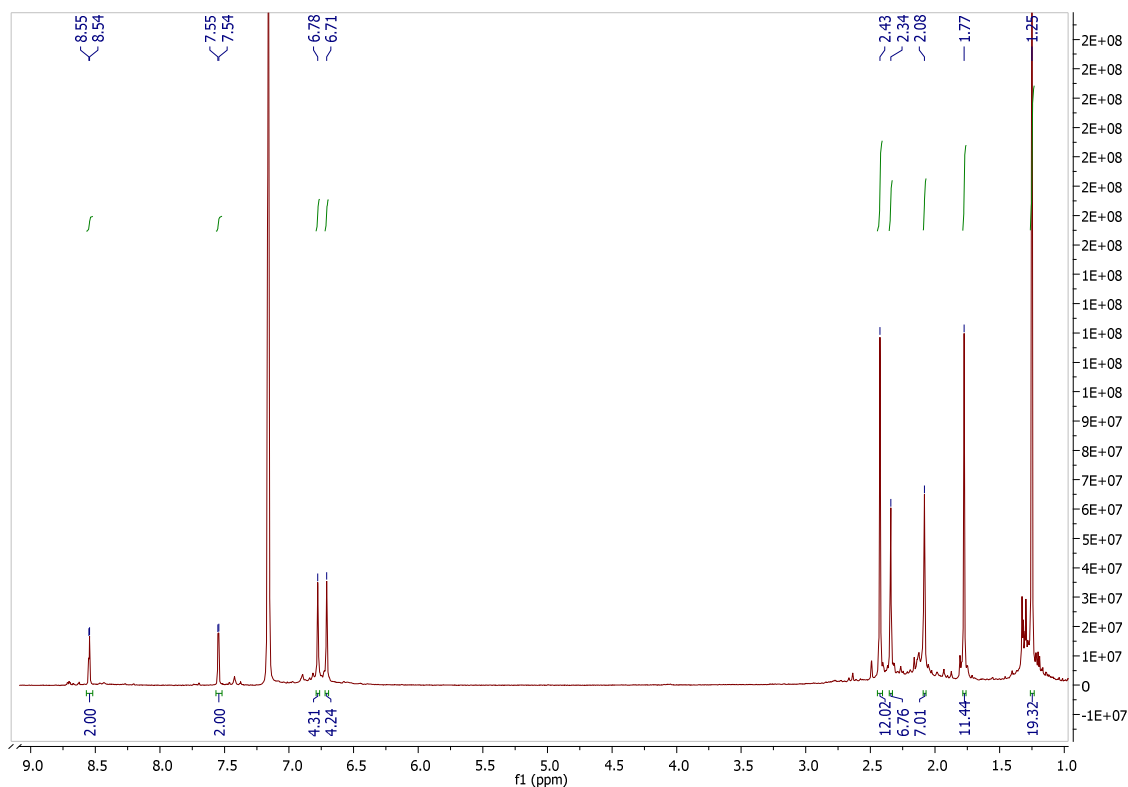
Figure 4.12: ^{1}H NMR of **20** in C_6D_6 solvent
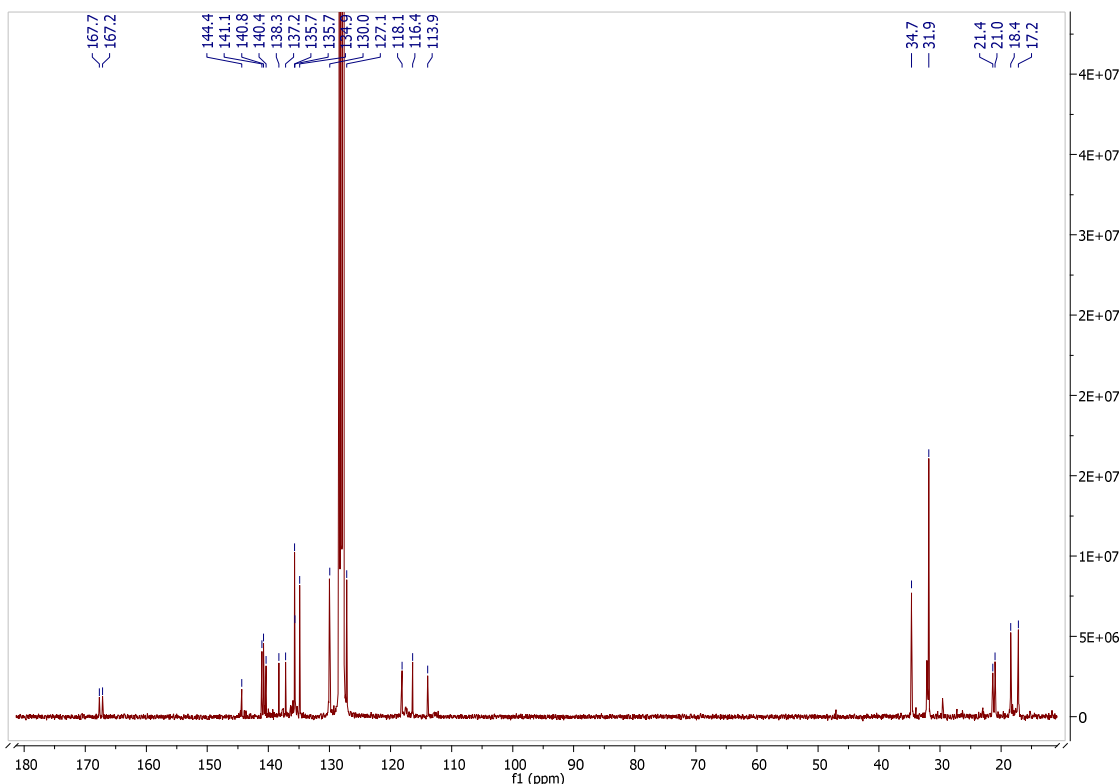
Figure 4.13: ^{13}C NMR of **20** in C$_6$D$_6$ solvent

4.3.6) Synthesis of 21

Carbon monoxide gas was bubbled through a solution of **20** (5.5 mg, 5.4 x 10^{-6} mol) dissolved in hexane (5 mL), until a colour change from dark to light brown was observed (Scheme 4.21). The solvent was evaporated, yielding an orange coloured residue that was determined to be **21** after NMR, IR and MS spectroscopic analysis. The product **21** was obtained with a yield of 77%. Crystal suitable for X-ray diffraction analysis could not be obtained.

Mes = 2,4,6-trimethylphenyl
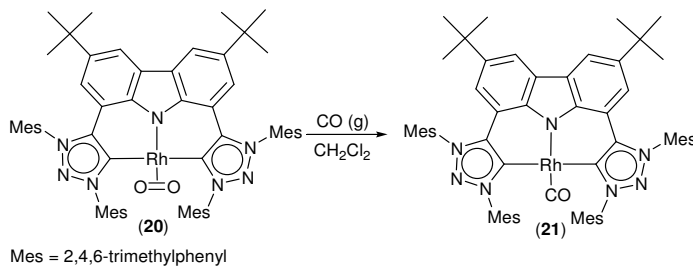
Scheme 4.21: Reacting **20** with carbon monoxide yielding **21**

With regard to **21**, the resonance of the ligand scaffold's aromatic protons have changed significantly from the resonance of the corresponding protons of **20**, as determined after proton NMR analysis

133

(Figure 4.14). Carbon NMR analysis further supports substitution of the molecular oxygen ligand in **20** with a carbonyl ligand, yielding **21**. Figure 4.15 displays the carbon spectrum of **21**. All carbons are accounted for. As is clearly evident from Figure 4.15, the carbene carbon of **21** resonates downfield by 6 ppm compared to the resonance of the carbene carbon for **20**. The carbene carbon of **21** resonates at 173.4 ppm with a [103]Rh(I)-[13]**C**carbene coupling constant of 41.5 Hz, which is 2.6 Hz more than the corresponding coupling constant of **20**. The larger coupling constant results from substitution of the L-donor oxygen ligand with a weaker L-donor carbonyl ligand. The carbene resonance of **21** is exactly the same as determined for **19**, while the [103]Rh(I)-[13]**C**carbene coupling constant of **21** is 0.1 Hz smaller compared to the corresponding coupling constant of **19**. The *sp*-hybridised carbonyl carbon of **21** resonates as a broad singlet at 194.4 ppm, and not as a doublet. The carbonyl carbon of **21** resonates upfield by 1 ppm compared to the Rh-**C**O resonance of **19**.
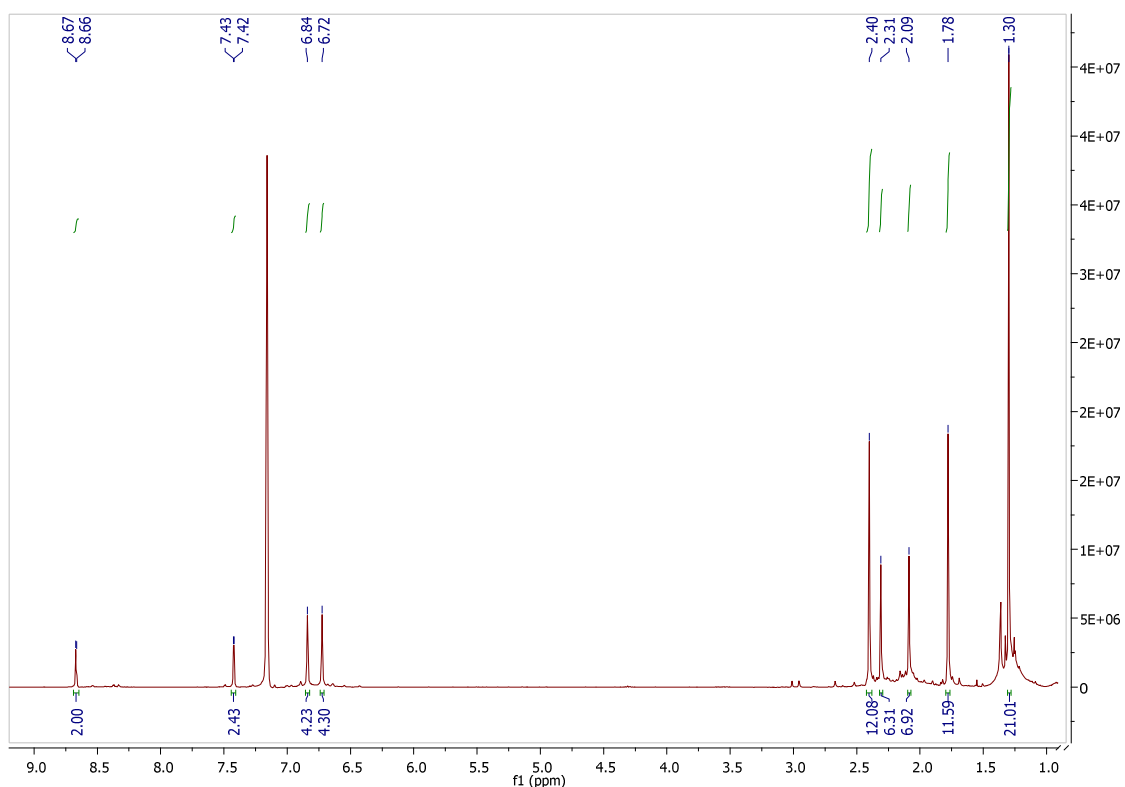
Figure 4.14: ^{1}H NMR of **21** in C_6D_6 solvent
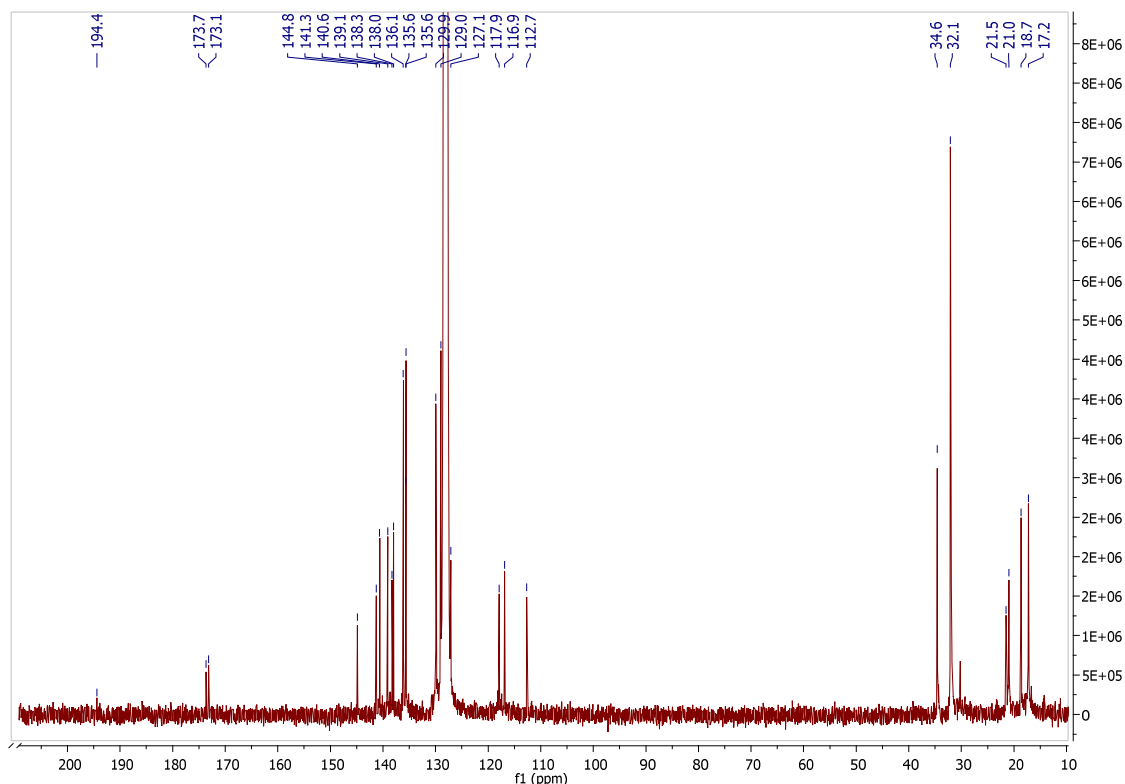
Figure 4.15: ^{13}C NMR of **21** in C$_6$D$_6$ solvent

Complex **21** was subjected to infrared spectroscopic analysis. The carbonyl ligand of **21** has a an even stronger absorption at 1941 cm^{-1}, compared to that of **19**, which was at 1955 cm^{-1}. As was determined for **19**, the ligand backbone **11** supporting the rhodium metal (complex **21**) is a strong σ-donor and weak π-acceptor ligand, directly resulting in the low absorption frequency determined for **21**. In fact, the ligand scaffold **11** is a stronger donor compared to the ligand scaffold **9**. The difference can be explained based on the wingtip functional groups. The 2,6-diisopropylphenyl functionalities have two carbon substituents on the benzene ring, while the 2,4,6-trimethylphenyl wingtip groups have three carbon substituent on the benzene ring. As is generally accepted, carbon substituents are σ-donors. Therefore, the ligand scaffold **11** has a slightly stronger donating ability compared to **9**. This results in a higher electron density donated to the rhodium metal, yielding a metal centre with a high nucleophilic character. The higher nucleophilic character of **21** compared to **19** will increase the ease of oxidative addition processes. The decreased steric bulk around the rhodium centre in **21** should allow easier access of substrates to the metal centre, increasing the rate of catalysis.

135

4.4) Catalytic activity of 20

The catalytic activity of **20** was tested towards the hydroamination of 1-pentyne with diethyl amine. The steric hindrance of **20** is less compared to the larger steric bulk of **17**, which could almost certainly result in **20** displaying higher catalytic activity, due to the greater ease with which the substrate would interact with the metal centre. In addition, the ligand scaffold **11** is a stronger σ-donor and weaker π-acceptor when compared to the ligand **9**, as was determined from the IR spectroscopic analysis for the rhodium(I)-carbonyl complexes, **19** and **21**. The reactivity of secondary amines is, in general, higher compared to primary amines. As such, a high pressure NMR tube was loaded with 0.4 mL deuterated benzene, 0.16 mmol of 1-pentyne, 0.16 mmol of diethyl amine and three mole percent of the catalyst, **20** (**I**, Scheme 4.22). The solution was heated up to 80 °C. Through NMR analysis, it could be determined that full conversion of the alkyne had occurred after just two hours. In contrast, the resonance and integration of the amine substrate was unchanged as determined through proton NMR analysis. The desired tertiary amine products were not obtained. Additional NMR experiments were conducted, and it was determined that the alkyne, in the presence of diethyl amine, was catalysed by **20** to the geminal (*gem*) enyne, namely 6-methylene-4-nonyne. The reaction was repeated, using the exact same amount of solvent, substrate and catalyst, but without the addition of secondary amine (**II**, Scheme 4.22). Again the alkyne was converted, with subsequent formation of the *gem*-enyne, which involves head-to-tail dimerisation of terminal alkynes[28] such as 1-pentyne. Figure 4.16 and 4.17 displays the ^{1}H and ^{13}C NMR spectra, respectively, of the catalytic reaction **II** in Scheme 4.22. The spectra indicate only the *gem*-enyne product, in addition to a small amount of uncatalysed alkyne still present in the reaction mixture. As is evident, only one product is formed, which is determined to be the *gem*-enyne, and not the *E*- and/or *Z*-isomers. The reaction proceeds in the absence of amine with a decrease in the rate of catalysis, as 40% of the alkyne had been converted after two hours. This is compared to full conversion after two hours in the presence of amine. After four hours, a 65% conversion was noted for **II**, Scheme 4.22.
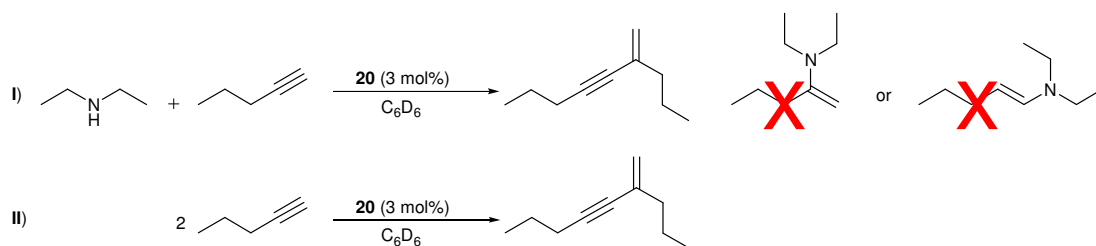
Scheme 4.22: Catalysis of 1-pentyne to 6-methylene-4-nonyne with **20** in **I**) the presence of diethyl amine and **II**) in the absence of diethyl amine

---

[28] L. Rubio-Pérez, R. Azpíroz, A. D. Giuseppe, V. Polo, R. Castarlenas, J. J. Pérez-Torrente, L.A. Oro, *Chem. Eur. J.*, 2013, **19**, 15304 – 15314, and references therein.

The proton NMR (Figure 4.16) indicates formation of only 6-methylene-4-nonyne, in addition to a small amount of uncatalysed 1-pentyne in the reaction mixture. The coupling constants for the *gem*-alkene protons are 2.4 Hz and 2.1 Hz, indicative of methylene proton coupling constants. This further supports *gem*-enyne formation, because the coupling constants for the *E*- and *Z*-isomers are four to eight times larger compared to the *gem*-isomers. In both spectra, the peaks corresponding to the **gem-enyne** are labelled numerically, with a bold font type in blue. The peaks corresponding to the small amount of uncatalysed *1-pentyne* are numerically labelled, with an italic font type in red.
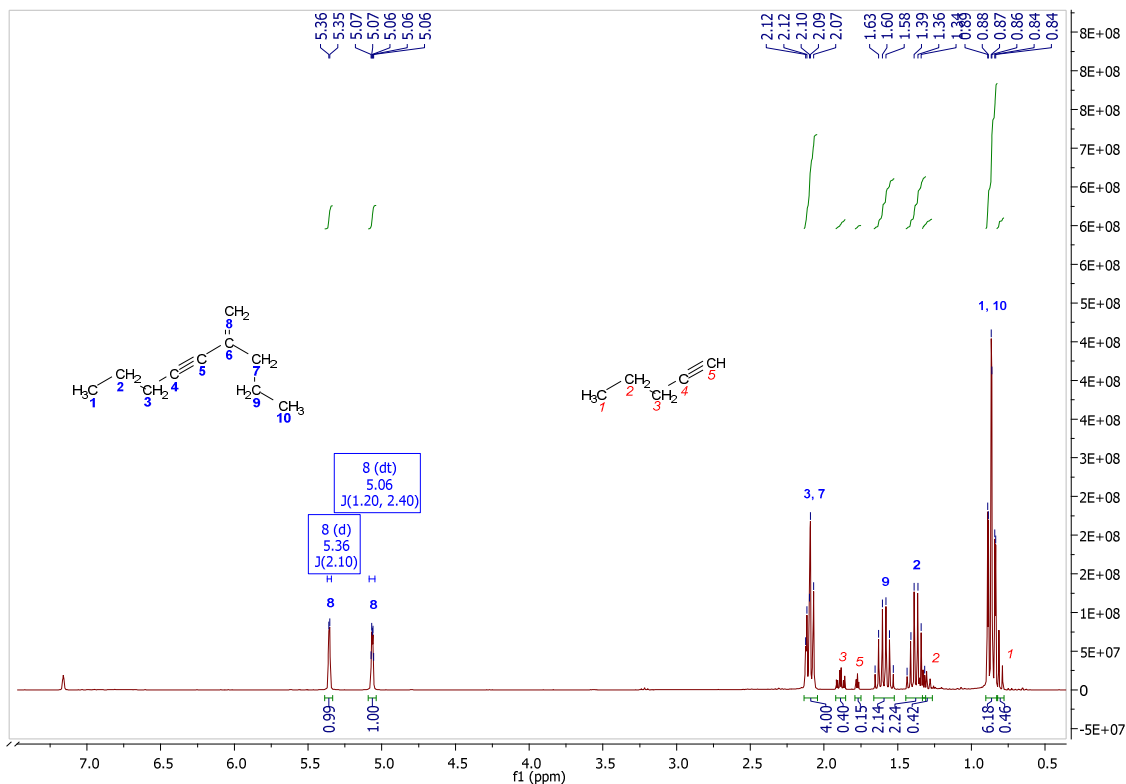
Figure 4.16: ^{1}H NMR after *1-pentyne* conversion to **gem-enyne** catalysed by **20** in the absence of amine with C_6D_6 as solvent
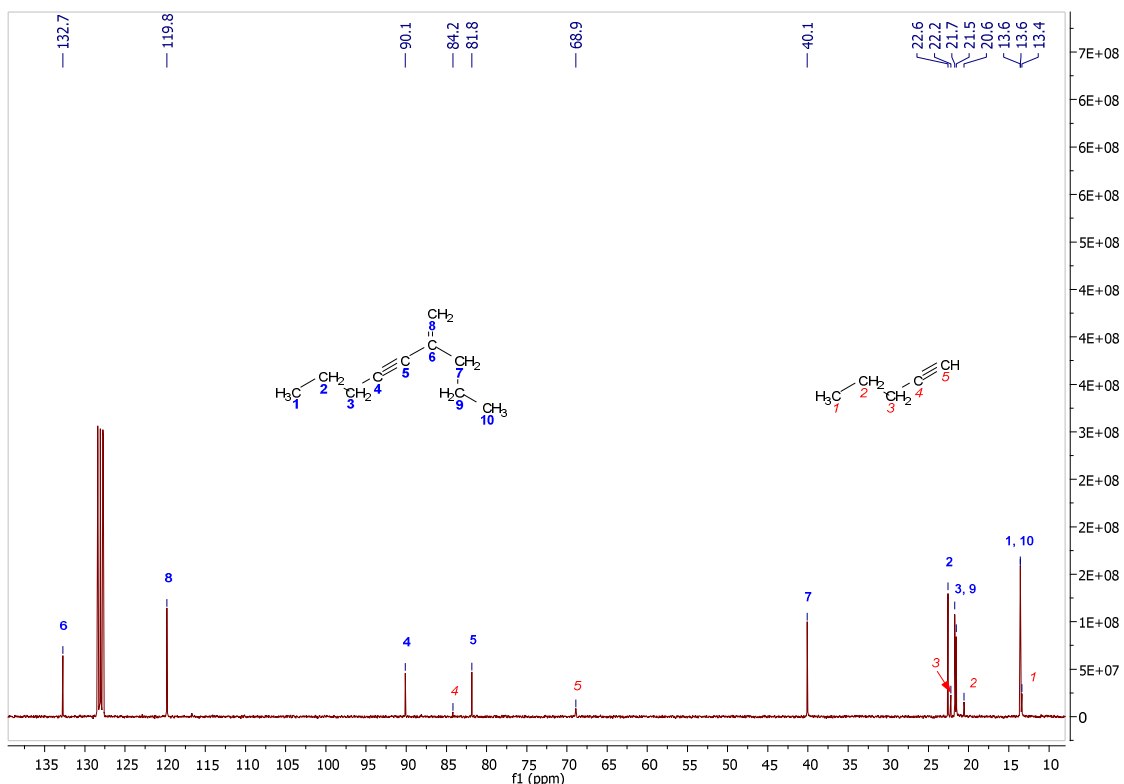
Figure 4.17: ^{13}C NMR after *1-pentyne* conversion to ***gem*-enyne** catalysed by **20** in the absence of diethyl amine in C_6D_6 solvent

Alkyne dimerisation involves a *sp*-hybridised C-H bond of an alkyne substrate that adds across a C≡C triple bond of a second alkyne.[29,30] The products of this process are conjugated enynyes. Alkyne dimerisation is a 100% atom economical process, but requires a catalyst. Various catalysts employing different metals have been reported to be active in this process. In general, three different enyne isomers are formed during the dimerisation of terminal alkynes. They are *E*-enynes, *Z*-enynes and *gem*-enynes. In addition, oligomer products have also been reported.[28,29,30] It should be noted that catalysis of terminal alkynes in general, proceed with low selectivity and/or stereospecificity, and the formation of two or even all three isomers is common. The catalytic reaction is initiated through π-coordination of the alkyne to the metal, followed by oxidative addition of the acidic C-H bond across the metal centre yielding the metal-hydride-alkynyl species.[28,29] The catalytic reaction, after the oxidative addition step had occurred, can then follow two main routes, depending on the catalyst employed and its selectivity and stereospecificity. The two main routes lead to the formation of

---

[29] C. J. Pell, O. V. Ozerov, *ACS Catal.*, 2014, **4**, 3470 – 3480, and references therein.

[30] For relevant articles and references therein see *a)* C. Jahier, O.V. Zatolochnaya, N. V. Zvyagintsev, V. P. Ananikov, V. Gevorgyan, *Org. Lett.*, 2012, **14**, 2846 – 2849, *b)* G. C. Midya, S. Paladhi, K. Dhara, J. Dash, *Chem. Commun.*, 2011, **47**, 6698 – 6700, *c)* V. Varga, L. Petrusová, J. Čejka, V. Hanuš, K. Mach, *J. Organomet. Chem.*, 1996, **509**, 235 – 240.

138

either the *E-* and/or *Z*-enyne isomers as products of the 'vinylidene' route, or the *E-* and/or *gem*-enyne isomers as products of the alternative route.

The *E-* or *Z*-enyne isomers are formed if the reaction proceeds through a vinylidene intermediate.[28,29] Isomerisation of the metal-hydride-alkynyl species, formed after oxidative addition had occurred, results to the formation of the vinylidene intermediate (Scheme 4.23).[28,29] Isomerisation is reported to be a non-reversible process.[29] Nucleophilic attack of the second alkyne on the electrophilic carbon of the vinylidene moiety, with subsequent reductive elimination, yields the catalyst and the *E-* and/or *Z*-enyne products.[28,29]
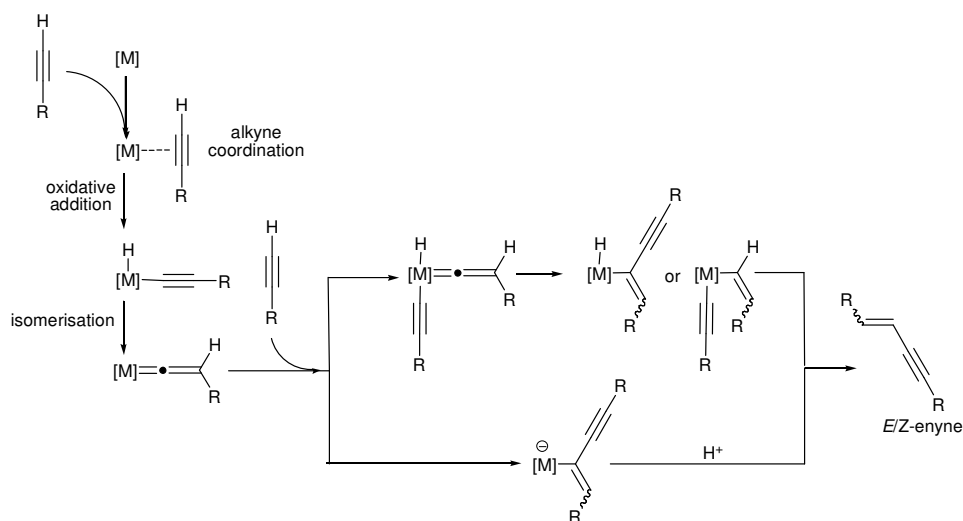
Scheme 4.23: *E/Z*-enyne catalysis through the vinylidene route[28]

The alternative route towards formation of the *E-* and/or *gem*-enyne isomers does not proceed through a vinylidene intermediate pathway. Instead, migratory insertion of a second alkyne into either the M-C (carbometalation) or M-H (hydrometalation) bond followed by reductive elimination yields the enyne and the active catalyst (Scheme 4.24).[28] This reaction pathway generally results in the formation of either *E-* and/or *gem*-enynes. In most cases, both isomers are formed with varying yields and selectivity. A 1,2- or 2,1-migratory insertion pathway can occur during the carbometalation or hydrometalation steps. Hydrometalation involving a 2,1-migratory insertion pathway yields the *gem*-enyne product after reductive elimination, while a 1,2-migratory insertion of the second alkyne will yield the *E*-enyne. Carbometalation following a 1,2-migratory insertion path yields the *gem*-enyne, while 2,1-migratory insertion leads to the formation of *E*-enynes (Scheme 4.24).[28]

139
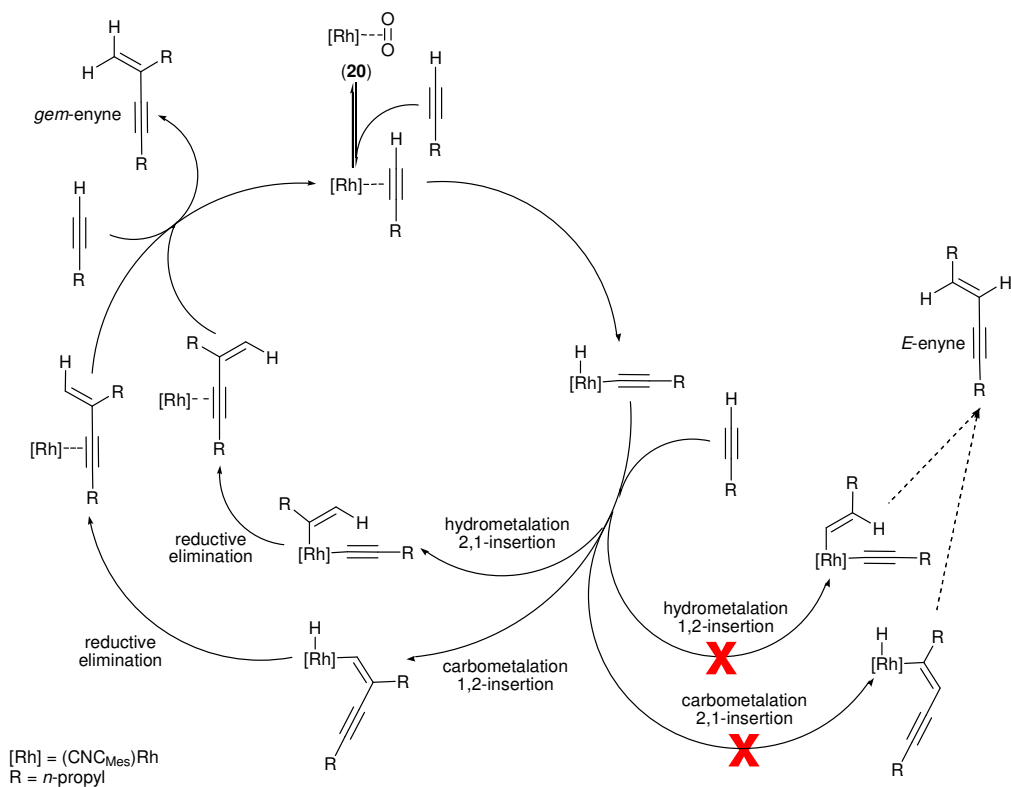
Scheme 4.24: Proposed reaction mechanism for the catalysis of 1-pentyne to *gem*-enyne by **20**

Based on the reported literature, as well as the in depth study regarding the mechanism of *E*- or *gem*-enyne formation by Oro and co-workers,[28] a possible mechanism for the catalysis depicted in Scheme 4.22 can be postulated. Formation of both *E*- and *Z*-enynes during the catalytic reaction of 1-pentyne catalysed by **20** (Scheme 4.22), could be ruled out due to formation of the *gem*-enyne as the sole product of the reaction (see Figure 4.16 and Figure 4.17). The *gem*-enyne, being the only product obtained after the catalytic reaction, is in all probability formed through hydrometalation that follows a 2,1-migratory insertion path, or through a carbometalation reaction which follows a 1,2-migratory insertion pathway. The postulated mechanism is depicted in Scheme 4.24.

It has been reported that the presence of a base, either weak or strong, can accelerate the catalytic rate. This is observed for the catalytic reaction depicted in Scheme 4.22. The catalytic activity of **20** in the presence of diethyl amine was higher, while the absence of the base decreases the catalytic activity. With regard to the catalytic tests conducted on **20**, Scheme 4.22, the basic diethyl amine can increase the catalytic activity of the reaction in either one of two ways. The basic amine can form hydrogen bonds to the terminal alkyne C-**H**, increasing the acidity of the proton. The C-**H** bond will be more polarised, which increases the oxidative addition step that could increase the rate of catalysis, if the oxidative addition step is the rate determining step. A second scenario exists, where

140

deprotonation of the acidic alkyne proton occurs. Upon π-coordination of the alkyne to the metal, the acidity of the proton could increase to such an extent that the basic amine can deprotonate the acidic terminal alkyne, yielding a relatively strong conjugated acid and the metal-alkynyl species, not the metal-hydride-alkynyl species. Dimerisation can then proceed only through carbometalation, following a 1,2-insertion pathway. The second alkyne can then enter the catalytic cycle, and upon reductive elimination, the *gem*-enyne and the metal-alkynyl catalyst is formed.

4.5) Conclusion

Several complexes of rhodium have been synthesised. The synthesis involved deprotonation of the ligand **7** or **10**, yielding the free carbene adduct **9** or **11** that was subsequently metallated *in situ* with the rhodium precursor $[Rh(C_2H_4)_2Cl]_2$. All attempts at isolating a rhodium 14-electron complex were unsuccessful. Instead, the 16-electron rhodium complexes **17** and **20**, coordinated by molecular oxygen, were obtained. Reacting **17** or **20** with either ammonia or carbon monoxide yielded novel rhodium complexes. In addition, the catalytic activity of **20** was investigated.

A Rh(I)-O_2 adduct **17** was isolated and crystal structure determination unambiguously confirmed its existence. The adduct **17** displayed thermal stability and could be manipulated in air without decomposition occurring. Relatively few examples regarding rhodium-oxygen adducts had been reported to date. The molecular oxygen π-coordinates to the rhodium(I) centre, while the oxygen-oxygen bond lengths gives an indication to a certain degree of rhodium to oxygen backbonding. The analogue of **17**, namely the rhodium(I) dioxygen adduct supported by **11**, was synthesised based on the same procedure as was used for the synthesis of **17**.

Reacting the Rh(I)-O_2 adduct **17** with ammonia gas resulted to the formation of the Werner complex, **18**. However, unlike most inert Werner complexes formed through coordination of an amine's lone pair to the metal centre, coordination of the ammonia ligand in complex **18** was determined to be reversible. The ammonia ligand in complex **18** could be removed by simply applying a vacuum followed by exposure to oxygen, yielding **17** again. To the best our knowledge, reversible ammonia coordination to a rhodium metal centre has not been reported to date. Attempts to obtain the oxidative addition product, namely the rhodium-amido-hydride complex, were unsuccessful.

The electronic properties of the ligand scaffold could be probed, by reacting either **17** or **20** with carbon monoxide, yielding the carbonyl complexes **19** and **21**, respectively. The rhodium-carbonyl complexes were subjected to infrared spectroscopic analysis. The IR stretching frequency for the

carbonyl ligand of **19** was determined to be 1955 cm^{-1}. Surprisingly, the carbonyl absorption band for the Rh(I)-CO complex **21** was observed at 1941 cm^{-1} during IR spectroscopic analysis. Both low energy values give evidence that the ligand scaffolds **9** and **11** are very strong σ-donors and weak π-acceptors. As such, it can be concluded that the ligand will readily donate electron density to the metal, yielding a metal centre with a high nucleophilic character.

The catalytic activity of **20** towards the hydroamination of 1-pentyne with diethyl amine was investigated. Hydroamination of the alkyne did not occur, and the tertiary amine was not formed. Instead, the rhodium complex **20** catalysed the dimerisation of the terminal alkyne yielding the *gem*-enyne, 6-methylene-4-nonyne. Only the *gem*-enyne product and not the *E*- and/or *Z*-isomers were obtained. This indicates that the catalyst **20** is selective only towards the *gem*-enyne product. Such selectivity is scarce, while some of the better performing alkyne dimerisation catalyst reported, catalyses the dimerisation with formation of one isomer as the major product, in addition to another isomer formed during the reaction. A mechanism for the catalytic reaction has been postulated to proceed through first oxidative addition of the terminal C-H bond across the rhodium metal, followed by either a carbometalation (1,2-insertion) or a hydrometalation (2,1-insertion) pathway; and concomitant reductive elimination yielding the active catalyst and the *gem*-enyne. This mechanism is only a postulation with regard to the catalytic reactions depicted in Scheme 4.22. Investigation of the reaction mechanism through varying the substrates used, will be attempted that could shed more light on the mechanism by which **20** catalyses the alkyne dimerisation reaction.

4.6) Experimental

4.6.1) (CNC$_{Dipp}$)RhO$_2$ (17)
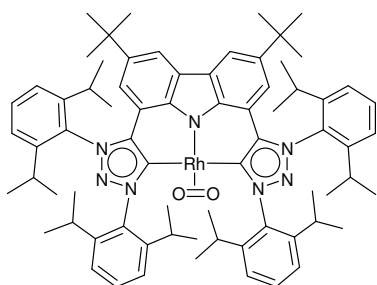
A flame dried Schlenk tube was loaded with **7** (200.0 mg, 1.6 x 10^{-4} mol), [Rh(C$_2$H$_4$)$_2$Cl]$_2$ (50.3 mg, 1.3 x 10^{-4} mol) and KN[Si(CH$_3$)$_3$]$_2$ (161.3 mg, 8.1 x 10^{-4} mol). The Schlenk tube was evacuated and purged with N$_2$ (g). The reaction vessel was cooled down to -78 °C, and the solids dissolved by addition of THF (20 mL) which was also cooled down to -78 °C. The solution was stirred for 30 min at -78 °C before being removed from the cold bath and stirred an additional 24 hours at room temperature. The solvents were evaporated *in vacuo*. The product was extracted with hexanes (4 x 15 mL). Evaporation of the solvent *in vacuo* yielded **17** as a brown solid (105.0 mg,

142

8.8 x 10^{-5} mol, 55%). Crystallisation from toluene yielded single crystals suitable for XRD analysis. NMR analysis was carried out in C$_6$D$_6$ as well as THF-d_8. ^{1}H NMR δ$_H$ (C$_6$D$_6$, 400 MHz) 8.40 (2H, d, J = 2.0 Hz, Ar**H**$_{carb}$), 7.49 (2H, d, J = 2.0 Hz, Ar**H**$_{carb}$), 7.34 (2H, t, J = 7.8 Hz, Ar**H**$_{Dipp}$), 7.30 (2H, t, J = 7.8 Hz, Ar**H**$_{Dipp}$), 7.16 (4H, d, Ar**H**$_{Dipp}$ overlaps with C$_6$D$_6$), 7.13 (4H, d, J = 8.0 Hz, Ar**H**$_{Dipp}$), 2.98 (4H, sept, J = 6.8 Hz, C**H**(CH$_3$)$_2$), 2.66 (4H, sept, J = 6.8 Hz, C**H**(CH$_3$)$_2$), 1.65 (12H, d, J = 6.8 Hz, CH(C**H$_3$**)$_2$), 1.23 (12H, d, J = 7.2 Hz, CH(C**H$_3$**)$_2$), 1.21 (18H, s, C(C**H$_3$**)$_3$), 1.05 (12H, d, J = 6.8 Hz, CH(C**H$_3$**)$_2$), 0.78 (12H, d, J = 6.8 Hz, CH(C**H$_3$**)$_2$). ^{13}C NMR δ$_C$ (C$_6$D$_6$, 100 MHz) 168.4 (d, J = 39.2 Hz, Rh-**C**$_{Carbene}$), 146.3 (Ar**C**$_q$), 145.4 (Ar**C**$_q$), 144.4 (Ar**C**$_q$), 141.6 (Ar**C**$_q$), 140.6 (Ar**C**$_q$), 137.5 (Ar**C**$_q$), 135.3 (Ar**C**$_q$), 131.7 (Ar**C**H), 129.1 (Ar**C**H), 125.5 (Ar**C**H), 121.6 (Ar**C**H), 119.6 (Ar**C**H), 116.7 (Ar**C**H), 113.2 (Ar**C**$_q$), 34.6 (**C**(CH$_3$)$_3$), 32.0 (C(**C**H$_3$)$_3$), 29.6 (**C**H(CH$_3$)$_2$), 29.1 (**C**H(CH$_3$)$_2$), 26.0 (CH(**C**H$_3$)$_2$), 24.8 (CH(**C**H$_3$)$_2$), 24.3 (CH(**C**H$_3$)$_2$), 23.2 (CH(**C**H$_3$)$_2$). ^{1}H NMR δ$_H$ (THF-d_8, 500 MHz) 8.18 (2H, d, J = 1.5 Hz, Ar**H**$_{carb}$), 7.73 (2H, t, J = 8.0 Hz, Ar**H**$_{Dipp}$), 7.60 (4H, d, J = 8.0 Hz, Ar**H**$_{Dipp}$), 7.32 (2H, d, J = 2.0 Hz, Ar**H**$_{carb}$), 7.15 (2H, t, J = 7.8 Hz, Ar**H**$_{Dipp}$), 6.92 (4H, d, J = 8.0 Hz, Ar**H**$_{Dipp}$), 2.63 − 2.57 (8H, m, C**H**(CH$_3$)$_2$), 1.36 (12H, d, J = 6.5 Hz, CH(C**H$_3$**)$_2$), 1.19 (12H, d, J = 6.5 Hz, CH(C**H$_3$**)$_2$), 1.13 (18H, s, C(C**H$_3$**)$_3$), 1.06 (12H, d, J = 7.0 Hz, CH(C**H$_3$**)$_2$), 1.00 (12H, d, J = 7.0 Hz, CH(C**H$_3$**)$_2$). ^{13}C NMR δ$_C$ (THF-d_8, 125 MHz) 168.5 (d, J = 39.0 Hz, Rh-**C**$_{Carbene}$), 146.8, 145.8, 144.5, 142.0, 141.2, 137.9, 135.9, 132.8, 129.3, 128.9, 128.7, 128.5, 126.5, 121.8, 119.9, 117.2, 113.3, 35.2, 32.3, 30.0, 29.9, 26.4, 24.4, 23.8. HRMS (FIA-ESI): Calculated for C$_{72}$H$_{90}$N$_7$RhO$_2^{2+}$ [M]$^{2+}$: 593.8105, found: 593.8127.

4.6.2) (CNC$_{Dipp}$)RhNH$_3$ (**18**)
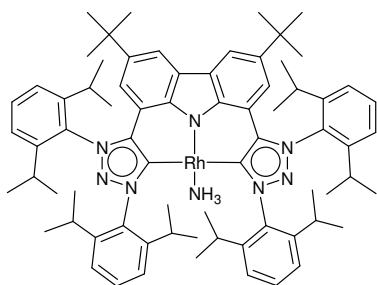
A Schlenk tube was loaded with **17** (20.0 mg, 1.7 x 10^{-5} mol), and dissolved by adding C$_6$D$_6$ (0.5 mL). At room temperature, NH$_3$ (g) was bubbled through the brown deuterated benzene solution. The colour of the solution instantaneously changed to a red coloured solution. From NMR analysis, it could be determined that a quantitative conversion of **17** to **18** had occurred. The reaction procedure was repeated, but deuterated thf was used as solvent instead of deuterated benzene. ^{1}H NMR δ$_H$ (C$_6$D$_6$, 300 MHz) 8.50 (2H, d, J = 1.8 Hz, Ar**H**$_{carb}$), 7.39 (2H, d, J = 1.8 Hz, Ar**H**$_{carb}$), 7.35 (2H, t, J = 7.8 Hz, Ar**H**$_{Dipp}$), 7.30 (2H, t, J = 7.8 Hz, Ar**H**$_{Dipp}$), 7.15 (8H, Ar**H**$_{Dipp}$ overlaps with C$_6$D$_6$), 2.94 (4H, sept, J = 6.8 Hz, C**H**(CH$_3$)$_2$), 2.70 (4H, sept, J = 6.8 Hz, C**H**(CH$_3$)$_2$), 1.45 (12H, d, J = 6.6 Hz, CH(C**H$_3$**)$_2$), 1.25 (18H, s, C(C**H$_3$**)$_3$), 1.22 (12H, d, J = 6.9 Hz, CH(C**H$_3$**)$_2$), 1.05 (12H, d, J = 6.9 Hz, CH(C**H$_3$**)$_2$), 0.82 (12H, d, J = 6.9 Hz, CH(C**H$_3$**)$_2$). ^{13}C NMR δ$_C$ (C$_6$D$_6$, 75 MHz) 169.2 (d, J = 34.8 Hz, Rh-**C**$_{Carbene}$), 146.2, 145.5, 144.3, 141.7, 137.8, 135.3, 131.6, 129.0, 127.2, 125.5, 121.9, 119.4, 117.2,

143

112.7, 34.6 (**C**(CH₃)₃), 32.2 (C(**CH₃**)₃), 29.4 (**C**H(CH₃)₂), 29.1 (**C**H(CH₃)₂), 26.4 (CH(**CH₃**)₂), 24.8 (CH(**CH₃**)₂), 23.9 (CH(**CH₃**)₂), 23.2 (CH(**CH₃**)₂). ^{1}H NMR δ $_H$ (THF-d_8, 500 MHz) 8.11 (2H, s, Ar**H**$_{carb}$), 7.68 (2H, t, J = 7.8 Hz, Ar**H**$_{Dipp}$), 7.55 (4H, d, J = 8.0 Hz, Ar**H**$_{Dipp}$), 7.23 (2H, t, J = 7.8 Hz, Ar**H**$_{Dipp}$), 7.08 (2H, s, Ar**H**$_{carb}$), 6.99 (4H, d, J = 8.0 Hz, Ar**H**$_{Dipp}$), 2.68 − 2.60 (8H, m, C**H**(CH₃)₂), 1.16 (12H, d, J = 6.5 Hz, CH(**CH₃**)₂), 1.14 (12H, d, J = 7.0 Hz, CH(**CH₃**)₂), 1.10 (18H, s, C(**CH₃**)₃), 1.03 (12H, d, J = 7.0 Hz, CH(**CH₃**)₂), 1.01 (12H, d, J = 6.5 Hz, CH(**CH₃**)₂). ^{13}C NMR δ $_C$ (THF-d_8, 125 MHz) 170.7 (d, J = 34.0 Hz, Rh-**C**$_{Carbene}$), 146.8, 146.2, 144.4, 142.2, 138.5, 137.6, 136.0, 132.5, 129.2, 128.0, 126.3, 122.4, 119.3, 117.6, 112.7, 35.0 (**C**(CH₃)₃), 32.5 (C(**CH₃**)₃), 30.8 (**C**H(CH₃)₂), 29.8 (**C**H(CH₃)₂), 27.1 (CH(**CH₃**)₂), 23.9 (CH(**CH₃**)₂). IR (CH₂Cl₂): 3407 cm^{-1} v(N-H), 1627 cm^{-1} δ (N-H), 1033 cm^{-1} δ (N-H).

4.6.3) (CNC$_{Dipp}$)RhCO (**19**)
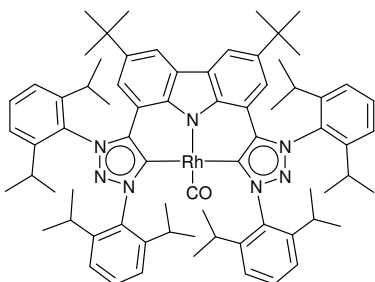
To a Schlenk tube was added **17** (20.0 mg, 1.7 x 10^{-5} mol), and dissolved by adding CH₂Cl₂ (2 mL) resulting in a brown coloured solution. At room temperature, CO (g) was bubbled through the solution which changed colour from brown to light brown. The solvent was removed *in vacuo* yielding **19** as a light brown coloured residue. From NMR analysis, it could be determined that a quantitative conversion of **17** to **19** had occurred. NMR δ $_H$ (C₆D₆, 300 MHz) 8.52 (2H, d, J = 1.8 Hz, Ar**H**$_{carb}$), 7.64 (1H, dd, J = 5.7 Hz, 3.3 Hz, Ar**H**$_{Dipp}$), 7.46 (2H, d, J = 1.5 Hz, Ar**H**$_{carb}$), 7.31 − 7.25 (6H, m, Ar**H**$_{Dipp}$), 6.93 (1H, dd, J = 5.7 Hz, 3.3 Hz, Ar**H**$_{Dipp}$), 3.04 (4H, sept, J = 6.8 Hz, C**H**(CH₃)₂), 2.62 (4H, sept, J = 6.8 Hz, C**H**(CH₃)₂), 1.55 (12H, d, J = 6.9 Hz, CH(**CH₃**)₂), 1.25 (18H, s, C(**CH₃**)₃), 1.16 (12H, d, J = 6.9 Hz, CH(**CH₃**)₂), 1.04 (12H, d, J = 6.9 Hz, CH(**CH₃**)₂), 0.78 (12H, d, J = 6.9 Hz, CH(**CH₃**)₂). ^{13}C NMR δ $_C$ (C₆D₆, 75 MHz) 195.4 (d, J = 70.2 Hz, Rh-**C**O), 173.4 (d, J = 41.6 Hz, Rh-**C**$_{Carbene}$), 146.3 (Ar**C**$_q$), 146.1 (Ar**C**$_q$), 144.4 (Ar**C**$_q$), 142.7 (Ar**C**$_q$), 138.2 (Ar**C**$_q$), 137.6 (Ar**C**$_q$), 135.7 (Ar**C**$_q$), 133.4 (Ar**C**$_q$), 131.5 (Ar**C**H), 130.9 (Ar**C**H), 130.8 (Ar**C**H), 129.1 (Ar**C**H), 127.2 (Ar**C**$_q$), 125.4 (Ar**C**H), 124.1 (Ar**C**H), 119.0 (Ar**C**H), 117.1 (Ar**C**H), 111.8 (Ar**C**$_q$), 34.5 (**C**(CH₃)₃), 32.3 (C(**CH₃**)₃), 29.3 (**C**H(CH₃)₂), 29.1 (**C**H(CH₃)₂), 25.6 (CH(**CH₃**)₂), 24.8 (CH(**CH₃**)₂), 24.2 (CH(**CH₃**)₂), 23.1 (CH(**CH₃**)₂). IR (CH₂Cl₂): 1955 cm^{-1} v(CO). HRMS (FIA-ESI): Calculated for C₇₂H₉₀N₇RhCO^{2+} [M + H]$^{2+}$: 592.8204, found: 592.8197.

144

4.6.4) (CNC$_{Mes}$)RhO$_2$ (20)
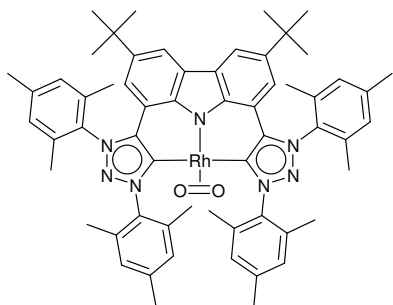
A flame dried Schlenk tube was charged with **10** (200.0 mg, 1.9 x 10^{-4} mol), [Rh(C$_2$H$_4$)$_2$Cl]$_2$ (58.2 mg, 1.5 x 10^{-4} mol) and KN[Si(CH$_3$)$_3$]$_2$ (186.7 mg, 9.4 x 10^{-4} mol). The reaction vessel was evacuated and purged with N$_2$ (g), and cooled down to -78 °C. The solids were dissolved by addition of THF (20 mL) which was also cooled down to -78 °C. The solution was stirred for one hour at -78 °C before being removed from the cold bath and stirred an additional 24 hours at room temperature. The solvents were evaporated *in vacuo* and the product was extracted with hexanes (4 x 15 mL). Evaporation of the hexane solvent, *in vacuo*, yielded **17** as a brown solid (130.0 mg, 1.3 x 10^{-4} mol, 68 %). Crystal suitable for X-ray diffraction could not be obtained. NMR δ $_H$ (C$_6$D$_6$, 300 MHz) 8.55 (2H, d, *J* = 1.8 Hz, Ar**H**$_{carb}$), 7.55 (2H, d, *J* = 1.8 Hz, Ar**H**$_{carb}$), 6.78 (4H, s, Ar**H**$_{Mes}$), 6.71 (4H, s, Ar**H**$_{Mes}$), 2.43 (12H, s, ArC**H**$_3$), 2.34 (6H, s, ArC**H**$_3$), 2.08 (6H, s, ArC**H**$_3$), 1.77 (12H, s, ArC**H**$_3$), 1.25 (18H, s, C(C**H**$_3$)$_3$). ^{13}C NMR δ $_C$ (C$_6$D$_6$, 75 MHz) 167.4 (d, *J* = 38.9 Hz, Rh-**C**$_{Carbene}$), 144.4, 141.1, 140.8, 140.4, 138.3, 137.2, 135.7, 135.7, 134.9, 130.0, 127.2, 118.1, 116.4, 113.9, 34.7 (**C**(CH$_3$)$_3$), 31.9 (C(**C**H$_3$)$_3$), 21.4 (Ar**C**H$_3$), 21.0 (Ar**C**H$_3$), 18.4 (Ar**C**H$_3$), 17.2 (Ar**C**H$_3$). HRMS (FIA-ESI): Calculated for C$_{60}$H$_{66}$N$_7$RhO$_2$$^{2+}$ [M + CH$_3$CN + 2H]$^{2+}$: 531.2377, found: 531.2393.

4.6.6) (CNC$_{Mes}$)RhCO (21)
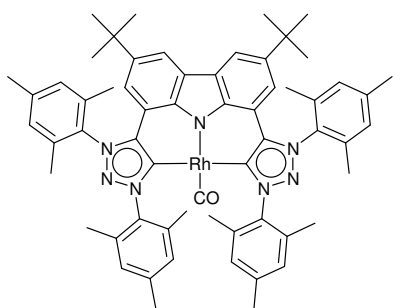
To a flame dried Schlenk tube was added **20** (5.5 mg, 5.4 x 10^{-6} mol). The reaction vessel was purged with N$_2$ (g). The brown solid was dissolved by adding hexane (5 mL). Carbon monoxide gas was bubbled through the solution for 5 minutes, resulting in a colour change from dark to light brown. The solvent was evaporated, *in vacuo*, yielding **21** (4.2 mg, 4.1 x 10^{-6} mol, 77%) as an orange solid. NMR δ $_H$ (C$_6$D$_6$, 300 MHz) 8.67 (2H, d, *J* = 1.8 Hz, Ar**H**$_{carb}$), 7.42 (2H, d, *J* = 1.8 Hz, Ar**H**$_{carb}$), 6.84 (4H, s, Ar**H**$_{Mes}$), 6.72 (4H, s, Ar**H**$_{Mes}$), 2.40 (12H, s, ArC**H**$_3$), 2.31 (6H, s, ArC**H**$_3$), 2.09 (6H, s, ArC**H**$_3$), 1.78 (12H, s, ArC**H**$_3$), 1.30 (18H, s, C(C**H**$_3$)$_3$). ^{13}C NMR δ $_C$ (C$_6$D$_6$, 75 MHz) 194.4 (Rh-**C**O), 173.4 (d, *J* = 41.5 Hz, Rh-**C**$_{Carbene}$), 144.9 (Ar**C**$_q$), 141.3 (Ar**C**$_q$), 140.6 (Ar**C**$_q$), 139.1 (Ar**C**$_q$), 138.3 (Ar**C**$_q$), 138.0 (Ar**C**$_q$), 136.1 (Ar**C**$_q$), 135.7 (Ar**C**$_q$), 135.6 (Ar**C**$_q$), 129.9 (Ar**C**H), 129.0 (Ar**C**H), 127.1 (Ar**C**$_q$), 117.9 (Ar**C**H), 116.9 (Ar**C**H), 112.7 (Ar**C**$_q$), 34.6 (**C**(CH$_3$)$_3$), 32.1 (C(**C**H$_3$)$_3$),

21.5 (ArCH$_3$), 21.0 (ArCH$_3$), 18.7 (ArCH$_3$), 17.3 (ArCH$_3$). IR (CH$_2$Cl$_2$): 1941 cm^{-1} ν(CO). HRMS (FIA-ESI): Calculated for C$_{60}$H$_{66}$N$_7$RhCO$^+$ [M]$^+$: 1015.4384, found: 1015.4407; calculated for C$_{60}$H$_{66}$N$_7$RhCO^{2+} [M + H]$^{2+}$: 508.7265, found: 508.7070.

4.6.7) Catalysis with 20

The catalytic studies were conducted as follows:

I)   Catalysis in the presence of diethyl amine

A high pressure NMR tube was loaded with C$_6$D$_6$ (0.4 mL), catalyst **20** (5.0 mg, 4.9 x 10^{-6} mol, 3 mol%), diethyl amine (16 μL, 1.6 x 10^{-4} mol) and 1-pentyne (17 μL, 1.6 x 10^{-4} mol) under a nitrogen gas atmosphere. A proton NMR experiment was conducted at the start of the reaction. The reaction mixture was heated up to 80 °C for two hours, before being subjected to NMR experiments. Through NMR analysis, it was determined that full conversion occurred after two hours.

II)   Catalysis without addition of diethyl amine

A high pressure NMR tube was loaded with C$_6$D$_6$ (0.4 mL), catalyst **20** (5.0 mg, 4.9 x 10^{-6} mol, 3 mol%) and 1-pentyne (17 μL, 1.6 x 10^{-4} mol) under a nitrogen gas atmosphere. A proton NMR experiment was conducted at the start of the reaction. The reaction mixture was heated up to 80 °C for two hours, before being subjected to NMR experiments. It was determined, through NMR analysis, that 40% of the alkyne had been converted to the enyne after two hours. The reaction was continued, and at each two hour interval, NMR experiments were conducted to determine the extent of conversion.

146

Chapter 5: A Golden Tale

5.1) Background

The chemistry of gold has lain dormant until the late 20th century, until a gold rush, with regards to research into gold and complexes of gold, occurred at the end of the 20th century. This explosion of interest and research in the chemistry of gold has not subsided in the 21st century. Gold and complexes of gold have unveiled interesting properties, giving it a unique character with reactivity contrasting to the well-established reactivity patterns of other late transition metals.[1]

The two most general oxidation states of gold are +1 and +3. In most cases, coordination of one or two ligands to a gold(I) metal centre yields linear complexes, while gold(III) generally prefers to form square planar complexes.[1] Relatively few examples have been reported regarding gold in an oxidation state of +2. The unpaired electrons of gold(II), generally results in an unstable complex.[1,2] However, this higher energy and thus reactivity of the gold(II) complex could be harnessed in catalysis, with potentially high catalytic output. Even fewer examples have been reported regarding the synthesis and isolation of gold(0) complexes. The group of Bertrand was able to synthesise and isolate gold(0) complexes stabilised by cyclic(alkyl)amino carbenes.[3] Remarkably, anionic gold complexes, were the negative charge is situated on the gold atom resulting in a fully occupied gold 6s-orbital, has been reported.[4]

Various reactivity and catalytic studies have been performed and reported, especially with regard to complexes of gold(I) and their coordination to and activation of unactivated, unsaturated carbon substrates (see review articles and references therein).[1,5,6,7,8] The activated carbon reagent can subsequently undergo nucleophilic attack, while the gold(I) metal centre never undergoes any oxidative addition or reductive elimination processes. On the other hand, complexes of gold(III) have

---

[1] H. G. Raubenheimer, H. Schmidbaur, *J. Chem. Educ.*, 2014, DOI: 10.1021/ed400782p.

[2] T. Dann, D-A. Roşca, J. A. Wright, G. G. Wildgoose, M. Bochmann, *Chem. Commun.*, 2013, **49**, 10169 – 10171.

[3] D. S. Weinberger, M. Melaimi, C. E. Moore, A. L. Rheingold, G. Frenking, P. Jerabek, G. Bertrand, *Angew. Chem. Int. Ed.*, 2013, **52**, 8964 – 8967.

[4] M. Jansen, *Chem. Soc. Rev.*, 2008, **37**, 1826 – 1835.

[5] R. A. Widenhoefer, X. Han, *Eur. J. Org. Chem.*, 2006, 4555 – 4563.

[6] E. Jiménez-Núñez, A. M. Echavarren, *Chem. Commun.*, 2007, 333 – 346.

[7] H. Schmidbaur, A. Schier, *Organometallics*, 2010, **29**, 2 – 23.

[8] *a)* M. Rudolph, A. S. K. Hashmi, *Chem. Commun.*, 2011, **47**, 6536 – 6544, *b)* A. S. K. Hashmi, *Chem. Rev.*, 2007, **107**, 3180 – 3211, *c)* A. S. K. Hashmi, *Gold Bull.*, 2003, **36**, 1 – 7.

even been studied for application as anti-cancer agents.[1,9] In some cases, various gold(I) and gold(III) complexes have been synthesised and their photoluminescent properties have been studied.[10]

5.1.1) Gold's Sparkling Personality

In order to appreciate the unique properties of gold with respect to its relativistic effect, a brief overview of the phenomena, which has been extensively studied, is given.[11] Electrons in atoms with high atomic numbers reach velocities approaching to the velocity of light. As such, Einstein's theories of relativity become applicable to these atoms and electrons. The term ve/vl needs to be considered, where ve represents velocity of the electron while the velocity of light is represented by the vl term.[11a] This term approaches unity for atoms with high atomic numbers such as is the case with gold. This directly results in the mass of the electron increasing dramatically while the Bohr radii decreases (the mass of an electron is inversely proportional to the Bohr radius of that electron orbiting the nucleus).[12] The 6s-orbital, and to a lesser extent the 6p-orbitals, contract while the 5d-orbitals expand.[1,12] The electrons located in the 6s-orbital have greater ionisation energy. The electrons in the 5d-orbitals are more shielded from the nucleus by the contracted orbitals, as expected, and experience a weaker nuclear attraction.[1,12] The contraction of the 6s-orbital greatly increases Au-L bond strength (L represents a ligand).[12] The relativistic effect on gold can actually be observed on a daily basis. The golden colour is a direct result of the 5d electrons that are excited to the Fermi level. The small bandgap of 2.38 eV, which indicates that gold absorbs blue visible light, is due to the relativistic contraction and expansion of the 6s-orbital and 5d-orbitals, respectively.[12] The same observation is not observed for silver.

Directly resulting from relativistic effects is the phenomenon termed aurophilicity, arising from the interactions between closed shell gold(I) centres.[11,13] This generally occurs in gold(I) complexes having low coordination numbers, as more ligands would result in steric repulsions and therefore decreases the tendency of gold(I)-gold(I) aurophilic interactions. The strength of aurophilic interactions has been compared to that of hydrogen bonding interaction, in addition to being

---

[9] N. Cutillas, G. S. Yellol, C. de Haro, C. Vicente, V. Rodríguez, J. Ruiz, *Coord. Chem. Rev.*, 2013, **257**, 2784 – 2797.

[10] *a)* K. M-C. Wong, L-L. Hung, W. H. Lam, N. Zhu, V. W-W. Yam, *J. Am. Chem. Soc.*, 2007, **129**, 4350 – 4365, *b)* V. W-W.Yam, K. K-W. Lo, *Chem. Soc. Rev.*, 1999, **28**, 323 – 334.

[11] *a)* H. Schmidbaur, *Gold Bull.*, 1990, **23**, 11 – 21, *b)* P. Pyykkö, *Chem. Rev.*, 1997, **97**, 597 – 636, *c)* P. Pyykkö, T. Tamm, *Organometallics*, 1998, **17**, 4842 – 4852, *d)* P. Pyykkö, *Angew. Chem. Int. Ed.*, 2004, **43**, 4412 – 4456.

[12] D. J. Gorin, F. D. Toste, *Nature*, 2007, **446**, 395 – 403.

[13] See relevant review articles and references therein *a)* H. Schmidbaur, A. Schier, *Chem. Soc. Rev.*, 2012, **41**, 370 – 412, *b)* H. Schmidbaur, A. Schier, *Chem. Soc. Rev.*, 2008, **37**, 1931 – 1951.

148

stronger than Van der Waals interactions.[11,13] A relatively flat energy profile, as well as the conformation of the complex upon aggregation, suggest that these gold-gold interactions exhibit attractive forces and not repulsive.[13] Various arrangements resulting from these d_{10}-d_{10} metallic interactions include dimeric structures, to polymers and even oligomeric cluster complex formation. Figure 5.1 represents but a few of the different conformations obtained due to aurophilic interactions between gold(I) complexes.[13]
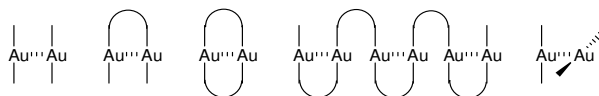
Figure 5.1: Various structure formation resulting from aurophilic interactions[13]

Gold is the metal with the highest electronegativity compared to all other transition metals.[1] In fact, the electronegativity of gold is comparable to that of carbon. Due to this similarity, the gold-carbon bond is less polar yielding a robust complex stable towards heterolytic cleavage by nucleophiles.[1] The electronegativity of gold has, to some extent, been attributed to the relativistic effect of gold. The electronegativity broadens the application of gold even further, specifically with regards to catalysis. The range of nucleophiles used during gold catalysis is widened, and the possibility of catalyst recycling increases.

5.1.2) Complexes of Gold(I)

Gold(I) has been described as a metal with decreased nucleophilic character.[12] This can be rationalised based on the following: the more diffuse 5d-orbitals, resulting from relativistic contraction and expansion, allow the electrons in the 5d-orbitals to be more dispersed and therefore experience less electron-electron repulsion. This ultimately results in the electrons being held with greater energy by the nucleus, compared to the electrons located in the 3d-orbitals of copper, making gold(I) less nucleophilic.[12] The advantage is that gold(I) is stable towards oxidative addition processes. In fact, gold(I) is stable towards oxygen due to disfavoured oxidation and has a high redox stability. The relativistic effect in gold(I) has been attributed as the reason behind gold(I) exhibiting a low-lying LUMO, which accounts for the high Lewis acidity of gold(I).[12] This also explains why gold has a high electronegativity (electronegativity generally correlates with Lewis acidity).

An intensive literature search failed to reveal any pincer complexes of gold(I), unlike the known gold(III) pincer complexes. The closest example demonstrating a ligand that has pinced around a

149

gold(I) metal centre, is the gold complex reported by Che *et al.* in 1998.[14] Reacting (tht)AuCl (tht = tetrahydrothiophene) with the dpdo ligand, followed by addition of LiClO₄, yielded the cationic, chelated gold(I) complex **a** (Scheme 5.1).[14] Crystal structure determination confirmed the formation of **a**. The dpdo ligand (dpdo = 1,8-bis(diphenylphosphino)-3,6-dioxaoctane) adopts a *trans*-chelating geometry, with the two coordinated gold(I) atom displaying an almost complete linear geometry. The P-Au-P bond angle is 172.2(1)°, while weak bonding interactions exist between the oxygens and the gold centre. The complex's photoluminescent properties were investigated.[14]
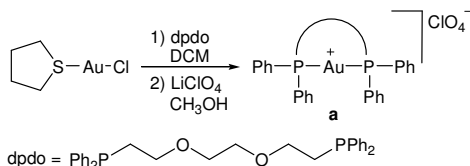
Scheme 5.1: Cationic gold(I) complex **a** with bidentate chelating supporting ligand[14]

A seminal report in 2008 regarding mononuclear gold(I) complexes, is that of Sadighi and co-workers who reported the synthesis, isolation and structural characterisation of an (NHC)Au(I)-H complex.[15] The gold-hydride complex **b** could be synthesised by reacting (NHC)Au(I)-Cl with LiBEt₃H (Scheme 5.2). Alternatively, the gold-hydride complex could also be prepared after reacting the (NHC)Au(I)-O^{t}Bu complex (obtained by reacting (NHC)Au(I)-Cl with NaO^{t}Bu) with (MeO)₃SiH (Scheme 5.2). Surprisingly, the gold(I)-hydride complex **b** was unreactive towards unactivated alkynes. It did however, react with dimethyl acetylenedicarboxylate yielding the vinylgold complex.[15] The hydride complex **b** was stable in the solid state indefinitely, but decomposed in solution after 6 hours only if it was exposed to air and moisture. A dinuclear gold complex **c** could also be synthesised, isolated and structurally characterised. The cationic dinuclear gold complex **c** was obtained by reacting **b** with (NHC)Au(I)-OTf. It was determined that aurophilic interactions were present between the two gold centres, with a hydride ligand bridging the two gold centres.[15]
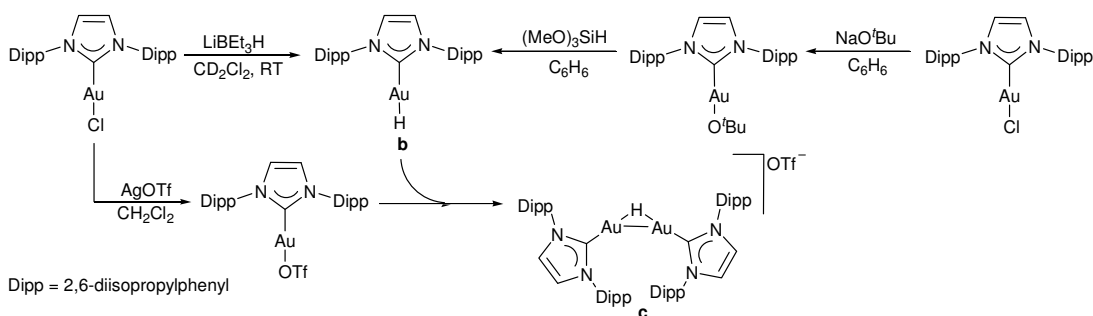
Scheme 5.2: Synthesis of a gold(I)-hydride complex **b** as well as the dinuclear gold complex **c**[15]

[14] W-H.Chan, T. C. W. Mak, C-M. Che, *J. Chem. Soc., Dalton Trans.*, 1998, 2275 – 2276.
[15] E. Y. Tsui, P. Müller, J. P. Sadighi, *Angew. Chem. Int. Ed.*, 2008, **47**, 8937 – 8940.

Gold hydroxide complexes have been reported to be intermediates in various catalytic reactions involving water and gold.[16] However, the chemistry of gold hydroxide complexes is vastly under-explored. Synthesis of gold hydroxide complexes would certainly broaden our understanding on these catalytic reaction mechanisms and ultimately lead to "green processes", in which gold catalysis is performed in non-toxic, environmentally friendly water as solvent.[16] As such, the group of Nolan *et al.* contributed to this underdeveloped area of research. They recently reported the synthesis, isolation and full characterisation of the first gold(I)-hydroxide complex.[17] The (NHC)Au-OH complex **d** was synthesised by treatment of the (NHC)Au-Cl complex, with either NaOH, KOH or CsOH (Scheme 5.3). The reaction is stated to be very robust, as it could be done in open air using technical grade solvents.[17] The proton resonance of the hydroxide ligand of **d** was only later reported to resonate as a broad singlet at -0.71 ppm.[18] However, both IR and X-ray diffraction analysis confirmed the formation of **d**.[17] It was demonstrated that the hydroxide complex **d** had a high basicity. Further investigations revealed that **d** reacted with a variety of reagents, including [(CH$_3$O)$_3$SiH] which yielded the gold(I)-hydride complex **e** (Scheme 5.3).
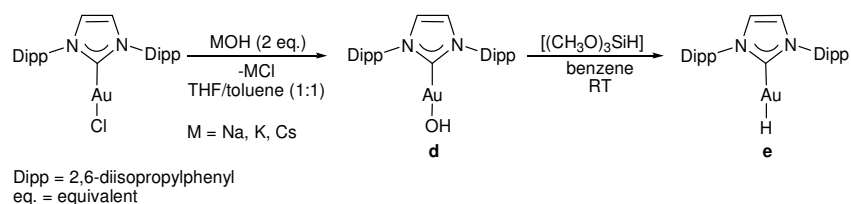
Scheme 5.3: Synthesis of (NHC)AuOH (**d**) and (NHC)AuH (**e**) complexes from (NHC)AuCl[17]

The group of Nolan further investigated various organogold species, focusing on a gold complex containing a peroxo unit. The importance and relevance of late transition metal complexes containing a peroxo unit has already been mentioned and discussed in Chapter 3. The synthesis of the first gold(I)-peroxo complex was achieved by reacting **d** (see Scheme 5.3) with ^{t}BuOOH, yielding the (NHC)Au(I)-OO^{t}Bu complex **f** (Scheme 5.4).[19] The reaction was carried out in the absence of light, employing technical grade solvents whilst the reaction could be exposed to air. Formation of **f** was unambiguously confirmed through crystal structure determination as well as NMR characterisation.[19] Complex **f** was further reacted with PPh$_3$, in order to determine the oxygen transfer ability of the (NHC)Au(I)-OO^{t}Bu complex (Scheme 5.4). One oxygen atom was transferred to the PPh$_3$ substrate, yielding the (NHC)Au(I)-O^{t}Bu complex **g** and triphenylphosphine oxide.[19]

[16] H. W. Roesky, S. Singh, K. K. M. Yusuff, J. A. Maguire, N. S. Hosmane, *Chem. Rev.*, 2006, **106**, 3813 – 3843.

[17] S. Gaillard, A. M. Z. Slawin, S. P. Nolan, *Chem. Commun.*, 2010, **46**, 2742 – 2744.

[18] A. Gómez-Suárez, R. S. Ramón, A. M. Z. Slawin, S. P. Nolan, *Dalton Trans.*, 2012, **41**, 5461 – 5463.

[19] A. Collado, A. Gómez-Suárez, Y. Oonishi, A. M. Z. Slawin, S. P. Nolan, *Chem. Commun.*, 2013, **49**, 10745 – 10747.
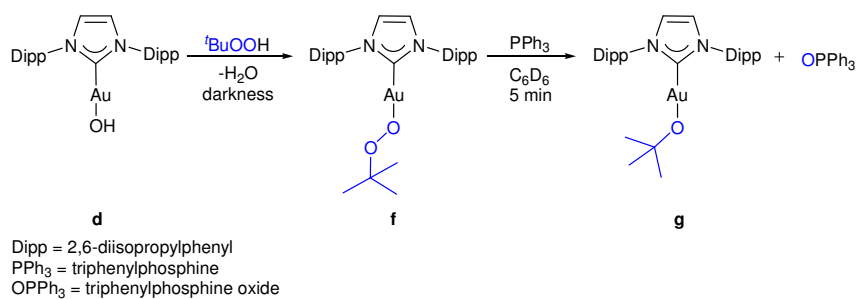
Scheme 5.4: Synthesis of (NHC)Au(I)-OO^{t}Bu (**f**) from (NHC)Au(I)-OH (**d**) and oxidation of PPh$_3$[19]

Gold(I) complexes featuring triazolylidene ligands were synthesised and characterised by the group of Albrecht.[20] Synthesis of complexes **h$_i$**, and its derivatives containing various R and R' functional groups, were attempted (**I**, Scheme 5.5). Metallation of the triazolium salts with silver oxide, followed by *in situ* transmetallation with a gold(I) precursor, yielded the (*trz*)Au-Cl complexes of the type **h$_i$** in moderate to good yields. These complexes are air and moisture stable, in both solution and in the solid state. The biscarbene cationic gold(I) complexes, **h$_{ii}$** and **h$_{iii}$**, could be synthesised by employing two independent methods (**I**, Scheme 5.5). The first involves chloride abstraction from complex **h$_i$**, using two equivalents of the gold complex to one equivalent of silver salt. This yields complex **h$_{ii}$** with a BF$_4^-$ counteranion. A direct method can also be employed, where two equivalents of the triazolium salt is first metallated with silver oxide, followed by *in situ* transmetallation with one equivalent of the gold precursor. This subsequently yields a gold salt **h$_{iii}$** with an ICl$_2^-$ counteranion.[20] As was observed during the synthesis of **h$_{ii}$**, abstraction of the chloride ligand from **h$_i$** occurs readily with the addition of AgBF$_4$ (**I**, Scheme 5.5). This yields a cationic gold(I) centre that is more electrophilic compared to the neutral starting gold complex. The vacant site formed can then be stabilised by addition of an L-type ligand, such as triphenylphosphine (PPh$_3$) or even an isonitrile derivative, yielding the cationic complexes **h$_{iv}$** and **h$_v$**, respectively (**II**, Scheme 5.5).[20] Synthesis of complex **h$_{vi}$** was accomplished using a similar method as used for the synthesis of **h$_i$** (**III**, Scheme 5.5).[20] However, the triazolium salt featured a carbamate functional group which resulted in the formation of dinuclear gold complex, bridged by two ligands. The carbamate NH is deprotonated and coordinates to gold as an X-type ligand, substituting the chloride ligand. Chelation does not occur and the geometry around the gold centre is still linear.[20]

---

[20] D. Canseco-Gonzalez, A. Petronilho, H. Mueller-Bunz, K. Ohmatsu, T. Ooi, M. Albrecht, *J. Am. Chem. Soc.*, 2013, **135**, 13193 – 13203.
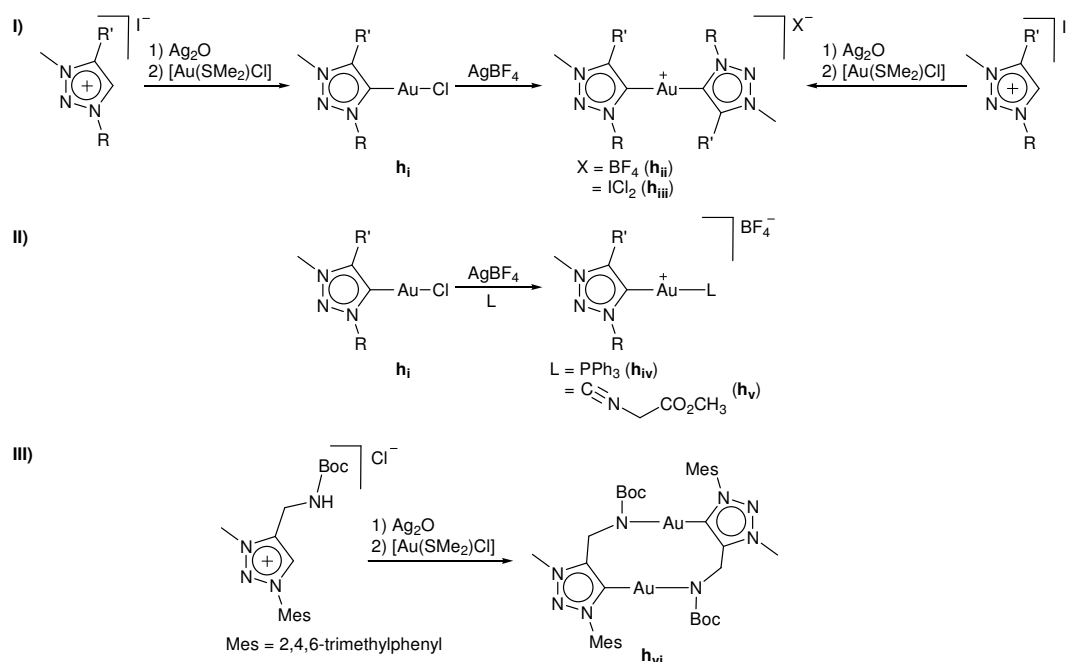
Scheme 5.5: Gold complexes featuring triazolylidene supporting ligands[20]

One of the major applications of gold(I) complexes, is in the catalysis of olefinic substrates with various nucleophiles. This, in general, involves gold intermediates with carbon based ligands obtained through coordination of the olefinic substrate.[1,8] Cationic gold(I) complexes has shown excellent properties towards the coordination of olefins, with subsequent π-activation of the olefin towards an incoming nucleophile. However, isolation of cationic gold(I)-olefin complexes is non-trivial, due to the ease of olefin dissociation from the gold centre. Isolation and structural characterisation of gold(I)-olefin complexes were recently accomplished.[21] Dias *et al.*[21a] was able to synthesise a cationic gold(I) tris(ethylene) complex, while Toste and co-workers[21b] reported various phosphine coinage metal π-complexes. However, these complexes were unstable to extremely unstable. A remarkably stable cationic gold(I)-olefin complex was synthesised by Russel and co-workers.[21c] Removal of a halide from a neutral gold(I) complex, using AgSbF$_6$ as halide scavenger, yielded the cationic gold(I) complex. Coordination of the olefin *in situ*, yielded the [(^{t}Bu)$_3$P-Au(I)-olefin][SbF$_6$] complexes, **i$_i$** and **i$_{ii}$**, after filtration and recrystallisation (Scheme 5.6). Crystal structure determination unambiguously confirmed the formation of the gold-olefin products.[21c] These complexes were determined to be stable in the presence of air, moisture and light. A high thermal stability was also reported for these complexes. The stability of the complexes was attributed to the sterically demanding P^{t}Bu$_3$ ligand with its σ-donor characteristics. The authors reported that

[21] *a)* H. V. R. Dias, M. Fianchini, T. R. Cundari, C. F. Campana, *Angew. Chem. Int. Ed.*, 2008, **47**, 556 – 559, *b)* N. D. Shapiro, F. D. Toste, *PNAS*, 2008, **105**, 2779 – 2782, *c)* T. N. Hooper, M. Green, J. E. McGrady, J. R. Patel, C. A. Russel, *Chem. Commun.*, 2009, 3877 – 3879.

coordination of the alkene occurs through donation of π-electron density into the gold 6s-orbital.[21c] This was reinforced with crystal structure analysis and density functional theory (DFT) calculations. These findings shed light with regard to the first step during gold catalysed olefin functionalisation.
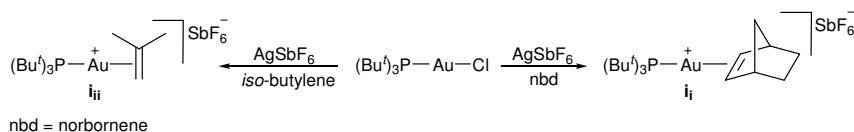
Scheme 5.6: Coordination of olefin to cationic gold(I) complex[21c]

5.1.3) Pincer Complexes of Gold(III)

Complexes of gold(III) have been less reported, compared to gold(I) complexes. This is largely due to the tendency of gold(III) to be reduced back to gold(I), yielding either the gold(I) analogue or decomposition products.[22] The reduction could be attributed to the strong oxidising gold centre with a high positive standard redox potential.[23] Appropriate supporting ligand scaffolds can circumvent the reduction and decomposition reactions of gold(III), thereby yielding a gold complex that is more stable towards both reductive elimination as well as temperature degradation.[22]

Gold(III) complexes containing either an amido or amino moiety were synthesised, in order to structurally compare these complexes with each other.[24] The [(NNN)Au(III)-Cl][BF$_4$] complex **j** was synthesised by reacting the ligand precursor with Na[AuCl$_4$], in the presence of NaBF$_4$ (Scheme 5.7). Spontaneous deprotonation of the amino moiety occurred, yielding the amido moiety which coordinated as an X-type ligand to the cationic gold(III) centre. Addition of excess triflic acid resulted in protonation of the amido moiety, yielding the amine and a dicationic gold(III) salt **k**, with elimination of HBF$_4$.[24] Complex **k** rapidly decomposed in acetone, but was more stable in methanol. In addition, the dicationic gold(III) salt displayed limited thermal stability. It was postulated that an equilibrium exists in solution, between both the amido and the amino derivatives. As intuitively expected, the amido N-Au bond length of **j** was shorter compared to the amino N-Au bond length, while the opposite trend was observed for the Au-Cl bond lengths. The reversible amido to amino and amino back to amido coordination between the two complexes, together with the properties of gold, can lead to catalytic systems that behave similarly as for the rhodium complexes reported by Milstein and co-workers, which was discussed in Chapter 4.[24]

---

[22] D-A. Roşca, D. A. Smith, M. Bochmann, *Chem. Commun.*, 2012, **48**, 7247 – 7249.

[23] A. S. K. Hashmi, *Angew. Chem. Int. Ed.*, 2012, **51**, 12935 – 12936.

[24] L. Cao, M. C. Jennings, R. J. Puddephatt, *Inorg. Chem.*, 2007, **46**, 1361 – 1368.
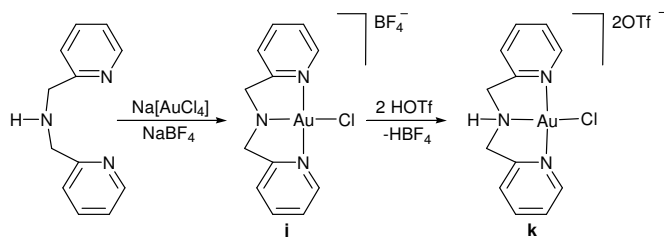
Scheme 5.7: Cationic gold(III) complexes supported by a tridentate ligand with an amido or an amino moiety[24]

A yellow gold(III)-hydroxide complex could be synthesised from the cyclometallated Au(III)-Cl starting reagent (**I**, Scheme 5.8).[22] Reacting the precursor gold complex **l** with CsOH in a mixture of toluene/THF/water (1:1:1) lead to the isolation of complex **m**, of which the structure was unequivocally proven with X-ray diffraction analysis (**I**, Scheme 5.8). Even though a few gold(III)-hydroxide complexes had been synthesised before, their reactivity towards various substrates were not reported. Complex **m** was reacted with various substrates, including terminal acetylenes and protic heterocycles, yielding the corresponding gold(III) derivatives in excellent yields.[22] These reactivity studies indicated that, the Au(III)-OH complex **m** is a milder base compared to the Au(I)-OH complex **d** reported by Nolan (see Scheme 5.3). The emission properties of the gold(III) complexes were also investigated, with most complexes displaying emission properties in the blue and yellow regions.[22]

A cyclometallated gold(III)-hydride complex was later synthesised by Bochmann and co-workers, and structural characterisation unambiguously confirmed the formation of complex **n** (**I**, Scheme 5.8).[25] The gold hydride complex was synthesised by reacting **m** with LiBEt$_3$H in toluene at -78 °C (**I**, Scheme 5.8). In solution, the gold hydride complex **n** was determined to be thermally stable under inert conditions, but decomposed upon exposure to air, moisture or light. Complex **n** however, was stable towards air and moisture in the solid state. It was determined that **n** was surprisingly unreactive towards alkene or alkyne substrates, as well as weak acids.[25] Treatment of **n** with trifluoroacetic acid resulted in an instantaneous reaction, yielding the cyclometallated gold(III)-OAc complex (OAc^F = trifluoroacetate). This could point to the hydridic character of **n** being less pronounced, when compared to the hydridic character of the gold(I)-hydride complex **b** (see Scheme 5.2). The reaction of **n** towards allene substrates were also investigated and, upon treatment of **n** with dimethylallene, a gold(III)-vinyl complex **o** was obtained (**II**, Scheme 5.8). Reductive condensation between the gold(III)-hydride **n** and gold(III)-hydroxide **m** yielded the dinuclear gold(II) complex **p** (**II**, Scheme 5.8).[25] The reaction could be carried out in either benzene or dichloromethane. Complex **p** exhibited photoluminescent properties, increasing the possibility of the complex towards various applications.

---

[25] D-A. Roşca, D. A. Smith, D. L. Hughes, M. Bochmann, *Angew. Chem. Int. Ed.*, 2012, **51**, 10643 – 10646.

The stability of the synthesised gold complexes was attributed to the rigid pincer ligand scaffold, which does not allow for a reductive elimination reaction to occur.[25]
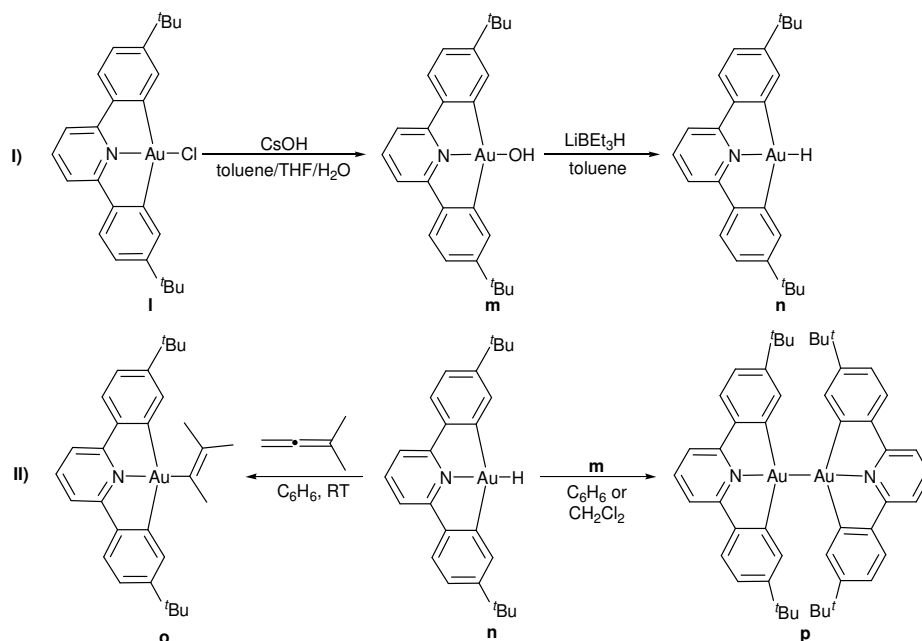
Scheme 5.8: Synthesis of gold(III)-hydroxide complex **m** and its reactivity towards various substrates[22,25]

Bochmann further investigated the reactivity of the cyclometallated gold(III) complex.[26] The gold trifluoroacetate complex **q**, readily synthesised by reacting **n** with trifluoroacetic acid, was treated with various olefins (Scheme 5.9). Adducts of gold olefin complexes where obtained, if the reaction was carried out in the presence of $B(C_6F_5)_3$. As illustrated in Scheme 5.9, the trifluoroacetato ligand is displaced by the ethylene ligand, which π-coordinates to the gold centre, yielding the cationic gold(III) complex **r**. It can be postulated that ligand dissociation occurs by coordination of $B(C_6F_5)_3$ to the oxygen atom of the acetate ligand, decreasing the Au-OAc^F bond strength. The reaction with olefin was determined to occur with quantitative conversion of **q** to the gold salt **r**.[26] The coordinated olefin could be substituted by addition of $S(CH_3)_2$, indicating that only weak olefin coordination occurs. If complex **q** was reacted with ethylene and without addition of $B(C_6F_5)_3$, an insertion reaction occurred where the ethylene inserted into the Au-OAc^F bond, yielding the gold(III)-alkyl-acetato complex **s**.[26]

---

[26] N. Savjani, D-A. Roşca, M. Schormann, M. Bochmann, *Angew. Chem. Int. Ed.*, 2013, **52**, 874 – 877.
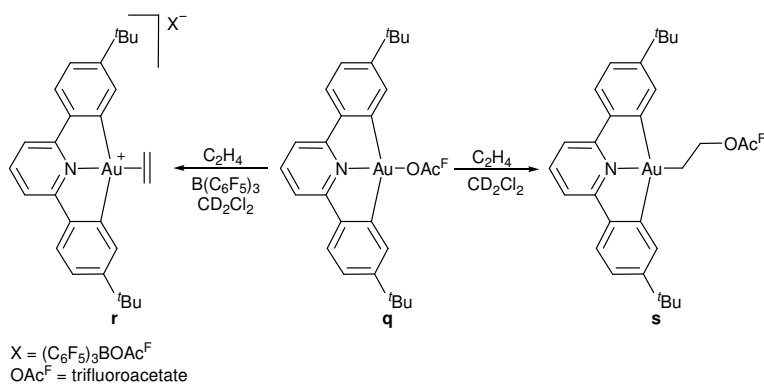
Scheme 5.9: Reactions of Au(III)-OAc^F with ethylene[26]

The gold(III) complexes (**I**, Scheme 5.10) where synthesised in order to study their luminescent properties.[27] The complexes **t$_i$** and **t$_{ii}$**, as well as their analogues not indicated, displayed strong absorption bands between 250 – 350 nm and between 375 – 440 nm. Further investigations revealed that complexes of the type shown in **I**, Scheme 5.10, have quantum yields of up to 58% and excited lifetimes of 200 microseconds and more, in solution at room temperature. The applicability of complexes displaying these long excited lifetimes and high quantum yield was mentioned and one example is displayed. The oxidation of the amine to the imine, in the presence of oxygen, was investigated.[27] Under aerobic conditions whilst irradiating with laser light at 756 nm, complex **t$_i$** furnished three turnovers of the amine to the imine (**II**, Scheme 5.10). No reaction was observed in the absence of **t$_i$**. It was concluded that solar energy could be harnessed for photochemical reaction employing gold(III) complexes of type **t$_i$**, exhibiting distinct and unique properties.[27]
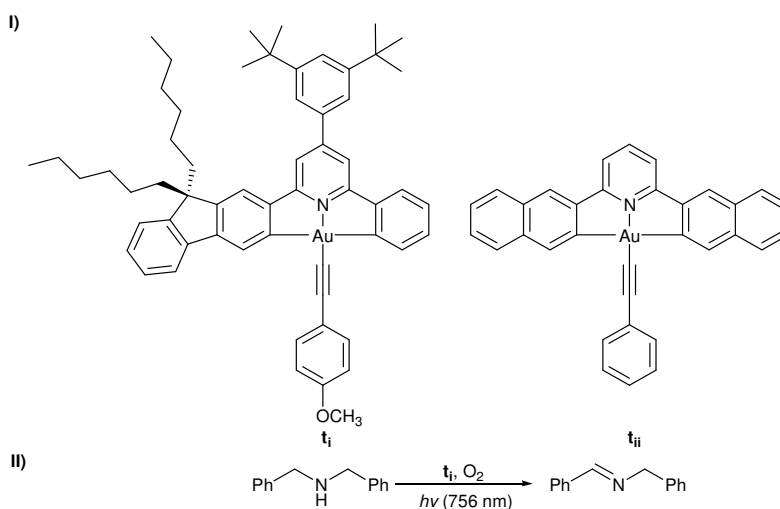
Scheme 5.10: Gold(III) complexes displaying photochemical/photocatalytic properties[27]

---

[27] W-P. To, K. T. Chan, G. S. M. Tong, C. Ma, W-M. Kwok, X. Guan, K-H.Low, C-M. Che, *Angew. Chem. Int. Ed.*, 2013, **52**, 6648 – 6652.

157

Cationic gold(III) complexes coordinated by olefins was postulated as reactive intermediates in various gold(III) catalytic reactions, but synthesis and isolation thereof remained elusive until very recently. The first fully characterised cationic gold(III) complex with an olefin coordinated to the gold centre was reported in 2013.[28] The cyclometallated neutral gold(III) complex was reacted with 2.2 equivalents of triflic acid, in deuterated dichloromethane at -78 °C, followed by heating up the reaction mixture to -40 °C (Scheme 5.11). A gold(III) complex u_i was obtained, which was further reacted with 1,5-cyclooctadiene yielding the olefin coordinated gold(III) cation u_{ii}, featuring a triflate counteranion (Scheme 5.11). The gold complex u_{ii} could also be synthesised directly from the cyclometallated gold(III) complex, by reacting the gold precursor with $[\{3,5\text{-}(CF_3)_2\text{-}C_6H_3\}_4B^-][(Et_2O)_2H^+]$ in deuterated dichloromethane, followed by addition of 1,5-cyclooctadiene (Scheme 5.11).[28] This method allowed for the isolation of u_{ii} exhibiting a $[\{3,5\text{-}(CF_3)_2\text{-}C_6H_3\}_4B]^-$ counteranion. NMR characterisation confirmed the formation of u_{ii}, with either OTf^- or $[\{3,5\text{-}(CF_3)_2\text{-}C_6H_3\}_4B]^-$ counteranion, while crystal structure determination of u_{ii}, with $[\{3,5\text{-}(CF_3)_2\text{-}C_6H_3\}_4B]^-$ counteranion unambiguously proved the formation of the cationic gold(III) complex.[28] Calculations revealed that weak but significant backbonding from the gold to the olefin π^*-orbital, stabilises the coordination of the olefin to the metal. This study confirms the formation of olefin coordinated, gold(III) cations, which validates their existence in gold(III) catalysed reactions.[28]

cod = 1,5-cyclooctadiene
X = OTf or $\{3,5\text{-}(CF_3)_2\text{-}C_6H_3\}_4B$
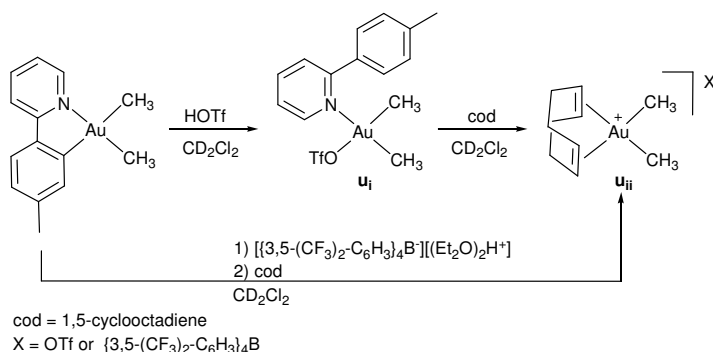
Scheme 5.11: Isolation of first cationic gold(III) complex coordinated by a olefin[28]

5.1.4) Catalysis going for Gold

Both gold(I) and gold(III) complexes have been reported to be active in various organic transformation reactions.[8,29] However, catalysts featuring a gold(I) centre have received considerably more attention than have complexes of gold(III). In particular, cationic gold(I) complexes are studied

[28] E. Langseth, M. L. Scheuermann, D. Balcells, W. Kaminsky, K. I. Goldberg, O. Eisenstein, R. H. Heyn, M. Tilset, *Angew. Chem. Int. Ed.*, 2013, **52**, 1660 – 1663.
[29] *a)* A. S. K. Hashmi, G. J. Hutchings, *Angew. Chem. Int. Ed.*, 2006, **45**, 7896 – 7936, *b)* Z. Li, C. Brouwer, C. He, *Chem. Rev.*, 2008, **108**, 3239 – 3265, *c)* D. J. Gorin, B. D. Sherry, F. D. Toste, *Chem. Rev.*, 2008, **108**, 3351 – 3378.

158

due to the fact that they have displayed good to excellent behaviour towards various catalytic reactions, with preference to activation followed by nucleophilic attack of unsaturated carbon substrates.[1] The cationic carbophilic gold centre selectively coordinates to the alkene/alkyne moiety. This is followed by metal slippage resulting in formation of a cationic centre that is vulnerable towards nucleophilic attack. Nucleophilic addition followed by protodeauration yields the organic product and the cationic gold(I) complex, ready to catalyse another transformation cycle.[1] The general catalytic cycle through which a cationic gold(I) complex catalyses the nucleophilic addition of a nucleophile across an alkyne substrate is indicated in Figure 5.2.[1]
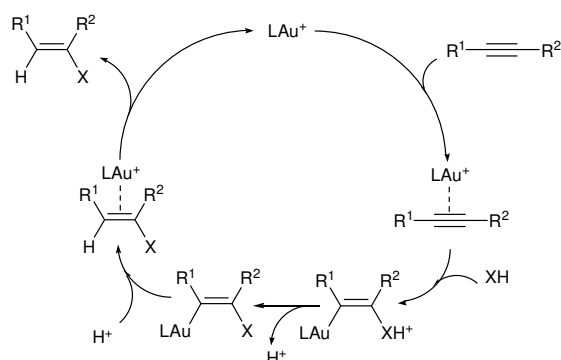
Figure 5.2: Catalytic mechanism through which cationic gold(I) complexes generally catalyses the transformation of organic substrates[1]

The gold hydroxide complex (**d**, Scheme 5.3), as reported by Nolan and co-workers, did show marked activity in various catalytic reactions, after the (NHC)Au(I)-OH complex had been manipulated.[30] A dinuclear gold complex with the hydroxide ligand bridging the two gold centres was synthesised by treatment of the (NHC)AuOH complex **d** (**I**, Scheme 5.12) with HBF$_4$·OEt$_2$ in benzene.[30a] The dinuclear gold(I) complex **v** could alternatively be synthesised from the (NHC)AuCl complex, simply by reacting it with AgBF$_4$ in acetonitrile followed by addition of water (**I**, Scheme 5.12).[30b] The gold complex **v** showed good to excellent catalytic activity towards various organic transformation reactions, including alkyne hydration (**II**, Scheme 5.12), nitrile hydration and the Meyer-Schuster rearrangement reactions. In addition, the catalytic activity of the [{Au(NHC)}$_2$(μ-OH)]BF$_4$ complex **v** towards the hydrophenoxylation catalysis of alkynes with phenols was also investigated.[31] This was the second report regarding the hydrophenoxylation of alkynes with phenols, employing a gold catalyst. In addition, research towards phenol addition across an alkyne has been relatively slow.[31] The catalytic complex **v** showed excellent reactivity, as observed when 97% conversion occurred for the reaction depicted in **III**, Scheme 5.12, after only one hour at 80 °C in toluene as solvent.

[30] *a)* R. S. Ramón, S. Gaillard, A. Poater, L. Cavallo, A. M. Z. Slawin, S. P. Nolan, *Chem. Eur. J.*, 2011, **17**, 1238 – 1246, *b)* A. Gómez-Suárez, Y. Oonishi, S. Meiries, S. P. Nolan, *Organometallics*, 2013, **32**, 1106 – 1111.
[31] Y. Oonishi, A. Gómez-Suárez, A. R. Martin, S. P. Nolan, *Angew. Chem. Int. Ed.*, 2013, **52**, 9767 – 9771.

Surprisingly, the catalyst was still active upon iterative additions of the substrate, reaching a turn over number of 3400.[31] The reaction mechanism was investigated, and it was postulated that a dual activation process occurs.[31] The dinuclear complex **v**, once in solution, is in equilibrium with the (NHC)Au(I)-OH and [(NHC)Au(I)]BF$_4$ complexes. The cationic gold complex [(NHC)Au(I)]BF$_4$, as is reminiscent of gold(I) complexes featuring a vacant site, activates the alkyne through π-coordination yielding the π-gold-alkyne complex. The gold(I)-hydroxide reacts with the phenol substrate, yielding the gold-phenoxide complex. The gold-phenoxide complex subsequently attacks the opposite side of the π-gold-alkyne complex forming the *gem*-diaurated intermediate that, after protodeauration, affords the vinyl ether as well as the gold(I)-hydroxide and gold(I) cationic complexes which again, is in equilibrium with the dinuclear gold complex **v**.
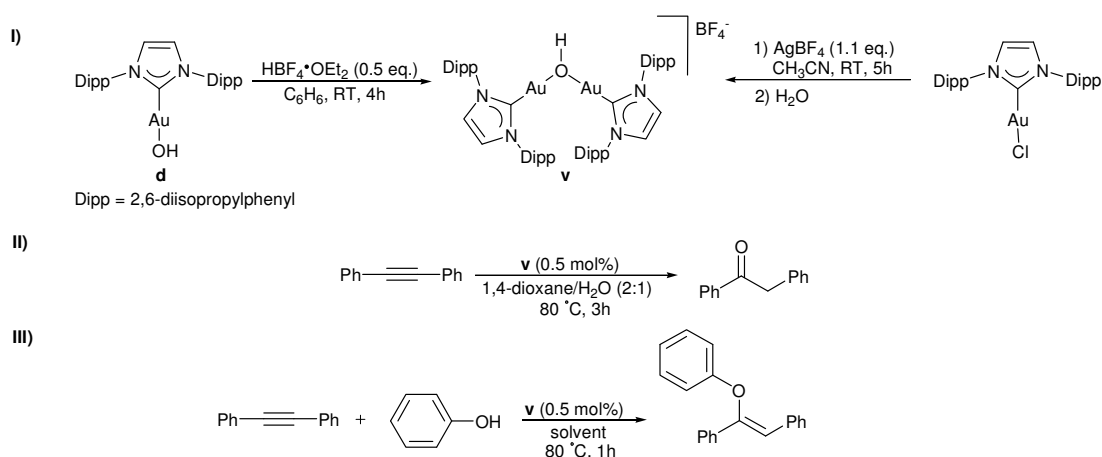
Scheme 5.12: Synthesis of **I)** [{Au(NHC)}$_2$(μ-OH)]BF$_4$ **v**, as well as its catalytic reactivity towards **II)** alkyne hydration and **III)** hydrophenoxylation reactions[30,31]

Whilst hydroamination of unactivated alkenes or alkynes with ammonia, as discussed in Chapter 4, seemed elusive when using rhodium or iridium transition metal catalyst, Bertrand and co-workers remarkably reported the hydroamination catalysis employing a cationic gold(I) complex. A series of CAAC gold(I) complexes were synthesised by stirring [(CH$_3$)$_2$S]AuCl in a THF solution of the free carbene precursor, overnight, in the absence of light and at room temperature (**I**, Scheme 5.13).[32] Full characterisation, including crystal structure determination, confirmed the formation of the (CAAC)AuCl complexes. Chloride abstraction and coordination of toluene yielded the cationic gold(I) complex **w$_i$**, the catalyst which is active towards the hydroamination of unactivated alkynes with ammonia (**II**, Scheme 5.13).[33] The reaction, as depicted by **II** in Scheme 5.13, was catalysed with 5

[32] G. D. Frey, R. D. Dewhurst, S. Kousar, B. Donnadieu, G. Bertrand, *J. Organomet. Chem.*, 2008, **693**, 1674 – 1682.
[33] V. Lavallo, G. D. Frey, B. Donnadieu, M. Soleilhavoup, G. Bertrand, *Angew. Chem. Int. Ed.*, 2008, **47**, 5224 – 5228.

160

mol% of **w_i** at 160 °C. After 3.5 hours, 95% of the alkyne had been converted to the primary imine. The cationic gold(I) complex **w_i** did not have to be isolated in order to be used as active catalyst.[33] The active cationic gold(I) complex could be generated *in situ*, upon addition of $KB(C_6F_5)_4$ to a solution of the neutral complex **w_ii**. The neutral (CAAC)AuCl complex did not catalyse the reaction if $KB(C_6F_5)_4$ was not added, showing the importance of generating the vacant site on the gold complex mediated by $KB(C_6F_5)_4$. It was further reported that the resting state of the catalyst, is the gold(I) ammonia adduct **w_iii** (**II**, Scheme 5.13).[33] The adduct **w_iii** was additionally characterised by crystal structure determination. All three complexes, **w_i-iii**, were active towards the catalytic hydroamination reaction. It was proposed that catalysis occurs *via* an insertion mechanism.
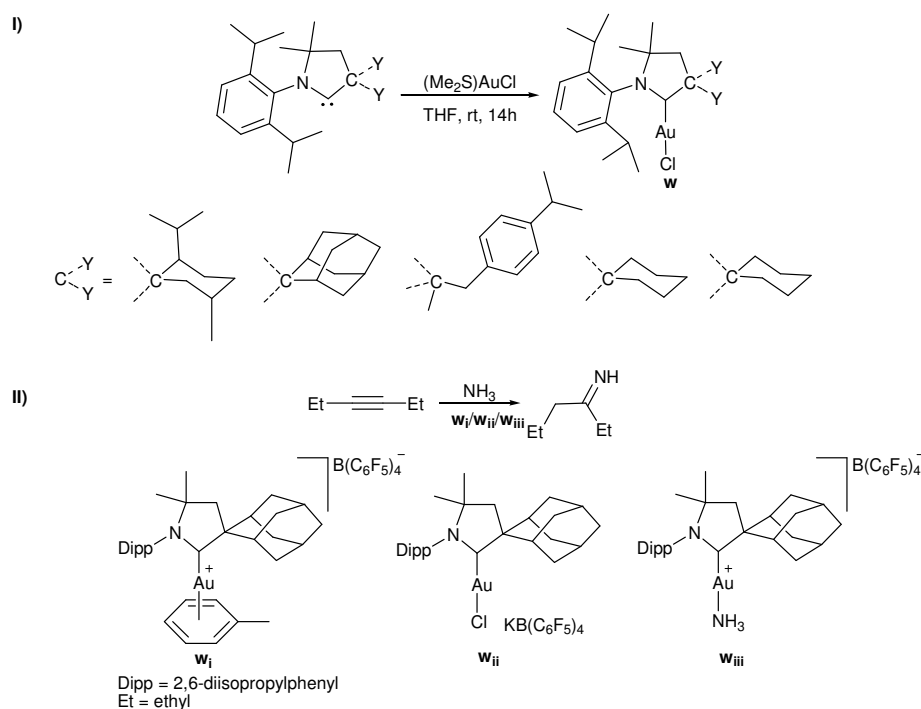
Scheme 5.13: **I)** Synthesis of (CAAC)AuCl complexes and **II)** hydroamination catalysis of unactivated alkynes with ammonia[32,33]

The catalytic activity of the (CAAC)Au(I) complex was further investigated, this time towards the hydroamination of unactivated alkynes and allenes with parent hydrazine. Treatment of the neutral gold(I) complex **w_ii**, in the presence of $KB(C_6F_5)_4$, with excess hydrazine yielded the cationic gold(I)-hydrazine adduct **w_iv** (Scheme 5.14).[34] The gold(I)-hydrazine adduct **w_iv** was characterised by crystal structure determination. Clean addition of hydrazine to the alkyne substrate was observed after 0.5 hours at 100 °C, in the presence of 5 mol% **w_iv** and deuterated benzene as solvent. The neutral complex **w_ii**, with $KB(C_6F_5)_4$ as additive, also catalysed the reaction and afforded the primary imine.[34]

---

[34] R. Kinjo, B. Donnadieu, G. Bertrand, *Angew. Chem. Int. Ed.*, 2011, **50**, 5560 – 5563.

161

The catalyst **w_{ii}** converted 95% of the alkyne after 6 hours at 150 °C, with as little as 1 mol% of catalyst loading.[34] Again, as observed for the hydroamination of alkynes with ammonia, in the absence of catalyst and in the presence of either AuCl, AuCl/KB(C_6F_5)_4, KB(C_6F_5)_4, or even **w_{ii}** without the addition of KB(C_6F_5)_4, no reaction was observed. Therefore, catalysis can only occur if a vacant site on the metal is present and if the CAAC ligand is coordinated.[34] The group of Bertrand again reported the same hydroamination catalysis, employing the gold(I) complex **w_v** which is supported by an anti-Bredt NHC ligand.[35] The complex **w_v** catalysed the same reaction as did complexes **w_{ii}** and **w_{iv}**. However, 91% of the alkyne was converted to the primary imine at room temperature and after just three hours, with a catalyst loading of 5 mol% in deuterated benzene. The increased catalytic activity of **w_v** versus **w_{ii}** or **w_{iv}**, was credited to steric factors since the electronic properties of anti-Bredt NHC ligands are similar to those of CAAC ligands.[35]
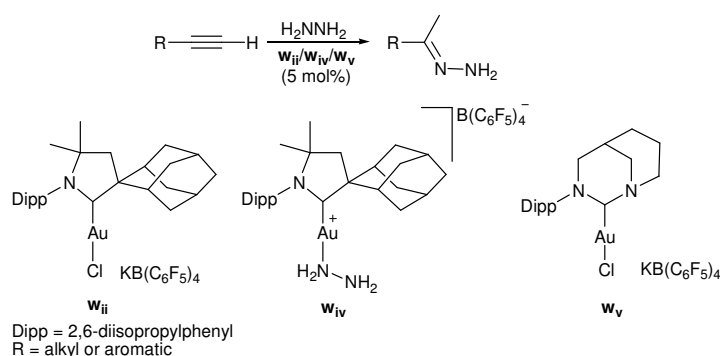
Scheme 5.14: Hydroamination of unactivated alkynes and allenes with gold(I) complexes[34,35]

Catalysis involving gold(III) complexes have been less reported, due to their tendency for reduction leading to the formation of gold(I) or decomposition products. In addition, gold(I) is less oxophilic compared to gold(III) complexes. However, as discussed below, employing certain ligand systems, such as those containing a carbene ligand, greatly increases the stability of the gold(III) complexes. This allowed, in certain cases, for the catalytic reaction to be carried out in the presence of air without decomposition or reduction of the gold(III) catalyst.

A cationic gold(III)-chloro complex was synthesised, with subsequent chloride abstraction employing AgOTf, which yielded the cationic gold complex **x_i** (I, Scheme 5.15).[36] Crystal structure determination revealed coordination of a water molecule. This was the second report in literature regarding gold(III) aqua complexes. The H_2O ligand could easily be replaced through introduction of a L-type ligand, yielding the corresponding cationic gold(III) complexes, **x_{ii}** (I, Scheme 5.15).[36] Various ligands

[35] M. J. López-Gómez, D. Martin, G. Bertrand, *Chem. Commun.*, 2013, **49**, 4483 – 4485.
[36] T. N. Zehnder, O. Blacque, K. Venkatesan, *Dalton Trans.*, 2014, **43**, 11959 – 11972.

162

were used, and a range of compounds were obtained and studied. In the solid state, the complexes were all stable towards air and moisture.[36] The photocatalytic activity of the synthesised complexes were investigated towards the oxidation of benzylic amines to the corresponding benzylic imines (**II**, Scheme 5.15). Photo-oxidation of the amine to the imine occurred whilst irradiating with a 125 W (watt) mercury lamp, in the presence of molecular oxygen, and using acetonitrile as solvent (**II**, Scheme 5.15). Even at low catalyst loading (0.50 mol%), all the complexes displayed poor to excellent activity, some catalysing full conversion after four hours. It is postulated that singlet oxygen is formed through interaction of molecular oxygen with triplet gold(III). The singlet oxygen can subsequently oxidise the amine.[36]
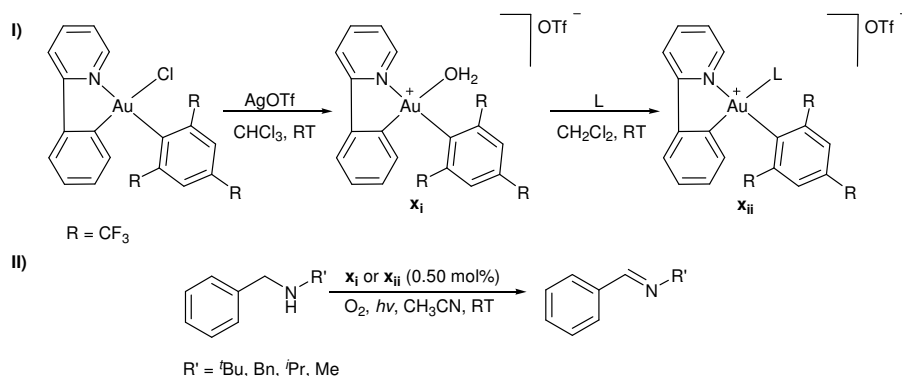
Scheme 5.15: Synthesis of **I)** cationic gold(III) complexes and the **II)** photocatalytic catalysis of an amine to the corresponding imine[36]

Not only does gold(I) complexes with carbene supporting ligands display catalytic activity, but also gold(III) complexes coordinated by carbenes. A water soluble (NHC)gold(III) complex y_i was synthesised by sequential treatment of the ligand salt with Ag_2O, [AuCl(SMe)$_2$] and finally PhICl$_2$ (**I**, Scheme 5.16).[37] Complex y_i, as expected, dissolves in water but establishes an equilibrium between y_i and the zwitterionic gold(III) complex y_{ii}. This occurs through release of HCl, with subsequent coordination of the pyridine moiety to the cationic gold(III) centre. An HCl zwitterionic salt is formed *in situ*, but this proved to be advantageous towards catalysis. The catalysis of a broad range of carboxylic acid substrates with alkyne functionalities was investigated (**II**, Scheme 5.16). Good to excellent catalytic conversion of the substrate to the corresponding lactone, catalysed by the gold(III) catalysts y_i at 2.5 mol%, was reported.[37] The catalytic reactions were carried out in a mixture of toluene and water (1:1), in air and at room temperature or at 80 °C. The catalyst could be recovered and reused for ten consecutive catalytic cycles. The formation of the cationic complex y_{ii} in solution opens up a vacant site on the gold centre, which is stabilised by the weakly coordinating

---

[37] E. Tomás-Mendivil, P. Y. Toullec, J. Díez, S. Conejero, V. Michelet, V. Cadierno, *Org. Lett.*, 2012, **14**, 2520 – 2523.

163

pyridine functionality.[37] The alkyne substrate can coordinate to the gold centre after the pyridine moiety had dissociated, which occurs readily.[37] The alkyne moiety can then be activated towards nucleophilic attack. The marked stability of the gold complex can be attributed to the carbene ligand, imparting increased stability to the complex compared to phosphine ligands.[37]
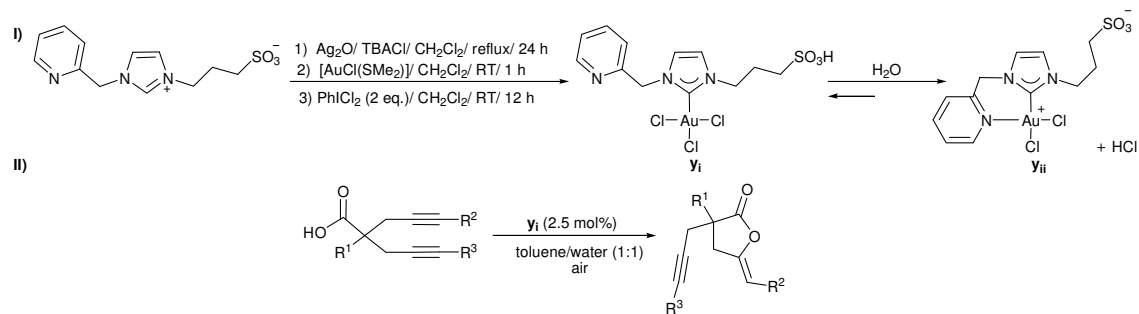
Scheme 5.16: Water soluble gold(III) complex active in the catalytic conversion of alkynes with carboxylic acids[37]

A cationic gold(III) complex with a supporting carbene ligand, displayed good catalytic reactivity towards a variety of organic transformation reactions.[38] A dichloromethane solution of an (NHC)Au(I)-Cl complex was treated with AgPF$_6$ in the presence of pyridine, yielding the cationic gold(I) complex (**I**, Scheme 5.17). This gold(I) complex was subsequently oxidised to the cationic gold(III) complex **z**, using iodobenzene dichloride as oxidant (**I**, Scheme 5.17). The various cationic gold(III) complexes, **z$_i$**-**z$_{iv}$**, were all stable upon exposure to air and light, either in solution or in the solid state (**I**, Scheme 5.17). The stability imparted by carbene ligands was again observed, upon attempted isolation of the phosphine analogues which lead to decomposition products. The catalytic activity of the complexes **z$_i$** and **z$_{iv}$** were tested towards five different organic transformation reactions.[38] Three of the five catalytic reactions are indicated in **II**, Scheme 5.17. The catalytic reactions were all initiated by the addition of AgSbF$_6$. Naphthalene was halogenated with *N*-bromosuccinimide (NBS) in the presence of one mol% catalyst (either **z$_i$** or **z$_{iv}$**), at 80 °C and after 20 hours, 58% conversion was achieved (**II**, Scheme 5.17). The *N*-(prop-2-yn-1-yl)benzamide was converted to the major product which was the 5-methyl-2-phenyloxazole, with unwanted formation of 5-methylene-2-phenyl-4,5-dihydrooxazole in minor amounts. The reaction was carried out with 5 mol% catalyst, in refluxing CH$_2$Cl$_2$. After 90 minutes, 75% of the substrate was converted to product (**II**, Scheme 5.17). The catalyst, either **z$_i$** or **z$_{iv}$**, also converted 2-methylundec-1-en-3-yn-5-yl acetate to 3-hexyl-5-methylcyclopent-2-enone (**II**, Scheme 5.17). Employing 1 mol% of **z$_i$** or **z$_{iv}$**, quantitative conversion could be observed after one hour in refluxing CH$_2$Cl$_2$.[38] The cationic gold(I) complex was

[38] S. Orbisaglia, B. Jacques, P. Braunstein, D. Hueber, P. Pale, A. Blanc, P. de Frémont, *Organometallics*, 2013, **32**, 4153 – 4164.

164

also tested towards the conversion reactions, but no AgSbF$_6$ needed to be added in order to activate the catalyst.[38] In addition, the authors reported that in some cases, the gold(I) catalyst decomposed during the catalytic reactions. The catalytic reactivity of the gold(III) complexes were slightly better compared to the gold(I) complexes. Also, only dry solvents could be used during the catalytic reactions catalysed by the gold(I) complex, while this was not the case for the gold(III) complexes.[38]

R = 2,6-diisopropylphenyl (z_i)
= 2,4,6-trimethylphenyl (z_{ii})
= cyclohexyl (z_{iii})
= *tert*-butyl (z_{iv})

NBS = *N*-bromosuccinimide
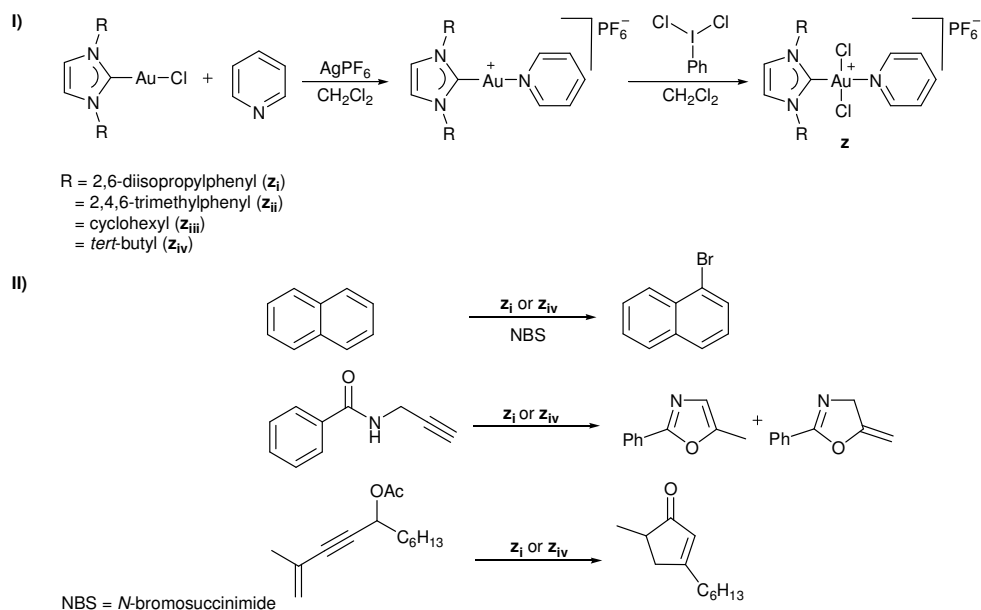
Scheme 5.17: Synthesis of **I)** cationic gold(III) complexes and **II)** organic transformations mediated by the gold(III) complexes[38]

5.2) Aim

Synthesis of various gold(I) and gold(III) complexes as possible future catalysts, employing the ligand scaffold **7** or **10**, will be attempted (Figure 5.3). Successful syntheses of the complexes will be confirmed by various spectroscopy techniques, as well as *via* X-ray diffraction analysis, if suitable single crystals are obtained. The properties of the synthesised complexes, such as its stability towards ambient conditions as well as light sensitivity, will be determined.

Ar = 2,6-diisopropylphenyl   M = Au(I), Au(III)
= 2,4,6-trimethylphenyl
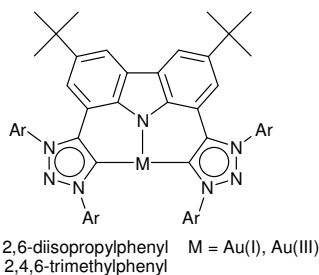
Figure 5.3: Proposed gold complexes

165

5.2.1) Synthetic Strategy

A well known, relatively simple procedure used in order to obtain the desired metal complex supported by the ligand of choice, involves metallation of the ligand with silver followed by transmetallation from the silver intermediate to the target complex. This method has already proven successful in the synthesis of various triazolylidene supported metal complexes.[39,40] The method involves metallation of the ligand precursor with excess silver oxide, in the presence of excess potassium bromide. The silver complex can either be isolated and purified followed by transmetallation,[40] or the formed silver complex can immediately be subjected to transmetallation without isolation and purification.[20,39] Isolation of the silver complex followed by transmetallation is a 'cleaner' method, with purification of the desired metal complex after transmetallation being trivial. As such, synthesis, purification and isolation of a silver complex will be attempted (Scheme 5.18). The method that will be employed will be similar to the method used by Crudden and co-workers.[40] This will involve treatment of the ligand precursor, **7** or **10**, with excess silver oxide and potassium bromide. After isolation and purification of the proposed silver species, a transmetallation reaction with (tht)AuCl will be launched in order to synthesise the desired gold(I) complex (Scheme 5.18).
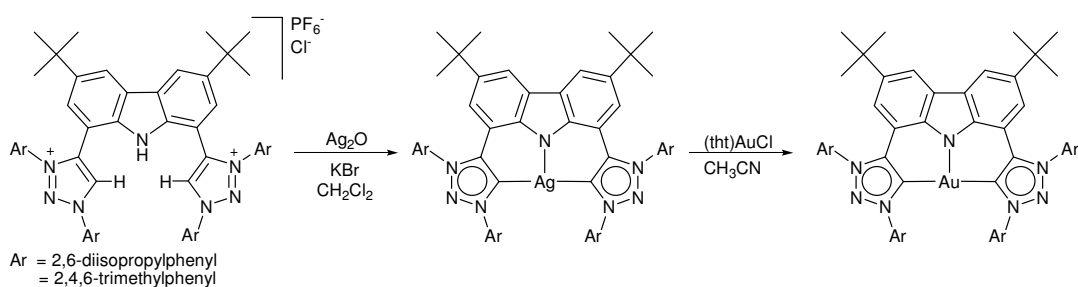
Scheme 5.18: Proposed synthesis of gold(I) complexes through transmetallation from silver

Gold(I), supported by either ligands **7** or **10**, can alternatively be synthesised through deprotonation of the ligand followed by *in situ* metallation of the free carbene adduct (**9** or **11**) with (tht)AuCl (Scheme 5.19). The tht ligand can easily be displaced by a stronger donor carbene ligand. In addition, the chloro ligand can readily be substituted by the amido X-type ligand, as has already been observed during the synthesis of other metal complexes discussed in Chapters 3 and 4.

[39] K. J. Kilpin, U. S. D. Paul, A-L. Lee, J. D. Crowley, *Chem. Commun.*, 2011, **47**, 328 − 330.
[40] E. C. Keske, O. V. Zenkina, R. Wang, C. M. Crudden, *Organometallics*, 2012, **31**, 456 − 461.
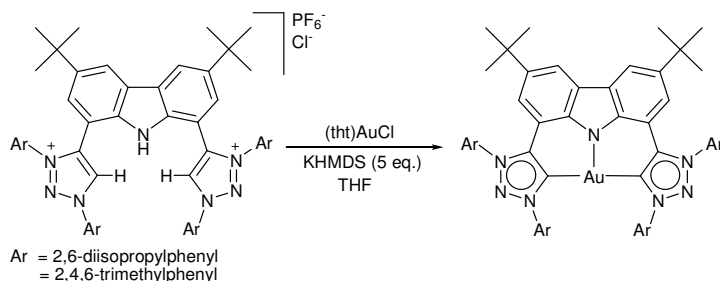
Scheme 5.19: Alternative synthesis of gold(I) complexes through *in situ* deprotonation followed by metallation

A cationic gold(III) complex can be synthesised from the corresponding gold(I) precursor complex, through oxidation using two equivalents silver hexafluorophosphate ($AgPF_6$) in the presence of dichloromethane. Silver(I) salts are generally employed as one-electron oxidants or as halide scavengers, as was mentioned and discussed throughout Section 5.1. The oxidising strength of silver salts is strongly dependant on the solvent used during the oxidation reaction.[41] In coordinating solvents such as acetonitrile, acetone or THF, the oxidising strength of silver salts is considerably decreased. However, in non-coordinating solvents such as dichloromethane, oxidation potential increases to such an extent that the silver salts behave as strong oxidants. This is the reason for attempting the reaction in CH_2Cl_2 as solvent (Scheme 5.20). Not only does the non-coordinating solvent result in increased oxidising strength of the silver salt, but coordination of the solvent to the gold vacant sites (after gold(I) to gold(III) oxidation had occurred), is expected to be negligible. The disadvantage of using silver(I) salts such as $AgPF_6$, is that they are very hygroscopic and light sensitive.[41]
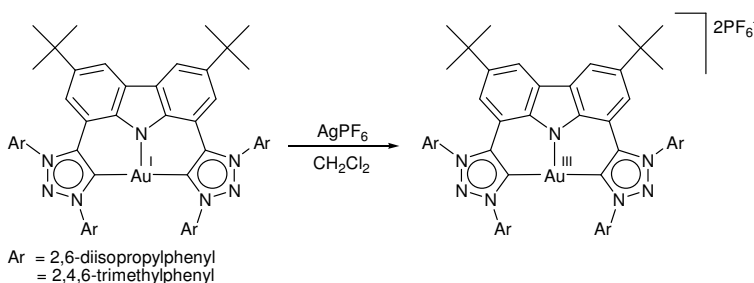
Scheme 5.20: Oxidation of gold(I) complexes to yield the gold(III) complexes

5.3) Results and Discussion

See Section 5.5 for synthetic procedures employed as well as the full characterisation of the synthesised compounds.

---

[41] N. G. Connelly, W. E. Geiger, *Chem. Rev.*, 1996, **96**, 877 – 910.

167

5.3.1) Synthesis of 22

The method employed during the synthesis of the (CNC)Ag(I) complex was similar to the method employed by Crudden and co-workers.[40] The dicationic ligand salt **7** was reacted with excess Ag_2O, in the presence of KBr using DCM as solvent (Scheme 5.21). After stirring the reaction mixture for five days at room temperature, in the absence of light, a dark orange residue was obtained after extraction from the crude mixture with Et_2O and *in vacuo* evaporation of the solvent. NMR, MS and X-ray diffraction analysis confirmed the formation of the silver(I) complex **22**. The neutral silver complex was determined to be thermally stable, as well as resistant towards decomposition in the presence of air. Complex **22** represents the first example of a silver(I) complex supported by a pincer triazolylidene ligand scaffold, where coordination of all three donor sites of the ligand to the metal occurs.
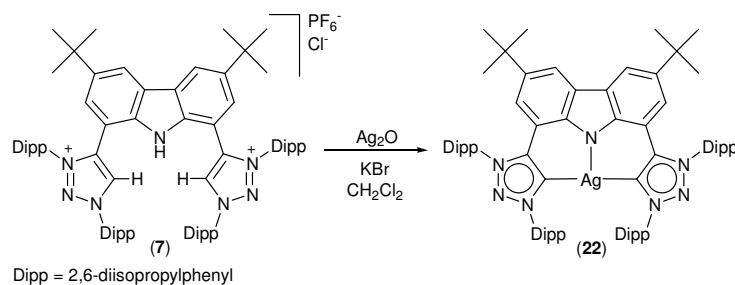
Scheme 5.21: Synthesis of silver complex **22**

Metallation of the ligand salt was confirmed through NMR spectroscopic analysis. There are no downfield resonating *trz***H** and N**H** protons, as determined from the proton NMR spectrum (Figure 5.4). The downfield resonance at 8.17 ppm corresponds to the carbazole's aromatic protons. A carbene signal is observed in the carbon NMR spectrum, resonating as a doublet of doublets at 177.4 ppm (Figure 5.5). The resonance for the carbene carbon of **22** is shifted downfield compared to the resonance of the (*trz*)Ag(I) complex reported by Crudden.[40] The doublet of doublet splitting pattern is observed for silver-carbene complexes due to two one bond interactions afforded by coupling of ^{13}C with both ^{107}Ag and ^{109}Ag isotopes.[42] The values of the two coupling constants observed for **22** are 185.3 Hz and 13.2 Hz. The ^{107}Ag isotope has a higher natural abundance at 51.8%, compared to the ^{109}Ag isotope with 48.2% abundance.[42] However, the larger coupling constant of 185.3 Hz is a result of the ^{13}C nuclei coupling with the nuclei of the heavier ^{109}Ag isotope.

---

[42] *NMR in Organometallic Chemistry*, P. S. Pregosin, WILEY-VCH Verlag GmbH & Co. KGaA, Weinheim, Germany, 2012, pp 207 – 277.
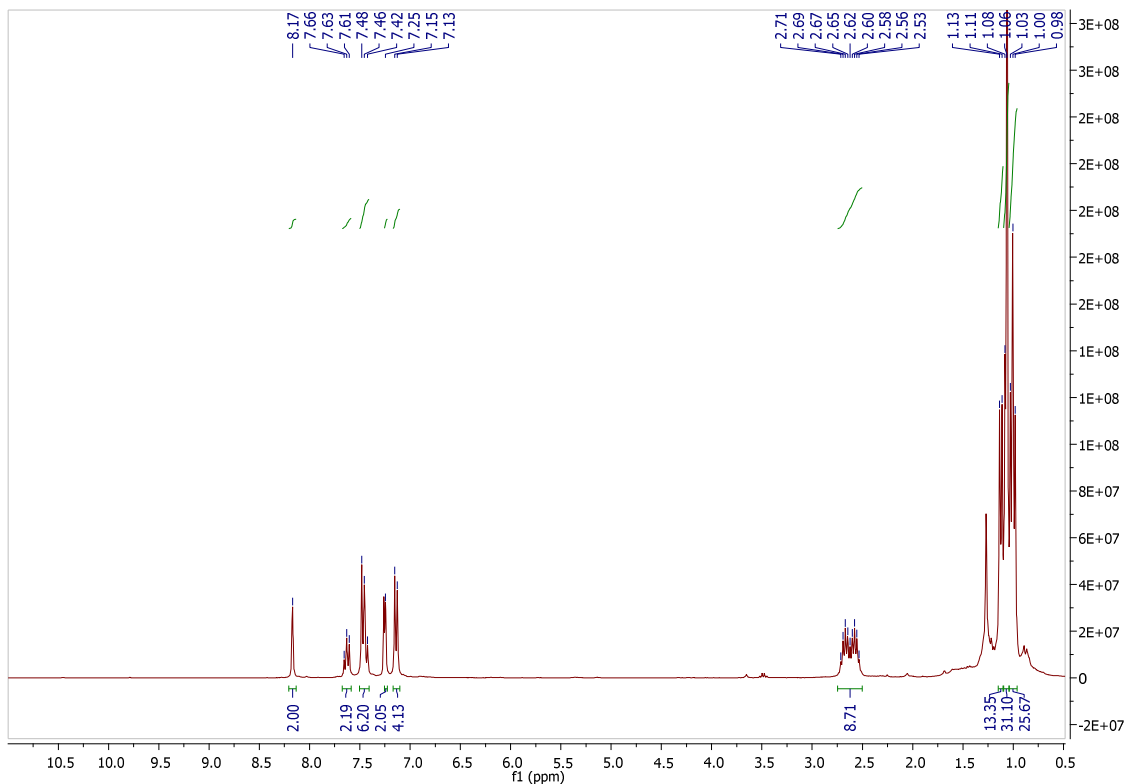
Figure 5.4: ^{1}H NMR of **22** in CDCl$_3$ solvent
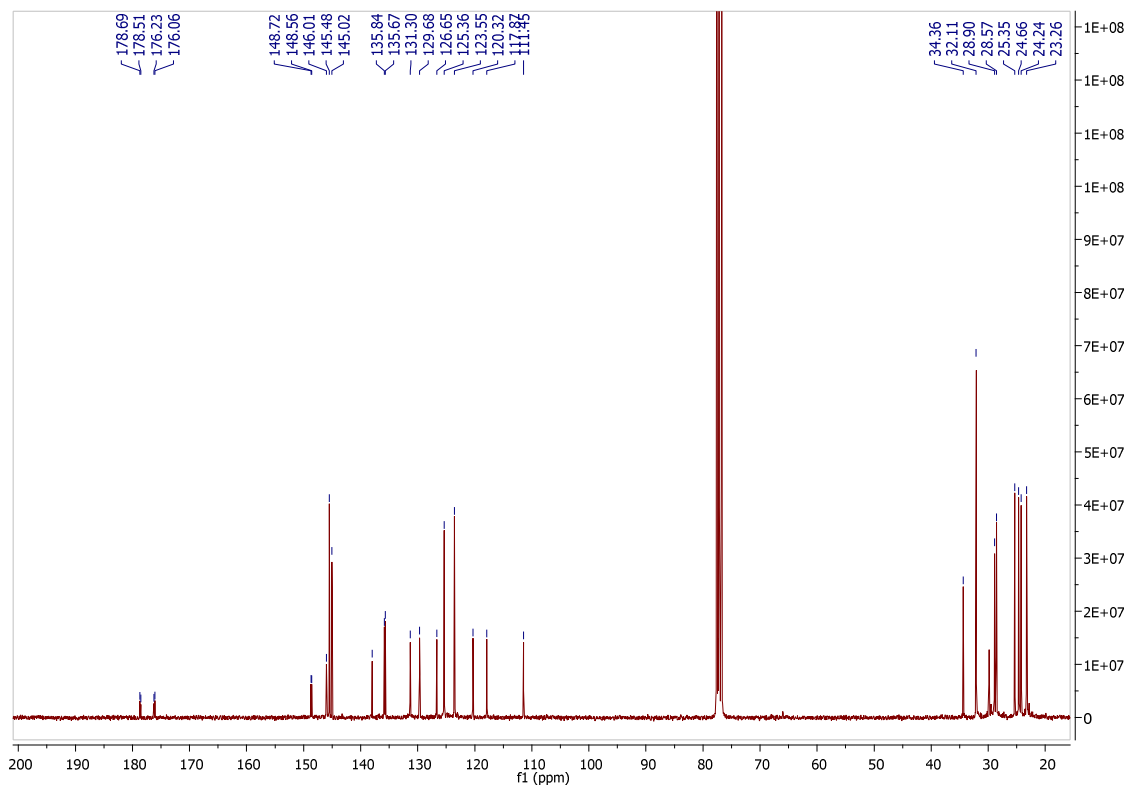
Figure 5.5: ^{13}C NMR of **22** in CDCl$_3$ solvent

169

A single crystal suitable for X-ray diffraction analysis was obtained from a CH_2Cl_2 solution of **22** layered with hexanes (Figure 5.6). The C10-C9-Ag1-C1 torsion angle has a value of 4.8(5)°. The C1-C2-N3-N2-N1 five-membered heterocycle deviates from the silver metal plane. This could be deduced from the C2-C1-Ag1-C9 torsion angle of 15.2(5)°. The deviation could be a result of steric repulsion between the wingtip functionalities. The triazolylidene moiety twists out of the silver metal plane, in order to decrease steric repulsion between the two 2,6-diisopropylphenyl wingtip groups. Both triazolylidene moieties are nearly in plane with the carbazole backbone. The C1-C2-C3-C4 and C9-C10-C11-C12 torsion angles are 1.9(3)° and 1.3(3)°, respectively. This is counter-intuitive, because the triazolylidene moiety that has twisted out of the silver metal plane, should have resulted in a large C1-C2-C3-C4 torsion angle. However, it is determined that the rigid carbazole backbone also deviates from planarity by twisting slightly in order to accommodate the large twist of the triazolylidene moiety out of the silver metal plane. The deviation from planarity in the carbazole backbone has been observed for the rhodium complex reported by Moser *et al.*[43]

As determined from the crystal structure, **22** has an unusual T-shaped geometry (Figure 5.6). However, the angles are not exactly perpendicular and linear as would be expected for a T-shaped complex. The C1-Ag1-C9 bond angle is 171.37(7)°, while the C1-Ag1-N7 and C9-Ag1-N7 bond angles are 85.58(6)° and 85.91(6)°, respectively. The bond angles that do not conform to an ideal T-shape could be due to either alleviation of steric repulsion, or, in order to increase orbital overlap between the silver and carbene carbon bonding orbitals.

The silver-carbene bond lengths for **22** is comparable to reported *trz*-Ag(I) silver-carbene bond lengths.[40] The C1-Ag1 and C9-Ag1 bond lengths are 2.0980(15) Å and 2.0990(14) Å, respectively. The N7-Ag1 bond length is longer compared to the silver-carbene bond lengths and has a value of 2.2844(15) Å.

The C2-C1-N1 bond angle (102.37(13)°) is more acute compared to the bond angle of **7**. Comparatively, the C10-C9-N4 bond angle, being 102.66(12)°, is also more acute than **7**. Both bond angles are larger when compared to the bond angles of **9**, as expected due to metallation of free carbene carbons that decreases s- and increases p-character of the σ-orbiral. The triazolylidene moieties are both planar, indicative of electron delocalisation and therefore aromaticity throughout the five-membered heterocycle. This is deduced from the torsion angle values for the triazolylidene moieties being close to zero. The C1-C2-N3-N2 torsion angle has a value of 0.36(19)°, while the C9-C10-N6-N5 torsion angle is 0.15(19)°.

---

[43] M. Moser, B. Wucher, D. Kunz, F. Rominger, *Organometallics*, 2007, **26**, 1024 – 1030.
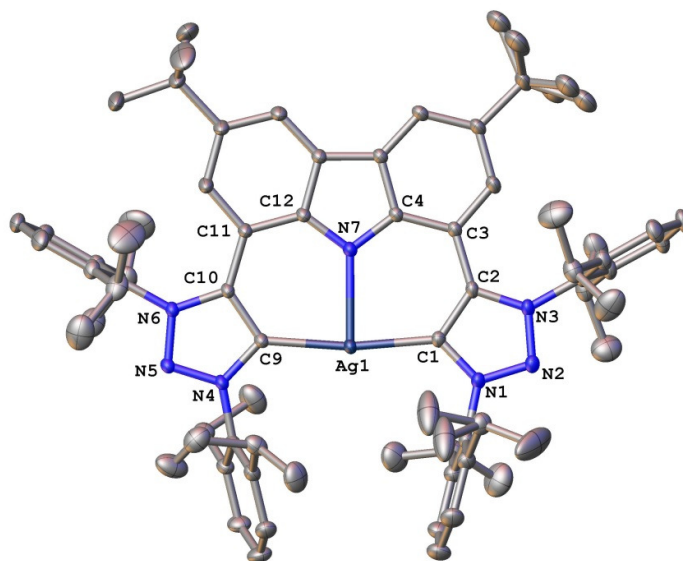
Figure 5.6: Crystal structure of **22**

5.3.2) Synthesis of 23

All attempted transmetallation reactions from **22** with (tht)AuCl failed to yield the desired gold(I) complex **23**. Various solvents were used, ranging from DCM to THF, as well as acetonitrile. The temperature of the reactions was also manipulated, ranging from room temperature to refluxing conditions. After each reaction, only the silver complex **22** was isolated. This indicated that **22** is extremely stable and that ligand coordination to the metal is accompanied by the formation of strong inert bonds. An alternative route had to be followed in order to prepare **23**.

The ligand salt **7** was deprotonated with a strong non-nucleophilic base (KHMDS), followed by *in situ* metallation of the formed adduct **9** with (tht)AuCl (Scheme 5.22). The residue was washed with hexanes, and the product extracted with Et$_2$O. Evaporation of the solvent, *in vacuo*, yielded a purple solid that was determined to be the gold(I) complex **23** by NMR, MS and XRD characterisation. To the best of our knowledge, **23** represents the first example of a T-shaped, mono-nuclear gold(I) complex supported by a organic tridentate pincer ligand scaffold.
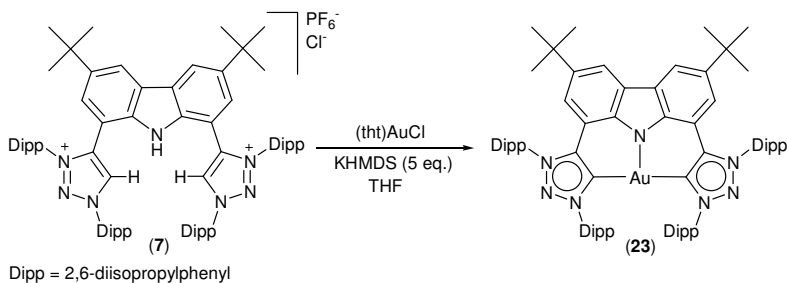
Scheme 5.22: Deprotonation of **7** followed by metallation with (tht)AuCl yielding **23**

171

The proton NMR spectrum (Figure 5.7) has a signal resonating downfield at 8.62 ppm. This resonance corresponds to the carbazole's aromatic protons. The clear disappearance of the acidic protons confirms successful deprotonation of **7**. A signal resonating in the carbon NMR spectrum as a singlet at 176.0 ppm correspond to the carbene carbon coordinated to the Au(I) metal (Figure 5.8). This in turn supports metallation of the adduct **9**, which was generated in the reaction mixture. The carbene resonance of **23** is similar to the carbene resonance for the (*trz*)-Au(I) complexes reported by Crowley.[39] In contrast, the resonance of **23** is significantly downfield compared to the carbene resonance of the (*trz*)-Au(I) complexes discussed in Section 5.1.2.[20] One carbon resonance is not observed in the carbon NMR spectra and that signal is in all likelihood, overlapped by the benzene-d_6 resonance.
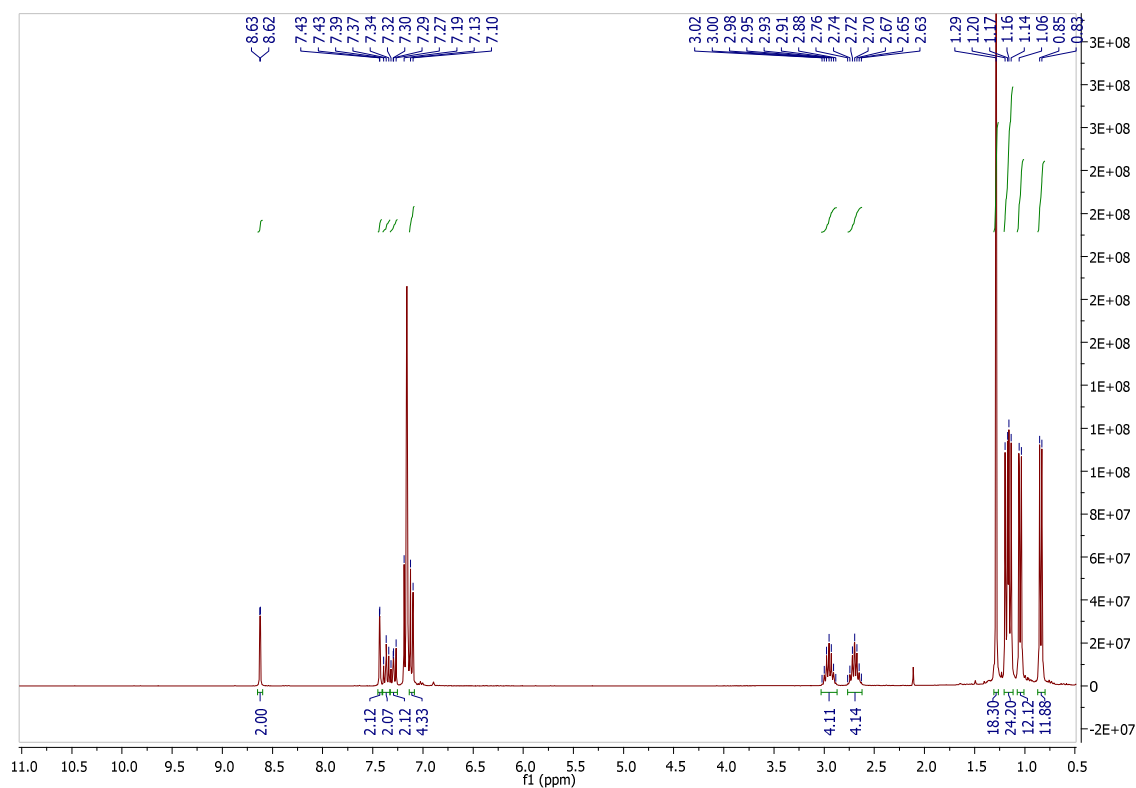
Figure 5.7: ^{1}H NMR of **23** in C$_6$D$_6$ solvent
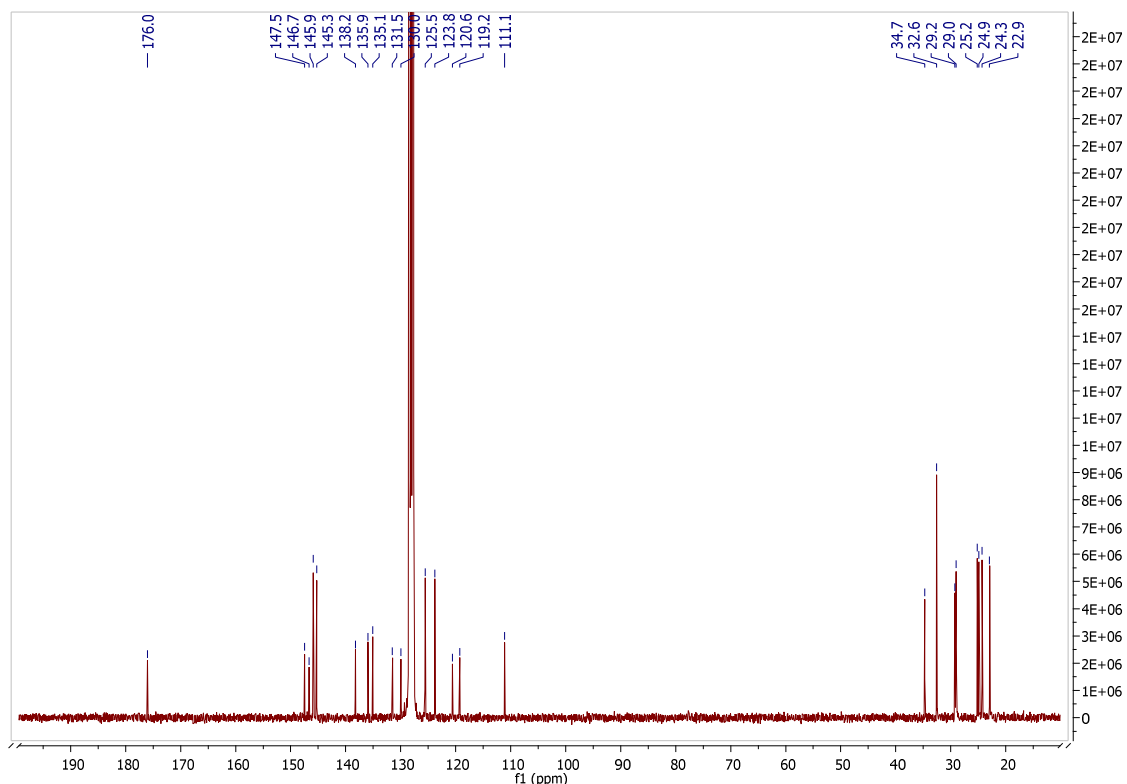
Figure 5.8: ^{13}C NMR of **23** in C$_6$D$_6$ solvent

The crystal structure of **23** (Figure 5.9) was analysed and revealed the following. The gold complex displays a T-shaped geometry around the metal centre. It is also determined that the molecule has a two-fold symmetry axis with the Au1 and N1 atoms lying on the axis. The symmetry axis is parallel to the unit cell's b-axis.

As was the case for **22**, the rigid carbazole backbone of **23** displayed a slight deviation from the expected planar system. The C11-C12-Au1-C12' and C11'-C12'-Au1-C12 torsion angles are 4.78(15)°, indicating that the triazolylidene moieties are twisted somewhat out of the gold centre plane. The two triazolylidene moieties are twisted in opposite directions with respect to each other. The ligand scaffold can compensate for this deviation by twisting both the triazolylidene moieties out of the carbazole plane, as well as the carbazole backbone itself. The C12-C11-C6-C1 torsion angle is 7.1(3)°. It is postulated that the deviation is a direct result of steric repulsion between the two 2,6-diisopropylphenyl wingtip groups.

The angles around the gold centre all deviate from the ideal T-shaped bond angles, similar to what was observed for **22**. The C12-Au1-C12' bond angle is 171.24(8)°, while the C12-Au1-N1 bond angle is smaller than 90°, with a value of 85.62(4)°. The gold-carbene (both C12-Au1 and C12'-Au1) bond length of 2.0143(14) Å is shorter than the **C**$_{Carbene}$-Ag1 bond distance of **22**, but elongated compared

173

to other triazolylidene carbene-gold(I) bond distances (for some examples, see **h$_{i-iv}$,** Scheme 5.5).[20,39] The shorter bond distance for **23** compared to **22**, is due to the soft L-donor carbene ligand forming stronger bonds to the softer gold(I) metal. The ligand *trans* to the carbene ligand in **23**, is a second strongly donating carbene ligand. The stronger *trans*-donor ligand will decrease the bond distance of the ligand in the *trans*-position. For the (*trz*)-Au(I) complexes reported by Albrecht *et al.* and by Crowley *et al.*, the ligands *trans* to the carbene ligands are weak donor ligands, which would not amount to a large elongation of the **C$_{Carbene}$**-Au(I) bond distance. The N1-Au1 bond length of **23** is longer than the **C$_{Carbene}$**-Au1 bond distance, at 2.3263(17) Å. The N1-Au1 bond distance of **23** is almost 0.1 Å longer compared to the N7-Ag1 bond length of **22**. The silver metal, with its smaller ionic radius, is a harder acid matched with the hard basic nitrogen ligand. Therefore, stronger bonds will form.

The C12-C11-N4-N3 torsion angle has a value of 0.55(18)°. This value, being close to zero, is indicative of aromaticity throughout the five membered heterocycle. The C11-C12-N2 bond angle (102.68(12)°) is larger than the corresponding bond angle of **9**, but smaller when compared to that of the ligand salt **7**. This is expected as the *σ*-orbital's s-character increases upon deprotonation and/or metallation of the ligand salt, resulting in a decrease of the X-**C$_{Carbene}$**-X bond angle.
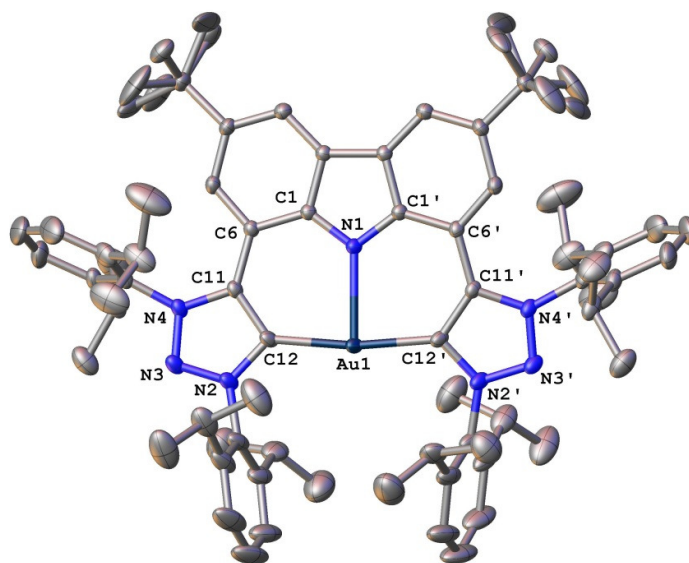
Figure 5.9: Crystal structure of **23**

5.3.3) Synthesis of 24

Oxidation of **23** with 2.3 equivalents of silver hexafluorophosphate lead to the formation and isolation of a gold(III)-hydroxo complex, **24** (Scheme 5.23). The reaction occurred with the deposition of a silver mirror on the sides of the reaction vessel, indicating reduction of Ag(I) to Ag(0). Upon completion of the reaction, complex **24** was isolated as a lime green solid after rinsing the crude solid with Et_2O, followed by extraction of the product with CH_2Cl_2 and subsequent evaporation of the solvent. The formation of the unexpected mono-cationic gold(III)-hydroxo species **24**, and not the desired dicationic gold(III) complex, was confirmed with NMR, MS and IR spectroscopic analysis. Crystals suitable for X-ray diffraction analysis could not be obtained. It is postulated that, even when working under dry and inert conditions, the presence of water in the reaction mixture (in all probability originated from the hygroscopic $AgPF_6$ solid) leads towards the reactive dicationic gold centre procuring an hydroxide ligand, yielding the mono-cationic complex **24**. It was further determined that **24** is stable in the presence of air and moisture. In fact, refluxing a solution of **24** in an acetonitrile:water mixture (9:1), did not lead to decomposition and **24** was again isolated as a mono-cationic gold(III)-hydroxo salt. When dissolved in CH_2Cl_2, complex **24** displayed some luminescence properties when irradiated with a UV-light at 356 nm wavelength. This gives an indication to the possibility of **24** exhibiting photoluminescent properties, and further investigation towards this property might reveal some interesting results.
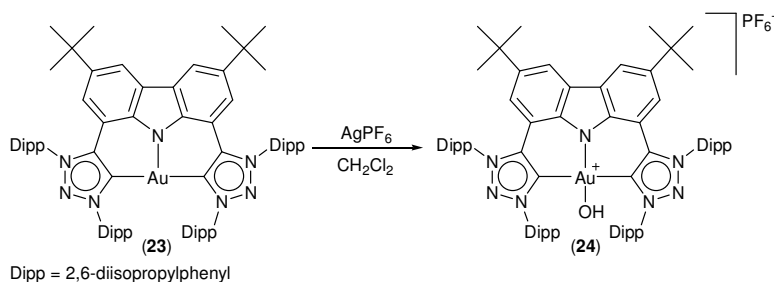
Scheme 5.23: Oxidation of **23** with $AgPF_6$ to obtain the cationic gold(III) complex **24**

As can be observed from the proton NMR spectrum of **24** (Figure 5.10), a resonance upfield at -0.75 ppm corresponds to the hydrogen of the Au-O**H** complex. The Au-O**H** resonance is comparable to the Au-O**H** resonance of a reported carbene-gold-hydroxide complex, also resonating upfield and not downfield as would be expected for the proton of an hydroxide moiety.[18] The carbon NMR spectrum is displayed in Figure 5.11, and further supports formation of a gold(III) complex. The distinctive carbene carbon resonance of the gold(I) complex **23** (see Figure 5.8) is not observed, and has shifted upfield to the aromatic region. All unequivalent carbons, which include the carbene carbon, are

175

accounted for and resonate in the aromatic region from 146.5 to 108.2 ppm and in the aliphatic region from 35.2 to 23.4 ppm. The upfield carbene resonance shift of gold(I) to gold(III) fits the general trend, as observed for other gold(III) complexes obtained through oxidation of gold(I).[38,44] This general trend, observed for carbene resonance shift of gold(I) to gold(III), exhibits a shift of 30 ppm or even more. Both ^{19}F and ^{31}P NMR characterisation of **24** confirms the presence of a hexafluorophosphate counteranion.
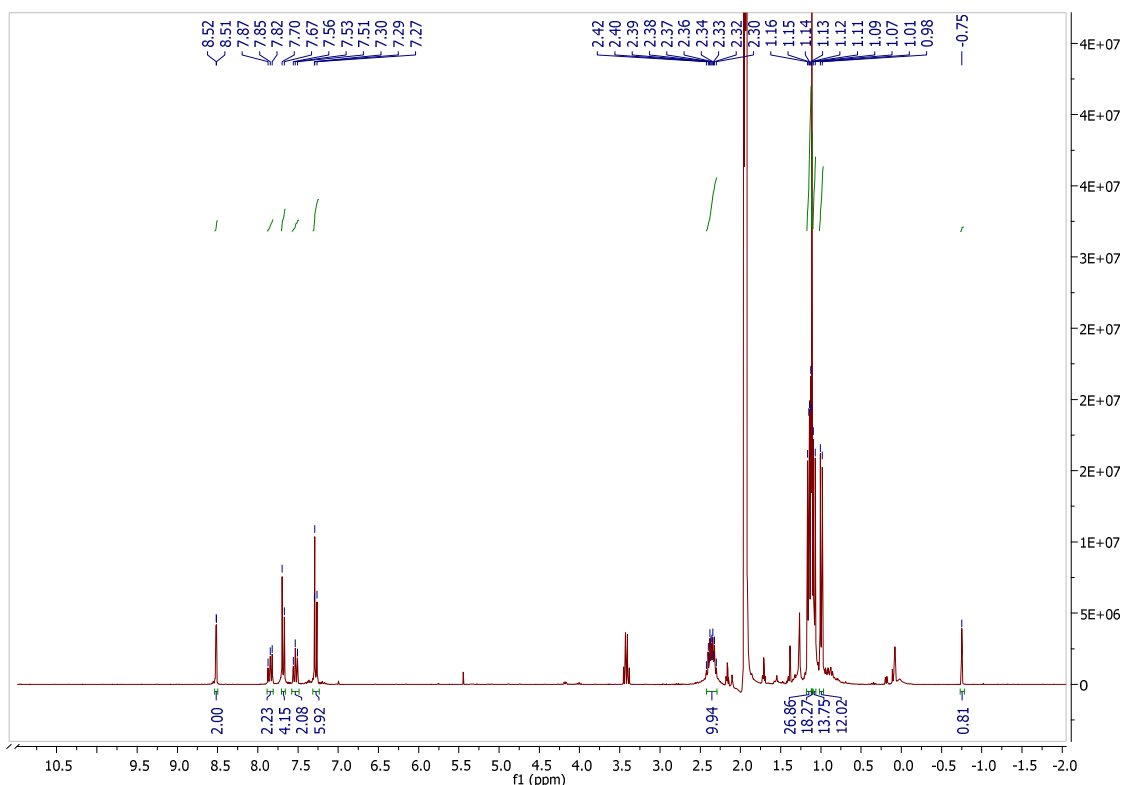
Figure 5.10: ^{1}H NMR of **24** in CD$_3$CN solvent

---

[44] M. Kriechbaum, D. Otte, M. List, U. Monkowius, *Dalton Trans.*, 2014, **43**, 8781 – 8791.
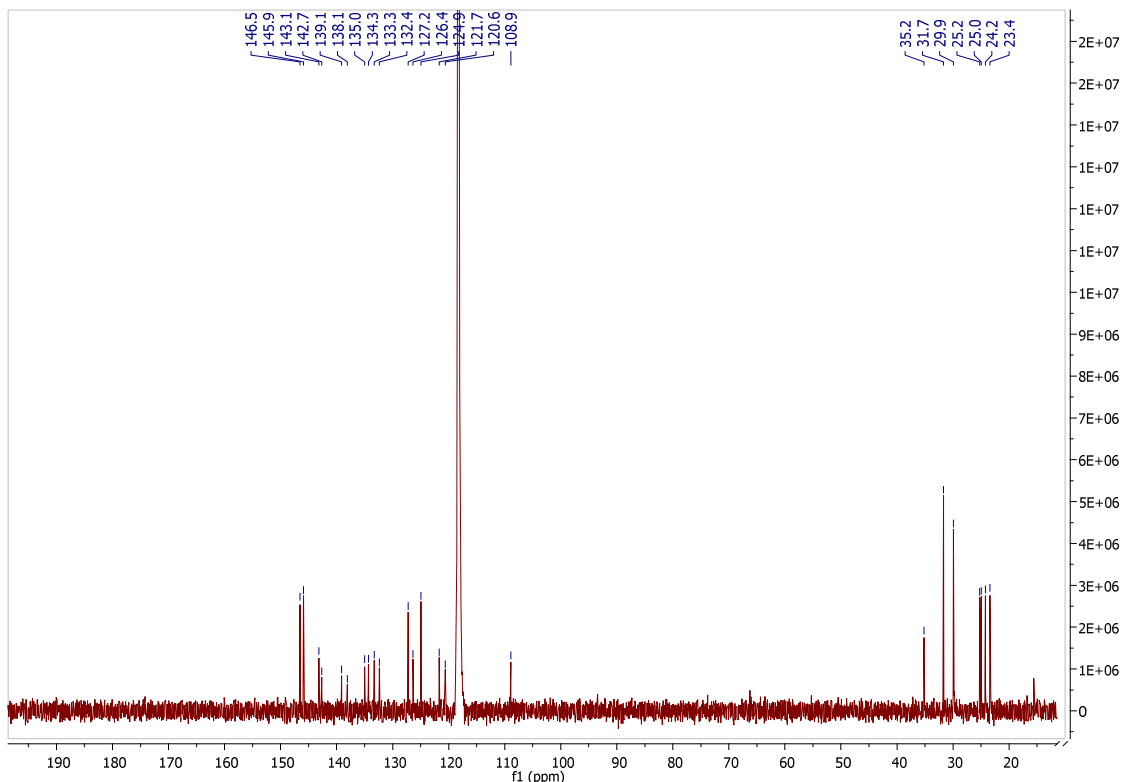
Figure 5.11: ^{13}C NMR of **24** in CD$_3$CN solvent

Determination of the characteristic O-H stretch in the infrared spectrum of **24** unambiguously confirmed the formation of a gold species coordinated to a hydroxide moiety. The O-H stretching frequency of **24** absorbs at 3602 cm^{-1}. This value lies well between the experimentally determined O-H stretching frequencies for gold dihydroxide and gold(I)-hydroxo complexes. The stretching frequency determined for gold dihydroxide complexes absorbs in the region of 3566 cm^{-1}.[45] The carbene gold(I)-hydroxo complex reported by Nolan features an O-H stretching frequency absorbing at 3627 cm^{-1} (**d**, Scheme 5.3).[17] Bochmann *et al.* did not report the absorption frequency for the synthesised gold(III)-hydroxo complex **m** (**I**, Scheme 5.8).[22] Therefore, concrete evidence towards a hydroxide moiety coordinated to the gold centre, i. e. formation of **24**, is obtained through infrared spectroscopy analysis.

MS analysis further supported formation of **24**. The theoretical mass for the mono-cationic complex **24** without the counteranion present is 1266.6950. Experimentally, it was determined that the mass to charge ratio of **24** is 1266.6998.

---

[45] *a)* X. Wang, L. Andrews, *Inorg. Chem.*, 2005, **44**, 9076 – 9083, *b)* X. Wang, L. Andrews, *Chem. Commun.*, 2005, 4001 – 4003.

177

5.3.4) Synthesis of 25

In order to synthesis **25**, the analogue of **23**, ligand salt **10** was deprotonated with KHMDS followed by *in situ* metallation of the adduct **11** with (tht)AuCl (Scheme 5.24). The residue was washed with hexanes, followed by extraction of the product with Et$_2$O. Evaporation of the solvent yielded a dark pink solid that was determined to be **25** through spectroscopic (NMR and MS) and X-ray diffraction analysis.
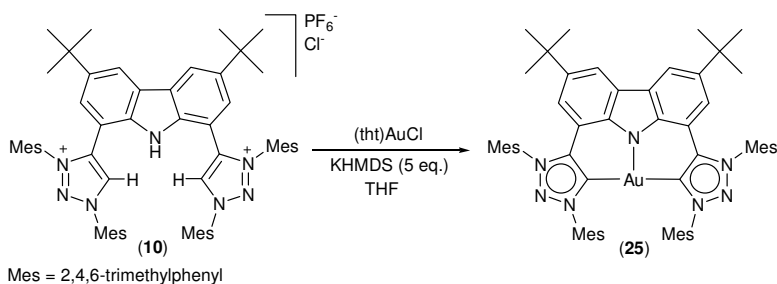
Scheme 5.24: Synthesis of **25** through *in situ* deprotonation of **10** followed by metallation

As was the case for **23**, the disappearance of the *trz*H and N**H** protons (Figure 5.12), as well as the observation of a carbene signal resonating at 175.8 ppm (Figure 5.13), gives clear evidence for the formation of a gold(I) complex **25**. The gold(I) complex **25** is symmetrical in solution, as can be observed from the proton NMR spectrum (Figure 5.12). The carbene resonance of **25** is similar to that of **23**.
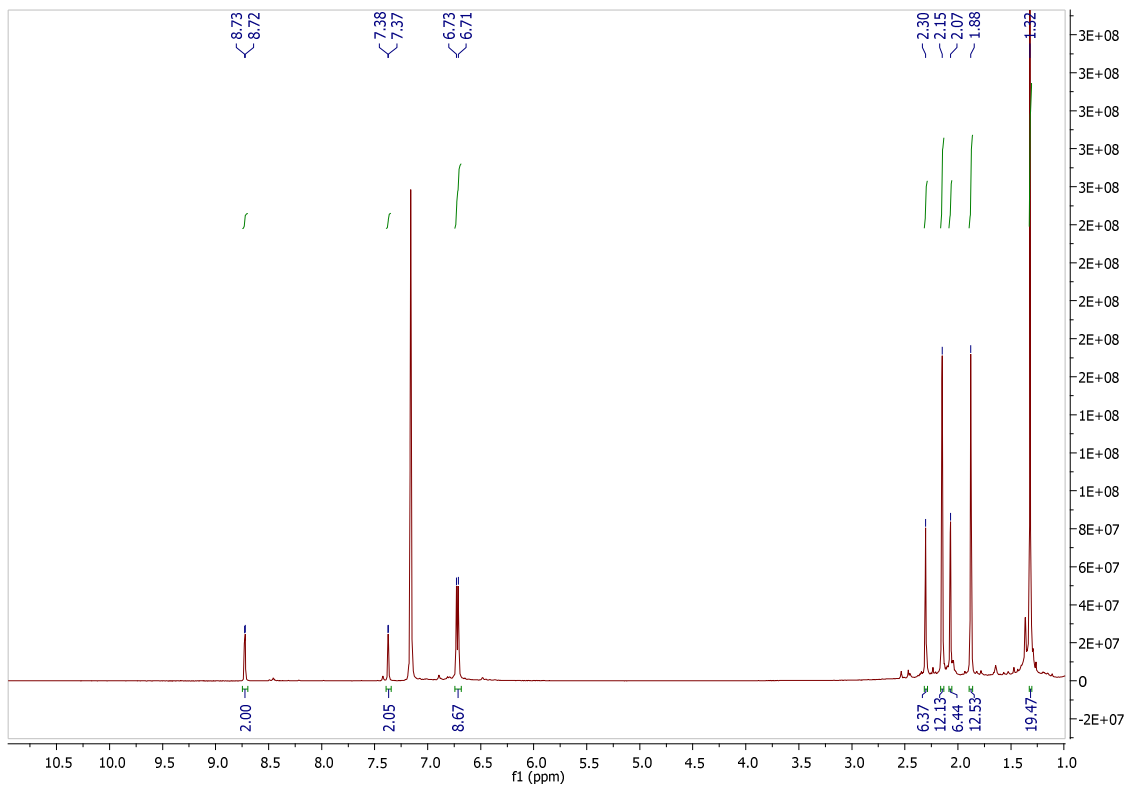
Figure 5.12: ^{1}H NMR of **25** in C$_6$D$_6$ solvent
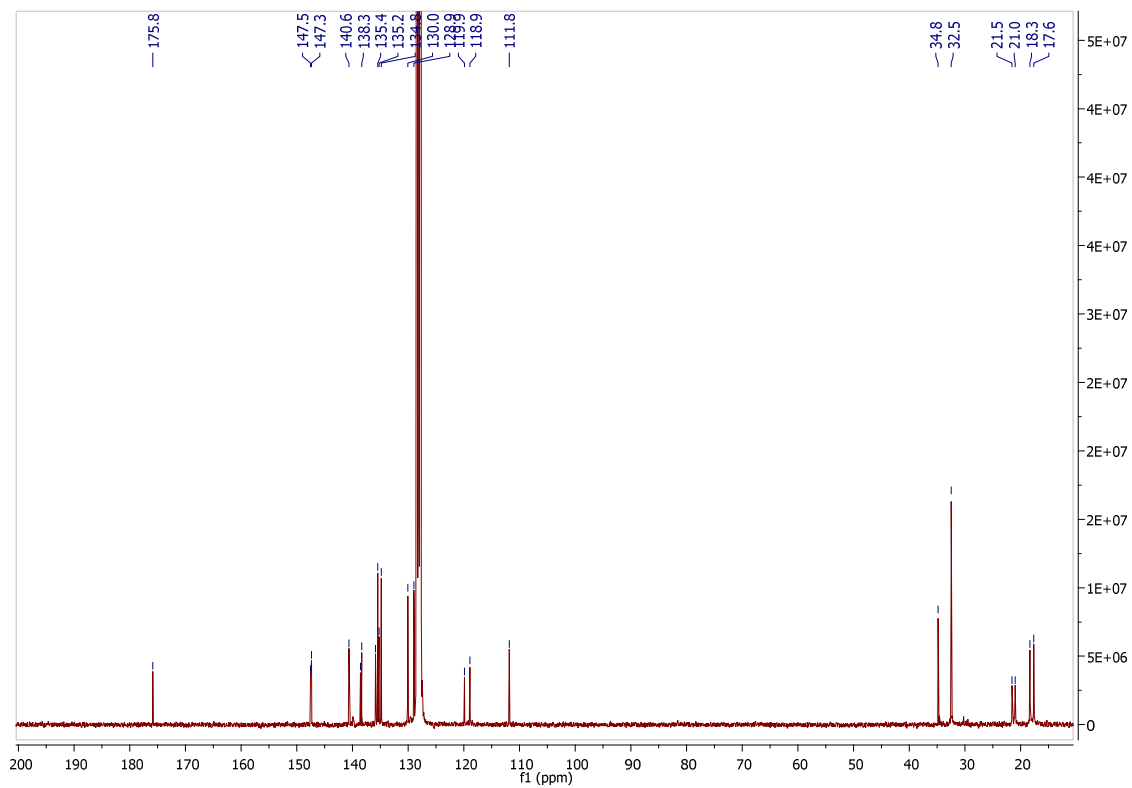
Figure 5.13: ^{13}C NMR of **25** in C$_6$D$_6$ solvent

179

The gold complex **25** is unsymmetrical in the solid state (Figure 5.14), contrasting to **23**. In addition to a frontal view (left, Figure 5.14), a view down the carbazole plane (right, Figure 5.14) is also displayed for clarity. The gold metal centre is orientated out of the ligand scaffold plane, as is clearly observed from the crystal structure (right, Figure 5.14). This gold metal, being positioned above and out of the carbazole plane, is similar to the observation made for the copper(II)chloro complex **14** (Section 3.3.3, Chapter 3). A C23-C24-Au1-C22 torsion angle of 52.7(11)° and a C21-C22-Au1-C24 torsion angle of 40.0(11)° gives concrete evidence for the substantial deviation from a planar or even remotely planar metal centre. The triazolylidene moieties of **25** are both orientated in the same direction. The carbazole backbone is also twisted, slightly, but with both sides pointing to the same direction which yields a concave carbazole structure. The triazolylidene moieties are twisted out of the carbazole plane, with torsion values of 21.1(8)° and 20.9(8)° for the C22-C21-C6-C1 and the C24-C23-C12-C7 angles, respectively.

The C22-Au1 bond length of 2.013(4) Å for **25** is comparable to the gold-carbene bond distance of **23**. The C24-Au1 bond length of **25** is also comparable, with a value of 2.040(4) Å. The nitrogen-gold bond distance for **25** is considerably longer compared to **23**. The N1-Au1 bond length is 2.412(3) Å and is almost 0.1 Å longer when compared to the corresponding bond length of **23**.

The bond angles around the gold centre of **25** differ significantly from the bond angle values expected for an ideal T-shaped complex. The C22-Au1-C24 bond angle is 167.28(17)°, which does not conform to linearity. In addition, the carbene-gold-nitrogen bond angles are considerably smaller than 90°. The C24-Au1-N1 bond angle is 83.23(12)°, while the C22-Au1-N1 has a bond angle of 86.75(13)°.

Electron delocalisation throughout the five-membered heterocycle of **25** has decreased, compared to the gold complex **23**. This is concluded from the C22-C21-N4-N3 torsion angle being 1.3(5)° and the C24-C23-N7-N6 torsion angle, which has a value of 1.6(6)°. The C21-C22-N2 and C23-C24-N5 bonding angles are 102.5(3)° and 103.4(3)°, respectively. Both bonding angles are more acute than the corresponding bond angles of **10**. The C21-C22-N2 bond angle is comparable to the corresponding bond angles of **23**, but the C23-C24-N5 bond angle is significantly larger. This indicates a decrease in the percentage of the σ-orbital's s-character. A direct result could be decrease bond strength, and this is observed for the C24-Au1 bond length.

The wingtip groups of **25** are smaller than the corresponding wingtip groups of **23**. Therefore various deviations from the expected values, or even from the values obtained from the crystal structure of **23**, is not a direct result of steric repulsion between the wingtip groups, as could be concluded for

23. A possible explanation regarding the observed differences can be made, with respect to the unfavourable coordination of gold(I) complexes with a coordination number of three adopting a T-shaped geometry. Steric repulsion in **23** resisted the significant deviations observed for **25**. The steric repulsion in **23** can be said to 'lock' the gold metal in the centre of the tridentate pocket. Therefore, unfavourable bond formation stabilisation can possibly result in the deviations observed for **25**.
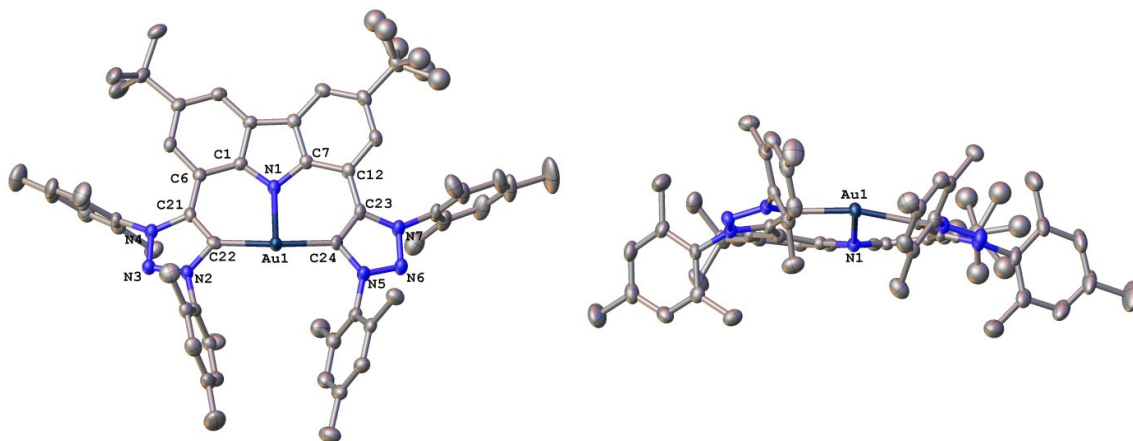
Figure 5.14: Crystal structure of **25** (Left: frontal and Right: side-on views)

5.4) Conclusion

A silver(I), two gold(I) and a gold(III) complex supported by either the ligands **7** or **10**, could be obtained through: 1) metallation with Ag_2O in the presence of KBr; 2) by deprotonation of the ligand salt with KHMDS followed by metalltion with (tht)AuCl and 3) by oxidation of gold(I) to gold(III) employing $AgPF_6$, respectively. These complexes were characterised through various techniques including, NMR, MS and IR spectroscopy, as well as X-ray diffraction analysis.

The silver(I) complex **22** is remarkably stable and inert, towards transmetallation reactions and even ambient conditions. However, **22** was protected from light as silver complexes are generally sensitive towards light. Complex **22** represents the first example of a three coordinated silver(I) metal supported by a tridentate ligand featuring triazolylidene functional groups.

To the best of our knowledge, synthesis and isolation of **23** represent the first example of a T-shaped mono-nuclear gold(I) complex supported by an organic tridentate pincer ligand, where chelation, and not dinuclear complex formation, occurred. The gold(I) complexes usually adopt a linear geometry if the coordination number is two and a trigonal planar geometry if the coordination number is three; so formation of a "naked" T-shaped gold(I) complex such as **23** is remarkable indeed. The carbene resonance is slightly deshielded when compared to (*trz*)-Au(I) complexes

reported by Albrecht and co-workers, but is similar to the (*trz*)-Au(I) complex reported by Crowley. The crystal structure of **23** displayed minor deviations, which could be attributable to steric repulsion or the fact that gold(I) resists formation of a T-shaped complex, resulting in structural irregularities upon coordination. The gold(I) complex **23** is stable towards high temperatures and under ambient conditions. The catalytic activity of **23** towards a broad range of organic transformation will be investigated as part of future work envisaged. The Au 6*p*-orbital should be occupied upon coordination of all three donor ligands of **9**. This might increase the energy of the 6*p*-orbital, resulting in a decrease between the HOMO-LUMO energy gap. This would be advantageous towards catalysis.

Oxidation of **23** to **24** with AgPF$_6$ in CH$_2$Cl$_2$ occurred readily. This could be a result of using the non-coordinating CH$_2$Cl$_2$ as solvent, which would increase the oxidising strength of the AgPF$_6$ oxidant. The mono-cationic gold(III) salt was obtained which was supported by **9** and also, by a hydroxo ligand. Gold substituted with a hydroxide as ligand is not uncommon, but is still relatively rare with only a few researchers active in this area of research. However, cationic gold(III) salts supported by a hydroxo ligand is, to the best of our knowledge, not reported. Gold(III) complex **24** displayed remarkable stability at high temperatures in the presence of air and water. Light exposure was kept to a minimum. In a solution of CH$_2$Cl$_2$, the complex **24** emits a weak green fluorescence upon irradiation with UV-light at 356 nm. The properties of **24** will be exploited when the catalytic activity of **24** is tested towards a broad range of organic transformations, including photochemical reactions. These properties include: 1) the surprisingly high stability of **24** rendering it a potentially robust catalyst; 2) the fact that the complex already exhibits some photoluminescent properties can render **24** as a catalyst which could be active in photochemical catalytic reactions; 3) the hydroxo ligand could yield a catalyst that would be able to catalyse similar reactions as reported by the groups of Nolan and Bochmann (see Section 5.1); and 4) a possible catalyst that can coordinate an olefin, activating it towards nucleophilic attack due to the presence of a vacant site on the gold centre.

As was the case for **23**, the gold(I) complex **25** displayed a T-shaped geometry around the gold(I) centre with coordination of all three donor sites. Crystal structure determination unambiguously confirmed the formation of the less steric crowded complex **25**. The crystal revealed significant distortions of **25** compared to **23**. The gold(I) metal protrudes out of the ligand scaffold plane. This could be a direct result due to the unfavourable chelation around a gold centre, employing a tridentate ligand. The effect in **25** is more pronounced compared to **23**, which could be due to less steric congestion, allowing for deviations to occur. The catalytic activity of **25** towards various organic transformation reactions will be investigated. The complex **25**, with its significant distortions,

182

bond and angle strain as well as less steric crowding, has the potential to exhibit good catalytic activity. In addition, due to the deviations, reversible carbene dissociation from the gold(I) centre can occur. This would open up a second vacant site on the metal, allowing for coordination of an incoming substrate to the metal, activating that substrate towards nucleophilic attack. It is anticipated that, the catalytic properties, upon investigation, can yield some very interesting results for complex **25**.

5.5) Experimental

5.5.1) (CNC$_{Dipp}$)Ag (**22**)
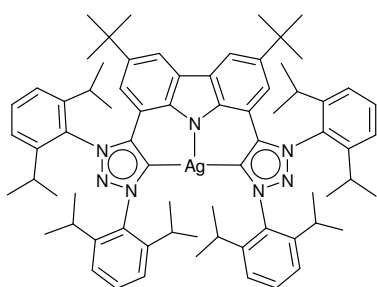
A flame dried Schlenk tube was loaded with **7** (200.0 mg, 1.6 x 10^{-4} mol), Ag$_2$O (131.1 mg, 5.7 x 10^{-4} mol), and KBr (192.4 mg, 1.6 x 10^{-3} mol). The reaction vessel was evacuated and purged with N$_2$ (g), followed by addition of DCM (25 mL). The black solution was stirred at room temperature for five days, in the absence of light. The solvent was evaporated *in vacuo*. The product was extracted from the residue with Et$_2$O (3 x 15 mL). Evaporation of the solvent *in vacuo*, yielded **22** (130.0 mg, 1.1 x 10^{-4} mol, 69%) as a dark orange solid. Crystallisation from DCM yielded single crystals suitable for XRD analysis. ^{1}H NMR δ$_H$ (CDCl$_3$, 300 MHz) 8.17 (2H, broad s, Ar**H**$_{carb}$), 7.63 (2H, t, *J* = 7.8 Hz, Ar**H**$_{Dipp}$), 7.47 (4H, d, *J* = 7.8 Hz, Ar**H**$_{Dipp}$), 7.45 (2H, m, Ar**H**$_{Dipp}$ overlaps with Ar**H**$_{Dipp}$), 7.25 (2H, broad s, Ar**H**$_{carb}$), 7.14 (4H, d, *J* = 7.8 Hz, Ar**H**$_{Dipp}$), 2.74 – 2.51 (8H, m, C**H**(CH$_3$)$_2$), 1.12 (12H, d, *J* = 6.9 Hz, CH(C**H**$_3$)$_2$), 1.07 (12H, d, CH(C**H**$_3$)$_2$ overlaps with C(CH$_3$)$_3$), 1.06 (18H, s, C(C**H**$_3$)$_3$), 1.02 (12H, d, *J* = 7.2 Hz, CH(C**H**$_3$)$_2$), 0.99 (12H, d, *J* = 7.2 Hz, CH(C**H**$_3$)$_2$). ^{13}C NMR δ$_C$ (CDCl$_3$, 75 MHz) 177.4 (dd, *J* = 185.3 Hz, 13.2 Hz, ^{109}Ag-^{13}**C**$_{Carbene}$, ^{107}Ag-^{13}**C**$_{Carbene}$), 148.7 (Ar**C**$_q$), 148.6 (Ar**C**$_q$), 146.0 (Ar**C**$_q$), 145.5 (Ar**C**$_q$), 145.0 (Ar**C**$_q$), 138.0 (Ar**C**$_q$), 135.8 (Ar**C**$_q$), 135.7 (Ar**C**$_q$), 131.3 (Ar**C**H), 129.7 (Ar**C**H), 126.7 (Ar**C**$_q$), 125.4 (Ar**C**H), 123.6 (Ar**C**H), 120.3 (Ar**C**H), 117.9 (Ar**C**H), 111.5 (Ar**C**$_q$), 34.4 (**C**(CH$_3$)$_3$), 32.1 (C(**C**H$_3$)$_3$), 28.9 (**C**H(CH$_3$)$_2$), 28.6 (**C**H(CH$_3$)$_2$), 25.4 (CH(**C**H$_3$)$_2$), 24.7 (CH(**C**H$_3$)$_2$), 24.2 (CH(**C**H$_3$)$_2$), 23.3 (CH(**C**H$_3$)$_2$). HRMS (FIA-ESI): Calculated for C$_{72}$H$_{90}$N$_7$Ag^{2+} [M + 2H]$^{2+}$: 580.8227, found: 580.8235.

5.5.2) (CNC$_{Dipp}$)Au (**23**)
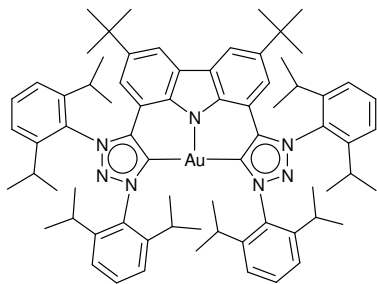
To a flame dried Schlenk tube was added **7** (200.0 mg, 1.6 x 10^{-4} mol), (tht)AuCl (62.2 mg, 1.9x 10^{-4} mol) and KN[Si(CH$_3$)$_3$]$_2$ (161.3 mg, 8.1 x 10^{-4} mol). The Schlenk tube was evacuated with N$_2$ (g) and cooled down to -80 °C. The reaction was initiated by the addition of THF (15 mL) also cooled down to -80 °C. The reaction was stirred for 30 min at -80 °C before being removed from the cold bath and left to warm up to room temperature whilst stirring overnight. A dark purple solution formed during the reaction. The solvent was evaporated *in vacuo*. The residue was washed with hexanes (5 x 15 mL) and the product extracted with Et$_2$O (4 x 15 mL). The solvent was evaporated *in vacuo*, yielding **23** (168.0 mg, 1.3 x 10^{-4} mol, 83%) as a purple solid. Crystallisation from toluene yielded single crystals suitable for XRD analysis. ^{1}H NMR δ $_H$ (C$_6$D$_6$, 300 MHz) 8.62 (2H, d, *J* = 1.5 Hz, Ar**H**$_{carb}$), 7.43 (2H, d, *J* = 1.5 Hz, Ar**H**$_{carb}$), 7.37 (2H, dd, *J* = 7.8 Hz, 7.8 Hz, Ar**H**$_{Dipp}$), 7.29 (2H, dd, *J* = 8.4 Hz, 6.9 Hz, Ar**H**$_{Dipp}$), 7.17 (4H, d, Ar**H**$_{Dipp}$ overlaps with C$_6$H$_6$), 7.11 (4H, d, *J* = 7.8 Hz, Ar**H**$_{Dipp}$), 2.95 (4H, sept, *J* = 6.9 Hz, C**H**(CH$_3$)$_2$), 2.70 (4H, sept, *J* = 6.9 Hz, C**H**(CH$_3$)$_2$), 1.29 (18H, s, C(C**H**$_3$)$_3$), 1.18 (12H, d, *J* = 6.6 Hz, CH(C**H**$_3$)$_2$), 1.15 (12H, d, *J* = 6.9 Hz, CH(C**H**$_3$)$_2$), 1.05 (12H, d, *J* = 6.9 Hz, CH(C**H**$_3$)$_2$), 0.84 (12H, d, *J* = 6.6 Hz, CH(C**H**$_3$)$_2$). ^{13}C NMR δ $_C$ (C$_6$D$_6$, 75 MHz) 176.0 (**C**$_{Carbene}$), 147.5, 146.7, 145.9, 145.3, 138.2, 136.0, 135.1, 131.5, 130.0, 125.5, 123.8, 120.6, 119.3, 111.1, 34.7 (**C**(CH$_3$)$_3$), 32.6 (C(**C**H$_3$)$_3$), 29.2 (**C**H(CH$_3$)$_2$), 29.1 (**C**H(CH$_3$)$_2$), 25.2 (CH(**C**H$_3$)$_2$), 24.9 (CH(**C**H$_3$)$_2$), 24.3 (CH(**C**H$_3$)$_2$), 23.0 (CH(**C**H$_3$)$_2$). HRMS (FIA-ESI): Calculated for C$_{72}$H$_{90}$N$_7$Au$^+$ [M + H]$^+$: 1250.7001, found: 1250.7035.

5.5.3) [(CNC$_{Dipp}$)Au(OH)]PF$_6$ (**24**)
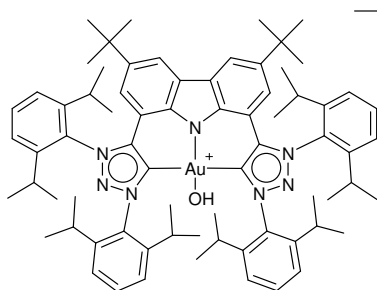
A Schlenk tube, that was flame dried, was charged with **23** (80.0 mg, 6.4 x 10^{-5} mol) and AgPF$_6$ (38.8 mg, 1.5 x 10^{-4} mol). The Schlenk tube was purged with argon gas. The reaction vessel was then cooled down to -80 °C. To the solid mixture was added DCM (10 mL), also cooled down to -80 °C. The reaction was stirred at -80 °C for 30 min before being removed from the cold bath and left to warm up to room temperature whilst stirring overnight. After stirring overnight, the solvent was evaporated *in vacuo*. The residue was washed with Et$_2$O (4 x 15 mL), followed by extraction of the product with DCM (3 x 15mL). The solvent was evaporated yielding **24** (31.0 mg, 2.2 x 10^{-5} mol, 34%) as a lime green solid. Crystals suitable for XRD analysis

could not be obtained. ^{1}H NMR δ $_H$ (CD$_3$CN, 300 MHz) 8.52 (2H, d, J = 1.8 Hz, Ar**H**$_{Carb}$), 7.85 (2H, t, J = 7.8 Hz, Ar**H**$_{Dipp}$), 7.68 (4H, d, J = 7.8 Hz, Ar**H**$_{Dipp}$), 7.53 (2H, t, J = 7.8 Hz, Ar**H**$_{Dipp}$), 7.29 (2H, d, J = 1.2 Hz, Ar**H**$_{Carb}$ overlaps with ArH$_{Dipp}$), 7.28 (4H, d, J = 7.5 Hz, Ar**H**$_{Dipp}$ overlaps with ArH$_{Carb}$), 2.42 − 2.30 (8H, m, C**H**(CH$_3$)$_2$), 1.15 (12H, d, J = 6.6 Hz, CH(C**H**$_3$)$_2$ overlaps with CH(CH$_3$)$_2$), 1.14 (12H, d, J = 6.6 Hz, CH(C**H**$_3$)$_2$ overlaps with CH(CH$_3$)$_2$), 1.11 (18H, s, C(C**H**$_3$)$_3$), 1.08 (12H, d, J = 6.9 Hz, CH(C**H**$_3$)$_2$), 0.99 (12H, d, J = 6.6 Hz, CH(C**H**$_3$)$_2$), -0.75 (1H, s, Au-O**H**). ^{13}C NMR δ $_C$ (CD$_3$CN, 75 MHz) 146.5 (Ar**C**$_q$), 146.0 (Ar**C**$_q$), 143.1 (Ar**C**$_q$), 142.7 (Ar**C**$_q$), 139.1 (Ar**C**$_q$), 138.1 (Ar**C**$_q$), 135.0 (Ar**C**$_q$), 134.3 (Ar**C**H), 133.3 (Ar**C**$_q$), 132.4 (Ar**C**H), 127.2 (Ar**C**H), 126.4 (Ar**C**$_q$), 125.0 (Ar**C**H), 121.7 (Ar**C**H), 120.6 (Ar**C**H), 108.2 (Ar**C**$_q$), 35.2 (**C**(CH$_3$)$_3$), 31.7 (C(**CH$_3$**)$_3$), 30.0 (**C**H(CH$_3$)$_2$), 25.2 (CH(**C**H$_3$)$_2$), 25.0 (CH(**C**H$_3$)$_2$), 24.2 (CH(**C**H$_3$)$_2$), 23.4 (CH(**CH$_3$**)$_2$). ^{19}F NMR δ $_F$ (CD$_3$CN, 282 MHz) -73.00 (d, J = 706.0 Hz, P**F$_6$**). ^{31}P NMR δ $_P$ (CD$_3$CN, 121 MHz) -144.7 (sept, J = 707.0 Hz, **P**F$_6$). IR (CH$_2$Cl$_2$): 3602 cm^{-1} ν(OH). HRMS (ESI-TOFMS): HRMS (FIA-ESI): Calculated for C$_{72}$H$_{90}$N$_7$AuOH$^+$ [M]$^+$: 1266.6950, found: 1266.6998.

5.5.4) (CNC$_{Mes}$)Au (25)
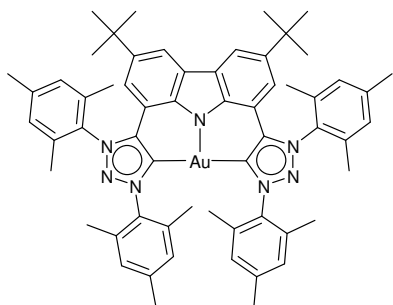
A similar procedure used for the synthesis of **23**, was employed for the synthesis of **25**. A Schlenk tube was loaded with **10** (200.0 mg, 1.9 x 10^{-4} mol), (tht)AuCl (72.0 mg, 2.2x 10^{-4} mol), KN[Si(CH$_3$)$_3$]$_2$ (186.7 mg, 9.4 x 10^{-4} mol), and subsequently evacuated and purged with N$_2$ (g). The reaction vessel was cooled down to -80 °C, followed by addition of THF (15 mL) which was also cooled down to -80 °C. The reaction mixture

was stirred for 30 min at -80 °C, removed from the cold bath and allowed to warm up to room temperature whilst stirring overnight. The solvent was evaporated *in vacuo*. The residue was washed with hexanes (4 x 15mL), and afterwards the product was extracted with Et$_2$O (3 x 15mL). Solvent evaporation, *in vacuo*, yielded **25** (83.0 mg, 7.7x 10^{-4} mol, 40%) as a dark pink solid. Crystals suitable for XRD analysis was obtained through slow evaporation of a toluene solution. ^{1}H NMR δ $_H$ (C$_6$D$_6$, 300 MHz) 8.72 (2H, d, J = 1.8 Hz, Ar**H**$_{carb}$), 7.37 (2H, d, J = 1.5 Hz, Ar**H**$_{carb}$), 6.73 (4H, s, Ar**H**$_{Mes}$), 6.71 (4H, s, Ar**H**$_{Mes}$), 2.30 (6H, s, ArC**H$_3$**), 2.15 (12H, s, ArC**H$_3$**), 2.07 (6H, s, ArC**H$_3$**), 1.88 (12H, s, ArC**H$_3$**), 1.32 (18H, s, C(C**H$_3$**)$_3$). ^{13}C NMR δ $_C$ (C$_6$D$_6$, 75 MHz) 175.8 (**C**$_{Carbene}$), 147.5 (Ar**C**$_q$), 147.4 (Ar**C**$_q$), 140.6 (Ar**C**$_q$), 138.5 (Ar**C**$_q$), 138.3 (Ar**C**$_q$), 135.8 (Ar**C**$_q$), 135.5 (Ar**C**$_q$), 135.2 (Ar**C**$_q$), 134.8 (Ar**C**$_q$), 130.0 (Ar**C**H), 128.9 (Ar**C**H), 127.5 (Ar**C**$_q$), 119.9 (Ar**C**H), 118.9 (Ar**C**H), 111.8 (Ar**C**$_q$), 34.8 (**C**(CH$_3$)$_3$), 32.5 (C(**CH$_3$**)$_3$), 21.5 (Ar**C**H$_3$), 21.0 (Ar**C**H$_3$), 18.3 (Ar**C**H$_3$), 17.6 (Ar**C**H$_3$). HRMS (FIA-ESI): Calculated for C$_{60}$H$_{66}$N$_7$Au$^+$ [M + H]$^+$: 1082.5123, found: 1082.5104.

Chapter 6: Conclusions and Future Perspectives

Carbenes have found a prominent position in organometallic chemistry, mainly as supporting ligands for various metal complexes designed to fulfil various roles. In particular, with regard to their use as ligands coordinated to catalytically active metal centres. Their ability to increase the stability of the catalyst, as well as increase electron density on the metal centre due to their strong donor ability, render carbenes a useful tool in synthesis and design of catalyst. In addition, ligand scaffolds substituted with one or more carbenes, have been shown to stabilise reactive metal complexes to such an extent, that these complexes can be isolated and even structurally characterised. During this study, we were able to exploit these properties of carbenes during the synthesis of reactive metal complexes, as well as a catalytically active metal complex.

The ligand salt **7** and **10**, were synthesised based on a 3 + 2 cycloaddition of the corresponding reagents, the 1,3-diaryl-2-azoniaallene salts and alkynes. The reaction was performed in the presence of *tert*-butylhypochlorite and KPF_6. This lead the formation and isolation of the two ligand salts, which could be deprotonated to yield the potassium free-carbene adducts **9** and **11**. The stability imparted by the rigid carbazole backbone and by the four bulky aromatic wingtip protecting groups on each ligand, allowed for the isolation of these extremely reactive species, which featured a high thermal stability under inert conditions. Both adducts feature a strong donating amido moiety, in addition to two triazolylidene functionalities, which are known for their strong σ-donor ability. As such, the electronic properties of the ligands were probed in order to determine just how strongly donating these ligands scaffolds are.

In order to probe the electronic properties of the ligand adducts **9** and **11** *via* determination of the effect on the v(CO) stretching frequencies, a metal carbonyl complex supported by the ligand scaffold, had to be synthesised. The ligand salts were treated with a base, followed by *in situ* metallation of the formed adduct **9** or **11** with $[Rh(C_2H_4)_2Cl]_2$, yielding the rhodium complexes **17** and **20**. These 16-electron rhodium(I) complexes feature molecular oxygen as a L-type ligand, π-coordinating to the metal centre. It has been shown that complexes of rhodium supported by carbenes resist oxidation in the presence of oxygen, which cannot always be said for rhodium complexes supported by other ligands. Bubbling carbon monoxide gas through a solution of either **17** or **20** yielded the corresponding rhodium(I)-carbonyl complexes **19** and **21**, respectively. These two complexes were subjected to infrared spectroscopic analysis. The Rh-CO complexes **19** and **21**

186

displayed strong absorptions at 1955 cm^{-1} and 1941 cm^{-1}, respectively. The ligand scaffolds **9** and **11** are found to be more donating then some of the most basic ligand systems reported, including phosphines, nNHCs and other triazolylidenes and 4-imidazolylidene ligands. The strong donating ability of our ligand scaffolds can be attributed to the strong σ-donor weak π-acceptor ability of the triazolylidene and amido moieties. The strongly donating ligand scaffolds will yield a metal centre with a high nucleophilic character, which could increase processes such as oxidative addition, which is an essential step in most catalytic reactions.

The stabilisation imparted by the ligand scaffolds, and in particular the carbene adduct **9**, to various reactive metal centres is as remarkable as the strong donor ability of the ligands. The synthesis, isolation and structural characterisation of the first neutral nickel(II)-hydride carbene complex **12**, support this argument. Nickel hydride complexes are known for their high reactivity and examples of these complexes are scarce. This is mainly due to their ease of decomposition, especially when not supported by a bulky, stabilising ligand. The analogue of **12**, namely the nickel(II)-hydride complex **13** which is supported by **11**, was also isolated and characterised by NMR and MS spectroscopy. The catalytic activity of **12** and **13** towards various organic transformations will be investigated in future. In particular, reduction of various carbonyl containing organic substrates will be attempted. Successful reduction of these organic substrate will be followed by determining the reactivity and catalytic activity of **12** and **13** towards carbon dioxide.

The stabilising ability of the ligand scaffold **9** was further investigated, when it was reacted with CuCl$_2$, yielding a rare example of a copper(II)-carbene complex. The Cu(II)-Cl complex **14** supported by **9**, was structurally characterised as an NMR-silent spectrum confirmed the existence of a paramagnetic complex. Complex **14** displayed a severely distorted sqaure-planar geometry around the metal centre approaching a geometry more characteristic to that of the see-saw type. Reduction of **14** to **15** occurred upon attempted substitution of the chloro ligand with a hydride ligand. However, **15** displayed a T-shaped geometry around the metal centre, which is unusual for copper(I) complexes. The analogue of **15**, namely the Cu(I) complex **16** could be synthesised through deprotonation of **10** followed by *in situ* metallation with CuI. As a continuation of the current work, all three complexes **14**, **15** and **16**, will be subjected to reactivity studies regarding the use of oxygen as reagent. Reactivity tests will be followed by catalytic investigations of the complexes towards the oxidation of organic substrates with oxygen, employing the complexes as catalyst.

Further surprising results originating from the stabilising effect of the ligand adducts **9** or **11**, were obtained by reacting the adducts with either silver(I) or gold(I) to yield complexes with unusual geometries around the metal centre. This term 'unusual geometry' is used with regard to the metals

187

silver(I) and gold(I) that, upon complexation, normally yields linear or trigonal planar complexes if the coordination number is two or three, respectively. However, complexes **22**, **23** and **25** all displayed distorted T-shaped geometries around the metal centre, as determined after crystal structure analysis, yielding a ''naked'' M(I) centre with a vacant site. Silver(I) and gold(I), especially the gold(I) metal, resist chelation by a pincer ligand, and is stable with just one or two ligands coordinated to the centre, in a linear fashion. The tendency of gold(I) to resist chelation was most pronounced in complex **25**, which formed the T-shaped gold(I) complex with significant deviations from the 'normal' T-shaped metal complexes. It can therefore be postulated that the pincer ligands 'lock' the metal in or close to the tridentate pocket. The distorted T-shaped gold(I) complexes **23** and **25**, will be scrutinised towards various organic transformation and catalytic reactions. Carbene dissociation in these two complexes could occur, due to bond and bond angle strain that would be alleviated. If this process occurs reversibly, a second site on the gold(I) centre can be vacated, which should coordinate and catalyse an incoming substrate.

Oxidation of gold(I) to gold(III) was successful when employing a silver(I) salt as oxidising agent. The gold(III) species **24** was attained upon oxidising **23** with 2.3 equivalents of $AgPF_6$. NMR, MS and IR spectroscopic analysis revealed the existence of the lime green solid **24**, supported by **9** in addition to a hydroxo ligand. ^{31}P and ^{19}F NMR analysis confirmed a hexafluorophosphate as counteranion. Complexes of gold coordinated by a hydroxide ligand are scarcely reported. In addition, cationic gold(III) complexes have also not been often reported, which could be explained by their tendency to reduce back to gold(I) or to yield decomposition products. A bulky, stabilising ligand would certainly decrease or prevent reduction or decomposition of gold(III) complexes. Our ligand scaffold **9** was certainly able to stabilise this cationic gold(III)-hydroxo complex as it was both thermally stable in the absence or presence of water. An extensive literature search failed to reveal examples of cationic gold(III)-hydroxo complexes. A gold(III)-hydroxo complex and its reactivity towards various substrates has been investigated (see Section 5.1.3, Chapter 5). Cationic gold complexes are known to coordinate and π-activate olefins. As such, it is proposed that **24** could accomplish various tasks. It could react with a substrate, i.e. deprotonation of an alcohol yielding the alkoxide, or coordinate through the vacant site to an olefin, activating that substrate to nucleophilic attack. This reactivity and possibly catalytic activity will be investigated in the near future.

As is clearly evident, the stabilisation imparted by the ligand scaffolds **9** or **11**, is remarkable. It is generally known that increasing the ligand bulk as well as increasing the stability of the complex, decreases catalytic activity. We set out to determine if, once metallated, the ligand would render the complex reactive towards ammonia, catalytically active towards the hydroamination reaction, or

188

not. Complexes **17** and **20** were used during the reactivity and catalytic activity tests. Bubbling ammonia gas through a solution of **17**, yielded a Rh(I)-NH$_3$ adduct **18**, not the product of oxidative addition, namely the rhodium(III)-amido-hydride complex. Remarkably, ammonia coordination to the rhodium(I) metal centre in **18** is reversible, and the ammonia ligand can simply be removed under vacuum, followed by exposure of the solution to oxygen which yielded **17** again. Hydroamination of 1-pentyne with diethyl amine was then investigated. The catalytic reaction was performed using **20** as catalyst. The hydroamination of 1-pentyne with the secondary amine was not catalysed. Instead, it was determined that **20** catalyses the dimerisation of 1-pentyne to the *gem*-enyne, 6-methylene-4-nonyne. The presence of the basic amine only served to increase the rate of catalysis. The *gem*-enyne is the sole product of catalysis, and formation of its isomers, the *E*- and *Z*-isomers, was not observed. This is surprising indeed, because the dimerisation catalysis of terminal alkynes is accompanied with the formation of a major product, as well as the other two isomers in minor yields. Not only is **20** selective towards the formation of the *gem*-enyne, but also the rate of catalysis high in the presence of the weak basic amine, with full conversion of alkyne to the *gem*-enyne in under two hours. The catalysis of 1-pentyne to the *gem*-enyne employing **20** as catalyst will further be investigated and the reaction conditions optimised. This will be followed by testing the scope of the catalyst towards other terminal alkyne substrates, including substrates with various functional groups substituted in the carbon backbone.

Chapter 7: Experimental

7.1) Standard Operating Procedures

7.1.1) Method

All synthetic manipulations were performed under an N_2 or Ar gas atmosphere using oven or flame dried glassware and standard Schlenk techniques. All solids that are hygroscopic and sensitive to oxygen were weighed off in a glove box under a N_2 gas atmosphere. Preparations of NMR and crystallisation of samples that also require an inert atmosphere were done in the glove box.

7.1.2) Materials

The reagent ^{t}BuOCl was prepared according to the general method of Mintz and Walling.[1] All other reagents were obtained from commercial sources and were used without any further purification. Unless otherwise stated, only anhydrous solvents were used during experimental procedures. Anhydrous THF and Et_2O were obtained after distillation over sodium and benzophenone under a N_2 gas atmosphere. Anhydrous PhMe and hexane were obtained after distillation over sodium under a N_2 gas atmosphere. Anhydrous CH_2Cl_2 was obtained after distillation over phosphorous(V) pentoxide under a N_2 gas atmosphere. Anhydrous CH_3CN was obtained after distillation over calcium hydride under a N_2 gas atmosphere. Deuterated solvents were purified through distillation under an Ar gas atmosphere.

7.2) Characterisation Techniques

7.2.1) Nuclear Magnetic Resonance Spectroscopy

Nuclear magnetic resonance (NMR) spectra were obtained using either a Bruker AVANCE-III-300 operating at 300.13 MHz for ^{1}H, 75.47 MHz for ^{13}C, 121.49 MHz for ^{31}P and 282.40 MHz for ^{19}F; or AVANCE-III-400 operating at 400.21 MHz for ^{1}H, 100.64 MHz for ^{13}C, 162.01 MHz for ^{31}P and 376.57 MHz for ^{19}F. A Varian Inova 500 spectrometer was also used which operated at 499.83 MHz for ^{1}H and 125.76 MHz for ^{13}C. ^{1}H Chemical shifts are reported as δ (ppm) values downfield from Me_4Si and

---

[1] M. J. Mintz, C. Walling, *Organic Synthesis, Coll.*, 1973, **5**, 184.

using residual non-deuterated solvents as internal standards (CD$_3$CN, 1.94 ppm; CD$_2$Cl$_2$, 5.32 ppm; CDCl$_3$, 7.26 ppm; C$_6$D$_6$, 7.16 ppm). ^{13}C chemical shifts are also reported as δ (ppm) values downfield from Me$_4$Si while using deuterated solvents as internal standards (CD$_3$CN, 1.32 ppm; CD$_2$Cl$_2$, 54.00 ppm; CDCl$_3$, 77.16 ppm; C$_6$D$_6$, 128.06 ppm). Proton coupling constants (*J*) are given in Hz. The spectral coupling patterns are designated as follows: s/S - singlet; d/D - doublet; t/T - triplet; q/Q - quartet; sept - septet; m - multiplet; br - broad signal. Quaternary carbons are designated as C$_q$.

Signal assignment in the ^{1}H NMR spectra is based on first-order analysis and when required were confirmed by two-dimensional (2D) (^{1}H-^{1}H) homonuclear chemical shift correlation (COSY) experiments. The ^{13}C shifts were obtained from proton-decoupled ^{13}C NMR spectra. Where necessary, the multiplicities of the ^{13}C signals were deduced from proton-decoupled DEPT-135 spectra. The signals of the proton-bearing carbon atoms were correlated with specific proton resonances using 2D (^{13}C-^{1}H) heteronuclear single-quantum coherence (HSQC) experiments. Standard Bruker pulse programs were used in the experiments.

7.2.2) Infrared Spectroscopy

7.2.2.1) Infrared Spectrometric Analysis for 17, 18, and 19

 Solution IR spectra were recorded on a Bruker ALPHA FT-IR spectrophotometer in CH$_2$Cl$_2$ as solvent, using a NaCl cell with a cell width of 0.5 mm. The range of absorption measured was from 4000-400 cm^{-1}.

7.2.2.2) Infrared Spectrometric Analysis for 20, and 21

 Solution IR spectra were recorded on a Perkin-Elmer Spectrum RXI FT-IR spectrophotometer in CH$_2$Cl$_2$ as solvent, using a NaCl cell with a cell width of 1.0 mm. The range of absorption measured was from 4000-600 cm^{-1}.

191

7.2.3) Mass Spectroscopy

7.2.3.1) Mass Spectrometric Analysis for 7, 8, 12, 14 and 15

Electrospray ionization (ESI)-Time of Flight (TOF)-Mass spectrometry (MS): ESI-TOFMS analyses were performed at the UC San Diego Mass Spectrometry Laboratory on an Agilent 6230 ESI-TOFMS by Dr. G. Ung.

7.2.3.2) Mass Spectrometric Analysis for 10, 13, 16, 17, 19, 20, 21, 22, 23, 24 and 25

Chemicals and reagents: MS-grade acetonitrile was purchased from Romil. Acetonitrile with 0.1% formic acid was purchased from Fluka.

Flow Injection Analysis (FIA)-Electrospray ionization (ESI)-Mass spectrometry (MS): ESI mass spectra were acquired, by Dr. D. Koot, in both positive and negative ionization mode using a Waters, Synapt G2 mass spectrometer (Milford, MA, USA). Prior to analysis, a 5 mM sodium formate solution was used to calibrate the instrument in resolution mode achieving a mass accuracy of of less than 0.5 mDa over a mass range of 100-1200 Da using the IntelliStart function of Masslynx software. For analysis, the instrument was operated under the following conditions: capillary voltage 2.8 kV (positive mode) 2.5 kV (negative mode); sampling cone (ramped from 20 V - 40 V), extraction cone 4 V, source temperature 100 °C, desolvation temperature 200 °C, Cone gas 100 L/h, desolvation gas 500 L/h, MS gas: nitrogen.

Samples were made up in 100% acetonitrile (MeCN) to an approximate concentration of 10 μg/ml. Flow injection using MeCN (0.1% formic acid) as mobile phase (with the aid of an Acquity auto sampler injecting 5 μl of sample) was used to introduce the compounds to the ionization source such that a minimum of 10 scans with a scan time of 0.5 seconds in continuum format could be combined across a bolus peak. A 2 ng/μl solution of Leucine enkephalin was constantly infused via a syringe through a separate ESI probe with an angle perpendicular to the sample spray at a flow rate of 3 μL/min and was sampled every 10 seconds to compensate for possible experimental drift. The mass spectral resolution attained was typically > 15000 (FWHM definition) as calculated using ResCalc (version 2.2.3). Quality control (QC) samples consisted of sodium formate clusters that were likewise analysed and used to confirm that the method was working. The attained spectrum list was saved as a txt file and further processed using mMass.

FIA-ESI mass spectra were acquired by Dr. D. Koot at the University of Pretoria.

7.2.4) X-Ray Diffraction Analysis

The CIF files for the complexes analysed by X-ray diffraction analysis, as well as all the data tables, are submitted in an electronic format.

7.2.4.1) X-Ray diffraction analysis for 12

Single crystal X-ray diffraction data were collected on a Bruker Apex II-CCD detector using Mo-K$_\alpha$ radiation (λ = 0.71073 Å) by Dr. Gaël Ung, at UC San Diego. Crystals were selected under oil, mounted on nylon loops then immediately placed in a cold stream of N_2 at 100 K. Using Olex2,[2] the structure was solved with the ShelXS[3] structure solution program using Direct Methods and refined with the ShelXL[4] refinement package using Least Squares minimisation.

Crystal data and structure refinement for 12: $C_{360}H_{433}N_{28}Ni_4O_4$ (M = 5451.16): monoclinic, space group C2/c (no. 15), a = 26.616(3) Å, b = 14.9450(17) Å, c = 20.524(3) Å, β = 106.507(3)°, V = 7827.6(17) Å^3, Z = 1, T = 100.0 K, μ(MoKα) = 0.299 mm^{-1}, $Dcalc$ = 1.156 g/mm^3, 28591 reflections measured (5.386 ≤ 2Θ ≤ 50.71), 7148 unique (R_{int} = 0.0457) which were used in all calculations. The final R_1 was 0.0368 (I > 2σ(I)) and wR_2 was 0.0850 (all data). The asymmetric unit contains a ½ formula unit located on a crystallographic inversion centre. Compound **12** co-crystallised with its corresponding Ni-OH derivative on a 51/49 ratio.

7.2.4.2) X-Ray diffraction analysis for 7, 9, 10, 14, 15, 17, 22, 23 and 25

Single crystal X-ray diffraction data were collected on a Bruker Apex II-CCD detector using Mo-K$_\alpha$ radiation (λ = 0.71073 Å), by Mr. David C. Liles, at the University of Pretoria. Crystals sensitive towards air and moisture, were selected under oil, mounted on nylon loops then immediately placed in a cold stream of N_2 at 150 K. Crystals stable towards ambient conditions were mounted on a needle at either 150 K or 273K. The structures were solved with the SHELXTS[3] structure solution program using Direct Methods and refined with both SHELXTL[4] and SHELXL[4] refinement packages using Least Squares minimisation.

---

[2] O. V. Dolomanov, L. J. Bourhis, R. J. Gildea, J. A. K. Howard, H. Puschmann, *J. Appl. Cryst.*, 2009, **42**, 339 – 341.
[3] G. M. Sheldrick, *Acta. Cryst.*, 2008, **A64**, 112 – 122.
[4] G. M. Sheldrick, *Acta. Cryst.*, 2008, **A64**, 112 – 122.

Crystal data and structure refinement for 7: $C_{153.04}H_{204}Cl_2F_{11.82}N_{14}O_3P_2$ (M = 2645.11): triclinic, space group P-1 (no. 2), a = 15.0299(3) Å, b = 20.9816(4) Å, c = 25.5308(5) Å, α = 90.0140(10)°, β = 94.3710(10)°, γ = 108.8090(10)°, V = 7596.4(3) Å^3, Z = 2, T = 150.15 K, μ(CuKα) = 1.141 mm^{-1}, $Dcalc$ = 1.156 g/mm^3, 237368 reflections measured (4.45 ≤ 2Θ ≤ 137.474), 27863 unique (R_{int} = 0.0566) which were used in all calculations. The final R_1 was 0.0679 (I > 2σ(I)) and wR_2 was 0.1837 (all data). The asymmetric unit contains two formula units along with three solvent molecules of acetone. A final difference Fourier map featured some strong remaining peaks. The SQUEEZE procedure was used to remove the strong peaks, which allowed a satisfactory refinement of the molecular structure.

Crystal Data and structure refinement for 9: $C_{72}H_{90}KN_7$ (M = 1092.60): triclinic, space group P-1 (no. 2), a = 14.4327(3) Å, b = 14.6585(3) Å, c = 17.8114(4) Å, α = 82.8410(11)°, β = 74.7310(10)°, γ = 68.2340(10)°, V = 3374.50(13) Å^3, Z = 2, T = 150.15 K, μ(CuKα) = 1.016 mm^{-1}, $Dcalc$ = 1.075 g/mm^3, 80987 reflections measured (5.146 ≤ 2Θ ≤ 140.134), 12717 unique (R_{int} = 0.0491) which were used in all calculations. The final R_1 was 0.0519 (I > 2σ(I)) and wR_2 was 0.1420 (all data).

Crystal Data and structure refinement for 10: $C_{60}H_{69}ClF_6N_7P$ (M = 1068.64 g/mol): monoclinic, space group P21/c (no. 14), a = 16.2214(4) Å, b = 24.0518(5) Å, c = 15.2494(3) Å, β = 108.8560(9)°, V = 5630.3(2) Å^3, Z = 4, T = 150(2) K, μ(CuKa) = 1.404 mm^{-1}, $Dcalc$ = 1.261 g/cm^3, 198184 reflections measured (5.756° ≤ 2Θ ≤ 144.492°), 11093 unique (R_{int} = 0.0378, R$_{sigma}$ = 0.0120) which were used in all calculations. The final R_1 was 0.0430 (I > 2s(I)) and wR_2 was 0.1148 (all data).

Crystal data and structure refinement for 14: $C_{42}H_{51}Cl_{0.5}Cu_{0.5}N_{3.5}$ (M = 654.35): orthorhombic, space group Pnma (no. 62), a = 17.200(3) Å, b = 31.200(6) Å, c = 14.700(3) Å, V = 7889(3) Å^3, Z = 8, T = 293(2) K, μ(MoKα) = 0.356 mm^{-1}, $Dcalc$ = 1.102 g/mm^3, 266907 reflections measured (4.484 ≤ 2Θ ≤ 51.532), 7676 unique (R_{int} = 0.0438) which were used in all calculations. The final R_1 was 0.0629 (I > 2σ(I)) and wR_2 was 0.1961 (all data). The asymmetric unit contains a 1/2 formula units along with a molecule of solvent, benzene. A final difference Fourier map featured some strong remaining peaks. The SQUEEZE procedure was used to remove the strong peaks. An small average phenyl C-C distance of 1.35 Å was obtained for C1B and C1D atoms of benzene, which does not affect to the satisfactory refinement of the molecular structure of **14**.

Crystal data and structure refinement for 15: $C_{90}H_{108}CuN_7$ (M = 1351.37): monoclinic, space group C2/c (no. 15), a = 26.4509(7) Å, b = 14.8717(4) Å, c = 20.6818(5) Å, β = 107.1470(10)°, V = 7774.0(4) Å^3, Z = 4, T = 293(2) K, μ(MoKα) = 0.330 mm^{-1}, $Dcalc$ = 1.155 g/mm^3, 29173 reflections measured (3.18 ≤ 2Θ ≤ 50.82), 6730 unique (R_{int} = 0.0220) which were used in all calculations. The

final R_1 was 0.0457 (I > 2σ(I)) and wR_2 was 0.1113 (all data). The asymmetric unit contains a ½ formula unit located on a crystallographic inversion centre.

Crystal data and structure refinement for 17: $C_{84.21}H_{103.1}N_7O_2Rh$ (M = 1348.26 g/mol): triclinic, space group P-1 (no. 2), a = 10.8323(5) Å, b = 15.4988(8) Å, c =24.8410(13) Å, α = 103.4480(14)°, β = 97.0590(13)°, γ = 107.0370(13)°, V = 3795.4(3) Å^3, Z = 2, T = 150(2) K, μ(MoKa) = 0.275 mm^{-1}, $Dcalc$ = 1.180 g/cm^3, 84650 reflections measured (4.428° ≤ 2Θ ≤ 51.56°), 14487 unique (R_{int} = 0.1258, R_{sigma} = 0.1067) which were used in all calculations. The final R_1 was 0.0658 (I > 2s(I)) and wR_2 was 0.1865 (all data).

Crystal data and structure refinement for 22: $C_{74}H_{94}AgCl_4N_7$ (M = 1331.23 g/mol): triclinic, space group P-1 (no. 2), a = 14.8607(5) Å, b = 15.7212(6) Å, c =18.0365(6) Å, α = 85.1075(14)°, β = 69.7219(13)°, γ = 63.4722(13)°, V = 3524.4(2) Å^3, Z = 2, T = 150(2) K, μ(MoKa) = 0.483 mm^{-1}, $Dcalc$ = 1.254 g/cm^3, 215708 reflections measured (4.558° ≤ 2Θ ≤ 68.38°), 29081 unique (R_{int} = 0.0372, R_{sigma} = 0.0263) which were used in all calculations. The final R_1 was 0.0464 (I > 2s(I)) and wR_2 was 0.1326 (all data).

Crystal data and structure refinement for 23: $C_{72}H_{90}AuN_7$ (M = 1250.47 g/mol): monoclinic, space group C2/c (no. 15), a = 25.5229(13) Å, b = 15.3460(8) Å, c = 16.4106(8) Å, β = 100.7610(15)°, V = 6314.6(6) Å^3, Z = 4, T = 150(2) K, μ(MoKa) = 2.377 mm^{-1}, $Dcalc$ = 1.315 g/cm^3, 180870 reflections measured (5.054° ≤ 2Θ ≤ 68.672°), 13233 unique (R_{int} = 0.0631, R_{sigma} = 0.0301) which were used in all calculations. The final $R1$ was 0.0294 (I> 2s(I)) and wR_2 was 0.0632 (all data). The asymmetric unit contains a ½ formula unit located on a crystallographic inversion centre.

Crystal data and structure refinement for 25: $C_{60}H_{66}AuN_7O_2$ (M = 1114.16 g/mol): monoclinic, space group C2/c (no. 15), a = 27.4209(14) Å, b = 18.0706(8) Å, c = 23.4524(12) Å, β = 108.7689(15)°, V = 11003.0(9) Å^3, Z = 8, T = 150(2) K, μ(MoKa) = 2.722 mm^{-1}, $Dcalc$ = 1.345 g/cm^3, 246113 reflections measured (4.508° ≤ 2Θ ≤ 51.494°), 10529 unique (R_{int} = 0.0841, R_{sigma} = 0.0285) which were used in all calculations. The final R_1 was 0.0345 (I > 2s(I)) and wR_2 was 0.0882 (all data).

7.2.5) Melting Point Determination

Melting points were measured with a Stuart SMP10 melting point apparatus.